Lars Klemet Jakobsson

Distribution of boron between silicon and $CaO\text{-}SiO_2$, $MgO\text{-}SiO_2$, $CaO\text{-}MgO\text{-}SiO_2$ and $CaO\text{-}Al_2O_3\text{-}SiO_2$ slags at 1600°C

Thesis for the degree of Philosophiae Doctor

Trondheim, November 2013

Norwegian University of Science and Technology
Faculty of Natural Sciences and Technology
Department of Materials Science and Engineering

NTNU – Trondheim
Norwegian University of
Science and Technology

NTNU
Norwegian University of Science and Technology

Thesis for the degree of Philosophiae Doctor

Faculty of Natural Sciences and Technology
Department of Materials Science and Engineering

ISBN 978-82-471-4790-0 (printed ver.)
ISBN 978-82-471-4791-7 (electronic ver.)
ISSN 1503-8181

Doctoral theses at NTNU, 2013:326

Printed by NTNU-trykk

Abstract

New energy sources are needed for a sustainable future. Solar cells have a huge potential as a sustainable energy source but further development of this technology is needed for solar cells to become cost-competitive with other energy sources. Silicon produced by metallurgical refining methods has the potential of reducing the cost of crystalline silicon solar cells significantly but boron has proven to be hard to remove from silicon by these methods. Slag refining is however a promising refining method for removal of boron from silicon. The aim of this thesis was to determine accurate data for the distribution of boron between silicon and selected slags.

All published values of the distribution coefficient of boron have been critically reviewed in this work. The thermodynamic properties and distribution of other major components of the system have also been reviewed. Several experiments with silicon and CaO-SiO_2, MgO-SiO_2, CaO-MgO-SiO_2 and CaO-Al_2O_3-SiO_2 slags have been conducted at 1600 °C under argon atmosphere. A series of experiments with ferrosilicon and CaO-SiO_2 slags have also been carried out.

Accurate data for the distribution of boron between silicon and CaO-SiO_2, MgO-SiO_2, CaO-MgO-SiO_2 and CaO-Al_2O_3-SiO_2 slags at 1600 °C has been determined. The distribution of other major slag components between slag and silicon has also been found in these slag systems. The distribution of calcium and boron between ferrosilicon and CaO-SiO_2 slags at 1600 °C has been determined. Activities of slag forming components have been determined in the CaO-SiO_2, MgO-SiO_2 and CaO-MgO-SiO_2 systems. The activity coefficient of $BO_{1.5}$ at infinite dilution in these slags has also been determined. Activity coefficients of calcium, magnesium and aluminium at infinite dilution in silicon and the activity coefficient of calcium and boron at infinite dilution in ferrosilicon have been determined. An alternative equation for mass transfer has been derived and the mass transfer coefficient of boron in a 37.9%CaO-62.1%SiO_2 slag has been estimated to be $k_s = 5.2 \cdot 10^{-7}$m/s.

The refining efficiency of CaO-MgO-SiO_2 slags has been found to be approximately the same independently of slag composition with a distribution coefficient of boron between 2 and 2.5. This also includes the binary CaO-SiO_2 and MgO-SiO_2 systems. The activity coefficient of $BO_{1.5}$ at infinite dilution in CaO-MgO-SiO_2 slags, including the binary CaO-SiO_2 and MgO-SiO_2 systems, has been found to follow the activity coefficient of SiO_2 where $\gamma^0_{BO_{1.5}} = 0.38\gamma_{SiO_2}$. A linear decrease of the distribution coefficient was found with increasing Al_2O_3 content in a ternary CaO-Al_2O_3-SiO_2 slag. This has been found to be caused by an increasing activity coefficient of $BO_{1.5}$ at infinite dilution in slag relative to the activity coefficient of SiO_2. The distribution coefficient of boron between ferrosilicon and CaO-SiO_2 slags was found to be unchanged with iron content in silicon.

Preface

This thesis is submitted to the Norwegian University of Science and Technology for partial fulfilment of the requirements for the degree of philosophiae doctor.

The doctoral work has been performed at the Department of Materials Science and Engineering, Norwegian University of Science and Technology, Trondheim, from August 2009 to September 2013 with Merete Tangstad as supervisor. Some of this work was carried out at the University of Tokyo between September 2011 and December 2011.

Parts of this work has been published in the proceedings of the following conferences and symposia:

- Fray International Symposium, Cancun 2011
- International Smelting Technology Symposium, TMS, Orlando 2012
- INFACON, Almaty 2013

I would like to thank my supervisor professor Merete Tangstad for invaluable help and support throughout the four years of this work. I am also grateful to professor Kazuki Morita for his supervision during my stay at the University of Tokyo.

I would also like to thank Syverin Lierhagen and Torill Sørlokk for the large number of analytical determinations required for this work. Their feedback on quality assessment of the analytical results is highly appreciated. I would like to thank Delphine Leroy and Harald Holm for their assistance in the laboratory and Aksel Alstad for constructive feedback and help with the design and making of new furnace parts. I am also thankful for the assistance from Kai Tang with FactSage calculations. The support from Torild Krogstad, Ove Darell and Birgitte Karlsen on parts of the tedious job of preparing samples for analysis is also appreciated.

This work was carried out as a part of the BASIC project, financed by the Research Council of Norway.

Trondheim, September 2013

Lars Klemet Jakobsson

Contents

Chapter 1

Introduction

The aim of this thesis was to determine accurate data for the distribution of boron between silicon and selected slags. Literature data on slag refining for boron removal is limited and experimental results are widely scattered. It is therefore important to verify existing data and to find new data for systems still not investigated.

1.1 Background and motivation

Energy is at present mainly provided through fossil fuels. Limited reserves of fossil fuels and concerns about pollution and climate change makes energy from other sources necessary and attractive both for energy security and human safety. There are many estimates of how long the fossil fuel reserves will last but they will become depleted at some point in the future. How abrupt the reserves will end is also debated and ranges from predictions of a sudden energy crisis to a gradual increase of price that makes alternative energy sources replace fossil fuels bit by bit.

A global warming of several degrees Celsius is predicted if releases of CO_2 from fossil fuels are continued at the current levels (IPCC, 2007). More extreme weather and an increased sea level are two definitive consequences of a global warming and this together with many other known and unknown negative consequences makes it preferable to avoid a global warming. Capturing CO_2 and storing it is one possible way to reduce the CO_2 emissions. This is however relatively hard and will thus make energy from fossil fuels more expensive. A consequence would however be that alternative energy sources could become more cost competitive to fossil fuels.

The world population is growing and the living standards are increasing in developing countries. More fossil fuels than ever is therefore burnt to meet the increasing energy demands even if this may have bad irreversible consequences for future generations. Fossil fuels dominate the global energy consumption while the total share of modern renewable energy sources accounts for less

than 10% as shown in figure 1.1.

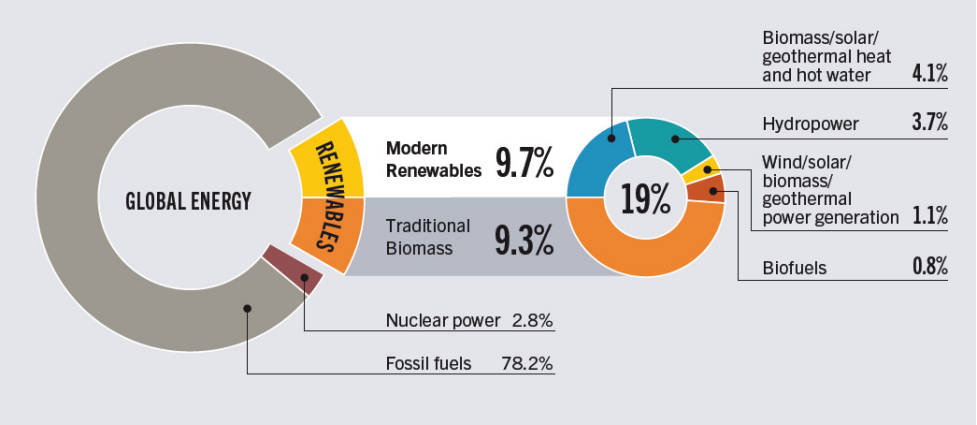

Figure 1.1: Estimated renewable energy share of global final energy consumption in 2011 from REN21 (2013).

A combined effort on many different areas is needed for the transition to sustainable energy sources. Energy efficiency and alternative energy technology development are two major fields where an ever-increasing effort is needed to make the transition possible without negative economic and social consequences. Strategies for handling the intermittent nature of solar and wind power are also needed if they are to become major energy sources.

The cost of energy from alternative sources can only be reduced through upscaling, know-how and technological advances. The two first criteria can be fulfilled through increased deployment of alternative energy sources while the last is dependent on research and development. A combined effort on all three is the most efficient approach since each of them will enhance the others. Advances in alternative energy technology will not come without research effort and the advances are most likely to be gradual like it is with any other technology. Postponing a transition from fossil fuels to alternative energy sources can in the worst case cause a catastrophic global warming and extremely high energy prices as the fossil fuels get more scarce.

Solar cells are predicted to be one of the major alternative energy sources in the future due to the abundance of energy from sunlight that can be converted to electricity through the photoelectric effect (Morton, 2006). The huge potential for solar energy is also visualized in figure 1.2. An exergy analysis of the global energy resources has also shown solar energy to have an enormous potential (Hermann, 2006). Solar cells are however in most countries still dependent on subsidies to be cost competitive with other electrical energy sources. It should be noted that fossil fuels also are subsidized in most countries. A gradual decline of cost is in any case decreasing the price gap between electricity from solar cells and other energy sources.

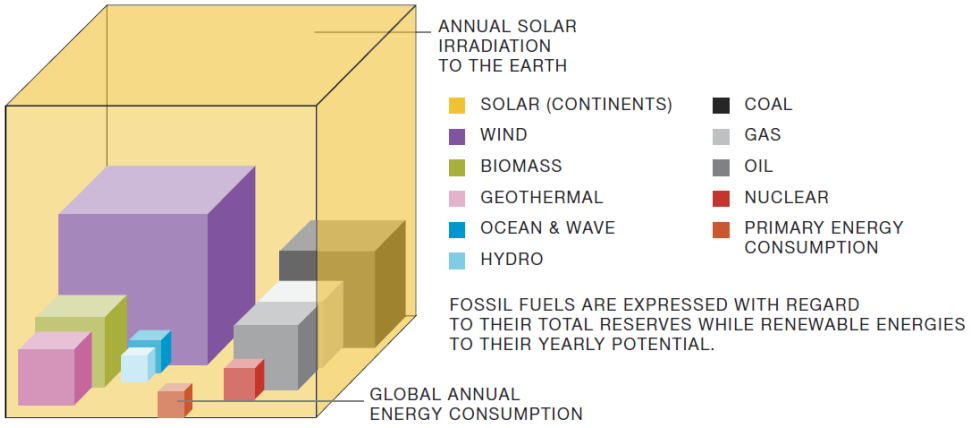

Figure 1.2: Solar irradiation versus established global energy resources (EPIA and Greenpeace, 2011).

Crystalline silicon solar cells dominate the solar cell market at present. Novel technologies are predicted to replace this technology in the future but crystalline silicon solar cells will remain as an important technology for several years to come due to its proven performance and durability. Using silicon as the primary material also has two major benefits being both non-toxic and very abundant as compared to many other materials. Crystalline silicon solar cells can only convert a limited range of the solar spectrum to electricity and the efficiency is therefore limited. Hybrid solar cells using the traditional crystalline silicon solar cell as a base combined with other cell concepts may however evolve as the technology advances.

Two drawbacks of the crystalline silicon solar cell technology is that a relatively large amount of silicon is required for each solar cell and that the silicon has to be extremely pure. The production of pure silicon is therefore contributing significantly to the cost of the solar cell both energy-wise and in terms of price.

1.2 Silicon for solar cells

Silicon is produced by reduction of silicon dioxide with carbon at temperatures above 1800 °C in an electric furnace through the overall reaction

$$SiO_2 + 2C = Si + 2CO \tag{1.1}$$

Huge deposits of relatively pure quartz or quartzite can be found worldwide due to the high abundance of SiO_2 in Earth's crust. Coal is the main source of carbon but high quality deposits are limited. Charcoal is however a renewable source that can replace coal in the future (Schei et al., 1998). The purity of the

produced silicon is dependent on the raw materials, but will in any case need to be further purified to meet the demands for solar cells. Metallurgical grade silicon is tapped from the furnace and refined to a purity above 98.5% (Tuset, 1985). This silicon is mostly used for alloying of aluminium but an increased amount is used for the production of solar cells. A purity of approximately 6N is however required for solar cells (SEMI, 2012).

As of today most silicon for solar cells is produced through a chemical distillation process called the *Siemens process* which is both expensive and very energy demanding. Metallurgical grade silicon purified by this process also tends to be purer than necessary for solar cells. The most energy intensive step in this process is the slow deposition of silicon from trichlorosilane at approximately 1100 °C. Silicon is deposited on silicon rods inside large bell jars where the walls have to be kept cold while the silicon rods are kept at 1100 °C. Obviously a lot of energy is needed to keep the silicon rods hot with a large heat flux from the rods to the inner walls of the bell jars. Production of solar grade silicon using fluidized bed reactors reduces the cost and energy consumption as compared to the Siemens process. The reduction of cost and energy consumption is however limited since silicon still has to be converted to silane or trichlorosilane and distilled before it is decomposed to pure silicon. Alternative methods for producing silicon of sufficient purity that are less energy demanding and less expensive are therefore of great interest.

Purification of silicon without going through gasification, distillation and decomposition could reduce both cost and energy use significantly. Metallurgical refining is an alternative that have this potential. Slag refining, gas blowing and acid leaching are metallurgical refining methods commonly used for purification of metallurgical grade silicon. Traditional use of these methods is however not sufficient to make solar grade silicon and directional solidification is in any case required as an additional final refining step to bring the impurity levels in silicon to a sufficiently low level for use in solar cells.

Directional solidification has the advantage of producing ingots used to make multicrystalline silicon solar cells. These ingots are cut into bricks and the bricks are sliced into wafers that are processed into solar cells. Some metal impurities can be eliminated after the wafers have been made by a process called gettering. Monocrystalline silicon can be made by the Czochralski process. Monocrystalline solar cells have higher purity demands and silicon made by the Siemens process is therefore preferred for these cells. Monocrystalline and multicrystalline solar cells have approximately equal shares of the market.

Most impurity elements have a very low solubility in solid silicon (Trumbore, 1960). The effective segregation coefficient for most impurity elements is therefore very low (Hopkins and Rohatgi, 1986) and can be effectively removed from silicon by directional solidification. Hopkins and Rohatgi also showed that the degradation threshold in solar cells and the segregation co-

efficient for most impurity elements are correlated so that impurity elements with a low degradation threshold have low segregation coefficients. The most harmful elements are therefore also the ones that are most efficiently removed by directional solidification. Boron and phosphorus are however not efficiently removed through directional solidification and must be removed using other refining methods.

Boron distributes almost evenly between the solid and liquid phase with a segregation coefficient of approximately 0.8 and can therefore not be removed by solidification methods. Phosphorus is not efficiently removed by solidification methods either since it has a segregation coefficient of approximately 0.35. (Coefficients from Schei et al., 1998). Phosphorus can however be removed by vacuum refining due to the high vapour pressure of this element while boron has a low vapour pressure. A recent review by Delannoy (2012) summarizes the purification methods of silicon for solar cells in larger detail than this introductory chapter. The reviews by Lynch (2009) and Johnston et al. (2012) may also serve as complementary reading on this topic. Figure 1.3 gives an overview of the route from quartz to solar cell.

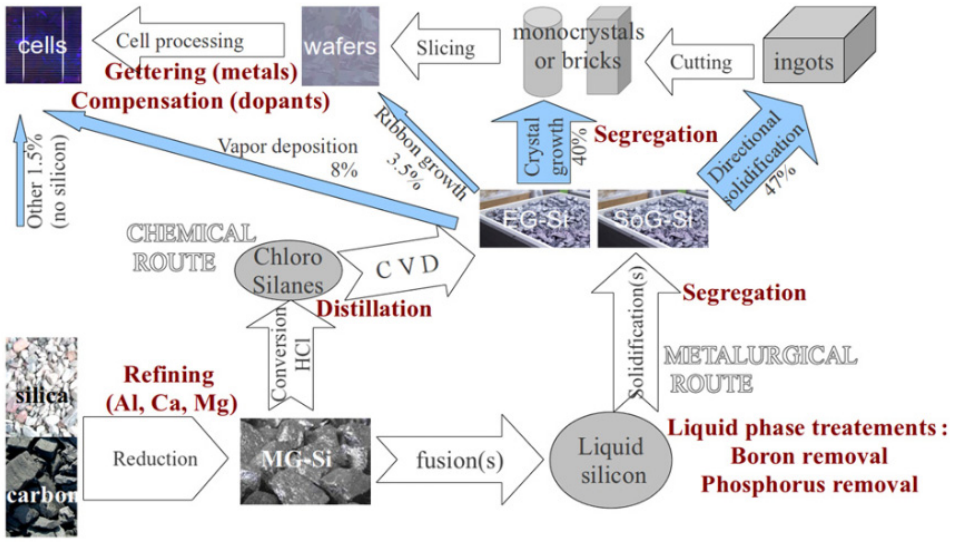

Figure 1.3: Silicon processing steps from raw material to solar cell (Delannoy, 2012).

Use of raw materials that does not contain any boron and phosphorus is one way to avoid the challenge of removing them at a later stage in the process. Enebakk et al. (2009) have shown that the maximum boron and phosphorus content in silicon for solar cells are 0.45 and 1.00 ppmw respectively. The levels of these elements are usually between 10 and 100 ppmw in metallurgical grade silicon. Boron or phosphorus have to be present as a dopant to make

the solar cell work and does therefore not need to be removed to ppbw-levels like most other impurities. Both can also be present at the same time but the ratio between them has to be accurately controlled.

Raw materials with boron and phosphorus at levels below 1 ppmw are very limited. It is therefore very hard to avoid higher levels of these elements in metallurgical grade silicon since most of the boron and phosphorus entering the furnace leaves with the silicon (Myrhaug and Tveit, 2000). Selecting raw materials with as low as possible levels of boron and phosphorus is crucial but less stringent requirements can be set if boron and phosphorus is removed from silicon by refining.

Slag refining was proposed as a possible method for removal of boron from silicon more than thirty years ago by Dietl and Wohlschläger (1981). Refining data and thermodynamic data are however still limited when it comes to slag refining for boron removal. It has also been shown that boron can be removed using hydrogen and water vapour as discovered by Theuerer (1956) but this work focuses primarily on removal of boron from silicon by slag refining.

Production of silicon with sufficient purity using metallurgical refining methods has already been demonstrated industrially by Elkem Solar. They use slag refining, acid leaching and directional solidification to bring the silicon to the purity level required for solar cells (Søiland et al., 2012). Their process sequence is shown in figure 1.4.

Figure 1.4: Process sequence for the refining method used by Elkem Solar (Hoffmann et al., 2008).

1.3 Thesis outline

The CaO-SiO_2, MgO-SiO_2, CaO-MgO-SiO_2 and CaO-Al_2O_3-SiO_2 slag systems were selected for this work. A temperature of 1600 °C was selected to achieve a large range of compositions in the liquid region of these slag systems. The equilibrium between iron and the binary CaO-SiO_2 slag system was also investigated with the aim of relating the data found with pure silicon to refining of ferrosilicon.

The next chapter of this thesis summarizes the most fundamental aspects of slag refining and its application to removal of boron from silicon. Several works has previously been conducted on slag refining for boron removal and a

critical review of these works are given in the first part of chapter 3. The chapter continues with a review of the distribution of other elements between slag and silicon relevant to this work. In the end of the chapter, thermodynamic activities relevant to the present work are reviewed. The following chapter, chapter 4, describes the experimental set-up and procedure. The procedure for sample preparation and chemical analyses are also described in detail. The last part of this chapter gives a detailed description of temperature measurement and control which is supported by temperature modelled in the furnace using COMSOL Multiphysics. Some details about the analyses are given in the end of this chapter.

The results are given in chapter 5 where all results for each slag system is given separately. The mass balance for some selected experiments is given in the end of the chapter to show the behaviour of the system during the experiments. The results are compared with previous works in chapter 6 and thermodynamic activity data for $BO_{1.5}$ and the major slag components are calculated in the CaO-SiO_2, MgO-SiO_2 and the ternary CaO-MgO-SiO_2 systems. Also the activity coefficients of calcium and magnesium at infinite dilution in silicon were determined. The activity coefficient of $BO_{1.5}$ and the activity coefficient of aluminium at infinite dilution in silicon were estimated in the CaO-Al_2O_3-SiO_2 system using thermodynamic activity data from FactSage. Activity data for boron and calcium in ferrosilicon were also determined. The mass transfer coefficient of boron for a binary CaO-SiO_2 slag was estimated using an equation for mass transfer based on the ratio of boron concentration in slag and silicon. The findings in the present work are summarized in the concluding chapter of this thesis.

Chapter 2

Fundamental aspects of slag refining for boron removal

The system investigated in this thesis is the chemical equilibrium between two immiscible liquids; one is a slag that consists of silicon dioxide and other selected metal oxides, and the other is liquid silicon containing different amounts of impurity elements. A slag can be used to remove unwanted impurity elements from silicon. Slag refining also has the potential to remove boron from silicon, but at present there is limited and scattered data on slag refining for boron removal from silicon.

A slag that does not contain any boron initially can remove boron from silicon even if it hardly absorbs boron. On the other hand it can also absorb boron from silicon even if it initially contains some boron if it has a high affinity for boron. Accurate data on the ability of a slag for absorption of boron is in any case necessary to evaluate the feasibility of the slag for purification of silicon.

The term *silicon* will from now on refer to a melt where mainly silicon is present in its elemental state. A melt where atoms in general are in their elemental state is from now on called *metal*. Silicon is a semiconductor when solid but has metallic conductivity when liquid and the term *silicon metal* is therefore often used in the smelting industry. This term will not be used here in order to avoid inconsistent terminology. All discussions that follow are regarding liquid slag and liquid silicon unless otherwise noted. The term *system* will therefore from now on refer to the combined system where liquid slag and metal is in physical contact with each other.

The main requirements for a slag are discussed next before the thermodynamics of boron removal is discussed. The kinetics of boron in the system is discussed in the last part of this chapter.

2.1 Slag requirements

Two main criteria have to be fulfilled for a metal oxide to be considered for slag refining. One is that the metal oxide has to be more stable than silicon dioxide and the other is that the metal oxide has to be fairly abundant. A metal oxide that is relatively rare and expensive can be ruled out due to the large quantities that would be needed for industrial scale refining. Toxic components are obviously not desirable for slag refining and neither are any volatile components. Another important criterion is that the liquidus temperature of a slag should not be significantly higher than the melting point of silicon which is 1414 °C (Haynes, 2012).

2.1.1 Physical requirements

Slags with a liquidus temperature up to 1600 °C are investigated in this work. A liquidus temperature of the slag within the desired range is relatively easily achieved by consideration of phase diagrams and selection of mixing ratios of components according to them. The viscosity must also to be considered. A very viscous slag will have a very low mass transfer rate for any impurities and have a very slow rate of demixing from silicon. A very viscous slag will therefore need vigorous stirring followed by a long settling time to have any refining efficiency and at the same time avoid too many inclusions.

A density difference between slag and silicon is also required, but it is a very narrow range of slag compositions that have the same density as silicon, and only a small change in slag composition is needed to avoid this potential problem. An industrial process will also have to be adjusted for a floating or sinking slag depending on the density of the slag. Finally the interfacial tension between slag and silicon has an important influence on the formation of liquid inclusions and the reaction kinetics, and will also have to be considered when evaluating a slag for industrial applications. The interfacial tension is however not considered in this work. Thermal and electrical conductivity are not considered in this work either, but will also have to be considered in an industrial process.

2.1.2 Thermodynamic requirements

A slag used for refining silicon will as previously mentioned contain silicon dioxide. It will in addition contain metal oxides that are more stable than silicon dioxide at refining temperature. Any metal oxides less stable than silicon dioxide will be reduced and absorbed into the molten silicon and thereby contaminate it. An Ellingham diagram with slag forming oxides relevant for this work is shown in figure 2.1. This diagram shows Gibbs energy of formation of oxides from elements as a function of temperature. The elements will distribute themselves between silicon and slag. Metal oxides that are much

more stable than silicon dioxide, will be heavily distributed towards the slag and only a small amount will be present in silicon at chemical equilibrium. As can be seen from figure 2.1, boron oxide is actually slightly less stable than silicon dioxide up to 1938 °C. This means that boron should not be oxidized into a slag if it behaves as an ideal solute in both slag and silicon. This is not the case and experiments have shown that boron has a somewhat higher affinity for slag than silicon when present as a dilute species. A review of these experiments is given in chapter 3. Calcium oxide is the most common metal oxide that is present together with silicon dioxide and they are usually mixed in almost equal amounts because of the relatively low liquidus temperature of this mixture, as can be seen in the phase diagram shown in figure 2.2.

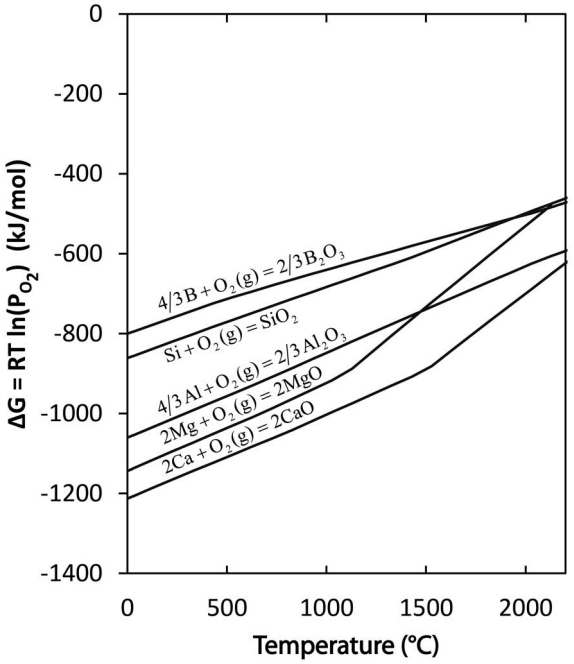

Figure 2.1: Ellingham diagram showing boron oxide, silicon dioxide and selected metal oxides that are more stable than silicon dioxide. Thermochemical data was taken from the NIST-JANAF Thermochemical tables (Chase, 1998)

2.2 Thermodynamics of boron removal

Boron is the element of primary concern in this work and it is present in silicon and slag in very low concentrations; typically in the mass range from 10 to 100 parts per million (ppm) in experimental works, industrial raw materials and metallurgical silicon. Such low concentrations mean that the activity of boron

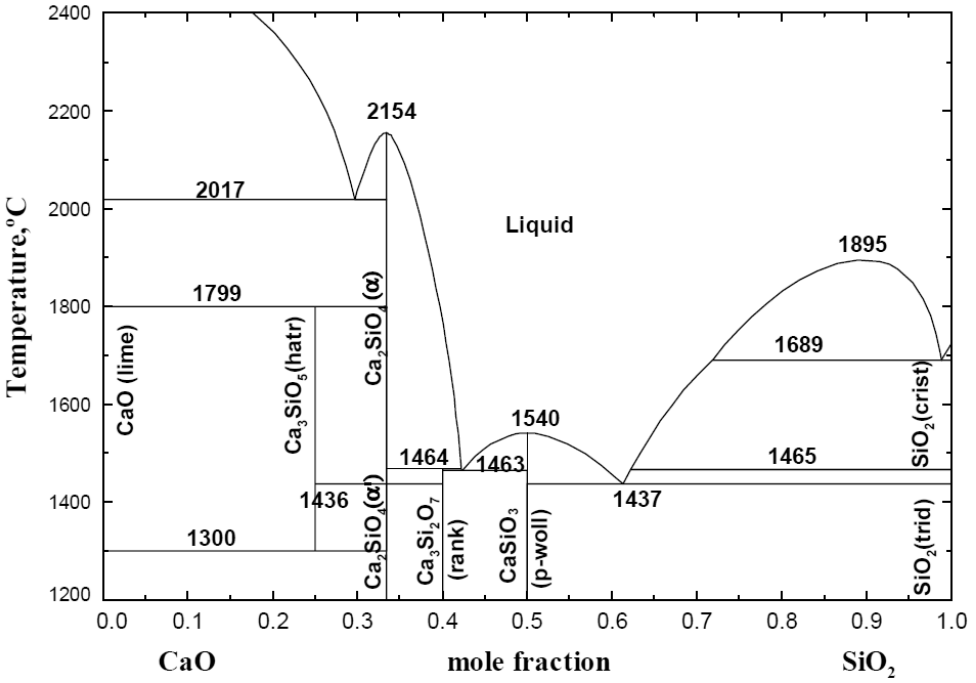

Figure 2.2: Phase diagram of the binary $CaO-SiO_2$ system from Jung et al. (2005). The lowest liquidus temperatures are in the area around equimolar mixture.

in both slag and metal is likely to change almost linearly with concentration of boron. This can be argued both from a statistical and mathematical point of view; statistically the activity of boron will increase linearly as long as the boron concentration is so low that boron atoms are surrounded only by the major components of the melt, and mathematically the quadratic and higher order terms of a Taylor expansion will be vanishing small when approaching infinite dilution. In other words we have a system where boron follows Henry's law. The activity of boron at and close to infinite dilution in slags is not known, but there are some works on the activity of boron in silicon.

Tanahashi et al. (1998) determined the self-interaction coefficient of boron in silicon by equilibrating silicon with boron nitride under controlled partial pressure of nitrogen, and found $\epsilon_{\mathrm{B}}^{\mathrm{B}}$ to be -164($\pm$8) at 1450 °C and -105($\pm$8) at 1500 °C. The interaction coefficient follows the relation $\epsilon = \alpha + \beta/T$ which with the results from Tanahashi and co-workers becomes:

$$\epsilon_{\mathrm{B}}^{\mathrm{B}} = 1928.14 - 3604760/T \tag{2.1}$$

The percent-wise change of the activity coefficient of boron is plotted as a function of boron content in silicon at 1450, 1500 and 1600 °C in figure 2.3. The self-interaction coefficient increases with increasing temperature and was

found to be 3.5 at 1600 °C by extrapolation using equation 2.1. Up to 100 ppmw of boron the activity coefficient does not change much as compared to the activity coefficient at infinite dilution. This is in accordance with the reasoning above. At 1600 °C the self-interaction coefficient becomes so close to zero that it hardly influences the activity coefficient within the range shown in figure 2.3.

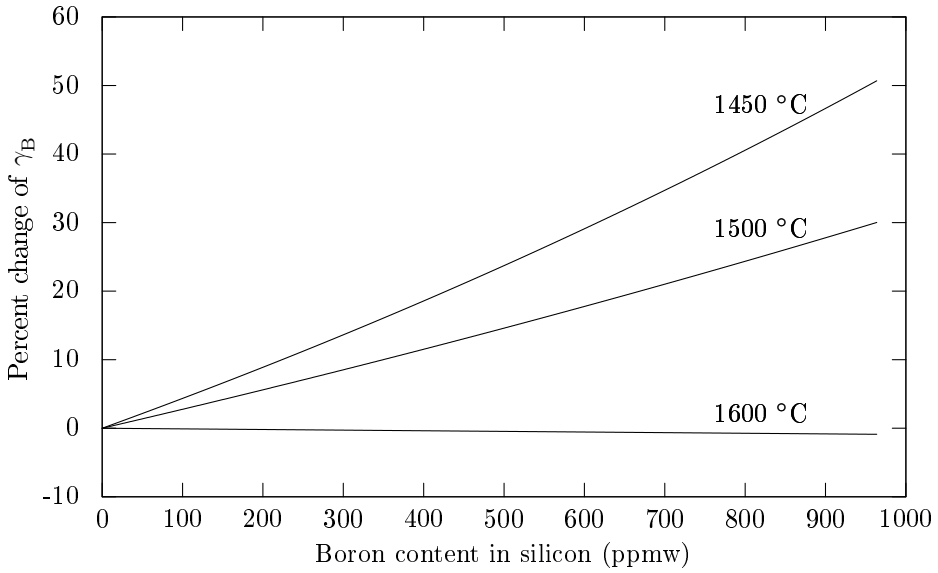

Figure 2.3: Percent-wise change of the activity coefficient of boron due to self-interaction from Tanahashi et al. (1998). The curve at 1600 °C is based on an extrapolation of their data (Equation 2.1).

The distribution of boron between slag and silicon has been shown to be constant up to 2500 ppm mass of boron in slag and 850 ppm mass of boron in silicon at 1550 °C in the binary calcium silicate system by Teixeira et al. (2009). A constant distribution indicates that the activity coefficient of boron in slag and silicon remains constant in this range. Constant activity coefficients may however not be the case if there is a very strong interaction of boron with any of the components present in the silicon - slag system. Such an interaction would lead boron to be heavily distributed towards one of the liquid phases or even towards a third phase. This would either solve the challenge of removing boron from silicon or in the opposite case make the compound useless for removing boron from silicon. No such strong interaction has so far been found with any components that have been tried for the silicon - slag system. It is therefore of more interest to start by investigating the boron distribution between slag and silicon with different slag compositions than to investigate the concentration dependence. A closer look at the concentration dependence would be appropriate if a slag with strong affinity for boron is discovered.

A closer look at the thermodynamics can explain the mechanisms behind the previously mentioned affinity that boron has for the slag phase. The redox reaction for oxidation of boron in terms of the molecular slag model is given by:

$$\mathrm{B}(l) + 3/4\mathrm{SiO_2}(s) = 1/2\mathrm{B_2O_3}(l) + 3/4\mathrm{Si}(l) \tag{2.2}$$

The equilibrium constant is given by:

$$K = \frac{a_{\mathrm{B_2O_3}}^{1/2} \cdot a_{\mathrm{Si}}^{3/4}}{a_{\mathrm{B}} \cdot a_{\mathrm{SiO_2}}^{3/4}} \tag{2.3}$$

From this equation it is seen that the equilibrium will be displaced towards the right if boron has a positive deviation from ideal behaviour in liquid silicon or a negative deviation from ideal behaviour in liquid slag. Either of these deviations will be beneficial for boron removal from silicon by slag refining.

It has previously been shown by Yoshikawa and Morita (2005) that boron has a positive deviation from ideal behaviour when present as a dilute species in silicon. They did an investigation where silicon was held together with a piece of boron nitride in a silicon nitride crucible under $\mathrm{N_2}$-10%$\mathrm{H_2}$ atmosphere and found the activity coefficient to be:

$$\ln \gamma_{\mathrm{B}}^{0} = 1.19(\pm 0.25) + \frac{289(\pm 450)}{T} \tag{2.4}$$

They also re-evaluated previous works and found a very good agreement with those, and based on that they set the validity range of the above expression to be from the melting point of silicon to 1850 °C. Within this temperature range the expression gives the activity coefficient to be virtually independent of temperature. This expression is considered to be the most accurate estimate for the activity coefficient that can be found in literature.

The activity of boron when present as a dilute species in slag is not well known. It is also seen that the equilibrium (2.2) should be displaced towards the left if the activity of silicon dioxide is reduced. This can however be counterbalanced by a positive interaction of boron oxide with other metal oxides that are added to the slag.

Silicon is so pure that it is expected to follow Raoult's law. The activity of silicon is hence equal to the molar fraction of silicon. Raoult's and Henry's law are related through the Gibbs-Duhem equation and silicon will therefore follow Raoult's law when an impurity element follows Henry's law (Gaskell, 2008).

2.2.1 The distribution coefficient of boron

The suitability of a slag for removal of boron from silicon is easiest expressed by the concentration difference between slag and silicon at chemical equilibrium.

The distribution coefficient of boron, L_{B}, is used to quantify this concentration difference and it is simply defined as the boron concentration in slag divided by the boron concentration in silicon at chemical equilibrium:

$$L_{\mathrm{B}} = \frac{(\%\mathrm{B})_{\mathrm{eq}}}{[\%\mathrm{B}]_{\mathrm{eq}}} \tag{2.5}$$

where $(\%\mathrm{B})_{\mathrm{eq}}$ and $[\%\mathrm{B}]_{\mathrm{eq}}$ is the boron concentration in slag and silicon at equilibrium.

The distribution coefficient can relatively easily be related to more fundamental thermodynamic properties of the system by using the equilibrium constant. We can start by using the relation

$$a_{\mathrm{B_2O_3}}^{1/2} = a_{\mathrm{BO_{1.5}}} \tag{2.6}$$

in equation 2.3 before expanding the activity of boron in slag and silicon into mole fractions and activity coefficients to get:

$$K = \frac{x_{\mathrm{BO_{1.5}}}\gamma_{\mathrm{BO_{1.5}}} \cdot a_{\mathrm{Si}}^{3/4}}{x_{\mathrm{B}}\gamma_{\mathrm{B}} \cdot a_{\mathrm{SiO_2}}^{3/4}} \tag{2.7}$$

The mole fraction of boron in silicon is given by:

$$\begin{aligned} x_{\mathrm{B}} &= \frac{n_{\mathrm{B}}}{n_{\mathrm{B}} + n_{\mathrm{Si}} + \sum n_{\mathrm{Me}}} \\ &= \frac{n_{\mathrm{B}}}{\frac{m_{\mathrm{B}}}{M_{\mathrm{B}}} + \frac{m_{\mathrm{Si}}}{M_{\mathrm{Si}}} + \sum \frac{m_{\mathrm{Me}}}{M_{\mathrm{Me}}}} \end{aligned} \tag{2.8}$$

where n_{Me} is the number of moles of other elements present in the liquid silicon. The mass percent of boron in silicon can in a similar way be expanded into moles and molar weight:

$$[\%\mathrm{B}] = \frac{m_{\mathrm{B}}}{m_{\mathrm{Tot}}} \cdot 100 = \frac{n_{\mathrm{B}} \cdot M_{\mathrm{B}}}{m_{\mathrm{Tot}}} \cdot 100 \tag{2.9}$$

where m_{B} is the mass of boron in the silicon phase and m_{Tot} is the total mass. By dividing equation 2.8 by equation 2.9 we get:

$$\begin{aligned} \frac{x_{\mathrm{B}}}{[\%\mathrm{B}]} &= \frac{n_{\mathrm{B}}}{\left(\frac{m_{\mathrm{B}}}{M_{\mathrm{B}}} + \frac{m_{\mathrm{Si}}}{M_{\mathrm{Si}}} + \sum \frac{m_{\mathrm{Me}}}{M_{\mathrm{Me}}}\right) \cdot \frac{1}{m_{\mathrm{Tot}}} \cdot n_{\mathrm{B}} \cdot M_{\mathrm{B}} \cdot 100} \\ \implies x_{\mathrm{B}} &= \frac{[\%\mathrm{B}]}{\left(\frac{[\%\mathrm{B}]}{M_{\mathrm{B}}} + \frac{[\%\mathrm{Si}]}{M_{\mathrm{Si}}} + \sum \frac{[\%\mathrm{Me}]}{M_{\mathrm{Me}}}\right) \cdot M_{\mathrm{B}}} \end{aligned} \tag{2.10}$$

This equation can be simplified since we have ppm-levels of boron in silicon.

$$x_{\mathrm{B}} = \frac{[\%\mathrm{B}]}{\left(\frac{[\%\mathrm{Si}]}{M_{\mathrm{Si}}} + \sum \frac{[\%\mathrm{Me}]}{M_{\mathrm{Me}}}\right) \cdot M_{\mathrm{B}}} \tag{2.11}$$

The mole fraction of boron oxide in the slag phase can be derived in a similar way. The mole fraction of boron in the slag is given by:

$$\begin{aligned} x_{\mathrm{BO}_{1.5}} &= \frac{n_{\mathrm{BO}_{1.5}}}{n_{\mathrm{BO}_{1.5}} + n_{\mathrm{SiO}_2} + \sum n_{\mathrm{MeO}_x}} \\ &= \frac{n_{\mathrm{BO}_{1.5}}}{\frac{m_{\mathrm{BO}_{1.5}}}{M_{\mathrm{BO}_{1.5}}} + \frac{m_{\mathrm{SiO}_2}}{M_{\mathrm{SiO}_2}} + \sum \frac{m_{\mathrm{MeO}_x}}{M_{\mathrm{MeO}_x}}} \end{aligned} \tag{2.12}$$

where n_{MeO_x} is the number of moles of other oxides in the slag. The mass percent of boron oxide in the slag is given by:

$$(\%\mathrm{BO}_{1.5}) = \frac{m_{\mathrm{BO}_{1.5}}}{m_{\mathrm{Tot}}} \cdot 100 = \frac{n_{\mathrm{BO}_{1.5}} \cdot M_{\mathrm{BO}_{1.5}}}{m_{\mathrm{Tot}}} \cdot 100 \tag{2.13}$$

By dividing equation 2.12 by equation 2.13 we get

$$\begin{aligned} \frac{x_{\mathrm{BO}_{1.5}}}{(\%\mathrm{BO}_{1.5})} &= \frac{n_{\mathrm{BO}_{1.5}}}{\left(\frac{m_{\mathrm{BO}_{1.5}}}{M_{\mathrm{BO}_{1.5}}} + \frac{m_{\mathrm{SiO}_2}}{M_{\mathrm{SiO}_2}} + \sum \frac{m_{\mathrm{MeO}_x}}{M_{\mathrm{MeO}_x}}\right) \cdot \frac{1}{m_{\mathrm{Tot}}} \cdot n_{\mathrm{BO}_{1.5}} \cdot M_{\mathrm{BO}_{1.5}} \cdot 100} \\ \implies x_{\mathrm{BO}_{1.5}} &= \frac{(\%\mathrm{BO}_{1.5})}{\left(\frac{(\%\mathrm{BO}_{1.5})}{M_{\mathrm{BO}_{1.5}}} + \frac{(\%\mathrm{SiO}_2)}{M_{\mathrm{SiO}_2}} + \sum \frac{(\%\mathrm{MeO}_x)}{M_{\mathrm{MeO}_x}}\right) \cdot M_{\mathrm{BO}_{1.5}}} \end{aligned} \tag{2.14}$$

The concentration of boron oxide in the slag is vanishing small compared to the concentration of the major slag forming oxides and can be ignored:

$$x_{\mathrm{BO}_{1.5}} = \frac{(\%\mathrm{BO}_{1.5})}{\left(\frac{(\%\mathrm{SiO}_2)}{M_{\mathrm{SiO}_2}} + \sum \frac{(\%\mathrm{MeO}_x)}{M_{\mathrm{MeO}_x}}\right) \cdot M_{\mathrm{BO}_{1.5}}} \tag{2.15}$$

In the slag phase we have that $x_{\mathrm{BO}_{1.5}} = x_{\mathrm{B}}$ and can insert equation 2.11 and equation 2.15 into equation 2.3 to get:

$$K = \frac{(\%\mathrm{BO}_{1.5}) \cdot \gamma_{\mathrm{BO}_{1.5}} \cdot a_{\mathrm{Si}}^{3/4} \cdot \left(\frac{[\%\mathrm{Si}]}{M_{\mathrm{Si}}} + \sum \frac{[\%\mathrm{Me}]}{M_{\mathrm{Me}}}\right) \cdot M_{\mathrm{B}}}{[\%\mathrm{B}] \cdot \gamma_{\mathrm{B}} \cdot a_{\mathrm{SiO}_2}^{3/4} \cdot \left(\frac{(\%\mathrm{SiO}_2)}{M_{\mathrm{SiO}_2}} + \sum \frac{(\%\mathrm{MeO}_x)}{M_{\mathrm{MeO}_x}}\right) \cdot M_{\mathrm{BO}_{1.5}}} \tag{2.16}$$

We also have that

$$(\%\mathrm{B}) = \frac{(\%\mathrm{BO}_{1.5}) \cdot M_{\mathrm{B}}}{M_{\mathrm{BO}_{1.5}}} \tag{2.17}$$

and we get

$$K = \frac{(\%\mathrm{B}) \cdot \gamma_{\mathrm{BO}_{1.5}} \cdot a_{\mathrm{Si}}^{3/4} \cdot \left(\frac{[\%\mathrm{Si}]}{M_{\mathrm{Si}}} + \sum \frac{[\%\mathrm{Me}]}{M_{\mathrm{Me}}}\right)}{[\%\mathrm{B}] \cdot \gamma_{\mathrm{B}} \cdot a_{\mathrm{SiO}_2}^{3/4} \cdot \left(\frac{(\%\mathrm{SiO}_2)}{M_{\mathrm{SiO}_2}} + \sum \frac{(\%\mathrm{MeO}_x)}{M_{\mathrm{MeO}_x}}\right)} \tag{2.18}$$

To simplify we can collect for the terms introduced when going from mole fraction to mass-%.

$$k_{x \to \%} = \frac{\frac{[\%\mathrm{Si}]}{M_{\mathrm{Si}}} + \sum \frac{[\%\mathrm{Me}]}{M_{\mathrm{Me}}}}{\frac{(\%\mathrm{SiO}_2)}{M_{\mathrm{SiO}_2}} + \sum \frac{(\%\mathrm{MeO}_x)}{M_{\mathrm{MeO}_x}}} \tag{2.19}$$

this coefficient can also be expressed in terms of mole fractions. We can generalize by including Si and SiO_2 into the sums and observing that

$$\sum \frac{[\%\mathrm{Me}]}{M_{\mathrm{Me}}} = 100 \sum \frac{x_{\mathrm{Me}}}{\sum x_{\mathrm{Me}} M_{\mathrm{Me}}} = \frac{100}{\sum x_{\mathrm{Me}} M_{\mathrm{Me}}} \tag{2.20}$$

The same is valid for the metal oxide sum and we get

$$k_{x\to\%} = \frac{x_{\mathrm{SiO_2}} M_{\mathrm{SiO_2}} + \sum x_{\mathrm{MeO}_x} M_{\mathrm{MeO}_x}}{x_{\mathrm{Si}} M_{\mathrm{Si}} + \sum x_{\mathrm{Me}} M_{\mathrm{Me}}} \tag{2.21}$$

after taking Si and SiO_2 out of the sums again. At chemical equilibrium we then have:

$$L_{\mathrm{B}} = \frac{K \cdot \gamma_{\mathrm{B}} \cdot a_{\mathrm{SiO_2}}^{3/4}}{k_{x\to\%} \cdot \gamma_{\mathrm{BO_{1.5}}} \cdot a_{\mathrm{Si}}^{3/4}} \tag{2.22}$$

The activity coefficient of boron oxide at infinite dilution in slags is mostly unknown and it is therefore not possible to calculate the distribution coefficient of boron using this equation. It is on the other hand possible to calculate the activity coefficient of boron oxide in the slag from L_{B} if both the activity coefficient of boron in silicon and the activity of silicon dioxide are known. A theoretical estimation of the distribution coefficient would also be possible if the activity coefficient of boron in slag could be calculated, but no one has so far managed to do a prediction that corresponds well with experimental data. Limited experimental data also makes it hard to assess the accuracy of theoretical calculations. It is therefore a need for more experimental data on the distribution coefficient of boron in order to understand the behaviour of boron in this system better.

2.2.2 Basicity, slag structure and the borate anion

It is seen from equation 2.22 that a reduced activity of silicon dioxide should decrease the distribution coefficient of boron. From earlier work it has been found that boron still has an affinity for slag despite the reduction of the activity of silicon dioxide with addition of other more reducing metal oxides to the slag (see chapter 3). This means that other reactions than the oxidation of boron plays a role for absorption into the slag. A closer look at the nature of slags can help explaining this.

Basicity is commonly used to express trends in properties of slags and it is dependent on the amount of acidic and basic oxides. The basicity of oxides can be grouped depending on which elements in the periodic table they are formed from. All metal oxides in group 1 and 2 in the periodic table except beryllium oxide are basic oxides. Acidic oxides are found among the metalloids, nonmetals and transition metal oxides in high oxidation states. Both boron oxide and silicon dioxide are acidic oxides. Transition metal oxides

can be acidic, amphoteric or basic. The oxide will be more acidic the higher the oxidation number of the transition metal is.

Pure silicon dioxide does not dissociate when it melts and the silicon atoms have four oxygen atoms shared with its neighbouring silicon atoms making up a fully polymerized three-dimensional network. B_2O_3 will not dissociate in pure silicon dioxide and will therefore be present together with pure silicon dioxide as a part of the silicate network. The polymerized structure is typical for acidic oxides. Basic oxides on the other hand dissociates as ions in a slag. Calcium oxide is basic and dissociates as Ca^{2+} and O^{2-} while acidic oxides tends to bind with oxygen anions. Boron oxide can therefore react with the oxygen anions that come from calcium oxide and be stabilized as BO_3^{3-} (borate) in the slag phase. This may compensate for the reduced partial pressure of oxygen in the slag caused by addition of calcium oxide. The ionic nature of the slag can in other words be used to better explain the incorporation of boron oxide into the slag. The oxidation and ionization reaction of boron in a calcium silicate slag is given by:

$$B + 3/4SiO_2 + 3/2CaO = BO_3^{3-} + 3/4Si + 3/2Ca^{2+} \tag{2.23}$$

It is therefore seen that both increased activity of silicon dioxide and an increased concentration of oxygen anions (in the form of CaO in this case) can shift the equilibrium of boron towards the slag phase. This representation of the ionic properties of the slag is however very simplified even though it better explains the behaviour of the slag than a pure molecular model. In a real slag boron may also be incorporated into the slag as different structural units than BO_3^{3-}.

2.2.3 Oxygen partial pressure and borate capacity

The oxygen partial pressure is fixed if the slag composition does not change with time provided that an element is a major component of both the slag and the metal. This is the case in the system with silicon and a calcium silicate slag. To demonstrate that the partial pressure of oxygen is indeed fixed in this system one can discuss what happens at 1600 °C when the partial pressure is increased and reduced respectively.

Silicon will be oxidized if the oxygen partial pressure is increased above the equilibrium partial pressure and the slag composition will be enriched with silicon dioxide until the slag and silicon is in equilibrium at the elevated oxygen partial pressure. All silicon may be oxidized before this happens if there are large amounts of slag compared to silicon. An increase of the oxygen partial pressure above the partial pressure of the equilibrium between pure liquid silicon and silicon dioxide will cause all the silicon to be oxidized in any case.

A reduction of the oxygen partial pressure will on the other hand reduce silicon dioxide to elemental silicon, and the slag will be depleted for silicon

dioxide until slag and silicon is in equilibrium with the reduced oxygen partial pressure. Silicon dioxide will be reduced until pure solid dicalcium silicate remains if the oxygen partial pressure is so low that equilibrium is not reached when the slag composition is at the liquidus line.

The partial pressure of oxygen is therefore defined by the system itself and not the surrounding atmosphere as long as no dramatic change in slag composition is seen. It is therefore possible to remove silicon and calcium from equation 2.23 and instead use an equilibrium in terms of oxygen partial pressure and oxygen anions:

$$\mathrm{B} + 3/4\mathrm{O}_2 + 3/2\mathrm{O}^{2-} = \mathrm{BO}_3^{3-} \tag{2.24}$$

where the oxygen partial pressure is given by the activity of silicon dioxide.

It is however hard to use this equation or equation 2.23 to calculate the equilibrium distribution of boron between slag and silicon because of lack of thermodynamic data; the equilibrium constant is not known, the activity of the oxygen anions is not known and the activity of BO_3^{3-} is not known. A borate capacity can be introduced using equation 2.24 and is given by

$$\mathrm{C}_{\mathrm{BO}_3^{3-}} = \frac{(\%\mathrm{BO}_3^{3-})}{a_{\mathrm{B}} \cdot p_{\mathrm{O}_2}^{3/4}} = \frac{K \cdot a_{\mathrm{O}^{2-}}}{\gamma_{\mathrm{BO}_3^{3-}}} \tag{2.25}$$

The borate capacity is a measure of the boron absorption capacity of the slag and is defined in this way because it becomes a function independent of oxygen partial pressure of the system and the activity of boron in the metal. It can therefore be used to predict the distribution of boron between the same slag and another metal under the same or a different oxygen partial pressure. The borate capacity also reveals the ability for a slag to absorb boron besides its oxidizing power.

2.3 Kinetics of boron removal

With limited data on the distribution coefficient of boron it follows that there is also limited data on the time necessary to reach chemical equilibrium. In fact almost no data exists on how long it takes before this chemical equilibrium is reached and it is therefore also necessary to investigate the kinetics of the system.

2.3.1 Transport theory

Boron will be transported from silicon to slag if we assume the initial boron concentration in slag to be lower than in silicon, and at the same time the boron concentration in slag to be higher than in silicon at equilibrium. These conditions are illustrated in figure 2.4. The transport of an impurity element

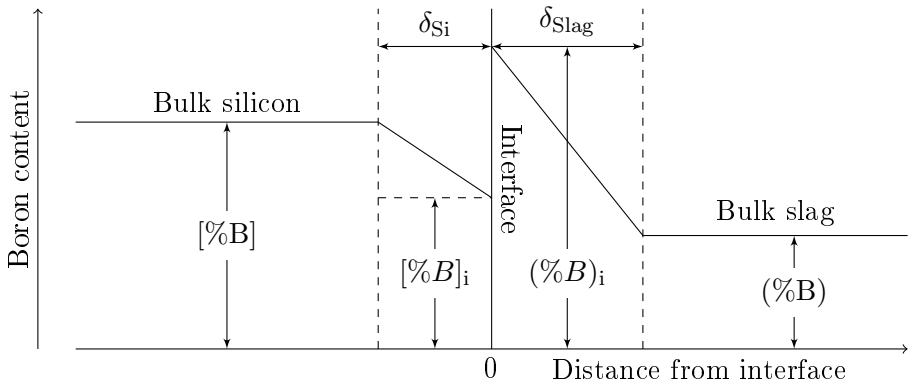

Figure 2.4: Concentration profile of boron in the silicon - slag system where boron will be transferred from silicon to slag. δ_{Si} and δ_{Slag} are the boundary layers at the silicon and slag side of the interface.

from silicon to slag has been investigated before for slag refining in a ladle by Engh et al. (1992). The same transport process can be applied for slag refining experiments in a crucible and it goes in five steps:

1. Transport of boron from bulk silicon to the silicon boundary layer.
2. Diffusion of boron through the silicon boundary layer.
3. Oxidation of boron at the silicon/slag interface.
4. Diffusion of oxidized boron through the slag boundary layer
5. Transport of oxidized from the slag boundary layer to bulk slag

The transport process has symmetrical characteristics across the slag-silicon interface and the nature of the transport is therefore similar at each side of the interface. Boron is first transported from bulk silicon to the silicon boundary layer at the interface. This transport can happen both by convection and diffusion. Forced convection is not applied in this work and two mechanisms that can cause convection remain; thermal gradients can give rise to natural convection and concentration gradients of major components can cause concentration driven convection. These types of convection may not be sufficient to completely mix the bulk silicon phase and concentration gradients of boron can therefore be present here until equilibrium is reached. Transport of boron from the slag boundary layer to the bulk slag is similar, but with a different magnitude of diffusion and convection because of different physical properties than silicon. Concentration gradients in bulk slag may also be present in the same way as in silicon before equilibrium is reached. One important practical consequence of inhomogeneous slag and silicon is that sampling has to be done properly before equilibrium is reached if bulk composition is to be determined.

Boron will be transported by diffusion through the silicon boundary layer where the driving force is the concentration gradient between bulk silicon and the interface. Oxidized boron will diffuse in the same way from the interface through the slag boundary layer. Diffusivity and thickness of the boundary layer will however be different from the silicon side to the slag side of the boundary layer. The oxidation reaction at the interface is due to high temperature expected to be so rapid that it has no influence on the transport of boron.

2.3.2 Previous experimental work

Nishimoto et al. (2012) recently investigated the mass transfer of boron between silicon and a slag with initial composition 55% CaO and 45% SiO_2 at 1550 °C and found the equilibrium time to be approximately 2 hours as can be seen in figure 2.5. They were also able to determine that the mass transfer was controlled by the slag phase. Their work proved at the same time that the mass transfer is not controlled by the reaction at the slag/silicon interface.

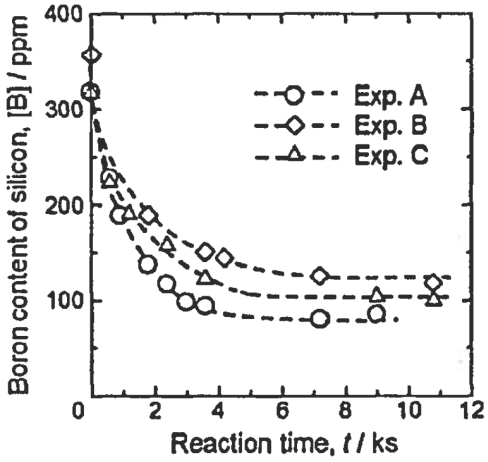

Figure 2.5: Change of boron concentration in silicon in reaction with a 55% CaO - 45% SiO_2 slag at 1550 °C. Exp. A, B and C contained silicon and slag in ratios 1.6g:4.0g, 3.0g:4.0g and 3.2g:4.0g respectively. Figure reprinted from Nishimoto et al. (2012).

Krystad et al. (2012) did a similar study as Nishimoto et al. (2012) where they investigated the mass transfer of boron from silicon to CaO-SiO_2, MgO-SiO_2 and CaO-MgO-SiO_2 slags. They used slag and silicon in a 1:1 or 1:2 ratio with a total mass of 30 grams at 1600 or 1650 °C and did also find the equilibrium time to be approximately two hours, as can be seen in figure 2.6.

Both Krystad et al. (2012) and Nishimoto et al. (2012) used a mass transfer model where the bulk phases are assumed to be completely mixed. No

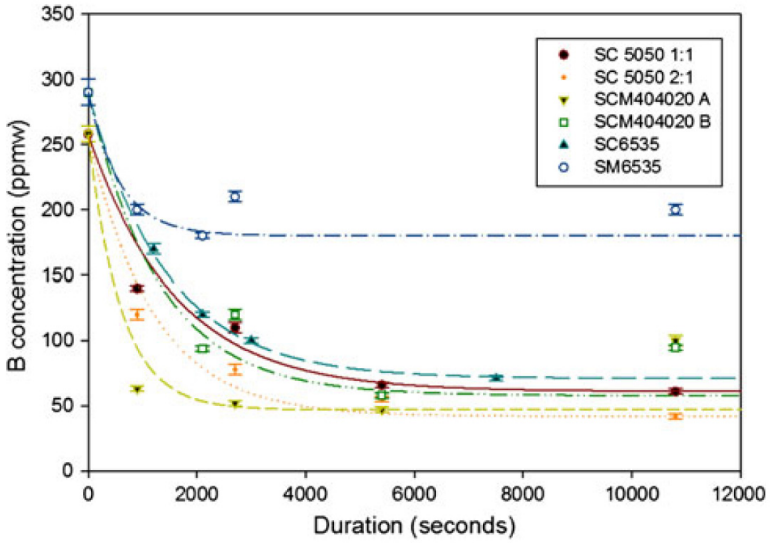

Figure 2.6: Change of boron concentration in silicon in reaction with CaO-SiO_2 (SC), MgO-SiO_2 (SM) and CaO-MgO-SiO_2 (SCM) slags from Krystad et al. (2012).

forced convection was employed during their experiments and the assumption of complete mixing of the bulk phases may therefore not be true. Still both studies show that the system behaves in accordance with this model and indicates that the model is a good approximation of the behaviour of this system. An introduction of average concentration for bulk slag and silicon in the transport equations may reflect reality better. The transport equations will still hold as a good approximation as long as the boundary layers are the main transport barriers. The overall mass transport equation for boron will then be:

$$\frac{[\overline{\%\mathrm{B}}] - [\%\mathrm{B}]_{\mathrm{eq}}}{[\%\mathrm{B}]_{\mathrm{in}} - [\%\mathrm{B}]_{\mathrm{eq}}} = \exp\left(-\frac{k_{\mathrm{t}}\rho A_{\mathrm{s}} t}{M}\left(1 + \frac{M}{M_{\mathrm{s}} L_{\mathrm{B}}}\right)\right) \tag{2.26}$$

where $[\overline{\%\mathrm{B}}]$ is the average concentration of boron in silicon at the time t. The rest of the transport equation is unchanged where $[\%\mathrm{B}]_{\mathrm{in}}$ is the initial boron concentration in silicon, $[\%\mathrm{B}]_{\mathrm{eq}}$ is the boron concentration in silicon at chemical equilibrium, k_{t} is the total mass transfer coefficient, ρ is the density of silicon, A_{s} is the slag/silicon interface area, M is the total mass of silicon, M_{s} is the total mass of slag, and L_{B} is the distribution coefficient of boron. The derivation of this equation can be found in the book by Engh et al. (1992).

The slag composition in the experiments by Nishimoto et al. (2012) are in the calcium rich liquid region of the binary calcium silicate slag system. The viscosity of a binary calcium silicate slag decreases with increasing calcium content as can be seen in figure 2.7. We have the diffusivity, D, as a function

of viscosity from Stokes-Einstein equation:

$$D = \frac{k_B T}{6\pi\eta r} \tag{2.27}$$

where k_B is Boltzmann's constant, T is temperature, η is viscosity and r is the radius of a diffusing spherical particle. We do not have diffusion of a spherical particle in the slag-silicon system and this equation is therefore not exact. The equation is in any case indicating the general relation between diffusivity and viscosity in liquids. Increasing viscosity gives lower diffusivity and the mass transfer of boron in a binary calcium silicate slag should therefore become lower with increasing silicon dioxide content in the slag. Boron transfer in a more silica rich slag than the one they investigated will therefore also be rate limited by mass transfer in the slag.

Krystad et al. (2012) found the mass transfer to be slower with a calcium oxide rich than with a silicon dioxide rich slag. They did however hold the silica rich slag at 1650 °C while the calcium oxide rich slag was held at 1600 °C and the viscosity decreases significantly with increasing temperature as can be seen in figure 2.7. This increases the diffusivity and convection which in turn increases the mass transfer. The results by Krystad et al. do hence indicate that a 50 °C change of temperature can influence mass transfer more than slag composition.

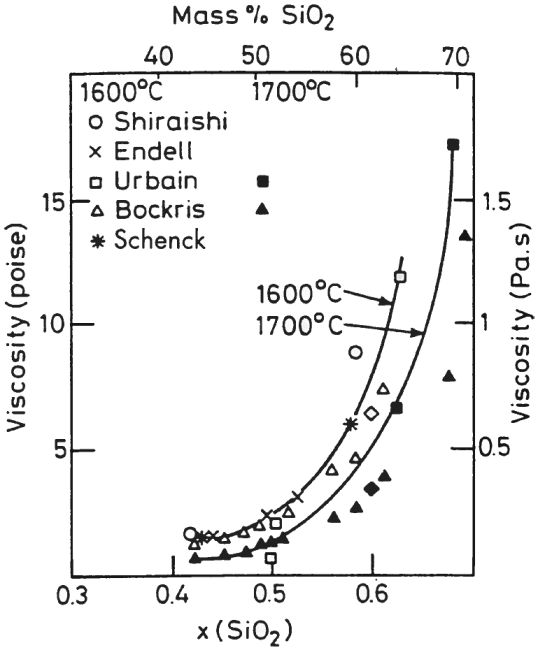

Figure 2.7: Viscosity of a binary calcium silicate slag as a function of silica content from the Slag Atlas (1995).

Chapter 3

Distribution equilibria and thermodynamic activities - A literature review

The distribution coefficient of boron is given by

$$L_{\mathrm{B}} = \frac{(\%\mathrm{B})_{\mathrm{eq}}}{[\%\mathrm{B}]_{\mathrm{eq}}} \tag{3.1}$$

where $(\%\mathrm{B})_{\mathrm{eq}}$ and $[\%\mathrm{B}]_{\mathrm{eq}}$ is the boron concentration in slag and silicon at equilibrium. The activity coefficient of boron oxide at infinite dilution in slags is, as discussed in chapter 2, the main unknown thermodynamic property needed for estimation of the distribution coefficient of boron. There is no known way to directly measure this activity coefficient and several studies have therefore been conducted to determine the distribution coefficient directly. The distribution coefficient can then be used to calculate the activity coefficient of boron at infinite dilution in slag.

The activity of boron at infinite dilution in silicon is needed for this estimate. This coefficient has already been discussed in chapter 2.2. The activity of SiO_2 must also be known since the equilibrium is given by

$$\mathrm{B}(l) + 3/4\mathrm{SiO_2}(s) = 3/4\mathrm{Si}(l) + 1/2\mathrm{B_2O_3}(l) \tag{3.2}$$

The activity of a slag forming element at infinite dilution in silicon can be used together with the equilibrium concentration of the same element in silicon to determine the activity of the respective oxide in the slag. Reversely the activity of a metal oxide in the slag can be used together with the equilibrium concentration of the respective element in silicon to determine the activity coefficient of the same element in silicon.

The distribution of boron, calcium, magnesium and aluminium between slag and silicon are discussed first in this chapter before the thermodynamic

activities of calcium, magnesium and aluminium at infinite dilution in silicon. The activities of CaO, MgO, Al_2O_3 and SiO_2 in slags are discussed in the last part of this chapter.

3.1 Distribution of boron between silicon and slags

The use of a slag for removing boron from silicon was first mentioned in a patent by Dietl and Wohlschläger (1981). The first work investigating the distribution coefficient of boron was done by Suzuki et al. (1990). Several works for different slag systems has been published since then, and it is getting to a point where an assessment of the accuracy of published values of the distribution coefficient of boron is getting more important. A critical review of present data for the distribution coefficient of boron for is given here where the slag systems that have been previously investigated are:

Binary slag systems
CaO-SiO_2 and Na_2O-SiO_2

Ternary slag systems
CaO-SiO_2-CaF_2, CaO-MgO-SiO_2, CaO-Al_2O_3-SiO_2, CaO-Na_2O-SiO_2, CaO-BaO-SiO_2, BaO-Al_2O_3-SiO_2, CaO-Li_2O-SiO_2 and CaO-SiO_2-LiF

Quaternary slag systems
CaO-MgO-Al_2O_3-SiO_2, CaO-MgO-SiO_2-CaF_2 and CaO-BaO-SiO_2-CaF_2

The experimental conditions for all works on the distribution coefficient of boron are summarized in table 3.1. The choice of crucible material will have a big influence the slag composition and is the most important factor for the behaviour of the system. All slags investigated in the current and previous works contain silicon dioxide. SiO_2 will react with carbon and form SiO and CO gas when slags containing silicon dioxide is held in a graphite crucible and the silicon dioxide content in the slag decrease slowly throughout the experiment. If an oxide is chosen as crucible material the slag will become enriched with that oxide until it becomes saturated at a liquidus line.

3.1.1 The binary CaO-SiO_2 system

The distribution coefficient of boron in the binary CaO-SiO_2 slag system has been investigated in more studies than any other slag system. Five separate works have been published until now and the most important details for each of these are discussed below and the results are summarized in figure 3.1. The system has been investigated using both graphite and quartz crucibles. The slag will become silica-saturated when it is held in a quartz crucible and the slag composition will rapidly settle at the liquidus line for the respective holding temperature. The distribution coefficient of boron is shown as a function of CaO/SiO_2 mass ratio in figure 3.1.

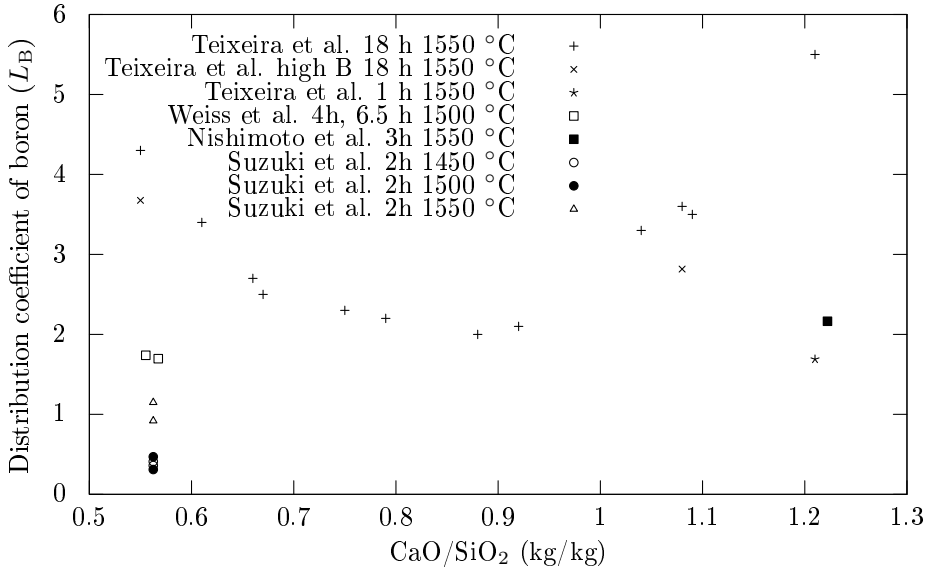

Figure 3.1: Distribution coefficient of boron for binary calcium-silicate slags.

Suzuki et al. (1990) were the first ones to investigate the distribution coefficient of boron between silicon and a binary calcium-silicate slag. They found the distribution coefficient of boron to be around one for a slag held in a graphite crucible at 1550 °C, and approximately 0.5 at 1450 and 1500 °C. They used both pure argon and argon with 12.5% CO_2, and found no difference for the distribution coefficient when using CO_2. The holding time was 2 hours and they used 10 grams of 6N pure silicon doped with 80 ppm-mass boron and 10 grams of slag with 36% CaO and 64% SiO_2 made from reagent grade chemicals.

Weiss and Schwerdtfeger (1994) did two experiments with a silica-saturated CaO-SiO_2 slag where they started with pure electronic grade silicon and 3% B_2O_3 in the slag phase. Their slags were also made from reagent grade chemicals. Silica-saturation was attained using quartz crucibles and they used 2 grams silicon and 5 grams slag. After holding the system at 1500 °C under argon atmosphere for 4 and 6.5 hours they found the distribution coefficient to be 1.74 and 1.70 respectively. These values are practically the same, indicating that their system may have reached equilibrium after 4 hours.

Teixeira and Morita (2009) were the first ones to investigate the distribution coefficient for several slag compositions in the binary calcium-silicate slag system, where they started with semiconductor grade silicon doped with 150 ppm-mass boron and slags made from reagent grade chemicals. An equilibrium time of 18 hours at 1550 °C was used. The system was held in graphite crucibles under argon atmosphere and they used 3 grams of silicon and 6.7 grams of slag. They found an u-shaped trend for the distribution coefficient

of boron as a function of CaO/SiO_2 mass ratio, where the lowest values were around 2 and the highest value was 5.5 for $CaO/SiO_2 = 1.21$. Teixeira and co-workers also investigated the influence of increasing boron concentration on the distribution coefficient and found no influence of increasing concentration within the range that they investigated. The highest concentration they investigated was 0.25 mass % boron in slag and 0.084 mass % boron in silicon. One value of the distribution coefficient for a holding time of one hour was also given. This value is significantly lower than the values for the same composition at 18 hours holding time.

Luo et al. (2011) did one experiment with a binary calcium-silicate slag with mass ratio of 1.21 and found the distribution coefficient to be 2.2. They used induction melting under argon atmosphere and had a holding time of one hour at 1500 °C in a silica crucible. The silicon initially contained 15 ppm boron and they used 3 kg silicon and 0.3 kg slag, both of unstated purity. The use of a silica crucible means that the slag composition has changed towards silica saturation, but they have not given the slag composition as measured after their experiments. Their value is therefore not included in figure 3.1.

Ding et al. (2012) have published one value of the distribution coefficient for a binary calcium silicate slag with a mass ratio of 0.82. Their experiments were performed at 1550 °C under argon atmosphere in an induction furnace with unknown holding time where they started with metallurgical grade silicon containing 22 ppm-mass boron. They used 70 grams of slag with unstated purity and an unstated amount of silicon and found the distribution coefficient to be 1.02. One difference to be noted between this study and the others is that they used an optical pyrometer instead of a thermocouple to control the temperature. Their apparatus also shows that the argon gas was bubbled through water before entering the furnace, adding moisture to the gas. Moisture may cause boron to evaporate as hydrogen boron oxide (Nordstrand and Tangstad, 2012) and cause the system to be a non-equilibrium system. This value is therefore not included in figure 3.1 either.

Nishimoto et al. (2012) found one value for the distribution coefficient of boron at 1550 °C under argon atmosphere. They used a graphite crucible and a holding time of 3 hours which is one hour longer than the equilibrium time they found. The CaO/SiO_2 mass ratio was 1.22 and they found the distribution coefficient to be 2.16.

Most experiments have been conducted with just a few grams of material under argon atmosphere using silicon doped with ppm-levels of boron. In addition most experiments have either been held at 1500 or 1550 °C. The work by Weiss and Schwerdtfeger (1994) differs from the others by having 3% boron oxide in the starting slag, but their results are still within the range of other published values. The work by Ding et al. (2012) and Luo et al. (2011) differs from the others by use of induction melting which may have agitated the melt and caused the system to reach equilibrium faster. Holding time

Table 3.1: Main parameters for experiments.

	Temperature °C	Holding time (h)	Atmosphere	Silicon mass	Slag mass
Suzuki et al.	1450 - 1550	2	Argon, CO_2, CO	10 g	10 g
Weiss et al.	1500	4, 6.5	Argon	2 g	5 g
Teixeira et al.	1550	1, 18	Argon	3 g	6.7 g
Nishimoto et al.	1550	3	Argon	Unknown	Unknown
Luo et al.	1500	1	Argon	3 kg	0.3 kg
Ding et al.	1550	Unknown	Argon	Unknown	70 g
Fujiwara et al.	1600	Unknown	Argon	2-3.5 g	4-6 g
Tanahashi et al.	1450-1500	2-12	Argon	10 g	5 g
Johnston et al.	1500	2	Argon	5.5 g	7.5 g
Cai et al.	1500-1700	1	Argon	Unknown	Unknown
White et al.	1600	48	Argon, CO, N_2	3 g	10 g
Zhang et al.	1500	1	Argon	667 g	333 g

	Crucible	Initial B in Si	Initial B in slag	Heating	Final slag composition
Suzuki et al.	Graphite	80 ppmw	Unknown	Restitive	Not measured
Weiss et al.	Quartz	0	3 wt%	Restitive	Measured
Teixeira et al.	Graphite	150 ppmw	Unknown	Restitive	Measured
Nishimoto et al.	Graphite	500 ppmw	0	Resistive	Not measured
Luo et al.	Quartz	15 ppmw	Unknown	Inductve	Not measured
Ding et al.	Graphite	Unknown	Unknown	Inductive	Not measured
Fujiwara et al.	Alumina	0	$<$ 2 wt%	Inductive	Measured
Tanahashi et al.	Quartz	0.3-1 wt%	Unknown	Restitive	Measured
Johnston et al.	Alumina, MgO	0.19-0.26 wt%	Unknown	Resistive	Measured
Cai et al.	Graphite	Unknown	Unknown	Inductive	Not measured
White et al.	Graphite	0	Unknown	Restitive	Measured
Zhang et al.	Graphite	Unknown	Unknown	Restitive	Not measured

is the parameter that differs the most between the different works, ranging from 1 to 18 hours, and only Nishimoto et al. (2012) give an experimental justification for their work to reach equilibrium within the chosen time.

The published values of the distribution coefficient of boron are in the range from 0.3 to 5.5. Significant scatter between the values can be seen from figure 3.1. Some of the differences may be explained by a consideration of the parameters used in the experiments. Starting with boron in silicon and using a too short equilibrium time will give a too low distribution coefficient, which in particular may be the case for the work by Suzuki and co-workers. A slag with a composition like the one they used is almost saturated with silica and very viscous compared to the slags with an equilibrium time of 2 hours in the work by Nishimoto et al. (2012). The holding time is therefore probably too short to reach equilibrium and the measured distribution coefficient of boron is likely to be lower than the equilibrium value. Only in the studies by Weiss and Schwerdtfeger (1994) and Teixeira and Morita (2009) are the slag compositions determined after the experiments. The slag compositions given in the studies by Suzuki et al. (1990) and Ding et al. (2012) have probably changed towards a more calcium rich slag due to formation of SiO gas in reaction with graphite through the reaction:

$$\mathrm{SiO_2}(l) + \mathrm{C}(s) = \mathrm{SiO}(g) + \mathrm{CO}(g) \tag{3.3}$$

There is no evident explanation for the discrepancy between the work by Weiss and Schwerdtfeger (1994) and the work by Teixeira and Morita (2009) for the most silica rich compositions. The distribution coefficient of boron should have been higher than the equilibrium value in the work by Weiss et al. if the system had not reached equilibrium. The high concentration of boron oxide in the slag phase of 1.22 to 1.25 mass% in the work by Weiss and Schwerdtfeger may however have led to boron not to act completely as a dilute species in the system. The value of the distribution coefficient found by Luo et al. (2011) is in the mid-range of the values found by others. The value that Ding and co-workers obtained is somewhat lower than the values found by Teixeira et al., but the potential non-equilibrium state of their system may be the cause of the lower value.

3.1.2 The CaO-SiO_2-CaF_2 system

Suzuki et al. (1990) investigated the CaO-30%CaF_2-SiO_2 system at 1450 °C under CO atmosphere. Also here they held ten grams silicon and ten grams slag for 2 hours in graphite crucibles. They found that the distribution coefficient of boron increased with increasing CaO/SiO_2 ratio to a peak value of approximately 1.7 at a CaO/SiO_2 mass ratio around 2.2. From there they found the distribution coefficient to decrease with increasing CaO/SiO_2 mass ratio as can be seen in figure 3.2. Suzuki and co-workers also investigated

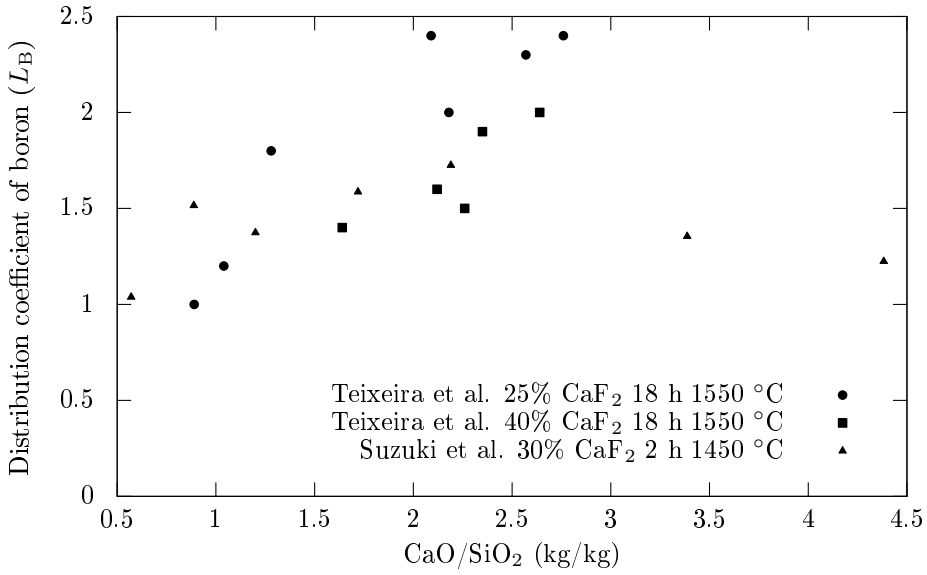

Figure 3.2: Distribution coefficient of boron for ternary CaO-SiO_2-CaF_2 systems as a function of CaO/SiO_2 mass ratio.

the temperature dependency of the distribution coefficient of boron for the 54%CaO-30%CaF_2-16%SiO_2 system and found that it increases with increasing temperature. This may however be caused by the system not having reached equilibrium and thereby an increased temperature could be giving a value of the distribution coefficient closer to the true equilibrium value.

Teixeira and Morita (2009) investigated the ternary CaO-SiO_2-CaF_2 slag system where they used the same experimental parameters as Teixeira et al. in the binary CaO-SiO_2 system. The influence of the CaO/SiO_2 mass ratio was investigated for a slag system containing 25% CaF_2 and a slag system containing 40% CaF_2. The distribution coefficient was found to increase with increasing CaO/SiO_2 ratio for both these systems in the range they investigated. The system containing 40% CaF_2 had slightly lower values than the system containing 25% CaF_2 as can be seen in figure 3.2 where the highest value of the distribution coefficient is 2.4. The values of the distribution coefficient are also lower than the highest values they found in the pure binary CaO-SiO_2 system.

Luo et al. (2011) did one experiment with CaF_2 where the initial slag composition was 49%CaO-10%CaF_2-41%SiO_2 and found that it to be 1.7 which is lower than the value they found in the binary CaO-SiO_2 system, and they did therefore not investigate CaF_2 containing slags further. They used the same parameters as in the binary CaO/SiO_2 system. The slag composition have therefore also here changed towards silica saturation because they used a silica crucible and their data is therefore not included in figure 3.2.

Cai et al. (2011) did a study of the distribution coefficient of boron between silicon and CaO-SiO_2-CaF_2 slags under argon atmosphere. They found the distribution coefficient of boron to vary with slag/silicon mass ratio which should not happen from a thermodynamic point of view. This indicates that they may not have interpreted the distribution coefficient of boron between silicon and slag as an equilibrium value and their results are therefore not evaluated any further.

The work by Teixeira and Morita (2009) and Suzuki et al. (1990) are compared in figure 3.2. It is seen that they are in good agreement except for two data-points in the most basic end of the work by Suzuki et al. This indicates that these systems may reach equilibrium within two hours and CaF_2 does not seem to have a big influence on the distribution coefficient of boron. Temperature does not seem to have much influence on the distribution coefficient either.

3.1.3 The CaO-MgO-SiO_2 system

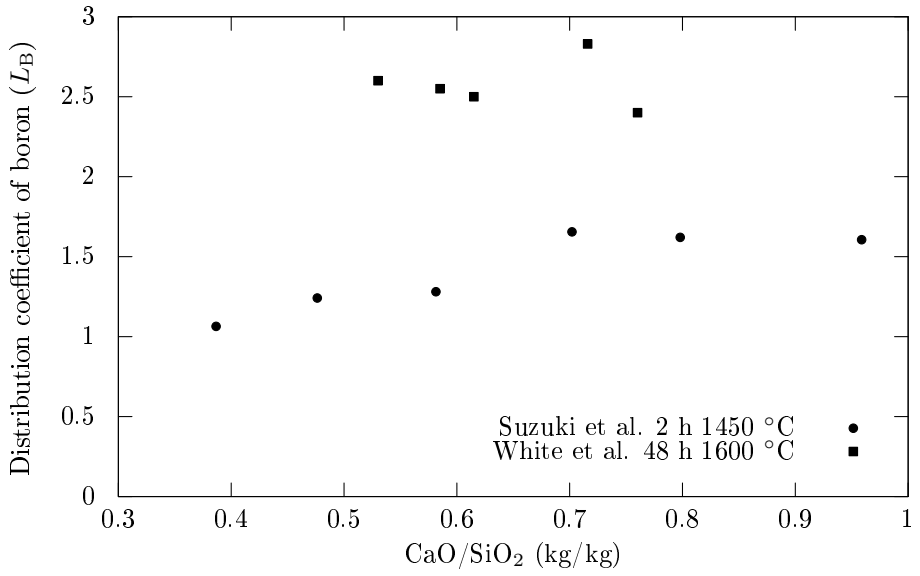

Figure 3.3: Distribution coefficient of boron for ternary CaO-10%MgO-SiO_2 systems as a function of CaO/SiO_2 mass ratio.

For a CaO-10%MgO-SiO_2 slag Suzuki et al. (1990) found that the distribution coefficient increased with increasing CaO/SiO_2 ratio to a value of 1.6 at a CaO/SiO_2 mass ratio of 0.8. The same parameters as in the CaO-CaF_2-SiO_2 system were used. They also investigated the temperature dependency of the distribution coefficient of boron for the 29%CaO-20%MgO-51%SiO_2 system and found that in the same way as in the 54%CaO-30%CaF_2-16%SiO_2 system

that it increases with increasing temperature. This may however be caused by the system not having reached equilibrium in the same way as explained for the 54%CaO-30%CaF_2-16%SiO_2 system.

White et al. (2012) did recently investigate the CaO-MgO-SiO_2 slag system at 1600 °C with a holding time of 48 hours. Both pure CO and CO diluted in argon gas was used and they found that an increased partial pressure of oxygen in the gas gave a somewhat higher distribution coefficient of boron. They also investigated the influence of N_2 on the distribution coefficient of boron and found that N_2 also increased the distribution coefficient of boron. A range of compositions were investigated under one bar CO and they did not find the slag composition to influence the distribution coefficient. The MgO concentration was varied from 1.0 to 14.3 % while the CaO/SiO_2 mass ratio was varied from 0.5 to 1.0. All values of the distribution coefficient they obtained were within the range 2.3 to 3.5.

The work by Suzuki et al. (1990) and White et al. (2012) in the ternary CaO-10%MgO-SiO_2 system is compared in figure 3.3. Slags with a content of 10 ± 1.1% MgO were selected from the study by White et al. for comparison with Suzuki et al. and it is seen that the values of the distribution coefficient given by White et al. is significantly higher than the values given by Suzuki et al. The holding time in the study by Suzuki et al. may have been too short for the system to reach equilibrium and hence giving values that are lower than the equilibrium value. The results by White et al. are compared with results obtained by others in the binary calcium silicate system in figure 3.6 and it is seen that they somewhat higher than the values obtained by others.

3.1.4 The CaO-Al_2O_3-SiO_2 system

Fujiwara et al. (2002) investigated the distribution coefficient of boron for CaO-Al_2O_3-SiO_2 slags at 1600 °C. They used high purity silicon and added less than 2 % boron to their slags. The samples were held in alumina crucibles in an induction furnace under argon atmosphere with unknown holding time. They used 4-6 g slag and 2-3.5 g silicon for each experiment. The range that they investigated was saturated with $CaAl_{12}O_{19}$ for the slags with highest SiO_2 concentration and with $CaAl_4O_7$ in the slags with lowest SiO_2 concentrations. The values of the distribution coefficient were in the range from 0.35 to 1.15 with the highest value close to the simultaneous saturation with $CaAl_{12}O_{19}$ and $CaAl_4O_7$ as can be seen in figure 3 below. From there the distribution coefficient decreased with increasing SiO_2 concentration as can be seen in figure 3.4.

Luo et al. (2011) found the distribution coefficient to increase both with time and temperature in a slag with initial composition of 49%CaO-10%Al_2O_3-41%SiO_2. The longest holding time they used was 2 hours and an increase of the distribution coefficient with time indicates that the transport of boron from silicon to slag has not reached equilibrium. Mass transfer speed increases

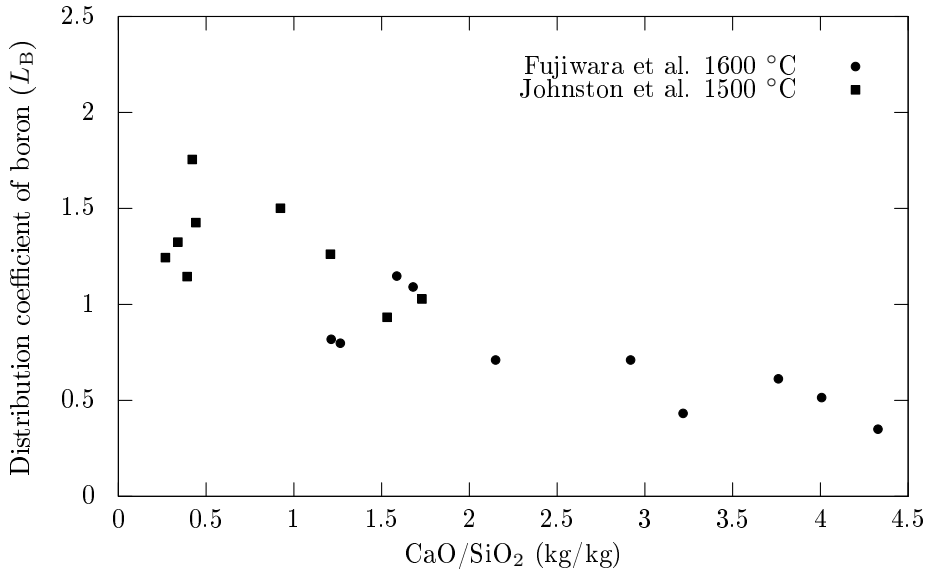

Figure 3.4: Distribution coefficient of boron for ternary CaO-Al_2O_3-SiO_2 systems held in alumina crucibles as a function of CaO/SiO_2 mass ratio.

with temperature and the increasing value of the distribution coefficient with temperature can also be an indication that mass transfer of boron may not have reached equilibrium. They increased the Al_2O_3 content with a fixed initial CaO/SiO_2 mass ratio of 1.21 and found that the distribution coefficient increased with increasing Al_2O_3 content in the slag. A holding time of 1 hour at 1550 °C was used in these experiments, and as discussed above this may not be long enough for the system to reach equilibrium. Al_2O_3 was found to give a maximum value of the distribution coefficient of 9.3 at an initial composition of 33%CaO-40%Al_2O_3-27%SiO_2, which is the highest value of the distribution coefficient ever published. Also here the slag composition is likely to have changed significantly during their experiments since they used silica crucibles and their results are therefore not included in figure 3.4.

In one series with quaternary slags Johnston and Barati (2010) held the systems in alumina crucibles and varied the CaO/SiO_2 mass ratio while the initial MgO and Al_2O_3 concentrations for all slags were 3% and 35% respectively. The systems were held for 2 hours at 1500 °C under argon atmosphere. The MgO content is here considered to be so low that the behaviour of this ternary system is comparable to the ternary CaO-Al_2O_3-SiO_2 system.

The work on the CaO-Al_2O_3-SiO_2 by Fujiwara et al. (2002) and Johnston and Barati (2010) are compared in figure 3.4. It is seen that the work by Johnston and Barati covers lower CaO/SiO_2 mass ratios than Fujiwara et al. and that they obtained somewhat higher values of the distribution coefficient. A decreasing trend with increasing CaO/SiO_2 mass ratio is seen but the Al_2O_3

content is also varying and may also have an effect. These slags do however not seem to have a higher affinity for boron than a binary calcium silicate slag.

3.1.5 The Na_2O-SiO_2 and CaO-Na_2O-SiO_2 systems

Tanahashi et al. (2002) investigated the distribution of boron between silica saturated CaO-Na_2O-SiO_2 slags and silicon where the holding time was 2 to 12 hours and silicon initially contained 0.3 to 1% boron. The system was held in quartz crucibles where they used 10 grams of >5N pure silicon which they doped with 99.5% pure boron before they added 5 grams of slag. They did experiments with five different compositions at 1450 °C and found the Na_2O concentration to decrease with time from slags containing 22 - 33.5% CaO. In one slag initially containing 13.5 % CaO and another only containing Na_2O and SiO_2 they found Na_2O to remain in the slag. They did not find any boron to be absorbed into the binary Na_2O-SiO_2 slag either. Silica rich slags are known to be very viscous and this may cause the evaporation of Na_2O and boron transport to be very slow. The holding times they used may therefore not have been long enough for any mass transfer to occur for these slags. They also did experiments with two different compositions at 1500 °C and found Na_2O to rapidly disappear. The distribution coefficient of boron was in most of their experiments found to increase with time to a peak value before decreasing again. This may have been caused by boron at first not having reached equilibrium due to slow mass transfer. Most of the Na_2O is gone for the longest holding times possibly giving less favourable conditions for oxidation of boron. The maximum value of the distribution coefficient in their work was 3.3.

Teixeira and Morita (2009) also added 7 and 10% Na_2O to a calcium silicate slag with a CaO/SiO_2 mass ratio of 1.21. The holding time was only one hour due to the volatile nature of Na_2O and it was found that the distribution coefficient was increased by the addition of Na_2O. The maximum value of the distribution coefficient was found to be 2.25.

Luo et al. (2011) investigated the CaO-Na_2O-SiO_2 system in addition to the previously mentioned systems. The same experimental parameters were used in these systems as in the other systems. They found the distribution coefficient to increase with holding time and temperature to a peak value and decreasing from there. This is in agreement with the previously discussed work by Tanahashi et al. (2002). They also increased the Na_2O content in their ternary slags with a fixed initial CaO/SiO_2 mass ratio of 1.21 and found that the distribution coefficient increased with increasing Na_2O content in the slag. Increasing distribution coefficient with increasing Na_2O is in agreement with the results from Teixeira and Morita (2009). The maximum value of the distribution coefficient with Na_2O was 5.8 at an initial composition of 33%CaO-40%Na_2O-27%SiO_2. The final composition of the slags will also be

significantly different from the initial composition because of SiO_2 dissolving into the slag from the crucible and decreasing Na_2O content due to evaporation.

Zhang et al. (2013) did a study on the distribution of boron between silicon and Na_2O-CaO-SiO_2 slags. They did however not consider the distribution coefficient of boron to be the equilibrium distribution between silicon and slag in liquid phase. They show the distribution coefficient as a function of weight ratio of silicon to slag, and the variation here may indicate the experimental uncertainty of their results since the distribution coefficient should not be dependent on slag/silicon mass ratio. Their results are therefore not evaluated any further.

Safarian et al. (2013) shows in a recent study using a Na_2O - SiO_2 slag that refining with Na_2O causes boron to evaporate from the slag. The Na_2O content in the slag is also showed to decrease with increasing holding time. Refining with a Na_2O slag is therefore not an equilibrium process and the distribution coefficient of boron is not applicable to the system. Their results are also very much in line with the results discussed above.

From previous works it is therefore seen that a slag containing Na_2O will have a higher affinity for boron than a binary calcium silicate slag. The Na_2O will however be lost within hours due to evaporation and this process is therefore not an equilibrium process.

3.1.6 Other slag systems

Suzuki et al. (1990) also investigated the ternary CaO-10%BaO-SiO_2 system and found the distribution coefficient to increase with increasing CaO/SiO_2 ratio in the same way as the CaO-10%MgO-SiO_2 system to a peak value of about 1.9. Also here the same parameters as in the CaO-CaF_2-SiO_2 system were used. The trend with increasing distribution coefficient with increasing CaO/SiO_2 ratio may be caused by the slags containing the most silicon dioxide not reaching equilibrium after 2 hours in the same way as the previously discussed binary CaO-SiO_2 system. They also added an unknown amount of CaF_2 to both the CaO-10%MgO-SiO_2 and the CaO-10%BaO-SiO_2 system at higher basicities and found this to decrease the distribution coefficient.

Johnston and Barati (2010) investigated the distribution coefficient of boron for BaO-Al_2O_3-SiO_2 and CaO-MgO-Al_2O_3-SiO_2 slags at 1500 °C under argon atmosphere. They determined the equilibrium time to be 2 hours and used this holding time for their main experiments. In one series with quaternary slags they held the systems in alumina crucibles and varied the CaO/SiO_2 mass ratio while the initial MgO and Al_2O_3 concentrations for all slags were 3% and 35% respectively. This series has been compared above with the ternary CaO-Al_2O_3-SiO_2 system. In another series with quaternary slags Johnston et al. held the slags in magnesia crucibles and varied the Al_2O_3/SiO_2 mass ratio while the initial CaO and MgO concentrations for all slags were

42% and 10% respectively. In the series with ternary BaO-20%Al_2O_3-SiO_2 slags they used alumina crucibles and varied the BaO/SiO_2 mass ratio. Depending on the crucible the slags would either change towards alumina or magnesium oxide saturation. The final composition of many of the slags is therefore significantly different from the initial composition.

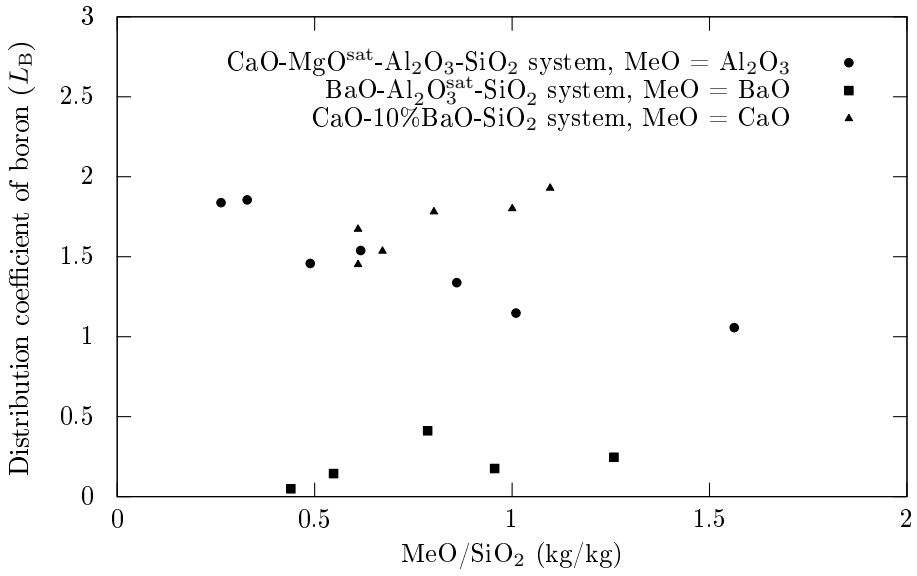

Figure 3.5: Distribution coefficient of boron for the CaO-MgO-Al_2O_3-SiO_2 and BaO-Al_2O_3-SiO_2 systems held at 1500 °C for 2 hours by Johnston and Barati (2010) and CaO-10%BaO-SiO_2 system held at 1450 °C for 2 hours by Suzuki et al. (1990).

They found the distribution coefficient of boron to be in the range between one and two for all their quaternary slags. For the ternary slags containing BaO the distribution coefficient of boron is between 0.05 and 0.5 for all compositions investigated. No trend was found for the distribution coefficient with changing BaO/SiO_2 mass ratio as can be seen in figure 3.5. A decreasing trend was found for the distribution coefficient of boron with increasing Al_2O_3/SiO_2 mass ratio in the 42%CaO-10%MgO-Al_2O_3-SiO_2 system where the maximum value of the distribution coefficient of boron is 1.8 as shown in figure 3.5. The trend seen with increasing Al_2O_3/SiO_2 leads them to suggest that a high oxygen partial pressure may be more beneficial for boron removal than the slag basicity.

Ding et al. (2012) investigated the distribution coefficient of boron for ternary CaO-Li_2O-SiO_2 and CaO-SiO_2-LiF systems at 1550 °C under argon atmosphere. The experimental parameters were the same as for the previously discussed experiment in the binary calcium silicate system. They used a fixed CaO/SiO_2 mass ratio of 45:55 and investigated the trend of the distribution

coefficient with increasing Li_2O and LiF content in the slag, where the maximum content of Li_2O and LiF was 40 %. The distribution coefficient of boron was determined by them to be in the range between one and three. The maximum value for the distribution coefficient was 2 at two mass-% Li_2O for the CaO-Li_2O-SiO_2 slag system and 2.8 at 5 mass-% LiF for the CaO-SiO_2-LiF system. They also observed a decreasing boron concentration with time for two ternary slags with the same CaO/SiO_2 mass ratio as above containing 20% Li_2O and 20% LiF respectively. They suggest that evaporation of boron oxide is the cause of this. When looking at their experimental setup it is seen that they blow argon gas through water before it enters the furnace. This will bring some moisture into the furnace and may cause boron to evaporate as hydrogen boron oxide as shown in the work by Nordstrand and Tangstad (2012).

None of the slag systems discussed in this chapter seems to be better for boron removal than any of the other slag systems discussed. A BaO-Al_2O_3-SiO_2 slag seems however to have a lower affinity for boron than any other slag that have been investigated.

3.1.7 Summary

Most equilibrium studies find the distribution coefficient of boron to be in the range from one to three as shown in figure 3.6. The study of the BaO-Al_2O_3-SiO_2 system by Johnston and Barati (2010) is not included because there is no CaO in the system. This system is also the system with the lowest distribution coefficient. The studies shown in figure 3.6 with long holding times have a higher distribution coefficient than the ones with short holding times. This has already been discussed for the binary calcium silicate system where a holding time of two hours may not be a sufficient holding time in the silica rich end of the slag system. It has also been discussed that the same may be the case for the CaO-10%MgO-SiO_2 system in the study by Suzuki et al. The CaO-Na_2O-SiO_2 system has not been included since it is a non-equilibrium system. Several other studies have not been included for various reasons discussed above. There is significant scatter between the different studies of similar slag systems indicating a need for more data in most of those systems. With present data, no slag system seems to be a clear candidate for boron removal by slag refining. The highest equilibrium values are however seen to have been found in the binary CaO-SiO_2 and the ternary CaO-MgO-SiO_2 system.

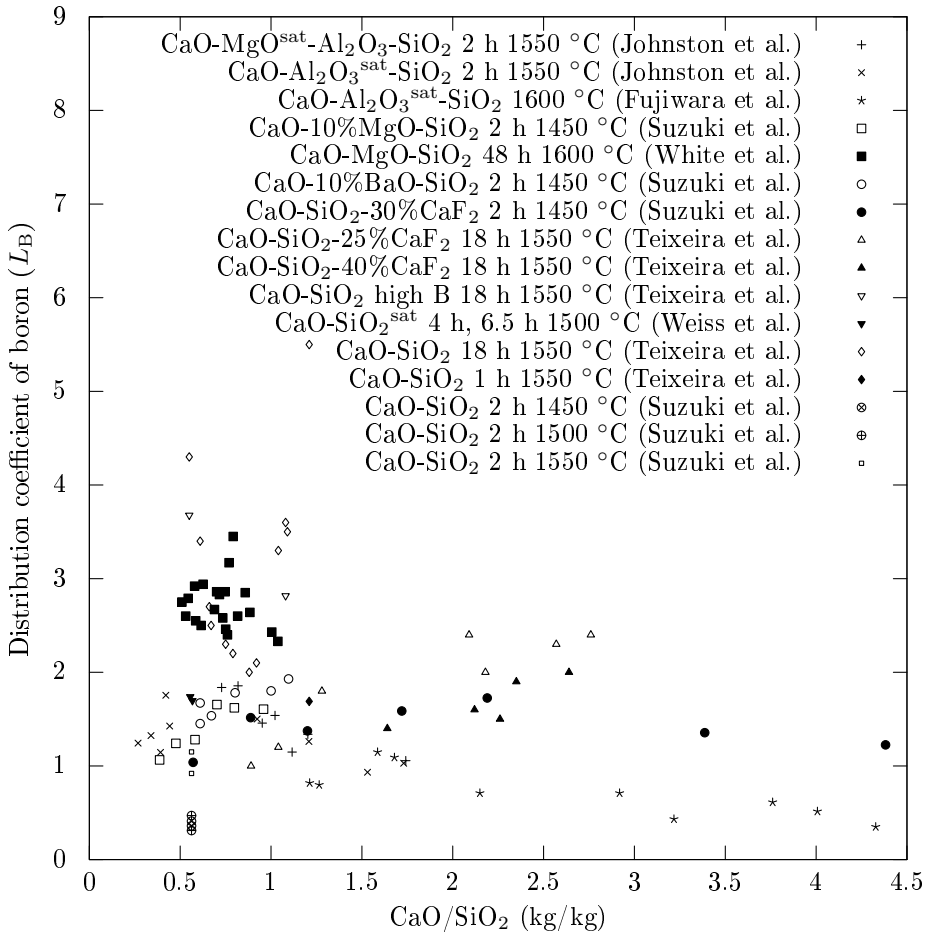

Figure 3.6: Distribution coefficient of boron for several systems with a varying CaO/SiO_2 mass ratio. The $BaO\text{-}Al_2O_3\text{-}SiO_2$ system is not included. Non-equilibrium systems and studies with insufficient data are not included either.

3.2 Distribution of calcium, magnesium and aluminium between silicon and slags

The overall thermodynamic properties of the system need to be well known in order to better understand the mechanisms behind the distribution of boron between silicon and slags. The activity of boron in silicon can be influenced by other elements present in silicon. The magnitude of the influence is dependent on the concentration and magnitude of the interaction between boron and the respective element. The distribution of slag forming elements between slag and silicon can therefore influence the distribution coefficient of boron. The distribution of slag forming elements between silicon and CaO-SiO_2, CaO-MgO-SiO_2 and CaO-Al_2O_3-SiO_2 slags are reviewed below.

3.2.1 The binary CaO-SiO_2 system

Several studies have been conducted under different conditions in this system. The distribution of calcium between silicon and slags can also be used to determine the activity of both CaO and SiO_2 in the slag. And the activity of CaO and SiO_2 can be used together with the distribution of calcium to calculate the activity coefficient of calcium in silicon. Silicon alloyed with calcium is also beneficial for acid leaching of silicon. Calcium will enter the silicon melt during slag refining where the amount of calcium in silicon is dependent on the slag composition. Several studies have been done on the distribution of calcium between silicon and calcium silicate slags. Most of these studies have been done with silica-saturated slags. Three studies have been done outside the silica saturated region using graphite crucibles, where two of these have been done in the calcium rich end of this slag system; one by Morita et al. (2000) and one by Teixeira et al. (2009). Both these studies are shown in figure 3.7 and a sharp increase in calcium concentration in silicon is seen from a CaO/SiO_2 mass ratio of about 0.8. In each study the highest calcium concentration was approximately 1.2 and 1.3 wt% respectively at a CaO/SiO_2 mass ratio of approximately 1.2. From the data obtained by Morita and co-workers it seems that the calcium concentration in silicon is not dependent on temperature. The data obtained by Teixeira and co-workers have a less clear trend and somewhat higher calcium concentration than Morita and co-workers.

The third study of the calcium distribution using graphite crucibles has been conducted by Wang et al. (2001) where they investigated the system with four different slags. Their results are shown in figure 3.7 and it is seen that two of their data-points agree well with the data by Morita et al. (2000) and Teixeira and Morita (2009). For the three most silica rich slag systems the results from Wang et al. show a decreasing trend with increasing CaO content in the slag. This contradicts known thermodynamic data for CaO

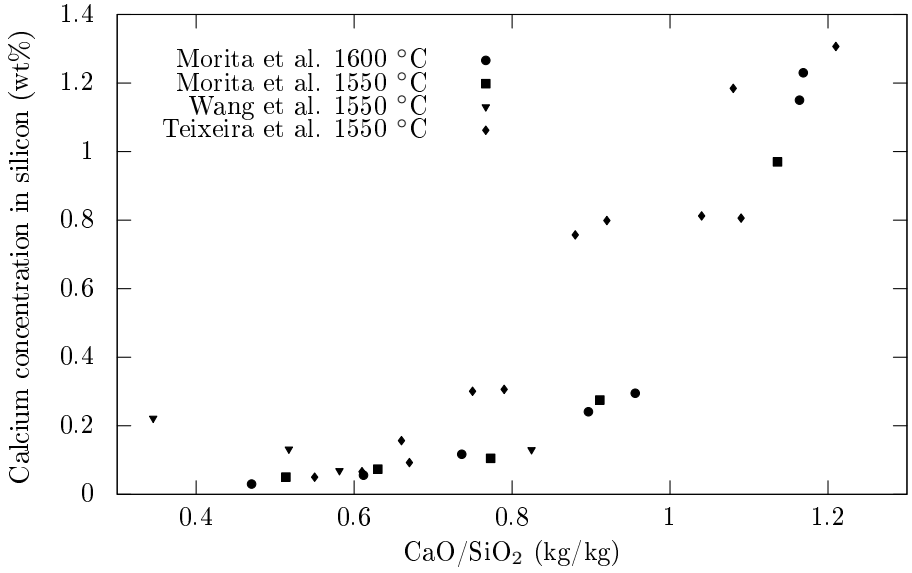

Figure 3.7: Calcium content in silicon equilibrated with calcium-silicate slags in graphite crucibles over the full liquidus range of the binary calcium-silicate slag system.

activity in the calcium silicate slag system and indicates that the measured calcium concentration in silicon for the two most silica rich slag systems may be incorrect. In addition their most silica rich slag is well beyond silica saturation at 1550 °C, indicating that the slag may be partly solid silica or that the measured slag composition is wrong.

Figure 3.8 shows the silica rich region of the calcium silicate system and includes the silica saturated slag systems. It is here clearly seen that the measured calcium concentration by Wang and co-workers for a CaO/SiO_2 mass ratio of 0.52 is significantly different from results obtained in other studies.

Miki et al. (1998) did a range of experiments at temperatures from 1450 to 1550 °C and found that the calcium concentration in silicon at silica saturation was independent of temperature in this range. Results from Weiss and Schwerdtfeger (1994) also indicate this, but they found the calcium concentration in silicon to be a little less than half of the findings by Miki et al. Weiss and Schwerdtfeger did several experiments using electronic grade silicon at 1500 and 1600 °C. They had holding times between 1 and 8 hours. Only the results where they determined the final slag composition is shown in figure 3.8. The closeness between the results for different holding times indicates that they have reached equilibrium already after 2.5 to 3 hours. Weiss and co-workers also did four experiments staring with metallurgical silicon containing between 0.07 and 0.1% calcium. Two of these experiments lasted 1 hour at 1500 °C giving the two data-points with lowest silica concentration. The composition

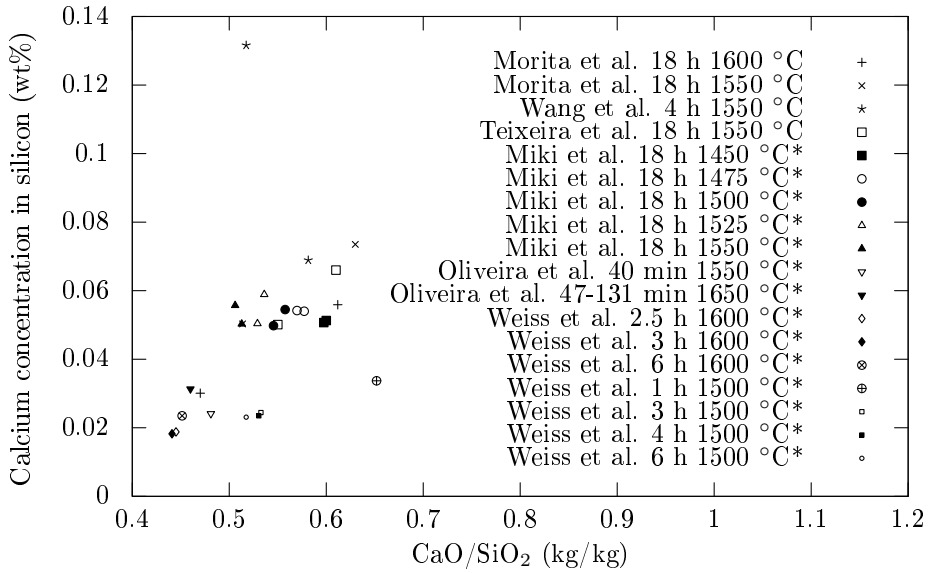

Figure 3.8: Calcium content in silicon equilibrated with calcium-silicate slags in the silica rich end of the binary calcium-silicate slag system. (* systems held in quartz crucibles)

of the slags in those experiments is seen to not have reached equilibrium with the silica crucible. The two other experiments lasted for 4 hours and have a CaO/SiO_2 mass ratio of 0.54 and 0.55 respectively. These is seen to have reached slag-silicon equilibrium since the calcium concentration is the same as for holding tomes of 3 and 6 hours when starting with electronic grade silicon. The data obtained by Weiss and co-workers at 1500 °C is somewhat lower than what others have found. Short equilibrium time as compared to many of the others does not seem to be the reason for this since the same values are found for different holding times. Starting with different calcium content in silicon also gives the same values for holding times of more than one hour. Weiss and Schwerdtfeger also found a higher SiO_2 concentration in the slag at silica saturation as compared to others, but they show that these data agree well with the known phase diagram. Miki et al. found a lower SiO_2 concentration that does not agree as well with the known phase diagram.

Pinto and Takano (2000) did several experiments using induction heating in a crucible that was open to atmosphere and blown from above with argon to protect the system from air. Induction will promote mixing and equilibrium time using induction heating is therefore shorter than when using resistive heating. They found that the equilibrium time was 40 minutes and excluded all data with a shorter holding time than this. The calcium concentration in silicon given in figure 3.8 for 1550 °C is an average of 19 samples, while the value for 1650 °C is an average of 7 samples. Details for the different studies

are summarized in table 3.2.

3.2.2 The CaO-MgO-SiO_2 and CaO-Al_2O_3-SiO_2 systems

The most recent study of the distribution of slag forming elements between the CaO-MgO-SiO_2^{sat} slag system at 1600 °C and the CaO-Al_2O_3-SiO_2^{sat} slag system at 1500 °C is given in the work by Morita et al. (2000). Their study is in good agreement with the study by Weiss and Schwerdtfeger (1994) with respect to aluminium while they obtained higher calcium and magnesium concentrations. They suggested that the temperature difference between the study by Weiss and Schwerdtfeger which was conducted at 1500 °C and their study may be the cause of the concentration differences. Morita et al. also shows that their study is in good agreement with the study by Fujiwara et al. (2002) in the CaO-Al_2O_3-SiO_2 system saturated with with Al_2O_3, $CaAl_{12}O_{19}$ and $CaAl_4O_7$. Morita and co-workers also determined the concentration of magnesium and aluminium in silicon across the entire liquid region of the CaO-MgO-SiO_2 and CaO-Al_2O_3-SiO_2 slag systems, but they did not calculate the isoconcentration curves from their data.

An estimate of isoconcentration curves for slag forming elements in silicon in equilibrium with the CaO-Al_2O_3-SiO_2 slag system at 1500 °C can be found on page 255 in the book by Schei et al. (1998). A more recent study by Wang et al. (2001) is in reasonable agreement with this estimate with respect to aluminium as can be seen in figure 3.9. They found higher calcium concentrations in the SiO_2 rich part of the slag system while there is a good agreement in the rest of the slag system as can be seen in figure 3.10. As previously discussed it should be noted that Wang et al. found unreasonably high calcium concentrations in silicon in equilibrium with the SiO_2 rich part of the binary calcium silicate slag system. The magnitude of the isoconcentration curves in the SiO_2 rich part of the slag system may therefore also be too high. Margaria et al. (1996) determined the isoconcentration curves for this system at 1450 °C and the same trends of the concentration curves was found there as in the other works. The magnitude of the concentrations are however somewhat lower than the estimate by Schei et al.

Table 3.2: Experimental details for works on the equilibrium distribution of calcium between calcium silicate slags and silicon.

	Temperature (°C)	Holding time	Atmosphere	Crucible
Miki et al	1450-1550	18 h	Argon	Quartz
Wang et al	1550	4 h	Argon	Graphite
Weiss et al	1500 and 1600	1-8 h	Argon	Quartz
Oliveira et al	1550-1650	40-124min	Argon blowing	Quartz
Morita et al	1550-1600	18 h	Argon	Graphite
Teixeira et al	1550	18 h	Argon	Graphite

	Silicon mass	Slag mass	Initial Ca in Si	Heating
Miki et al	4g	12g	0.10 %	Unknown
Wang et al	1 part (12x40 mm)	1.5-2 parts (12x40 mm)	0.01-0.25 %	Resistive
Weiss et al	2g	5g	0-0.1 %	Resistive
Oliveira et al	10g	40g	0-0.92 %	Induction
Morita et al	8g	16g	Unknown	Resistive
Teixeira et al	3g	6.7g	0	Resistive

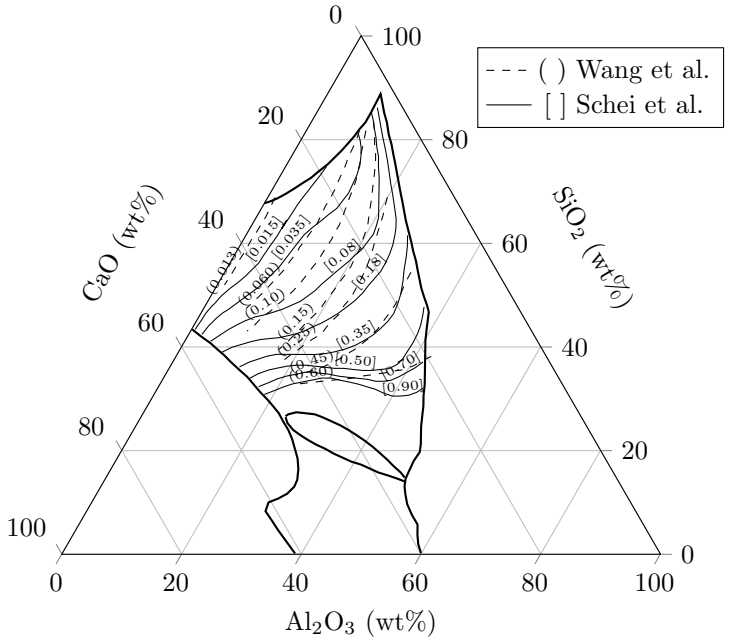

Figure 3.9: Isoconcentration curves for aluminium at 1550 °C as found by Schei et al. (1998) and Wang et al. (2001).

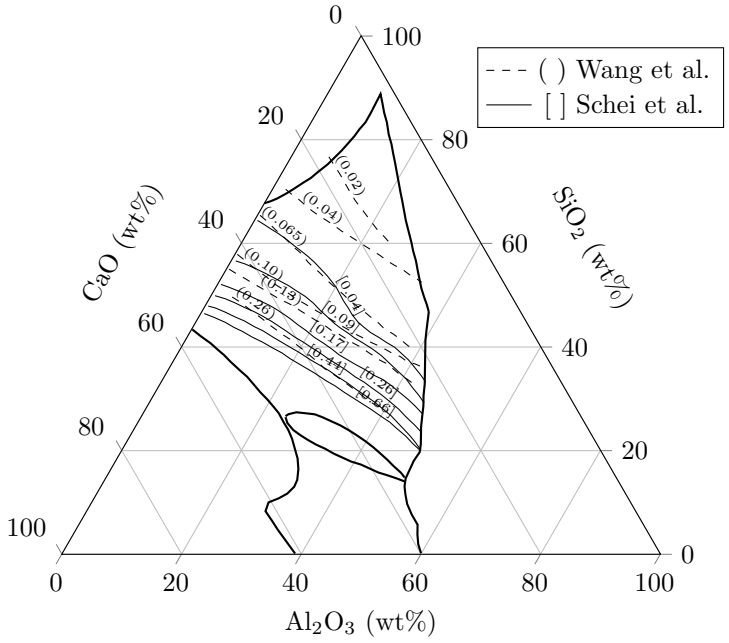

Figure 3.10: Isoconcentration curves for calcium at 1550 °C as found by Schei et al. (1998) and Wang et al. (2001).

3.3 Activities at infinite dilution in silicon

There are several experimental determinations of the activity coefficient at infinite dilution in silicon. The activity coefficients in this chapter are all at infinite dilution in silicon even if they are just referred to as the activity coefficient. Estimates of the activity coefficient of elements at infinite dilution in silicon have also been done using approximations and extrapolation, but they are not considered here. More extensive thermodynamic models which are incorporated into thermodynamic software can also be used to calculate the activity coefficient.

3.3.1 The activity coefficient of calcium

The activity coefficient of calcium at infinite dilution in silicon has been determined experimentally in four separate works. Estimates by extrapolation of experimental and thermochemical data can also be found in literature. Schürmann et al. (1975) as one example determined the activity coefficient of calcium using vapour pressure measurements in the temperature range 1210 to 1350 °C. The highest silicon concentration in their study was $x_{\mathrm{Si}} = 0.7$. Tuset (1985) did an extrapolation of these data to 1550 °C and $x_{\mathrm{Si}} = 1$ and found the activity coefficient to be $\ln \gamma^0_{\mathrm{Ca}} = -7.11$. Only direct experimental determinations are considered below.

Miki et al. (1998) used the equlilibrium

$$\mathrm{SiO_2} + 2\mathrm{Ca} = \mathrm{Si} + 2\mathrm{CaO} \tag{3.4}$$

and Gibbs energy of formation of CaO from Wakasugi and Sano (1989) together with their data for the distribution of calcium between silicon and slag to calculate the activity coefficient. For the activity of CaO they used the data from Eriksson et al. (1994). They investigated the activity coefficient of calcium in the range from 1450 - 1550 °C and found it to follow the relation

$$\ln \gamma^0_{\mathrm{Ca}} = -17661/T + 3.52 \tag{3.5}$$

In another study Miki et al. (1999) equilibrated silicon with lead. From these measurements they could both calculate the temperature dependence of the activity coefficient and self-interaction coefficient of calcium in silicon. They used the activity coefficient of calcium at 1450 °C from their previous study as a calibration point for the calculations in this study. The two studies are therefore connected, but the activity coefficient from the most recent study is considered to be more accurate since it takes into account the self-interaction of calcium. The activity coefficient was found to be

$$\ln \gamma^0_{\mathrm{Ca}} = -14300/T + 1.55 \tag{3.6}$$

In both studies they investigated the activity coefficient in 25 °C intervals from 1450 - 1550 °C

Pinto and Takano (2000) used the same method as Miki et al. (1998) used in their first study to determine the activity coefficient of calcium at infinite dilution in silicon. Pinto and Takano investigated the activity coefficient at 1550 and 1650 °C and found that it could be expressed by

$$\ln \gamma^0_{\mathrm{Ca}} = -15427/T + 1.02 \tag{3.7}$$

where they used the Gibbs energy of formation for CaO and SiO_2 from the NIST-JANAF tables (shown in figure 2.1), and the liquidus line at silica saturation from the Slag Atlas (1995).

Margaria et al. (1996) have also published values for the activity coefficient of calcium at infinite dilution in silicon. They equilibrated silicon with slag in graphite crucibles for 12 to 48 hours and analysed the distribution of calcium between slag and silicon after air quenching. To check the validity of these values they also performed a series of experiments using an effusion cell coupled with mass spectrometry to determine the partial pressure of calcium above the liquid metal. They give one value of the activity coefficient at at 1450 °C ($5.2 \cdot 10^{-4}$) and one value at 1550 °C ($8.6 \cdot 10^{-4}$). A temperature dependence can therefore be estimated from their results:

$$\ln \gamma^0_{\mathrm{Ca}} = -15803/T + 1.61 \tag{3.8}$$

In the book by Schei et al. (1998) a study by Ottem (1993) is described where silicon was equilibrated with SiO_2 saturated CaO-SiO_2 slags. Activities of CaO from Rein and Chipman (1965) was used together with the experimental data to determine the activity coefficient of calcium at infinite dilution in silicon where

$$\ln \gamma^0_{\mathrm{Ca}} = -23006/T + 5.45 \tag{3.9}$$

The activity coefficient of calcium at infinite dilution in silicon as obtained in the different works are shown in figure 3.11. The temperature dependence of the activity coefficient is seen to be almost the same for all works except the study by Ottem where the activity coefficient increases more with temperature than in the other works.

There has been some debate about the Gibbs energy of formation of CaO, but the most recent investigation by Jacob and Varghese (1996) supports the value given in the NIST-JANAF Tables. Miki et al. used a Gibbs energy of formation of CaO that is significantly different from the value found in the NIST-JANAF tables. They did therefore find an activity coefficient that is significantly different from the work by Pinto and Takano (2000). The distribution of calcium between slag and silicon is also found to be different in the two works as can be seen in figure 3.8, and this would lead the calculated activity coefficient of calcium to be different even if the same thermochemical data had been used in both the studies.

The activity coefficient of calcium can also be calculated from other values of the calcium concentration in silicon equilibrated with a silica-saturated slag. The activity of SiO_2 is unity in a silica saturated slag while the activity of silicon have been shown by Morita et al. (2000) to follow Raoult's law up to 2 wt% calcium. The calculation is also dependent on the activity of CaO at silica saturation and the activity data for CaO and SiO_2 are therefore reviewed in chapter 3.4.

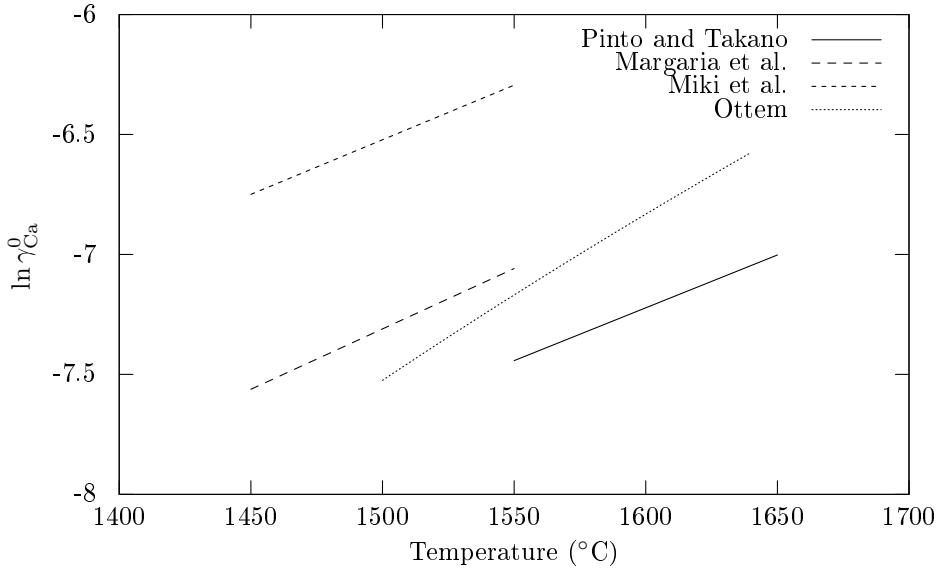

Figure 3.11: Temperature dependence of the activity coefficient of calcium at infinite dilution in silicon.

3.3.2 The activity coefficient of magnesium and aluminium

The only studies determining the activity coefficient of magnesium at infinite dilution in silicon is by Miki et al. (1998) and Miki et al. (1999). In the first study they determined the activity coefficient by equilibrating silicon with MgO-Al_2O_3-SiO_2 slags at double saturation with SiO_2 and $MgSiO_3$. Using thermochemical data and the magnesium concentration in silicon they calculated the activity coefficient. In the second study they also investigated the concentration dependence of the activity coefficient by equilibrating magnesium alloyed silicon with lead. The concentration dependence was found to be so small that the activity coefficient at infinite dilution from the first study was kept unchanged to be

$$\ln \gamma^0_{Mg} = -11300/T + 4.51 \tag{3.10}$$

in the range from 1425 to 1525 °C.

Miki et al. (1998) also determined the activity coefficient of aluminium at infinite dilution in silicon in their first study. For these experiments they equilibrated silicon with a crucible made from Al_2O_3 and $Al_6Si_2O_{13}$. In the second study (Miki et al., 1999) they investigated the concentration dependence of the activity coefficient in the same way as with magnesium and re-investigated the temperature dependence using a Knudsen cell. They found the activity coefficient to be

$$\ln \gamma^0_{\mathrm{Al}} = -3610/T + 0.452 \tag{3.11}$$

in the range from 1450 to 1550 °C.

Margaria et al. (1996) equilibrated silicon with CaO-Al_2O_3-SiO_2 slags and used the concentration of aluminium and activities of slag components from literature to determine the activity coefficient of aluminium at infinite dilution in silicon. The activity coefficient at 1500 °C was found to be

$$\gamma^0_{\mathrm{Al}} = 0.45 \pm 0.9 \tag{3.12}$$

and negligible variation of the activity coefficient in the range from 1425 to 1575 °C. They calculated the activity coefficient to be 0.53 using data from the study by Weiss and Schwerdtfeger (1994) at 1550 °C. The activity coefficient found by Miki et al. (1999) is 0.19 at 1450 °C and 0.22 at 1550 °C respectively. This is seen to be less than half of the values found by Margaria et al.

3.4 Activities in binary calcium silicate slags

The thermodynamic activities of the major components of slags are detrimental for understanding the thermodynamics of the two phase slag-silicon system. A complete review of the activity of CaO and SiO_2 in the binary calcium silicate slag system is given below.

Some earlier works (e.g. Rey (1948) and Richardson (1953)) used available thermodynamic data together with the phase diagram of the CaO-SiO_2 system to estimate the activity of CaO and SiO_2 in the slag. The estimate by Rey of the activity of SiO_2 is close to experimentally measured values while the activity of CaO is one order of magnitude higher than experimental data. Neither the activity of CaO or SiO_2 are in agreement with experimental data in the work by Richardson. The Gibbs energy of formation of SiO_2 was at that time erroneous as have been shown later by Chipman (1961). Calculations involving this value did therefore give wrong results.

3.4.1 The activity SiO_2

The first experimental determination of the activity of SiO_2 in binary calcium silicate slags was done by Chang and Derge (1946). The activities were determined using reversible cell measurements with silicon carbide-graphite

electrode pairs from 1500 to 1600 °C with 25 °C intervals. The activities they found are close to findings in later works but show a discontinuity around $CaSiO_3$.

The most recent work determining the activity of SiO_2 in calcium silicate slags is by Morita et al. (2000). They use the equilibrium distribution of calcium between binary calcium silicate slags and silicon to do a Gibbs-Duhem integration from silica saturation and found a good agreement with previously published values.

Rein and Chipman (1965) calculated the activity of SiO_2 in the calcium silicate system based on the distribution of silicon between slag and Fe-Si-C alloys saturated with either graphite or silicon carbide. The activty was determined at 1550 and 1600 °C, and the activity coefficient of silicon in iron was also used in these calculations. They also determined the activity of CaO by Gibbs-Duhem integration as shown in figure 3.13 and it is seen to be slightly higher than other experimental data. The activity product $CaO \cdot SiO_2$ was found to be in excellent agreement with thermochemical data at 1550 °C at the composition 50 wt% CaO 50 wt% SiO_2.

Omori and Sanbongi (1961) did reverse cell EMF measurements to determine the activity of SiO_2 in CaO-SiO_2 slags at 1630 °C. They also estimated the activity of CaO by Gibbs-Duhem integration. For this integration they needed the activity of CaO at one slag composition, and they used erroneous thermodynamic data to calculate the activity of CaO at Ca_2SiO_4 saturation. The Gibbs-Duhem integration was therefore started with the wrong value for the activity of CaO.

Kay and Taylor (1960) measured the CO pressure above calcium silicate slags in graphite crucibles together with the equilibrium

$$SiO_2 + 3C = SiC + 2CO \tag{3.13}$$

to determine the activity of SiO_2. They considered the results in this publication to be more correct than in a previous publication by Baird and Taylor (1958). The same experimental technique was used in both works, but accuracy was improved in the work done by Kay and Taylor. They also calculated the activity of CaO by Gibbs-Duhem integration using Ca_2SiO_4 saturation as a reference point and they calculated the activity of CaO in $CaSiO_3$ saturated slags. The calculated activities are in good agreement with Carter and Macfarlane (1957).

Yang et al. (1958) determined the activity of SiO_2 at 1637 °C using a Knudsen Cell. They measured pressures of SiO and O_2 gas above the slags and pure cristobalite and calculated the activity of SiO_2 from these pressures.

Fulton and Chipman (1954) did a study of the distribution of silicon between carbon saturated iron and calcium silicate slags. They did however use a Gibbs energy of formation of SiO_2 to calculate the activity of SiO_2 that was later shown by Chipman (1961) to be incorrect. They also estimated

the activity of CaO by Gibbs-Duhem integration, but this value also becomes incorrect since their estimate of the activity of SiO_2 was erroneous.

Sakagami (1953a) did a similar study of the activity of SiO_2 at 1550, 1575 and 1600 °C in binary calcium silicate slags from using electrochemical measurements. They also determined the activity of CaO at 1550 and 1600 °C where the standard state is $a_{CaO} = 1$ at Ca_2SiO_4 saturation.

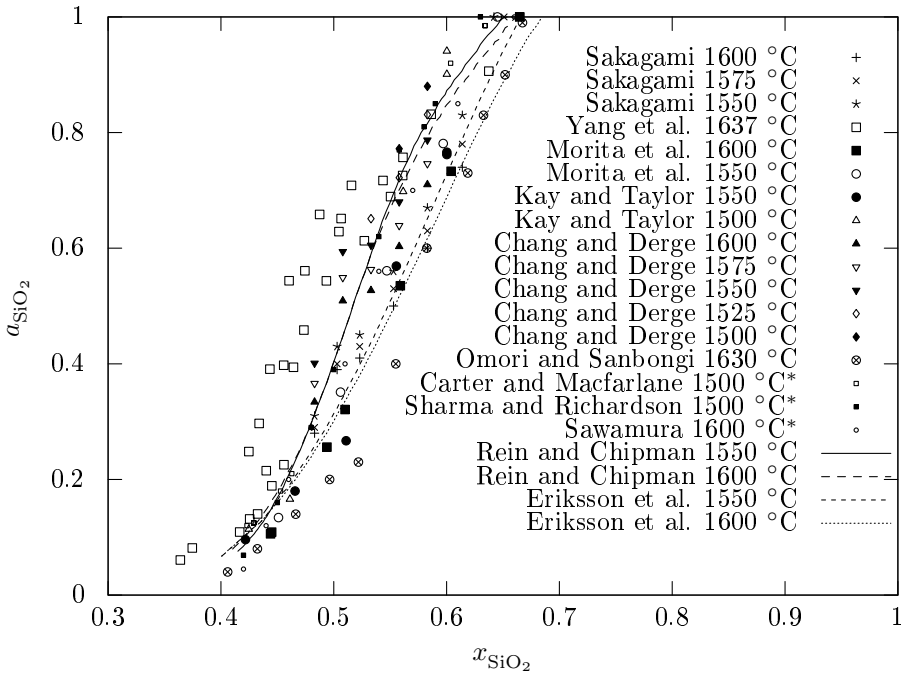

Figure 3.12: Activity of SiO_2 in a binary CaO-SiO_2 slag. (* determined by Gibbs-Duhem integration of the activty of CaO)

The activity of SiO_2 determined in the works discussed above is shown in figure 3.12. A somewhat higher activity of SiO_2 is seen in the work by Yang et al. compared to the others. Except the work by Yang et al. a discontinuity in the activity curve is seen around $CaSiO_3$ in all the works that does not involve Gibbs-Duhem integration. This indicates that there may be a source of error that has not been accounted for in these works.

Eriksson et al. (1994) did a critical evaluation of all thermodynamic and phase diagram data for the CaO-SiO_2 system. From these data they did an optimization to get one set of model equations for the Gibbs energies of all phases as functions of temperature and composition. Using these equations they calculated the thermodynamic properties and phase diagram of the calcium silicate system. They used the modified quasichemical model to represent the Gibbs energies of the molten slag phases. The calculated activity of SiO_2 at 1550 and 1600 °C is seen in figure 3.12. The calculated activity

is among the lowest experimental measurements close to silica saturation and in good agreement with all experimental data in the calcium rich part of the slag system.

3.4.2 The activity of CaO

Carter and Macfarlane (1957) did a study of the activity of CaO and SiO_2 in calcium silicate slags at 1500 °C where they equilibrated binary calcium silicate slags with CO-CO_2-SO_2 gas mixtures. They could then determine the activity of CaO by measuring the concentration of sulphur in the slags after the experiments. They assumed the activity coefficient of CaS to be constant for the range of CaO-SiO_2 slags that they investigated and used Gibbs-Duhem integration to find the activity of SiO_2.

Sharma and Richardson (1962) did a similar study as Carter and Macfarlane (1957) but also included the variation of the activity coefficient of CaS with slag composition. Their activity data can therefore be regarded as more accurate than the activities derived by Carter and co-workers, but still there is a close agreement between them. They observed that the melting point of the slag was lowered to below 1500 °C at compositions around $CaSiO_3$. They also did additional experiments at 1550 °C in this region that confirmed the results at 1500 °C. The activity of CaO was in other words found to be independent of temperature. Their gas composition was a mixture of N_2, H_2S, H_2 and CO_2. They also compared the activity product of CaO and SiO_2 with Gibbs energy of formation of $CaSiO_3$ from thermal data and found an excellent agreement with these at 1550 °C. They also assumed that the activity of CaO rose proportionally to the mole fraction of CaO, as the mole fraction of CaS fell to zero.

Sawamura (1961) measured the activity of CaO in binary calcium silicate slags at 1600 °C by double cell EMF measurements. These measurements agree very well with measurements by Sharma and Richardson (1962). Sawamura also calculated the activity of SiO_2 by extrapolating the activity of CaO to silica saturation and doing Gibbs-Duhem integration from there.

Morita et al. (2002) used the same method to determine the activity of CaO at 1550 and 1600 °C as they used to determine the activity of SiO_2. They used γ_{Ca} from the previously discussed work by Miki et al. (1999) and Gibbs energy of formation of CaO from the work by Wakasugi and Sano (1989) to calculate an initial value for the integrals. In fact this means that they used the activities of CaO given by Eriksson et al. at silica saturation as their initial values.

The results obtained from the different works determining the activity of CaO in calcium silicate slags are shown in figure 3.13. The measured activities are seen to be in good agreement with each other. Sawamura (1961) obtained a somewhat higher activity of CaO than the others at Ca_2SiO_4 saturation.

Several of the works determining the activity of SiO_2 used Gibbs-Duhem

integration to determine the activity of CaO. The initial value of the integral is dependent on thermochemical data and this has resulted in many erroneous estimates because some of the thermochemical data at that time was incorrect. In particular the earlier mentioned error for the formation of SiO_2 caused many erroneous estimates. On the other hand it should be noted that the Gibbs-Duhem integration of the activity of CaO to find the activity of SiO_2 is not dependent on thermochemical data when the integration is done from silica saturation. These also agree very well with experimental data on the activity of SiO_2 as can be seen in figure 3.12.

Eriksson et al. (1994) also calculated the activity of CaO at 1500 °C from their model equations. The calculated activity is seen in figure 3.13 to be slightly higher than experimental values except in the CaO rich part of the system.

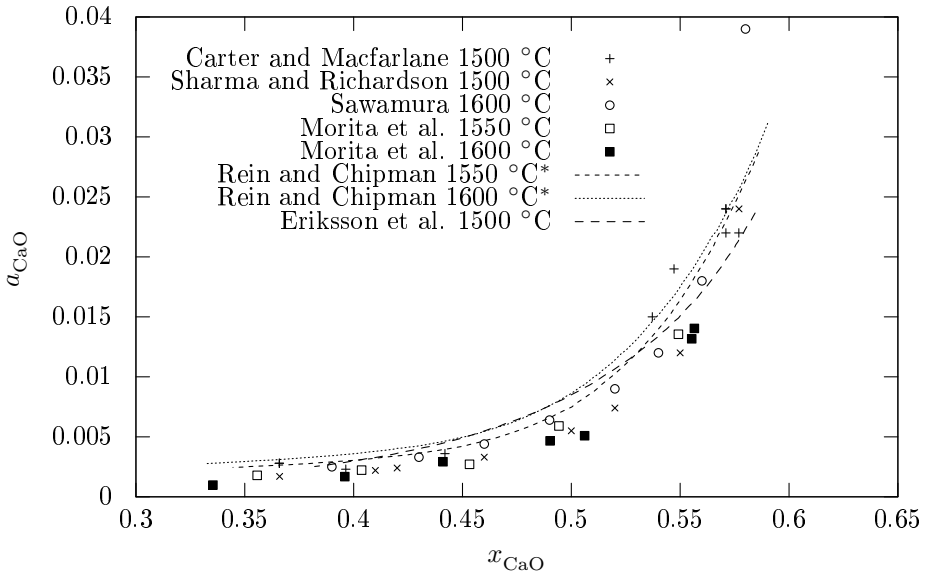

Figure 3.13: Activity of CaO in the binary CaO-SiO_2 system. (* determined by Gibbs-Duhem integration of the activity of SiO_2)

3.5 Activities in the CaO-MgO-SiO_2 system

Rein and Chipman (1965) determined the activity of SiO_2 in CaO-MgO-SiO_2 slags at 1600 °C by equilibrating silicon alloyed iron in graphite or silicon carbide crucibles with CaO-MgO-SiO_2 slags under CO atmosphere. They used the concentration of silicon in the alloy after equilibration together with the activity coefficient of silicon in iron to calculate the activity of SiO_2 in slag in the same way as they did in the binary CaO-SiO_2 system.

Morita et al. (2000) did the most recent work on the ternary CaO-MgO-SiO_2 system. They used Gibbs-Duhem integration and the equilibrium distribution of magnesium and calcium to determine the activity of SiO_2 for the whole liquid region of the CaO-MgO-SiO_2 system at 1600 °C. Their results are mostly in good agreement previous work by Rein and Chipman (1965) as can be seen in figure 3.14, but it is seen that Morita et al. obtained a somewhat higher activity of SiO_2 than Rein and Chipman in the magnesium rich part of the system.

Jung et al. (2005) did a critical evaluation of all thermodynamic and phase diagram data for the CaO-MgO-SiO_2 system. An optimized set of model equations was obtained in the same way as in the work by Eriksson et al. in the binary CaO-SiO_2 system. These model equations were used to calculate the activity of SiO_2 at 1600 °C across the entire liquid region of the CaO-MgO-SiO_2 system. The calculated activity of SiO_2 is shown in figure 3.14. It is seen that the activity of SiO_2 is somewhat lower than found by the others in the SiO_2 rich region of the phase diagram while it is in between the results by Morita et al. (2000) and Rein and Chipman (1965) in the rest of the liquid region.

Both Morita et al. (2002) and Rein and Chipman (1965) also determined the activity of CaO and MgO using Gibbs-Duhem integration. The activities for CaO are shown in figure 3.15 and it is seen that Morita and co-workers obtained somewhat lower activities than Rein and Chipman. The activities for MgO are shown in figure 3.16 and it is seen that Morita et al. obtained somewhat higher activities than Rein and Chipman.

Sawamura (1961) investigated the CaO-MgO-SiO_2 system at 1600 °C and obtained the iso-activity lines for CaO up to 11 wt% MgO. They found the activity of CaO to increase with increasing MgO content in the slag and this is not in agreement with the activities others have found. Thermodynamically an increase of the activity of CaO with decreasing concentration of CaO should not happen either.

Kalyanram et al. (1960) determined the activity of CaO in this system using the same method as Carter and Macfarlane (1957) used in the binary CaO-SiO_2 system. They investigated compositions up to 26 wt% MgO and determined iso-activity lines that show the same trend as Morita et al. (2002) and Rein and Chipman (1965). The activities they determined are however

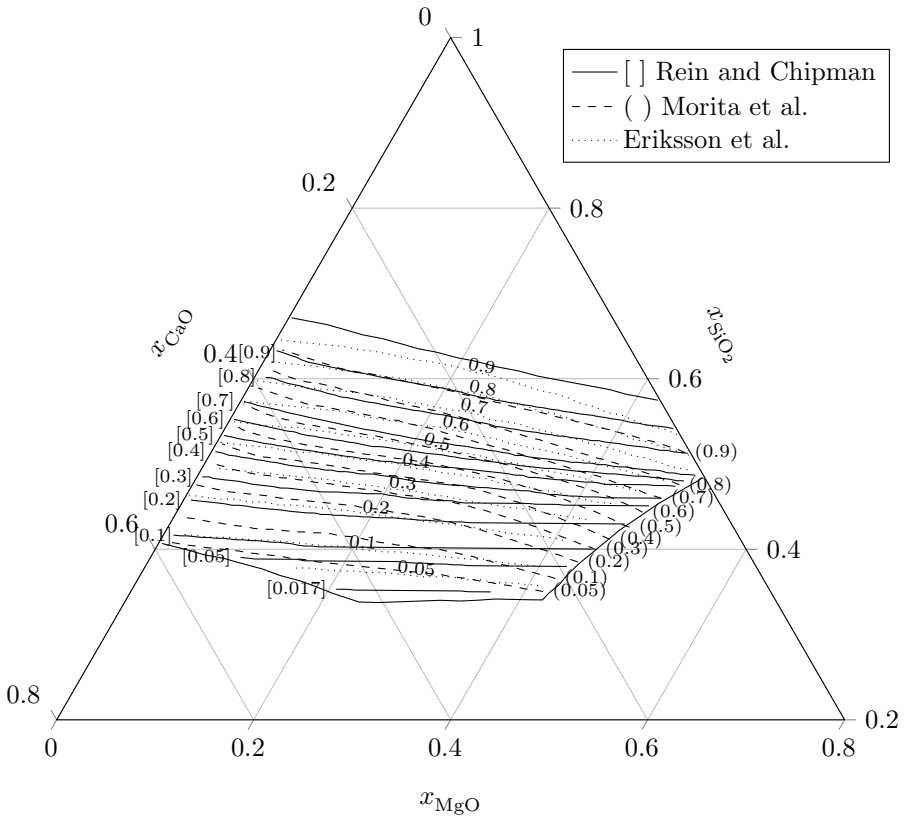

Figure 3.14: Activity of SiO_2 at 1600 °C in the ternary CaO-MgO-SiO_2 system.

somewhat higher than found by the others.

Rein and Chipman (1965) also used their data to find the activity of MgO and SiO_2 in the binary MgO-SiO_2 system and these data are compared with the work by Kambayashi and Kato (1983) and Wu et al. (1993) at 1600 °C. The activities are in relatively good agreement as can be seen in figure 3.17. Kambayashi and Kato found the activities using mass spectrometry and Gibbs-Duhem integration. The activity of SiO_2 found by Wu et al. is calculated after a thermodynamic optimization of the system. This estimate is considered to be more accurate than earlier theoretical estimates compiled by Elliott et al. (1963). The earlier estimates are therefore not included in figure 3.17.

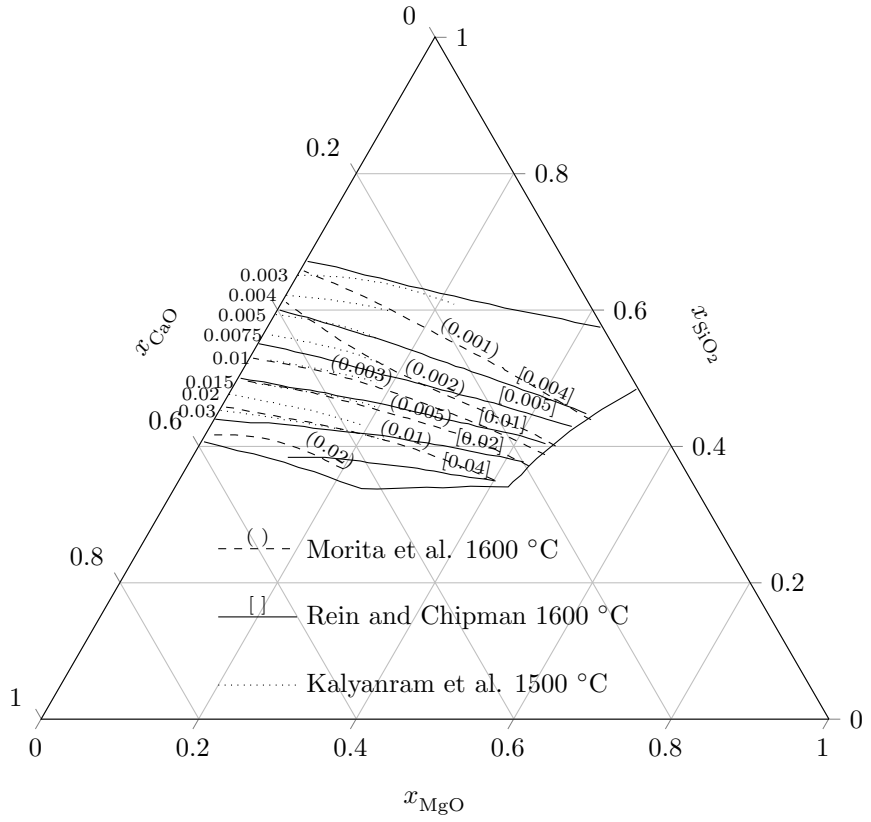

Figure 3.15: Activity of CaO in the ternary CaO-MgO-SiO_2 system.

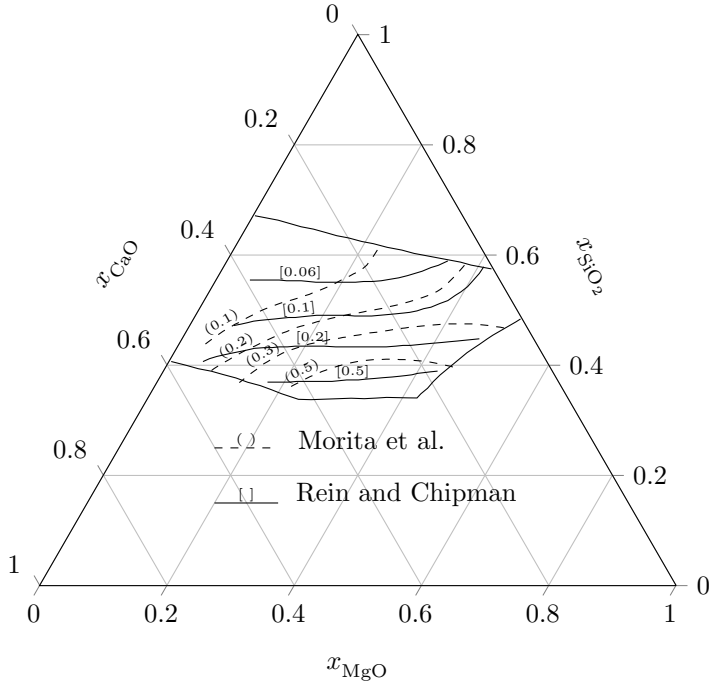

Figure 3.16: Activity of MgO at 1600 °C in the ternary CaO-MgO-SiO_2 system.

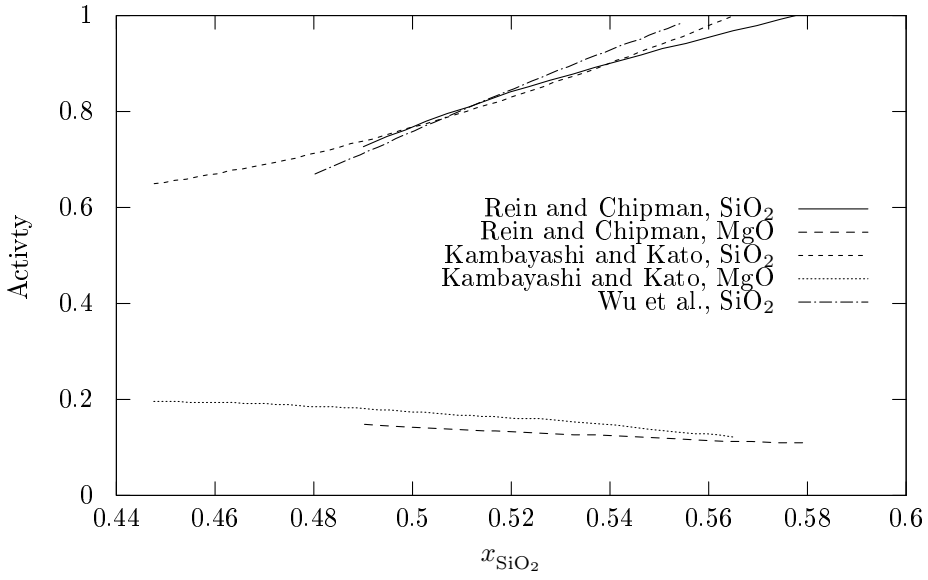

Figure 3.17: Activity of MgO and SiO_2 at 1600 °C in the binary MgO-SiO_2 system.

3.6 Activities in the CaO-Al_2O_3-SiO_2 system

Chang and Derge (1946) investigated the ternary CaO-SiO_2-Al_2O_3 system by electrochemical measurements in the same way as they investigated the binary calcium silicate system. They were however not able to calculate thermodynamic properties of the system due to insufficient fundamental thermodynamic data.

Sakagami (1953b) did also extend their study from the binary calcium silicate system into the ternary CaO-Al_2O_3-SiO_2 system and were able to estimate the activity of CaO and SiO_2 at 1500-1540 °C. The activity of SiO_2 is not far from findings in later studies but the trends of the activity curves do not agree with later studies.

Kay and Taylor (1960) determined the activity of SiO_2 in the CaO-Al_2O_3-SiO_2 system from 1450 to 1550 °C using the same method as previously described for the binary CaO-SiO_2 system. They also estimated activities at 1600 °C by extrapolation. The SiO_2 activities agree well with the work by Rein and Chipman (1965). They also derived the activity of CaO and Al_2O_3 using Gibbs-Duhem integration. The activities of Al_2O_3 are much lower than the findings by Rein and Chipman and the shape of the activity curves of CaO are also significantly different.

Kalyanram et al. (1960) determined the activity of CaO in this system at 1500 °C using the same method as they used in the ternary CaO-MgO-SiO_2 system. The iso-activity lines they found agree well with the work by Morita et al. (2002) and Rein and Chipman (1965).

Sawamura (1961) also investigated this ternary slag system at 1600 °C and found the iso-activity lines of CaO up to 20% Al_2O_3. These lines are in a fairly good agreement with others.

Omori and Sanbongi (1961) investigated the ternary CaO-Al_2O_3-SiO_2 system at 1630 °C using electrochemical measurements. Their results agree somewhat with Rein and Chipman (1965) and hence also with Kay and Taylor (1960), but there is a bend in the iso-activty curve of SiO_2 that is not observed in the work by the others. They also determined the activity of Al_2O_3 using electrochemical measurements, and obtained activities that are much lower than in other works. They determined the activity of CaO by Gibbs-Duhem integration, but the thermochemical data they used was not correct and hence they also found wrong activity of CaO.

Rein and Chipman (1965) investigated the ternary CaO-Al_2O_3-SiO_2 system at 1550 and 1600 °C using the same method as previously described for the binary CaO-SiO_2 and ternary CaO-MgO-SiO_2 systems. Fulton and Chipman (1954) had also done a similar study many years earlier. The results from the later study by Rein and Chipman are more extensive. As previously mentioned Chipman (1961) found an error in the value of the Gibbs energy of formation of SiO_2 which had made the calculated activities in the previous

study to be erroneous. They also determined the activities of CaO and Al_2O_3 by Gibbs-Duhem integration.

Zhang et al. (1986) determined the activity of CaO in the CaO rich part of the liquid region of the CaO-Al_2O_3-SiO_2 system at 1600 °C. They used Sn as a solvent and determined the activity of CaO based on the slag-metal equilibria.

Ohta and Suito (1996) investigated the activities of SiO_2 along the liquidus lines in the CaO-Al_2O_3-SiO_2 system at 1550 and 1600 °C. These activities were used together with the activities found by Rein and Chipman (1965) to reassess the activities of CaO and Al_2O_3 for the whole liquid region at 1550 and 1600 °C. The activity of Al_2O_3 agree better with the work by Rein and Chipman than the work by Kay and Taylor (1960) while the iso-activity curves of CaO agree better with the work by Kay and Taylor.

Morita et al. (2000) have done the most recent work on the activity of SiO_2 in the CaO-Al_2O_3-SiO_2 system. They used the same method as previously described for the binary CaO-SiO_2 and ternary CaO-MgO-SiO_2 systems at 1550 °C. Morita et al. (2002) also determined the activities of CaO and Al_2O_3. The activity curves for CaO agree well with the work by Rein and Chipman (1965) but the magnitude of the activities are somewhat lower. The activity curves for Al_2O_3 agree well with Rein and Chipman but the activities are lower above 30 mol% Al_2O_3.

A thermodynamic assessment of the system has also been done by Mao et al. (2006) and the activities they found are in relatively good agreement with Rein and Chipman (1965). Mao et al. also found a good agreement with Kalyanram et al. (1960) and Zhang et al. (1986) with respect to the activity of CaO.

The work by Rein and Chipman (1965) is considered to be most representative for the ternary CaO-Al_2O_3-SiO_2 system at 1600 °C because of the close agreement with the work by Morita et al. (2000) at 1550 °C.

Chapter 4

Experimental

A detailed description of the experimental procedure is given in this chapter starting with the preparation of materials. Apparatus and experimental procedure is then described in detail before the procedure for sample preparation and analysis. Much effort was put on accurate control of temperature and this work is also described here. Some important details about the analyses are given in the last part of this chapter.

4.1 Preparation of materials

Silicon used for the experiments had a purity of at least 8N. Boron powder with a purity of 99.7 % was used to dope (alloy) silicon with about 100 ppmw of boron. The boron doped silicon was made by melting the boron powder together with silicon in a graphite crucible under argon atmosphere. An induction furnace was used for the melting and the molten alloys were quenched in a water-cooled copper mold. The boron doped silicon was then crushed and sieved to a size fraction of 0.125 mm to 2.0 mm and cleaned by etching in hydrofluoric acid before washing in deionized water. The master alloys had a weight of several hundred grams and could be used for a series of experiments. Three batches of boron doped were made altogether where the first batch was used in the binary CaO-SiO_2 system. The second batch was used in the binary MgO-SiO_2 and ternary CaO-MgO-SiO_2 systems, while the third batch was used in the ternary CaO-Al_2O_3-SiO_2 system.

Master slags with a total weight of approximately 300 g each were made from 99.5 % pure or purer oxides bought from commercial suppliers. They were made by weighing and mixing the oxides to achieve the compositions given in table 4.1 before melting each mixture in a graphite crucible under argon atmosphere. The slags were melted and quenched in the same furnace as the silicon master alloy, but the slags were remelted at least two more times to ensure homogeneous composition. The slags were crushed to a powder in a tungsten carbide disk mill between each melting and crushed to -0.25 mm after

Table 4.1: Target composition of master slags in wt%.

ID.	CaO	MgO	Al_2O_3	SiO_2
M1	55	0	0	45
M2	36	0	0	64
M3	30	25	0	45
M4	0	35	0	65
M5	50	0	40	10
M6	50	0	10	40
M7	20	0	40	40
M8	20	0	10	70
M9*	50	0	0	50

*Doped with approximately 100 ppm boron

Table 4.2: Measured composition of master slags in wt% after normalization. Recovery before normalization is also shown.

ID.	CaO	MgO	Al_2O_3	SiO_2	Recovery (%)
M1	54.2	0.1	0.1	45.5	102.5
M2	36.2	0.1	$<$0.1	63.7	103.1
M3	30.8	23.6	0.1	45.3	100.8
M4	0.4	33.9	0.1	65.5	99.9
M5	50.1	0.1	38.9	10.7	102.8
M6	50.4	0.0	9.8	39.5	101.7
M7	20.9	0.1	40.9	38.0	101.3
M8	20.9	0.0	10.3	68.6	99.8
M9*	48.9	0.3	0.1	50.5	100.8

*Doped with approximately 100 ppm boron (as B_2O_3)

the final melting. One of the master slags was also doped with approximately 100 ppmw boron (as 99.98%B_2O_3). The composition of the master slags was measured by XRF after preparation and the measurement results are shown in table 4.2. The measured composition is seen to be in relatively good agreement with the targeted composition of the master slags. A recovery close to 100% before normalization also indicates good performance of the XRF instrument. Approximately 0.1% Fe_2O_3 was also detected in all master slags. The total amount of other oxides was measured to be less than 0.1%. In other words all the slags was measured to consist of at least 99.8% CaO, MgO, Al_2O_3 and SiO_2 in total. All measurement results of slag composition by XRF are given after normalization in the rest of this thesis.

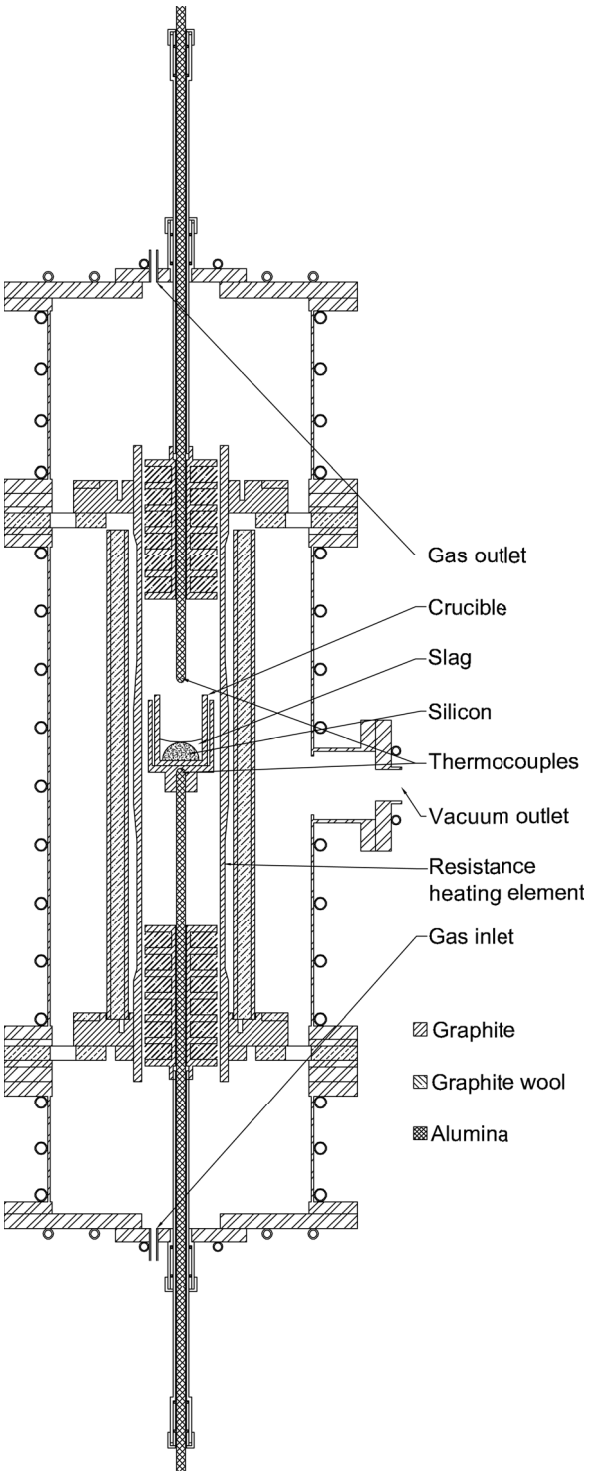

Figure 4.1: Drawing of furnace with a second thermocouple inserted from top that could be used for calibration of thermocouples.

4.2 Apparatus

A furnace of in house design was used for the majority of the experiments. Figure 4.1 shows a detailed drawing of the furnace. The furnace is heated by passing an electrical current through a graphite resistance tube. Graphite has a very high thermal shock resistance and the furnace can withstand rapid thermal cycling since only graphite is present in the hot zone of the furnace. The use of graphite restricts the atmosphere in the furnace to be either inert or reducing, and all experiments in this work were conducted under argon atmosphere at one bar pressure. B-type thermocouples (Pt-6%Rh/Pt-30%Rh) were used both to control and measure the temperature because they are known to be stable for very long periods of time at temperatures up to 1600 °C. Other benefits with the B-type thermocouple is the insensitivity to fluctuations around room temperature at the end connected to the logger (cold junction), and that pure copper can be used as extension wires.

A Eurotherm 2408 PID controller was connected to the thermocouple used to control the temperature while another thermocouple was used to measure and log the temperature right under the crucible throughout every experiment. Some of the initial experiments were performed with the controller connected to an S-type thermocouple placed outside the resistance heating tube. More easy regulation of temperature was however achieved by using a dual B-type thermocouple placed under the crucible where one was connected to the PID controller and the other was connected to the data logger.

4.3 Procedure

Equal amounts of slag and silicon was used for all experiments and most experiments were performed with 15 grams of silicon and 15 grams of slag. High purity graphite crucibles were used for most experiments and the crucibles were filled with silicon and slag before they were placed inside the furnace. The furnace was then evacuated to less than 3 millibar and refilled with 4N or 5N pure argon three times. Heating was started after the third evacuation and 1600 °C was reached in approximately 15 minutes, and the samples were held at this temperature for 0.6 to 18 hours. The heating was stopped after the targeted holding time and the samples cooled to the melting point of silicon in two minutes. The temperature was 150 °C below the melting point of silicon another two minutes after that again.

A somewhat different procedure was used for a series of experiments where silicon was alloyed with iron. For each experiment a graphite crucible was filled with a mixture of iron with 99.99 % purity and silicon with 8N purity. Five compositions with a total weight of 15 grams in the range from 50% iron and 50% silicon to 100% silicon were used. These mixtures were held at 1600 °C under argon atmosphere for one hour before being cooled to room temperature

again. This was done in the same furnace using the same procedure as in the majority of the experiments. A binary calcium silicate slag with 50 % CaO and 50% SiO_2 that had been doped with approximately 100 ppm boron (as 99.98 % B_2O_3) was then filled into the crucible on top of the solidified ferrosilicon alloy. The slag was made by mixing 150 g 99.98 % pure CaO with 150 g 99.99% pure SiO_2 and melting three times in the same way as the other master slags. The crucible was again placed inside the furnace and held at 1600 °C for 6 hours using the same procedure as previously described.

4.4 Sample preparation

Bulk composition of both slag and silicon was to be determined with as high accuracy as possible. Solidified slag and silicon were therefore separated after the crucible was cooled to room temperature aiming at keeping as much of both slag and silicon as possible. Possible inhomogeneities due to crystallization and segregation effects during solidification could in this way be minimized. This also minimized inhomogeneities that could be caused by non-equilibrium conditions.

A careful procedure was followed to achieve a good separation of graphite, slag and silicon. At first most of the graphite was machined away before the last thin layer of graphite was removed using a diamond grinder. Silicon and slag were after that broken away from each other piece by piece. Any visible remains of slag on silicon pieces and silicon on slag pieces were grinded away. The surfaces of the slag and silicon pieces was subsequently washed in HF or isopropanol and acetone before a second inspection of the surfaces of the slag and silicon pieces was done to ensure no remaining slag on the silicon pieces and no remaining silicon on the slag pieces respectively.

Sealed plastic bags and nitrile gloves were used when handling the materials after cleaning to avoid contamination. A tungsten carbide disk mill was used to crush the slag and silicon pieces to a homogeneous powder. Silicon with 9N purity was first crushed three times to ensure the crusher to be clean with respect to other elements than silicon, carbon, tungsten and cobalt. The crusher was cleaned and rinsed with acetone between each sample. Silicon samples were crushed before slag samples to avoid cross-contamination of silicon with slag forming elements.

4.5 Analysis

The ICP-MS instrument *Thermo Scientific Element 2* was used to determine the boron content in both silicon and slag samples. This instrument was also used to determine the concentration of slag forming elements and iron in silicon. Three sub-samples of 20-45 mg was taken from each powdered sample and analysed. Each sub-sample was dissolved in 1.5 mL ultrapure 68% HNO_3

(in house) and 0.5 mL Suprapur® 40% HF (Merck) before they were diluted to 216 or 250 mL with deionized water.

Any significant inhomogeneity of the samples would be seen as a large standard deviation between the sub-samples. Very high reaction rates were observed for the dissolution of the silicon samples. In later analyses 0.5 mL of deionized water was added to the silicon sample before the acids to bring down both the temperature and reaction rate. The analysis results were the same as before when doing this, but a less vigorous dissolution was obtained. The slag samples needed an additional treatment after adding acids in order to dissolve. In this treatment the slag samples were heated to 240 °C at 100 bars pressure and held at this temperature for 10 minutes using a Milestone UltraCLAVE.

A metallurgical silicon standard reference material from NIST was analysed together with all silicon samples while either a geological reference material or a slag was analysed together with the slag samples. The analyses of these materials were in reasonable agreement with the reference values with respect to boron for all analysis runs. The composition of the slag samples with respect to the major elements were determined by XRF using fused glass disks with 0.5 grams of sub-sampled slag.

The Thermo Scientific Element 2 is a double focusing magnetic sector field inductively coupled plasma mass spectrometer which has a much higher resolving power than the more common quadrupole-based ICP-MS instruments. Most mass interferences encountered using a quadrupole instrument is eliminated because of the much higher resolution. Detection limits are also better than for a quadrupole instrument because of extremely low background levels and very high sensitivity. The book by Thomas (2004) describes this type of mass spectrometer in detail and more details about mass spectroscopy can also be found there.

4.6 Temperature control

Knowledge of the temperature profile in the region with the most uniform temperature inside the furnace is needed for accurate temperature measurements. The temperature profile in the hot zone was measured both from top and bottom of the furnace using a B-type thermocouple. Measurement both from tom and bottom was mainly done to eliminate uncertainties caused by the thermocouple acting as a hot or cold finger on the shoulders of the hot zone. Figure 4.2 shows the measured temperature and a significant difference in measured temperature is seen in both ends of the hot zone of the furnace because of this effect.

A more uniform temperature of the hot zone was desired and the furnace was modified so that the vertical position of the radiation shield above and below the hot zone became adjustable. Figure 4.1 shows the furnace after

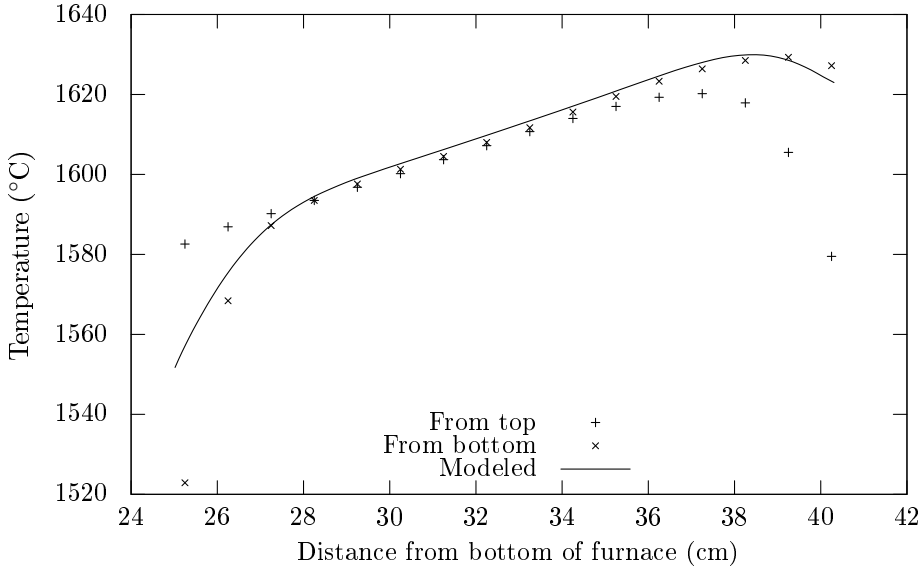

Figure 4.2: Measured and modelled temperature profile of the furnace.

this modification. It was however found that adjustment of these did not give any significant change to the temperature profile of the hot zone. Therefore the temperature inside the furnace was also modelled using COMSOL Multiphysics.

The temperature inside the furnace was modelled by adjusting the voltage on the electrical connectors in the model until a temperature of 1600 °C was reached in the middle of the hot zone of the furnace. The outer walls of the furnace were fixed at 20 °C in the model. Thermal and electrical conductivity data from the graphite heating element supplier was used. The modelled temperature profile can be seen in figure 4.2. An excellent agreement is seen between the modelled and measured temperature profile in the middle of the hot zone. The geometry of the Comsol model is shown in figure 4.5. The model was only compared with temperature measurements around the hot zone because this was the region where the temperature has to be accurately determined. Outside this region the thermocouples could also act as hot or cold fingers, preventing accurate temperature measurements there.

Adjustment of the different parts of the furnace was done in the model in order to find a suitable way to get a more homogeneous temperature in the hot zone of the furnace. From the model it was found that adjustment of the vertical position of the heating element was the most simple and efficient way of adjusting the temperature profile in the hot zone of the furnace. Adjustment of the element was done according to the model and the new temperature profile is shown together with the modelled temperature profile in figure 4.3.

The measured temperature profile is seen from figure 4.3 to have a sad-

dle shape. From the model it was found that increasing the thickness of the graphite felt surrounding the heating element would eliminate this. A thicker layer of graphite felt was inserted to the furnace according to this. The temperature profile given in figure 4.4 was obtained after some trial and error with fine adjustment of the thickness of the graphite felt and the position of the heating element. The bottom of the crucible stand was subsequently adjusted to be 34.25 cm above the bottom of the furnace.

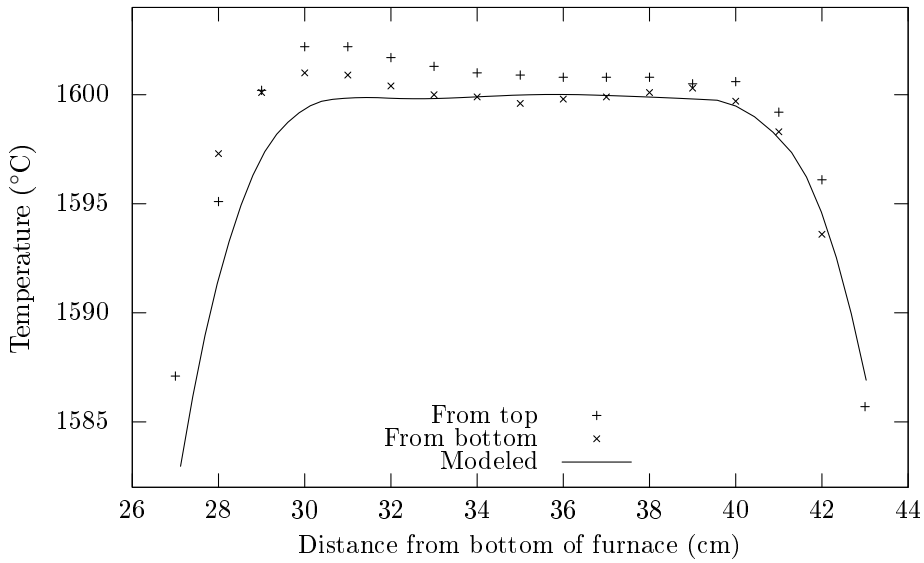

Figure 4.3: Improved temperature profile of the furnace after adjustment according to the model.

The temperature profile shown in figure 4.4 was considered to be so uniform that the furnace could be used to check the calibration of thermocouples. A thermocouple that had been UKAS[1] calibrated at 1550 °C was used to check the calibration of the thermocouple used to measure the temperature during the experiments in this work. The thermocouples were inserted from opposite ends of the furnace with the tips of the alumina protection tubes touching in the middle of the hot zone of the furnace. The corresponding distance between the thermocouple junctions were approximately 1 cm and the temperature gradient in the hot zone is at most 0.1 °C per cm. A temperature difference of 0.4 °C was found between the thermocouples, which is much less than the uncertainty of ±1.7 °C (95 % confidence interval) of the calibrated thermocouple.

[1] United Kingdom Accreditation Service

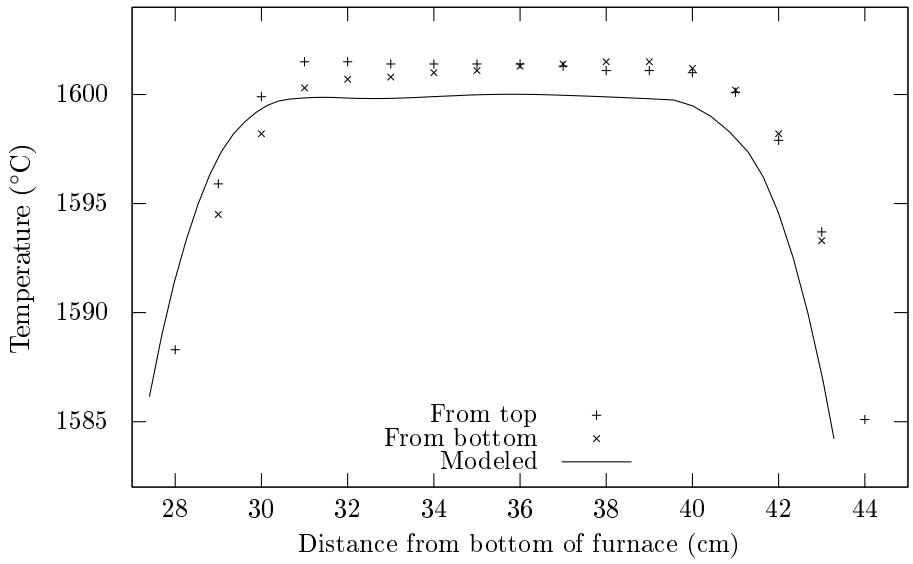

Figure 4.4: Final temperature profile of furnace after fine adjustment of heating element and thickness of graphite felt surrounding the heating element. The crucible stand was placed with the bottom at 34.25 cm.

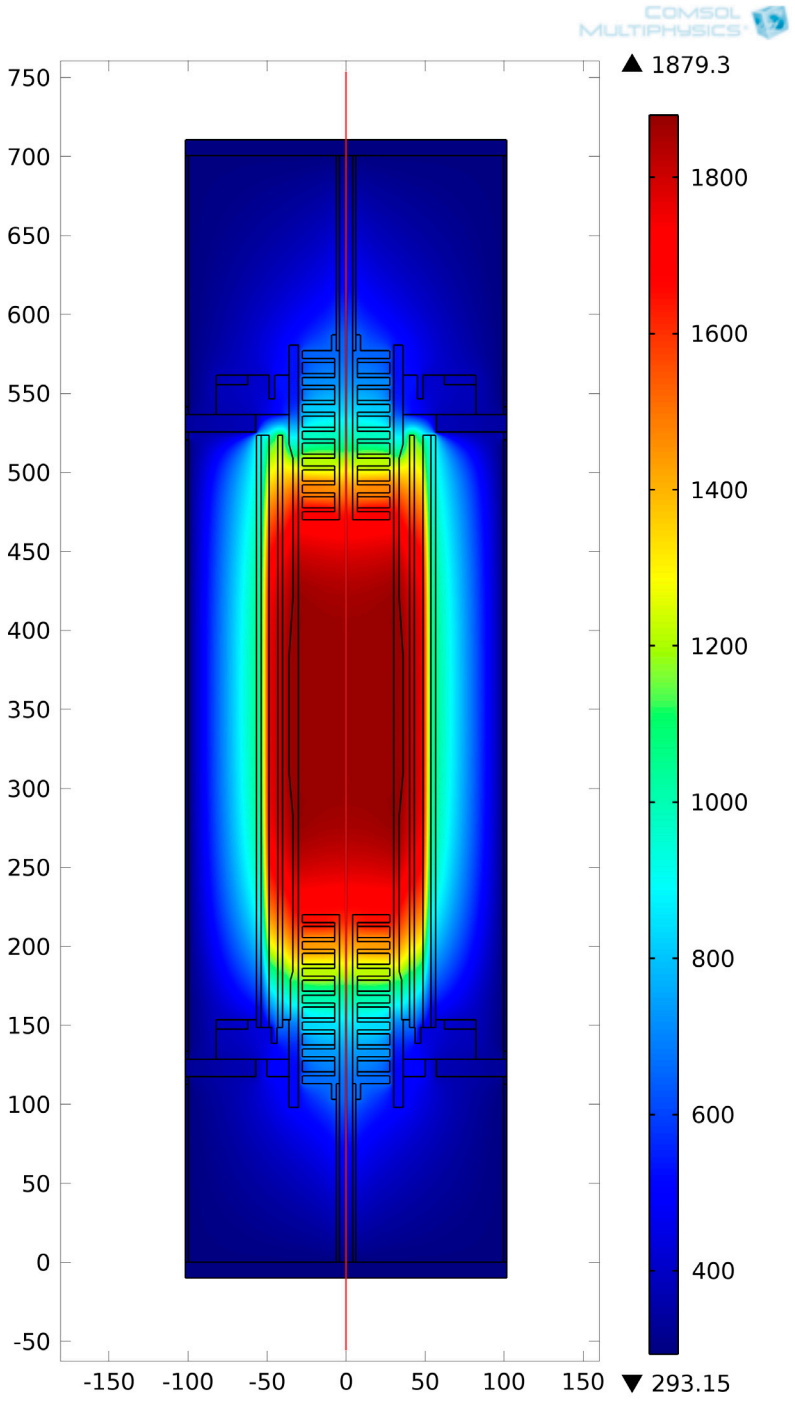

Figure 4.5: Geometry used in COMSOL Multiphisics and modelled temperature distribution where the unit on the axes is in millimetres and the temperature is in Kelvins. Rotation symmetry around $r = 0$ was used in the model.

4.7 Some analytical considerations

A few details related to the ICP-MS analyses needs special consideration. One is the presence of outliers and another is dissolution of slag and silicon before analysis. Also the repeatability of the measurements from one one analytical run to another is of high importance.

Analytical repeatability

Experiment MS7 (table 5.5) was analysed in three replicate splits on three different days. The confidence intervals for this experiment is therefore calculated from the three repeated analyses of three replicate splits. It is seen from the confidence intervals that the dispersion of the results between analysis runs is of the same magnitude as the dispersion between three replicate splits within one analytical run. Some of the other experiments were also reanalysed and almost same results were found in both analyses. The average value of these analyses were used where the confidence intervals are based on the pooled standard deviation of the three replicate splits.

Outliers

Classical statistical methods were used in this work. Classical statistical methods break down on data with large outliers and these outliers had to be considered separately. Only a few outliers was found in the analyses and they are underlined in table 4.3. These outliers were identified by observation of the large relative standard deviation of the three replicate splits as compared all other samples. Also the significant deviation of the outlier from the two other analyses was taken as an indication of the outlier. The mean and the confidence interval for these samples were therefore calculated from the two remaining analyses.

The outlier for the analysis of CS0 could also be identified by the low measured concentration of silicon shown in the table. A measured concentration of just 73% silicon was taken as an indication that either the weighing of the sample was incorrect or that silicon was not completely dissolved. Incomplete dissolution of silicon may have happened if less than 0.5 mL HF was added. The concentration of silicon was measured for all the samples and was mostly found to be between 90 and 100%. Silicon is the sample matrix and an exact measurement of the expected 100% was therefore not possible when using ICP-MS. Large deviations like the one for CS0 can however be used as a possible indication of an outlier. Especially when the relative deviation is correlated between silicon and other measured elements like it is for with boron the analysis of CS0.

Estimates of the average and the dispersion of the data by robust statistical methods would not have been affected by these outliers. The closeness between

the median (a robust estimator) before elimination of the outliers and the mean (not robust) after elimination of the outliers demonstrates this for the data in table 4.3.

Table 4.3: Analyses where an outlier was found in one of the replicate splits. The outliers are underlined and the unit of the numbers is ppmw except for silicon. (RSD = Relative Standard Deviation)

ID.	CS0	CS0	CS13	CMS8	CMS17	CMS20	CAS1
Element	B	Si (wt%)	B	Mg	Mg	Ca	B
Split 1	<u>96.1</u>	<u>73.0</u>	<u>69.5</u>	<u>2882</u>	750	137	<u>53.5</u>
Split 2	120.1	91.2	57.9	2035	715	<u>873</u>	40.3
Split 3	116.3	89.4	56.5	2029	<u>1848</u>	139	39.2
RSD (%)	12	12	12	21	58	111	18

Dissolution of slag and silicon

Some of the first slag samples were held in an ultrasonic bath for one hour at approximately 70 °C. This was found to be insufficient to completely dissolve the slag. The measured slag composition for these samples are shown in table 4.4. The main thing to notice is that the recovery of boron in the system is low when using these analytical results. The calculated distribution coefficient is also lower since the measured concentration of boron in slag is lower than it should be. Using an UltraCLAVE gave a recovery of boron close to 100% for almost all samples indicating that the slag is completely dissolved.

Some heat was generated by the reaction taking place during dissolution of silicon. BF_3 is a volatile component that may evaporate during sample dissolution if the temperature is too high. A 90-100% recovery of silicon for most samples is however taken as an indication that the temperature has been kept sufficiently low to avoid this. The concentration of silicon is several orders of magnitude higher and SiF_4 has a similar volatility as BF_3 and silicon should therefore be lost from the system before loss of boron occurs.

Table 4.4: Measured boron concentration in slag when using an ultrasonic bath at approximately 70 °C for one hour to dissolve the slag. Boron recovery is calculated using the boron concentration from CS0.

	B in Slag	L_B	Recovery
CS3	63.8 ± 2.4	1.7	86.2
CS6	69.6 ± 10.1	2.0	88.9
CS7	53.4 ± 2.1	1.7	76.2
CS8	65.5 ± 6.2	1.5	87.6
CS11	81.9 ± 3.3	2.2	100.8

Chapter 5

Results

The main focus of this work has been to determine the equilibrium distribution of boron between silicon and $CaO\text{-}SiO_2$, $MgO\text{-}SiO_2$, $CaO\text{-}MgO\text{-}SiO_2$ and $CaO\text{-}Al_2O_3\text{-}SiO_2$ slags. It is important to know if equilibrium is reached and the time to reach equilibrium therefore had to be determined. Experiments to determine the equilibrium time were thus performed first for each of the slag systems before the rest of the experiments were performed. Hence, equilibrium time is discussed first before the thermodynamic data for each slag system. Most experiments have been conducted with boron doped silicon, but some experiments have also been conducted with pure silicon to approach equilibrium by transfer of boron from slag to silicon. The slag contained boron for all these experiments, and they are labelled *pure silicon*. The influence of iron on the distribution coefficient has also been investigated by adding up to 50 wt% iron to silicon and the results from these experiments are presented. Mass loss from the system is considered in the end of this chapter. The error bars in this chapter indicates a 95% confidence interval based on three replicate splits.

Figure 5.1 shows a cross-section of the crucible after 6 hours for the most silica-rich slag in the binary $CaO\text{-}SiO_2$ system. The silicon is seen to be in the middle surrounded by slag. This geometry was the same for most experiments except for the series with iron alloying of silicon. In these experiments the alloy was premelted in the crucible before slag was added and the alloy remained in the bottom of the crucible for all these experiments, as can be seen in figure 5.2 for the experiment with 35% iron in the alloy.

5.1 The binary $CaO\text{-}SiO_2$ system

The main parameter determining the rate of transfer of boron from silicon to slag is the diffusivity of boron in the system. It is known from Nishimoto et al. (2012) that the mass transfer is controlled by the slag phase. Krystad et al. (2012) found the equilibrium time to be approximately 2 hours at 1600 °C when using 15 g silicon and 15 g slag containing 50% CaO and 50% SiO_2.

Figure 5.1: Cross-section of crucible after 6 hours experiment with the most silica-rich binary CaO-SiO_2 slag.

Figure 5.2: Cross section after complete removal of crucible from experiment with ferrosilicon containing 35% iron.

From the Stokes-Einstein equation (2.27) we know that diffusivity is inversely proportional to viscosity and in figure 2.7 we see that the viscosity increases significantly with increasing SiO_2 content in the slag. The most SiO_2 rich master slag was therefore selected for determination of equilibrium time. Table 5.1 shows the initial composition and final composition after different holding times. The slag compositions are shown in figure 5.3 as a function of time and it is seen that the SiO_2 content in the slag decreases while the CaO content increases. The change is relatively small and will therefore not have a big influence on the equilibrium values. This indicates that SiO_2 is lost from the slag and the reaction

$$SiO_2(l) + C(s) = SiO(g) + CO(g) \tag{5.1}$$

is probably the main cause of this loss. In later experiments also the mass loss was measured and was found to be increasing approximately linearly with time.

The calcium and boron concentrations in silicon and the boron concentrations in slag after different holding times are shown in table 5.1. The initial concentrations are also shown in the table and it is seen that the boron content in the starting slag is very low. Equilibrium is therefore approached by transfer of boron from silicon to slag. For calcium on the other hand equilibrium is reached by mass transfer from slag to silicon. The distribution coefficient is shown as a function of time in figure 5.4 and equilibrium is seen to be reached within 6 hours. One experiment was conducted with pure silicon and a boron doped slag, and the distribution coefficient is seen to have approximately the

Table 5.1: Initial composition and final composition after different holding times in the experiments performed to determine equilibrium time in the binary CaO-SiO_2 system. Uncertainty is given as 95% confidence intervals based on the analysis of three replicate splits.

ID.	Time (h)	SiO_2 (wt%)	CaO (wt%)	B in Slag (ppmw)	B in Si (ppmw)	Ca in Si (ppmw)
CS0	0	63.7	36.2	< 3	$118.2 \pm 24.0^{\dagger}$	< 30
CS1	0.6	63.2	36.3	21.2 ± 5.0	102.1 ± 2.0	355 ± 173
CS2	3	62.3	37.4	74.4 ± 3.1	45.1 ± 3.1	393 ± 162
CS3	6	60.3	39.4	81.5 ± 3.0	36.0 ± 3.7	840 ± 276
CS4[(1)]	9	57.7	42.1	57.3 ± 8.1	26.8 ± 3.4	630 ± 117
CS5[(2)]	6	62.1	37.7	98.8 ± 4.1	46.4 ± 3.6	644 ± 214

[1] Boron doped silicon from the batch used in the MgO-SiO_2 slag system.
[2] Pure silicon and a separately made boron doped slag.
[†] Based on two replicate splits.

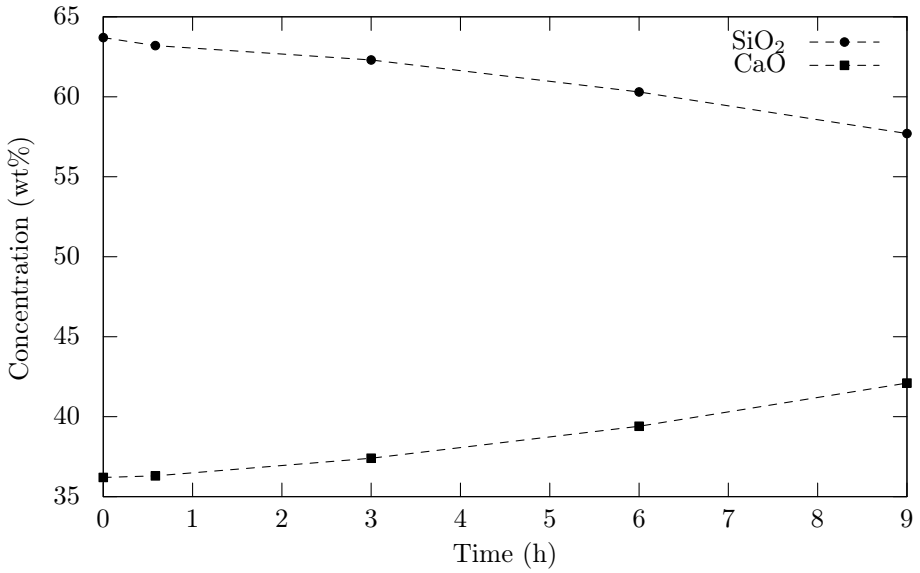

Figure 5.3: Change of slag composition with holding time in the experiments performed to determine equilibrium time in the binary CaO-SiO_2 system.

same value as the experiments with boron doped silicon with 6 and 9 hours holding time. This confirms that equilibrium has been reached in 6 hours and an equilibrium time of 6 hours was chosen for most experiments in the rest of the binary CaO-SiO_2 system.

The boron recovery is defined as the sum of boron detected in slag and silicon relative to the initial content in slag and silicon. The initial boron

content in slag for the experiments with boron doped silicon is so low that it is set to zero for the recovery calculations. Boron recovery is also shown in figure 5.4 and it is seen to be approximately 100% for all experiments except the 9 hour experiment. No obvious explanation has been found for the low recovery of boron in this experiment. A 100 % recovery of boron in the liquid phases (slag and silicon) indicates that no boron is lost as a gaseous species. It also indicates that the analytical measurements are consistent; no boron is lost through the sample preparation, both slag and silicon are completely dissolved and there is no contamination of the samples.

The calcium concentration in silicon as a function of time is shown in figure 5.5 and it seems reasonable to assume that equilibrium has been reached within 6 hours even though the data are somewhat scattered.

The slag composition will as mentioned above change somewhat during the equilibration time and a new equilibrium corresponding with the new slag composition may therefore cause a continuous non-equilibrium state. The change of slag composition is however relatively small and equilibrium is seen to be reached within 6 hours. It can therefore be concluded that equilibrium between slag and silicon is reached so fast that they are in equilibrium even if the slag composition changes somewhat with time.

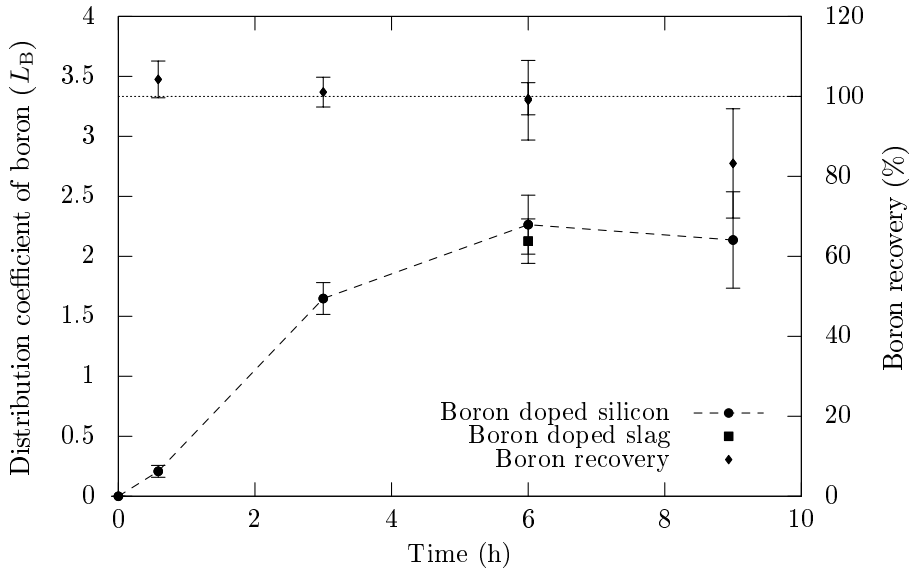

Figure 5.4: Distribution coefficient of boron as a function of time. Recovery of boron relative to the total boron content in slag and silicon initially is also shown.

Equilibrium results from the experiments in the binary CaO-SiO_2 system is shown in table 5.2. The distribution coefficient of boron is shown as a function of slag composition in figure 5.7 where the experiments with 6 and 9

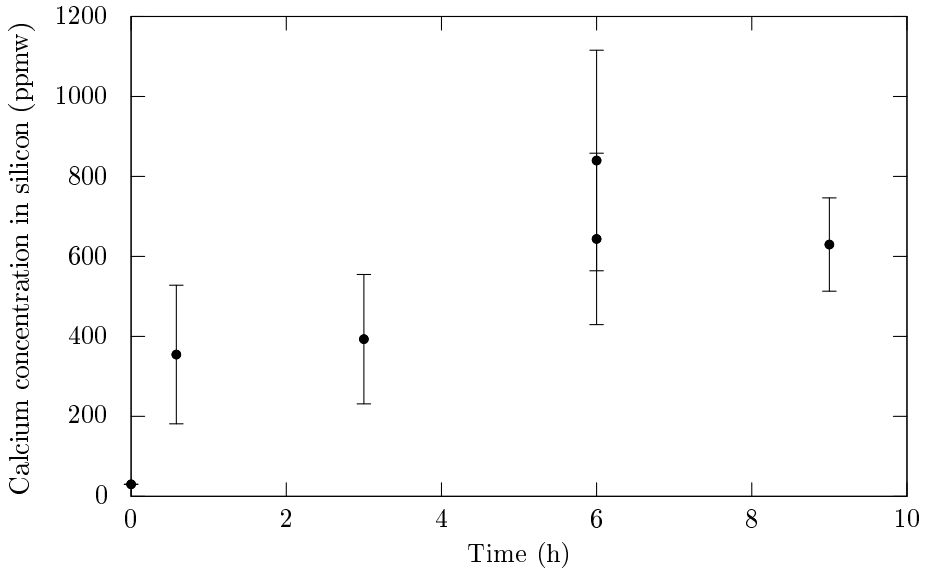

Figure 5.5: Calcium concentration in silicon as a function of time.

hours holding time from table 5.1 also are included. A linear trend is seen with $L_B = 2.0$ in the silica rich end of the system and $L_B = 2.5$ in the CaO rich end. The recovery of boron is also shown in the figure and it is around 100% for most experiments indicating that no boron is lost during experiments or analysis. The equilibrium time was expected to be shorter than 6 hours for experiments in the CaO rich end of the system because of the lower viscosity. Two experiments confirm that equilibrium has been reached already after 3 hours when the CaO/SiO_2 mass ratio is larger than one. Three experiments were also conducted with a boron doped slag to approach equilibrium by mass transfer in the opposite direction. The distribution coefficient found from these experiments confirms the values obtained in the other experiments. One experiment was also conducted in a silica crucible to attain silica saturation. A holding time of 18 hours was used because the slag has a very high viscosity at this composition. Pure silicon and a boron doped slag were used for this experiment and the value of the distribution coefficient was found to be in line with the other experiments.

The calcium concentration in silicon in equilibrium with $CaO\text{-}SiO_2$ slags is shown in figure 5.8 and it is seen to increase significantly when the CaO/SiO_2 mass ratio becomes higher than one. The final slag compositions are shown in the binary $CaO\text{-}SiO_2$ phase diagram in figure 5.6 and it is seen that the SiO_2 saturated slag as expected has a composition close to the liquidus line. The most CaO-rich slag on the other hand seems to be slightly outside the liquid region indicating that the slag may be partially solid. The activity of the slag should however not change after the composition has crossed the liquidus line.

In other words the calcium concentration in silicon should remain constant with changing slag composition on this side of the liquidus line.

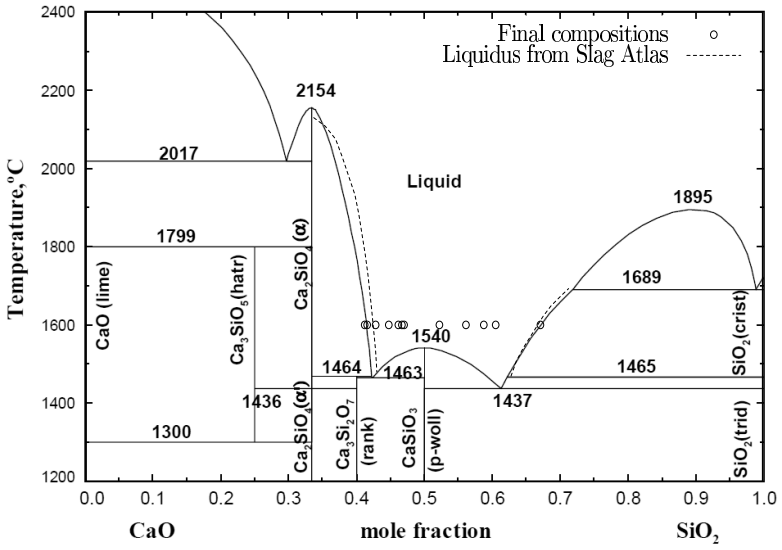

Figure 5.6: Final slag compositions shown in the CaO-SiO_2 phase diagram (Jung et al., 2005). The liquidus line from the Slag Atlas (1995) around 1600 °C is also indicated in the figure.

Four silicon samples were analysed for boron and calcium content and four slag samples were analysed for boron content by ICP-OES at an external laboratory. The results from these analyses are shown in table 5.3. The boron concentrations from these analyses are somewhat lower than the analyses by ICP-MS. The initial boron concentration in silicon is even lower with a measured concentration of 83 ppmw as compared to 118 ppmw measured by ICP-MS. The measured value of 83 ppmw is not consistent with the other measurements as illustrated by boron recovery relative to initial concentration at the bottom of table 5.3. The measured distribution coefficient of boron on the other hand is almost identical with the ICP-MS measurements as can be seen in figure 5.7. This illustrates an important point about determination of the distribution coefficient of boron. The measured concentration of boron may be biased but the measured distribution coefficient will be accurate as long as the bias is the same for both slag and silicon. Measurement of boron concentration in slag and silicon should therefore preferentially be done at the same time at the same instrument to minimize bias and all measurements in this work have been conducted according to this. In figure 5.8 the calcium concentration in silicon measured by ICP-OES is seen to agree very well with the ICP-MS measurements. Both the distribution coefficient of boron and the calcium concentration in silicon are therefore considered to be accurately determined by ICP-MS.

Table 5.2: Main experiments in the binary CaO-SiO_2 system. Initial and final slag composition is shown to the left. Boron and calcium concentration in silicon and boron concentration in slag is shown to the right. Uncertainty is given as 95% confidence intervals based on the analysis of three replicate splits.

	Before (wt%)		After (wt%)		B in Slag	B in Si	Ca in Si
ID.	SiO_2	CaO	SiO_2	CaO	(ppmw)	(ppmw)	(ppmw)
CS6[1]	59.1	40.7	53.8	45.9	82.4 ± 6.7	36.6 ± 7.7	1061 ± 151
CS7[1]	54.6	45.2	48.6	51.1	82.7 ± 7.0	34.7 ± 4.9	3723 ± 634
CS8[1,2]	50.0	49.7	47.7	51.9	90.4 ± 1.9	36.9 ± 2.2	3903 ± 144
CS9			46.3	53.4	90.7 ± 5.3	38.9 ± 1.9	4504 ± 1192
CS10[2]	45.5	54.2	44.3	55.3	85.6 ± 2.4	34.0 ± 3.6	7422 ± 1348
CS11[1]			43.1	56.6	90.0 ± 8.3	35.6 ± 0.7	14141 ± 469
CS12[3]	∼65	∼35	68.4	31.2	43.9 ± 1.3	21.5 ± 4.3	372 ± 63
CS13[4]	45.5	54.2	42.6	56.8	128.3 ± 5.3	$57.2 \pm 9.1^{\dagger}$	17638 ± 1450
FS5[5]	50.5	48.9	48.2	51.3	66.0 ± 3.0	25.7 ± 2.9	3006 ± 217

[1] Average calcium concentration from two analyses. Confidence interval based on pooled standard deviation.
[2] 3 hours holding time
[3] Silica saturated slag, boron doped silicon and 18 hours holding time
[4] Silicon alloyed with 5% calcium and boron doped slag
[5] Experiment also shown last in table 5.12
† Based on two replicate splits.

Table 5.3: Analyses performed at an external laboratory by ICP-OES. Two slag samples and two silicon samples were selected from the equilibrium time experiments and two slag samples and two silicon samples were selected from the main experiments.

	CS0	CS3	CS7	CS11
B in slag (ppmw)	1.1	67	66	70
B in Si (ppmw)	83	29	29	27
Ca in Si (wt%)	0.007	0.08	0.38	1.3
Boron recovery	100 %	114 %	113 %	115 %

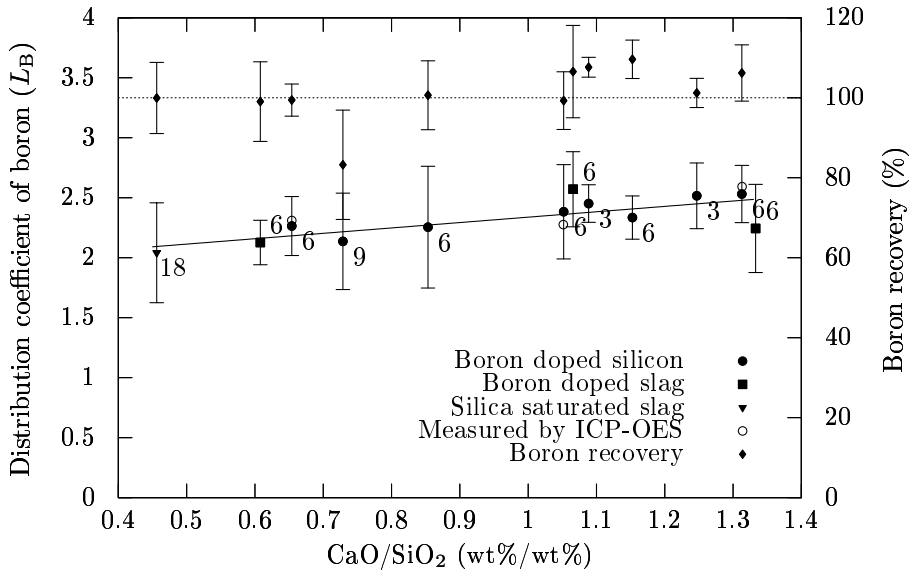

Figure 5.7: Distribution coefficient of boron as a function of slag composition in the binary CaO-SiO_2 system. Holding time is shown beside the data points. Recovery of boron relative to total initial content in slag and silicon.

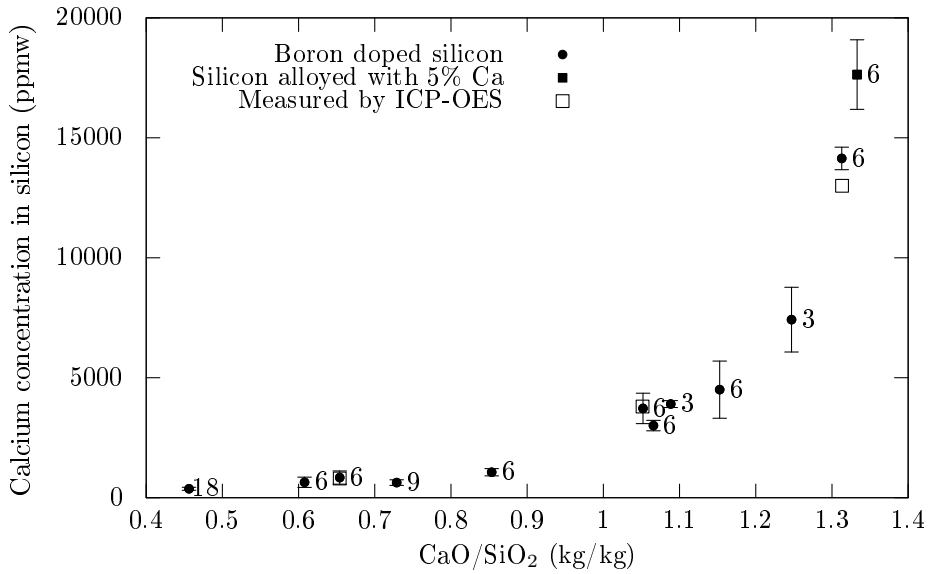

Figure 5.8: Calcium concentration in silicon as a function of slag composition in the binary CaO-SiO_2 system. Holding time is shown beside the data points.

5.2 The binary MgO-SiO_2 system

Both magnesium and MgO are known to be volatile. All experiments except one in this system were therefore carried out with lid to decrease mass loss. Six experiments were conducted with 5 g slag and 5 g silicon in graphite crucibles in an alumina tube furnace. One of these experiments had a holding time of 18 hours but too little material was left after the experiment for proper analysis to be done. This experiment is therefore not discussed any further. Table 5.4 shows the change of slag composition and mass loss with time. Two experiments with 15 g slag and 15 g silicon and one experiment with silicon coated crucible walls were conducted in the graphite resistance tube furnace used for the majority of the experiments in this thesis. These three experiments are also included in table 5.4. Pure silicon and a crucible without lid was used in one of the experiments with 15 g slag and 15 g silicon, and equilibrium was hence approached by transfer of boron from slag to silicon instead of by transfer from silicon to slag as in the other experiments.

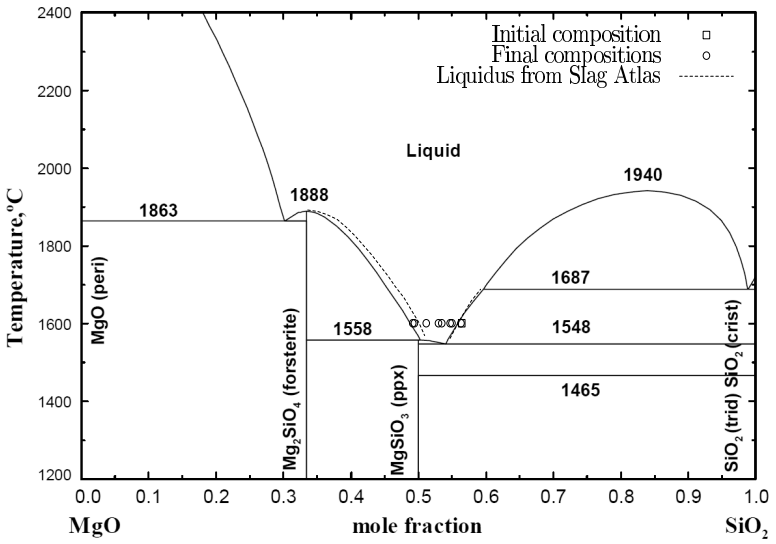

Figure 5.9: Initial and final slag compositions shown in the MgO-SiO_2 phase diagram (Wu et al., 1993). The liquidus line from the Slag Atlas (1995) around 1600 °C is also indicated in the figure.

The initial and final slag compositions are shown in the phase diagram for the MgO-SiO_2 slag system in figure 5.9. The change of slag composition with time is shown together with mass loss in table 5.4 and figure 5.10 for the experiments conducted in an alumina tube furnace. It is seen that the SiO_2 content in the slag decreases with time while the CaO and MgO content increases. The mass loss was much larger for the experiments with 15 g slag and 15 g silicon. The larger mass loss is expected since the total masses were

Table 5.4: Slag composition and mass loss for experiments in the MgO-SiO_2 slag system.

ID.	Time (h)	SiO_2 (wt%)	MgO (wt%)	CaO (wt%)	Mass loss (g)
MS0	0	65.5	33.9	0.38	0
MS1	1	65.3	34.0	0.41	0.10
MS2	2	64.1	35.2	0.42	0.31
MS3	3	63.8	35.4	0.42	0.40
MS4	6	62.7	36.6	0.43	0.65
MS5	9	58.6	40.6	0.50	1.28
MS6[1]	6	58.9	40.5	0.43	3.25
MS7[1,2]	6	60.4	38.6	0.58	4.43
MS8[3]	12	62.2	37.0	0.58	0.56

[1] 15 g silicon 15 g slag
[2] No lid and starting with pure silicon
[3] Silicon coated crucible walls

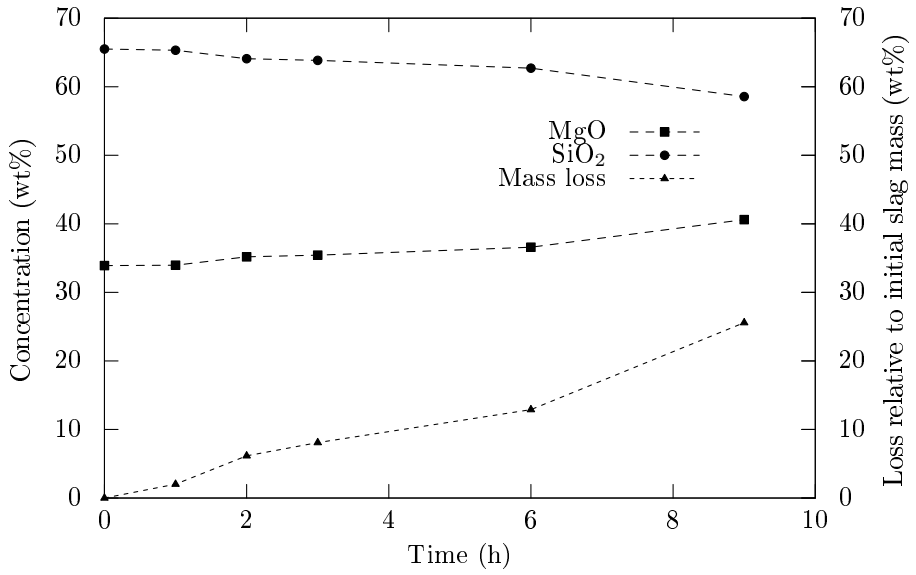

Figure 5.10: Change of slag composition for MgO and SiO_2 on the left axis as a function of time. Mass loss is on the right axis and it is seen to increase with time.

larger, but also the relative mass loss was larger than for the experiments with 5 g slag and 5 g silicon. Graphite crucibles from a different supplier were used for the experiments with larger mass and this graphite may have been more reactive towards the slag causing a larger mass loss through reaction (5.1). A film of silicon was observed between the slag and the crucible wall after

the 12 hour experiment. The mass loss was lower in this experiment than in experiments with a shorter holding time. The film probably prevented direct reaction between SiO_2 in the slag and the graphite crucible causing the lower mass loss. The mass loss and change of slag composition is seen in table 5.4 and figure 5.10 to be correlated; larger relative mass loss gives lower SiO_2 concentration in the slag.

Table 5.5: Magnesium and boron concentration in silicon and boron concentration in slag in the binary MgO-SiO_2 system. Uncertainty is given as 95% confidence intervals based on the analysis of three replicate splits.

ID.	Time (h)	B in Slag (ppmw)	B in Si (ppmw)	Mg in Si (ppmw)
MS0	0	69.7 ± 1.1	101.1 ± 10.7	< 10
MS1	1	67.3 ± 2.2	94.0 ± 9.5	466 ± 173
MS2	2	74.3 ± 11.5	92.7 ± 11.1	586 ± 234
MS3	3	79.6 ± 8.5	83.1 ± 3.1	747 ± 76
MS4	6	110.5 ± 2.4	52.8 ± 0.8	1044 ± 175
MS5	9	125.2 ± 1.9	52.0 ± 1.5	1533 ± 318
MS6[1]	6	99.9 ± 4.3	51.8 ± 2.2	1059 ± 212
MS7[1,2]	6	47.6 ± 7.4	21.6 ± 2.7	818 ± 50
MS8[3]	12	112.2 ± 17.1	53.4 ± 9.7	791 ± 75

[1] 15 g silicon 15 g slag. Analysed two times.
[2] No lid and starting with pure silicon. Analysed three times.
[3] Silicon coated crucible walls

The initial and final concentrations of boron in slag and silicon are shown in table 5.5 together with the magnesium concentration in silicon. The initial concentration of boron in silicon was approximately 100 ppmw while the initial concentration in slag was approximately 70 ppmw. The boron in the slag came together with the MgO used to make the slag. Equilibrium was hence approached by transfer of boron from slag to silicon in the experiments performed with pure silicon. No additional doping of the slag with boron was necessary for these experiments since the slag already contained boron. The distribution coefficient of boron is shown in figure 5.11 together with the recovery of boron. The distribution coefficient is seen to reach equilibrium in six hours with an equilibrium value of 2.1 in the most silica rich side of the system and with a maximum value of 2.4 in the MgO rich side of the system.

After one hour it is seen that the concentration of boron in slag and silicon is almost identical with the initial concentration in slag and silicon. The slag composition has not changed much either, but both slag and silicon was observed to have been melted. After two and three hours the slag composition has changed somewhat more, but the distribution coefficient of boron is still

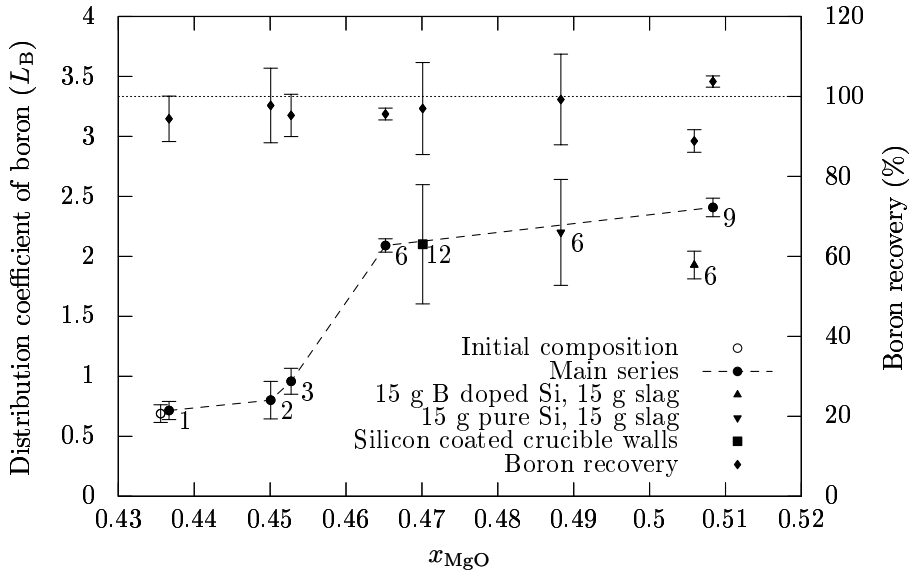

Figure 5.11: Distribution coefficient of boron (L_B) as a function of slag composition. The recovery of boron is also shown. Holding time (hours) is shown beside each data point. It should be noted that the slag contained 70 ppmw boron initially for all experiments.

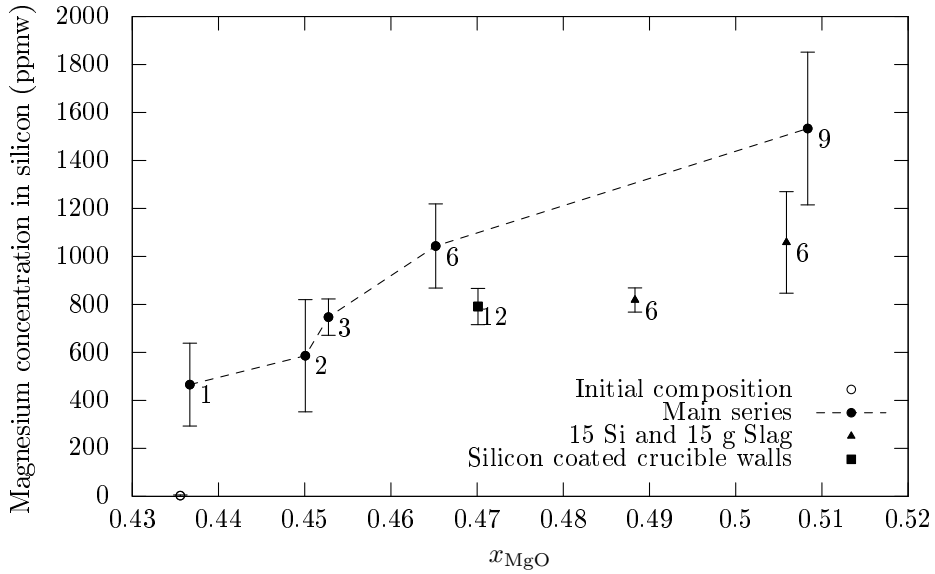

Figure 5.12: Magnesium concentration in silicon as a function of slag composition. Holding time (hours) is shown beside each data point.

almost the same as the initial value. Significant transfer of boron from silicon to slag does not start until the holding time has exceeded three hours. A combination of two factors may explain the delayed onset of mass transfer. Firstly the temperature was not measured inside the furnace for the experiments in the alumina tube furnace, and slow heating of the crucible and its contents may have caused the slag and silicon to remain partially solid for a while. Secondly the initial slag composition is seen in figure 5.9 to be slightly outside the liquid region even at 1600 °C and the mass transfer may therefore have been slower initially because the slag was partially solid SiO_2.

The recovery of boron is close to 100% and increases slightly with change of slag composition. This increase correlates with mass loss (and hence change of slag composition) indicating that boron is not lost from the system. The experiment with 15 g of boron doped silicon and 15 grams of slag is seen not to be in line with the other experiments. Both the recovery of boron and the distribution coefficient of boron is lower than the trend seen from the other experiments. No obvious explanation for this deviation has been found.

The magnesium concentration in silicon is shown in figure 5.12 as a function of slag composition. No clear trend towards equilibrium is seen, but it seems fair to assume that equilibrium between slag and silicon with respect to magnesium has been reached within six hours. The experiments performed in the alumina tube furnace are seen to give a higher concentration of magnesium in silicon than the experiments performed in the graphite tube furnace. No reasonable explanation for this difference has been found.

5.3 The ternary CaO-MgO-SiO_2 system

Twenty experiments were performed in the ternary CaO-MgO-SiO_2 system in addition to the experiments in the binary CaO-SiO_2 and binary MgO-SiO_2 systems. All twenty experiments had a holding time of 6 hours at 1600 °C and were performed with 15 g slag and 15 g silicon. Viscosity data was used as a basis for determining equilibrium time also in this system. Diffusivity is, as mentioned earlier, inversely proportional to viscosity and the most viscous slags are therefore expected to have the longest equilibrium time. Figure 5.13 shows the viscosity of the ternary CaO-MgO-SiO_2 system at 1500 °C and it is seen to be almost constant with constant SiO_2 content. The equilibrium time of 6 hours found in the binary CaO-SiO_2 and binary MgO-SiO_2 systems were therefore also used in the ternary system. These experiments were performed with the same batch of boron doped silicon as the experiments in the binary MgO-SiO_2 system.

The initial and final slag compositions are shown in table 5.6. The initial slag compositions are also shown in figure 5.14 while the final compositions are shown in figure 5.15. These two figures also include the binary systems. Reaction between carbon and SiO_2 was probably the main mechanism for

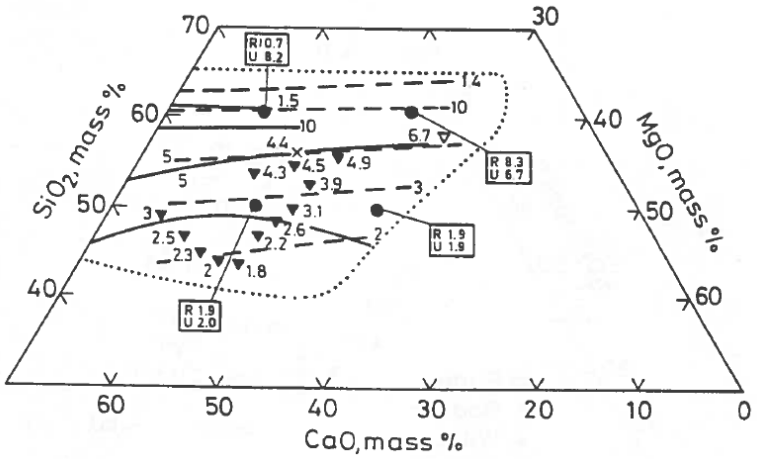

Figure 5.13: Viscosity of the ternary CaO-MgO-SiO_2 system at 1500 °C from the Slag Atlas (1995).

mass loss and change of slag composition, where the mass loss was between 1.7 and 4.4 g for all experiments.

Table 5.7 shows the boron concentration in slag and silicon after all twenty experiments in the ternary CaO-MgO-SiO_2 system. The distribution coefficient of boron is shown for all twenty experiments in figure 5.16 and it is seen to be between 1.8 and 2.5 without any clear trends. It should be remembered that all MgO containing slags also contained boron, and with that in mind experiments with pure silicon were performed for the three most SiO_2 rich slags to approach equilibrium by transfer of boron from the slag to silicon. In that way it was possible to ensure that equilibrium was reached within 6 hours. These experiments are marked with an asterisk and the values of the distribution coefficient for these experiments compared with the experiments with boron doped silicon indicate that equilibrium has been reached within 6 hours. In the same way one additional experiment with pure silicon were also conducted for the 30%CaO-25%MgO-45%SiO_2 system and the distribution coefficient was found to be the same ($L_B = 2.33$) as for the experiment with boron doped silicon ($L_B = 2.32$).

The results can be divided into two groups depending on SiO_2 content as shown in figure 5.15. The slags with high and low SiO_2 content is compared in figure 5.17 and it is seen that the dependence of L_B on SiO_2 content in the binary CaO-SiO_2 system not continues into the ternary CaO-MgO-SiO_2 system. It is also seen that the distribution coefficient is unchanged when CaO is replaced with MgO.

The calcium and magnesium concentrations in silicon after all twenty experiments are also shown in table 5.7. The concentration of calcium in silicon in equilibrium with CaO-MgO-SiO_2 slags are shown in figure 5.18 and it is

Table 5.6: Initial and final slag compositions in the CaO-MgO-SiO_2 system.

	Before (wt%)			After (wt%)		
ID.	SiO_2	CaO	MgO	SiO_2	CaO	MgO
CMS1	59.1	34.8	6.0	54.5	38.6	6.7
CMS2	54.5	33.5	11.8	49.6	37.0	13.2
CMS3	49.9	32.2	17.7	46.8	36.7	16.3
CMS4	45.3	36.7	17.7	45.1	41.0	13.6
CMS5	45.5	48.3	6.0	43.7	52.0	4.1
CMS6	60.5	13.8	25.5	53.9	16.8	29.1
CMS7	45.4	42.5	11.9	44.5	46.2	9.0
CMS8	55.5	27.3	17.0	49.8	32.0	18.0
CMS9	50.5	40.7	8.5	46.9	44.8	8.0
CMS10	50.3	23.2	26.2	47.6	25.8	26.4
CMS11	55.4	15.6	28.8	50.1	18.0	31.7
CMS12	60.4	8.0	31.3	52.7	9.3	37.7
CMS13	45.3	30.8	23.6	46.5	34.4	18.9
CMS14*				45.4	33.7	20.7
CMS15	64.1	27.2	8.5	57.8	32.6	9.4
CMS16*				61.8	28.3	9.6
CMS17	64.6	18.3	17.0	58.6	22.0	19.2
CMS18*				57.0	23.2	19.6
CMS19	65.0	9.3	25.4	58.9	11.3	29.6
CMS20*				61.3	10.0	28.4

* Experiment with pure silicon

seen that the calcium concentration increases significantly with decreasing MgO and SiO_2 content in the slag. Magnesium has a somewhat different trend as can be seen in figure 5.19. The magnesium concentration increases with decreasing SiO_2 content in the slag while it does not have a increasing trend with decreasing CaO content in the slag. The experiments with pure silicon works as replicates with respect to calcium and magnesium, but the final slag composition is somewhat different than for the experiments with the same slags and boron doped silicon. The concentration of calcium and magnesium obtained from these experiments does however agree well with the trend obtained in the other experiments.

Table 5.7: Concentration of boron in slag and concentration of boron, calcium and magnesium in silicon after experiments. Uncertainty is given as 95% confidence intervals based on the analysis of three replicate splits.

ID.	B in slag (ppmw)	B in Si (ppmw)	Mg in Si (ppmw)	Ca in Si (ppmw)
CMS1	65.1 ± 1.6	30.0 ± 4.3	293 ± 69	734 ± 125
CMS2	72.8 ± 6.0	33.9 ± 3.0	1354 ± 204	1726 ± 191
CMS3	83.1 ± 6.5	36.8 ± 2.9	2846 ± 383	3231 ± 436
CMS4	82.6 ± 5.6	37.7 ± 2.7	3862 ± 316	6264 ± 511
CMS5	69.6 ± 3.2	29.2 ± 2.8	1690 ± 321	13076 ± 1389
CMS6	90.3 ± 5.4	38.0 ± 5.2	1551 ± 216	265 ± 26
CMS7	78.7 ± 1.0	32.5 ± 2.7	3632 ± 328	8208 ± 986
CMS8	80.9 ± 6.6	33.6 ± 1.9	$2032 \pm 40^{\dagger}$	1710 ± 247
CMS9	71.1 ± 2.5	28.6 ± 1.4	975 ± 129	3139 ± 1059
CMS10	104.7 ± 9.3	42.3 ± 3.2	5113 ± 487	2010 ± 107
CMS11	99.9 ± 6.8	43.6 ± 1.0	3433 ± 420	656 ± 127
CMS12	110.6 ± 6.0	43.9 ± 3.9	2090 ± 234	155 ± 55
CMS13	102.3 ± 4.5	44.2 ± 1.4	5373 ± 326	5691 ± 703
CMS14*	37.3 ± 2.4	16.0 ± 0.9	7445 ± 794	6215 ± 826
CMS15	67.0 ± 1.8	29.4 ± 1.8	282 ± 29	346 ± 19
CMS16*	14.1 ± 2.1	7.7 ± 1.1	324 ± 42	342 ± 28
CMS17	75.1 ± 3.2	33.6 ± 0.8	$733 \pm 223^{\dagger}$	327 ± 96
CMS18*	23.4 ± 1.3	9.8 ± 1.0	775 ± 142	397 ± 69
CMS19	94.1 ± 10.4	38.3 ± 1.8	905 ± 51	92 ± 2
CMS20*	40.6 ± 1.8	16.1 ± 4.0	721 ± 166	$138 \pm 4^{\dagger}$

* Experiment with pure silicon

† Based on two replicate splits.

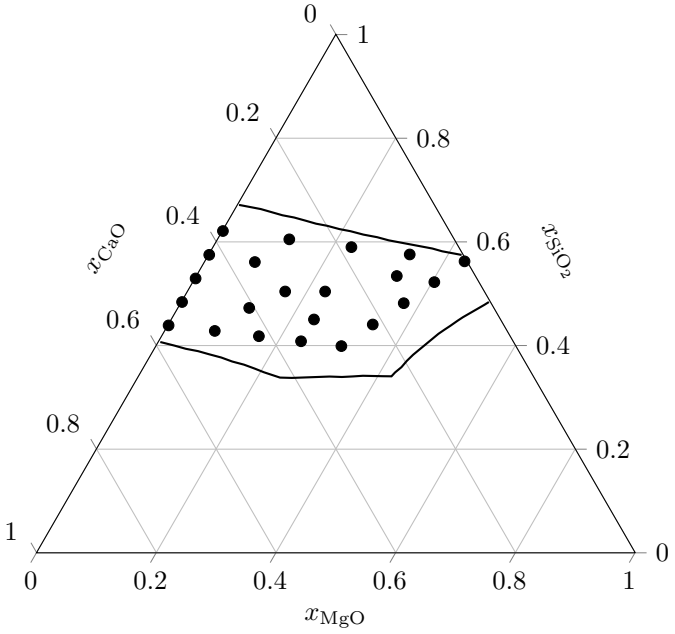

Figure 5.14: Inital compositions in the ternary CaO-MgO-SiO_2 system including the binary systems.

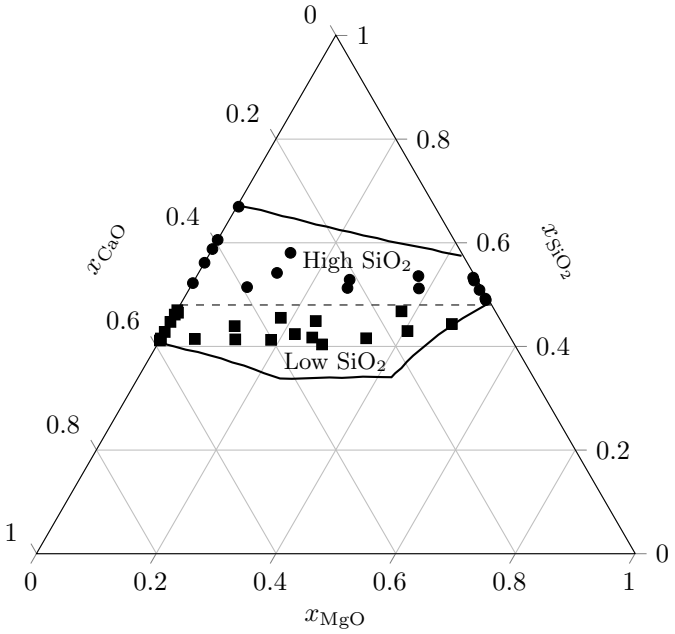

Figure 5.15: Final compositions in the ternary CaO-MgO-SiO_2 system including the binary systems. The system is divided into two regions with high and low SiO_2 content respectively.

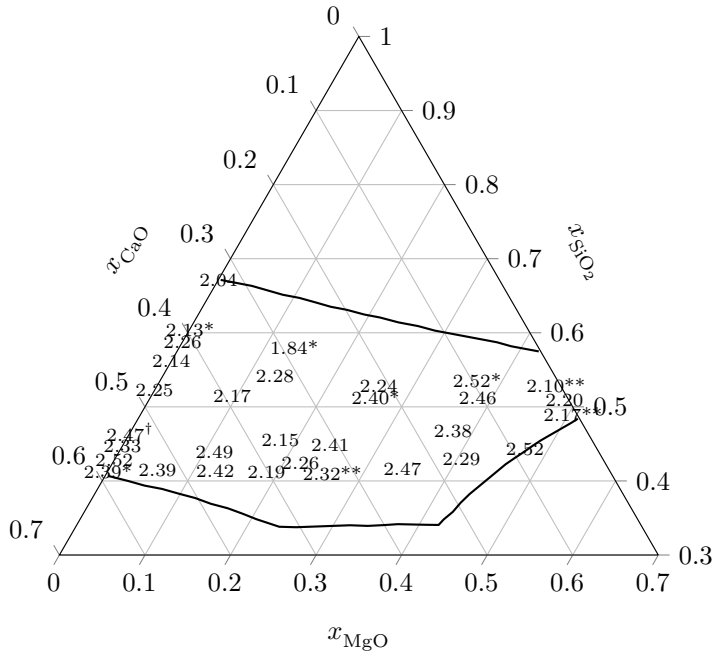

Figure 5.16: Distribution coefficient of boron in the ternary CaO-MgO-SiO_2 system. (* Experiment with pure silicon. ** Mean value of experiment with pure silicon and experiment with boron doped silicon. † Mean value of three experiments)

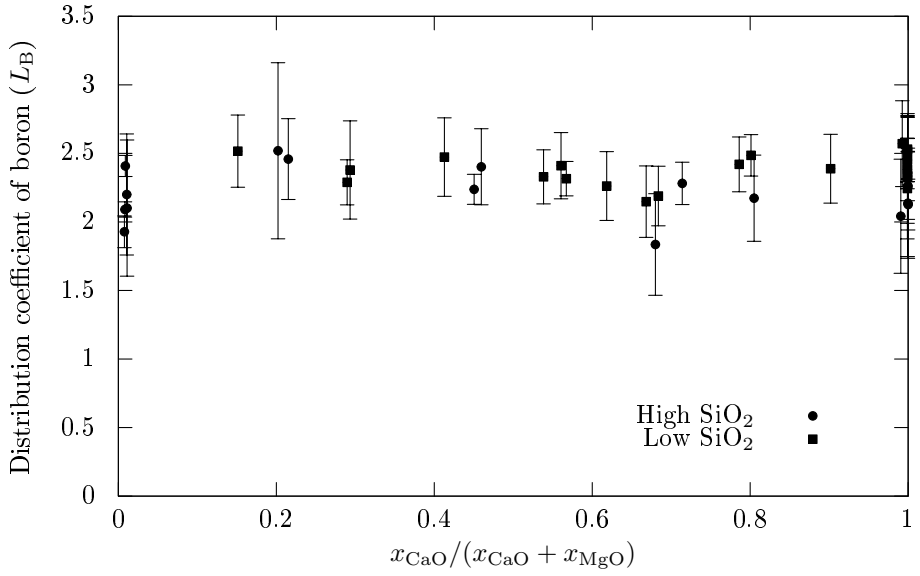

Figure 5.17: Distribution coefficient of boron for slags with a high and low SiO_2 content in the CaO-MgO-SiO_2 system including the binary systems.

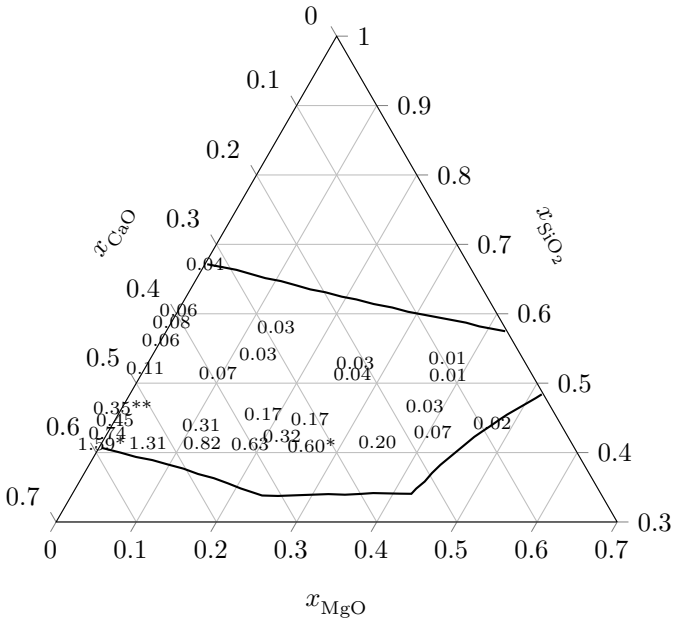

Figure 5.18: Concentration of calcium in silicon in equilibrium with ternary CaO-MgO-SiO_2 slags as found in the present study. (* Mean value of two experiments. ** Mean value of three experiments.)

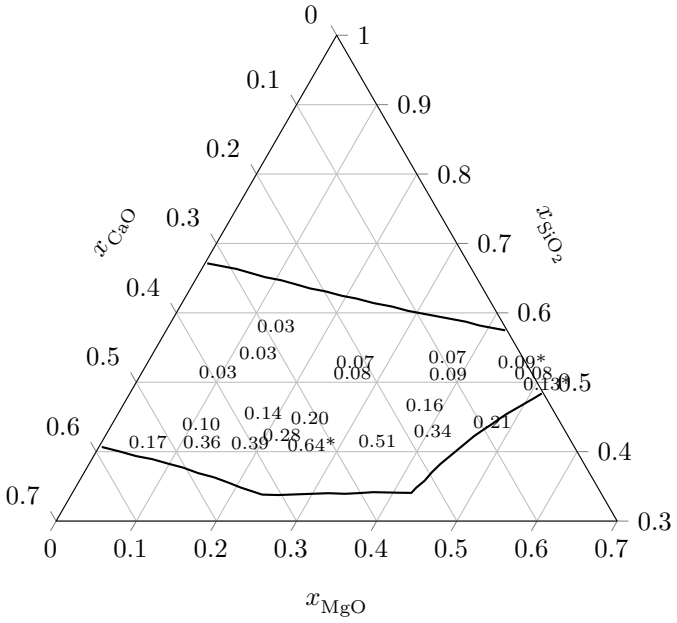

Figure 5.19: Concentration of magnesium in silicon in equilibrium with ternary CaO-MgO-SiO_2 slags as found in the present study. (* Mean value of two experiments.)

5.4 The ternary CaO-Al_2O_3-SiO_2 system

Six slag compositions were investigated in the ternary CaO-Al_2O_3-SiO_2 system. These slag compositions are shown in figure 5.20 where three of them have a higher CaO content than the three others. These two groups are denoted "High CaO" and "Low CaO" respectively.

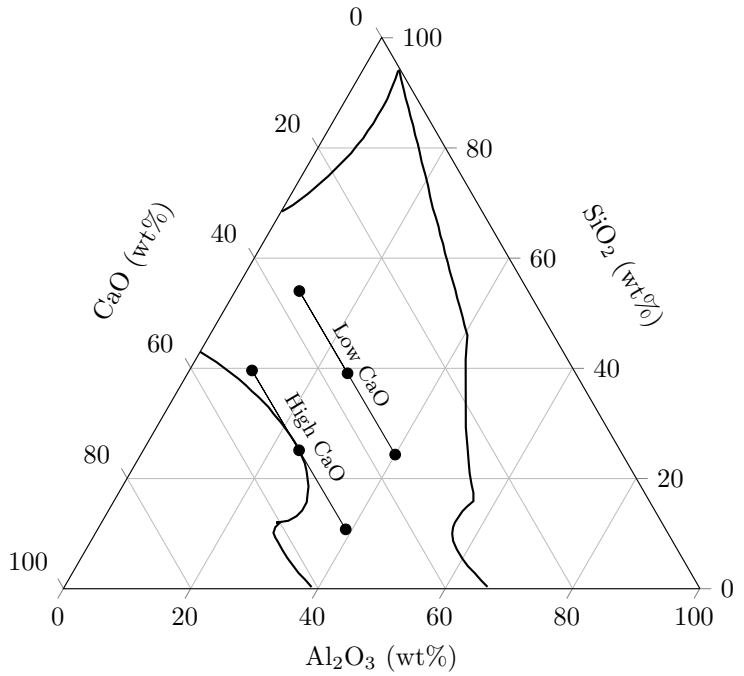

Figure 5.20: Initial slag compositions in the CaO-Al_2O_3-SiO_2 system.

The slag composition 35.7%CaO-40.0%Al_2O_3-24.3%SiO_2 was used to determine the equilibrium time in this slag system where the holding time was 3, 5.8 and 9 hours. This slag was chosen because it has the highest viscosity of the two slags with the highest Al_2O_3 content. It is seen in figure 5.21 that viscosity is approximately constant for constant CaO content. Diffusivity is inversely proportional to viscosity and the most viscous slags are therefore expected to have the longest equilibrium time. The three slags in the "Low CaO" group are therefore considered to have approximately the same equilibrium time. The three slags in the "High CaO" group are in the same way considered to have approximately the same equilibrium time which should be shorter than for the "Low CaO" group due to the lower viscosity.

Initial slag composition and slag composition after different holding times are shown in table 5.8 together with the mass loss. The mass loss was found by weighing the graphite crucible before and after each experiment. The graphite crucibles themselves had no mass loss when heated empty and neither had the

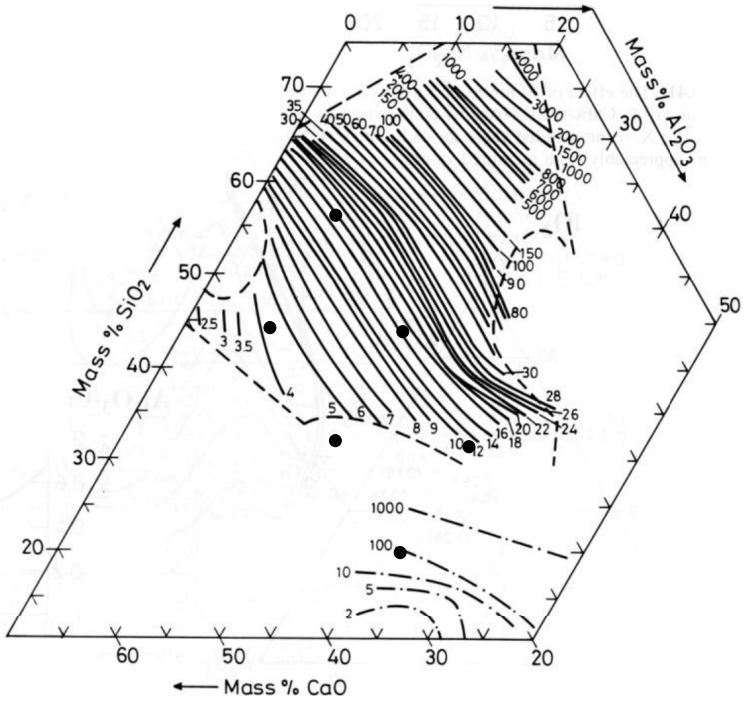

Figure 5.21: Viscosity of the ternary CaO-Al_2O_3-SiO_2 system at 1500 °C from the Slag Atlas (1995). Initial slag compositions are also indicated.

slags when heated in a platinum crucible and the mass loss was therefore caused by reactions between graphite, slag and silicon. The slag composition and mass loss is shown in figure 5.22 as a function of time. At first the SiO_2 content increased while the CaO and Al_2O_3 content decreased indicating that the predominating reaction at first was reduction and dissolution of calcium and aluminium into the silicon phase. From three hours holding time and upwards the SiO_2 concentration decreased while the CaO and Al_2O_3 increased indicating loss of SiO_2 from the slag.

Table 5.8: Slag composition and mass loss after different holding times.

ID.	Time (h)	CaO (wt%)	Al_2O_3 (wt%)	SiO_2 (wt%)	Mass loss (g)
CAS0	0	35.5	39.9	24.4	0.00
CAS1	3	34.9	38.0	26.9	0.24
CAS2	5.8	35.1	38.2	26.5	0.44
CAS3	9	35.6	38.5	25.7	0.74

The boron concentration in slag and silicon is shown in table 5.9 where the initial boron content was approximately 84 ppmw in silicon and 7 ppmw

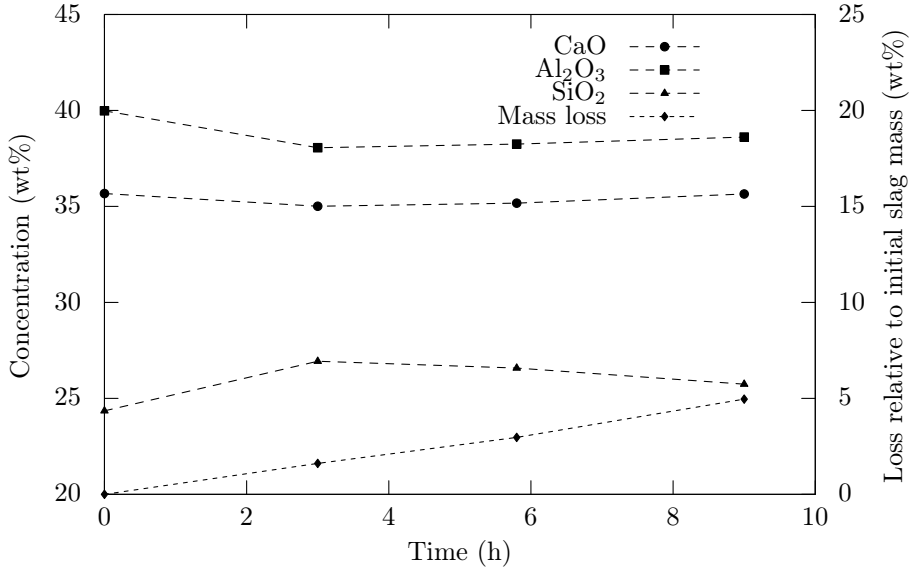

Figure 5.22: CaO, SiO_2 and Al_2O_3 concentration in slag as a function of time on the left axis. Mass loss is on the right axis and is seen to increase linearly with time.

in the slag. Also the calcium and aluminium content in silicon is shown in this table. The distribution coefficient of boron and recovery of boron in the system is shown in figure 5.23. It is seen that no boron is lost from the system and that equilibrium with respect to boron is reached after 3 hours with an equilibrium value of 1.3 for the distribution coefficient of boron.

Table 5.9: Calcium, aluminium and boron concentration in silicon, and boron concentration in slag. Uncertainty is given as 95% confidence intervals based on the analysis of three replicate splits.

ID.	Time (h)	B in slag (ppmw)	B in Si (ppmw)	Ca in Si (wt%)	Al in Si (wt%)
CAS0	0	7.3 ± 1.2	84.4 ± 7.3	< 0.025	< 0.001
CAS1	3	51.1 ± 3.3	$39.7 \pm 7.2^{\dagger}$	0.80 ± 0.07	1.23 ± 0.07
CAS2	5.8	52.4 ± 3.8	39.3 ± 3.0	0.86 ± 0.08	1.27 ± 0.09
CAS3	9	52.7 ± 1.9	38.2 ± 1.3	1.11 ± 0.09	1.48 ± 0.11

† Based on two replicate splits.

In figure 5.24 it is seen that the calcium and aluminium concentration in silicon increased significantly from the initial concentrations after three hours holding time. This coincide with the change of slag composition during the same time period discussed above and confirms that the change of slag

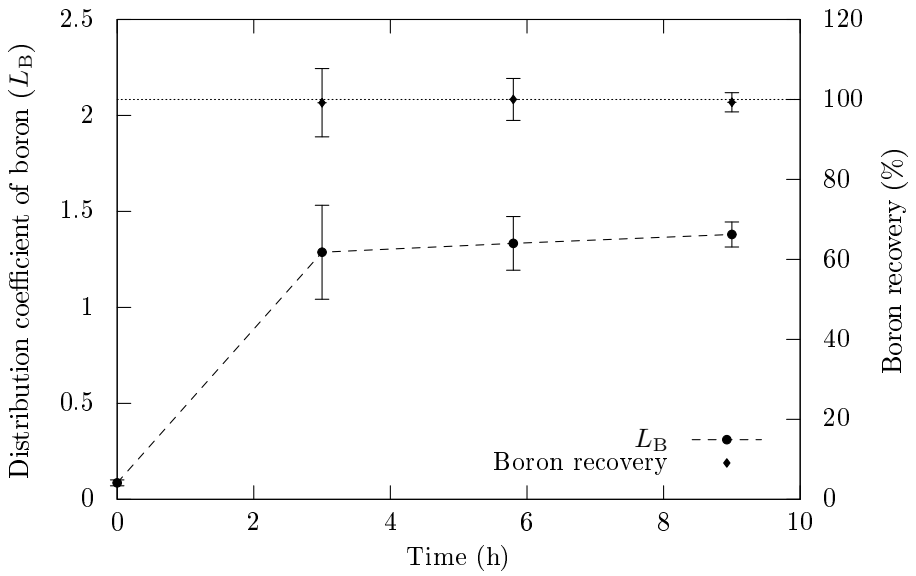

Figure 5.23: Distribution coefficient of boron (L_B) and boron recovery as a function of time. No boron is lost from the system and equilibrium with respect to boron is reached after 3 hours.

composition after the three first hours is caused by reduction of calcium and aluminium into the silicon phase. The calcium and aluminium concentration in silicon is approximately the same after three and six hours while it is somewhat higher after nine hours. It seems that the equilibrium time with respect to calcium and aluminium also was three hours. The increased concentration of both calcium and aluminium from six to nine hours is probably caused by decreased activity of SiO_2 and increased activity of CaO and Al_2O_3 caused by decreased SiO_2 content in the slag.

A holding time of 9 hours was chosen for the three slags with the lowest CaO content. The equilibrium time has previously been shown to be 6 hours in the SiO_2-rich side of the binary calcium silicate system and 9 hours should therefore with good margin be a long enough holding time for these slags. A holding time of 6 hours was deemed to be sufficient holding time for the slags with the highest CaO content since they have a much lower viscosity, as can be seen in figure 5.21.

The slag composition before and after experiments are shown in table 5.4. The mass loss was between 0.4 and 2.0 grams for these experiments. Table 5.11 shows the boron, calcium and aluminium concentration in silicon and the boron concentration in slag after the experiments. The distribution coefficient of boron is shown as a function of slag composition in figure 5.25. Two values of the distribution coefficient from the binary calcium silicate system is also included in this figure. It is seen that the distribution coefficient decreases with

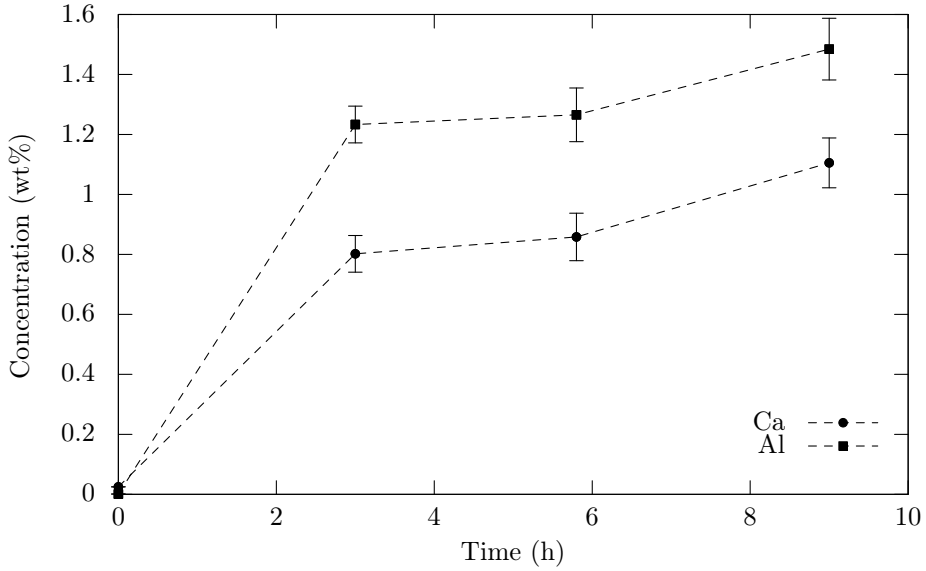

Figure 5.24: Calcium and aluminium concentration in silicon as a function of time.

increasing Al_2O_3 content to a value of approximately 1.3. The decrease is also seen in figure 5.26 as a function of $x_{Al_2O_3}/x_{SiO_2}$ for high and low CaO content. The CaO content does not seem to have much influence in the distribution coefficient of boron in this system either, but it is seen to be higher for the two of three slags with a high CaO content. This tendency agrees with the trend found in the binary CaO-SiO_2 system. The calcium and aluminium concentration in silicon in equilibrium with CaO-Al_2O_3-SiO_2 slags is shown in figure 5.27 and 5.28 respectively. The concentration of calcium and aluminium increases as expected with decreasing SiO_2 content in the slag.

Table 5.10: Slag composition before and after experiments.

	Time	Before (wt%)			After (wt%)		
ID.	(h)	CaO	Al_2O_3	SiO_2	CaO	Al_2O_3	SiO_2
CAS4	6	50.4	9.8	39.5	50.6	9.4	39.9
CAS5	6	50.3	24.3	25.1	45.4	22.3	32.1
CAS6	9	50.1	38.9	10.7	42.4	35.7	21.7
CAS7	9	35.7	10.1	54.1	39.6	10.8	49.5
CAS8	9	35.7	25.4	38.8	37.8	24.9	37.2

Table 5.11: Calcium, aluminium and boron concentration in silicon, and boron concentration in slag.

ID.	Time (h)	B in slag (ppmw)	B in Si (ppmw)	Ca in Si (wt%)	Al in Si (wt%)
CAS4	6	68.9 ± 11.0	33.2 ± 5.7	1.95 ± 0.13	0.33 ± 0.02
CAS5	6	66.5 ± 3.9	39.0 ± 1.0	4.56 ± 0.23	1.28 ± 0.05
CAS6	6	56.2 ± 9.2	42.3 ± 7.2	6.69 ± 0.71	2.55 ± 0.29
CAS7	9	60.9 ± 8.6	31.2 ± 6.7	0.12 ± 0.03	0.054 ± 0.013
CAS8	9	59.4 ± 6.1	38.0 ± 8.4	0.49 ± 0.06	0.51 ± 0.08

Uncertainty is given as 95% confidence intervals based on the analysis of three replicate splits.

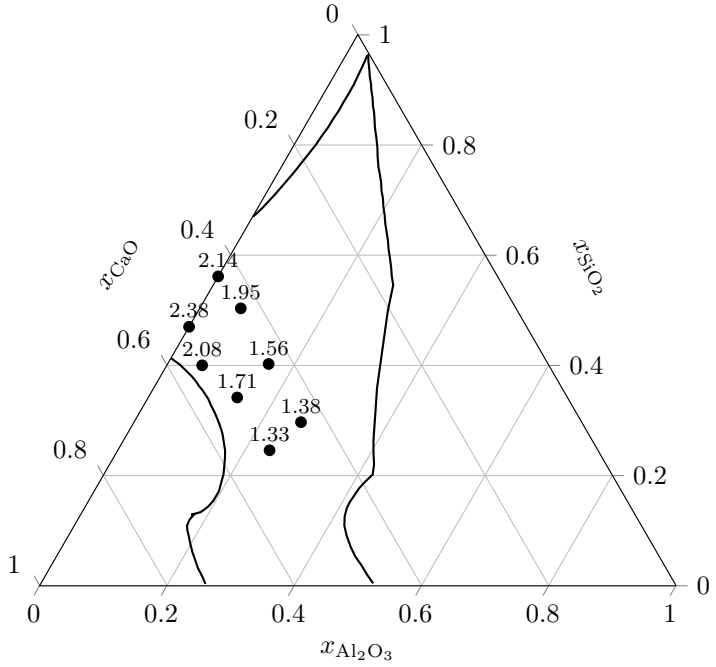

Figure 5.25: Distribution coefficient of boron for different slag compositions in the CaO-Al_2O_3-SiO_2 system.

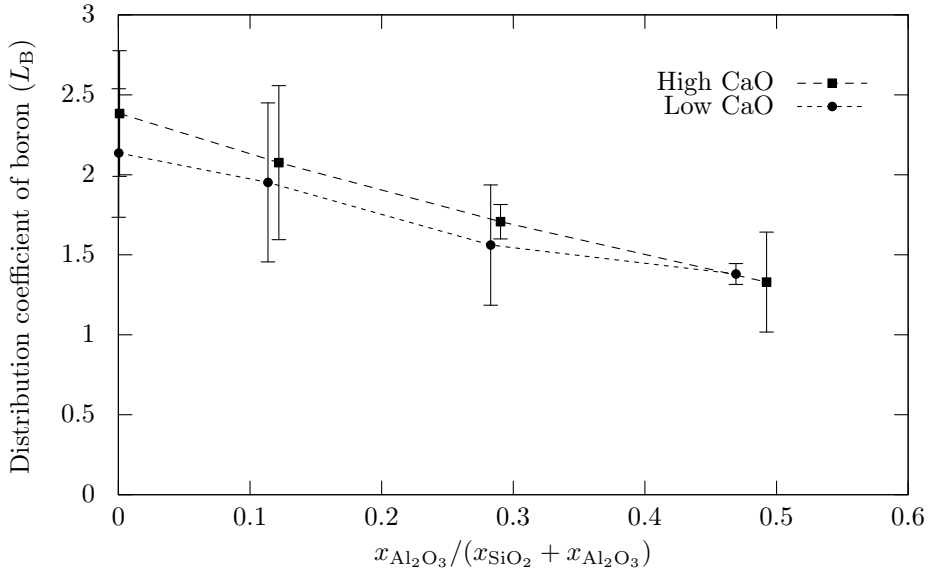

Figure 5.26: Distribution coefficient of boron when SiO_2 is replaced with Al_2O_3 in the CaO-Al_2O_3-SiO_2 system.

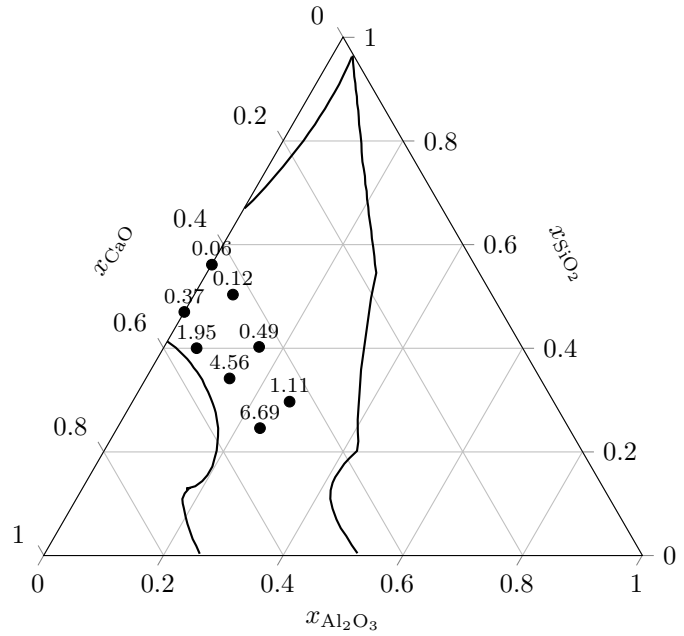

Figure 5.27: Calcium concentration in silicon in equilibrium with CaO-Al_2O_3-SiO_2 slags (wt%).

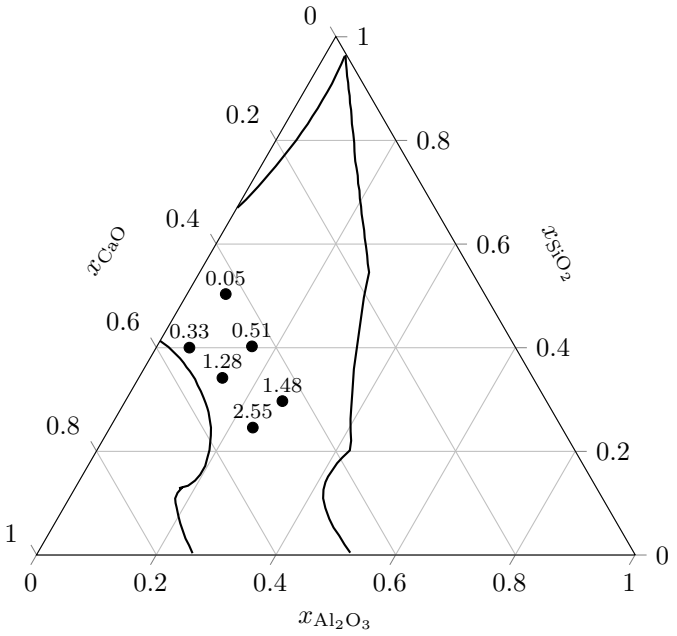

Figure 5.28: Aluminium concentration in silicon in equilibrium with CaO-Al_2O_3-SiO_2 slags (wt%).

5.5 A binary CaO-SiO_2 slag and ferrosilicon

Calcium silicate slags in equilibrium with ferrosilicon containing up to 50 wt% iron was investigated. The aim was to investigate the influence of iron on the distribution coefficient of boron. The same master slag with 48.9 % CaO and 50.5 % SiO_2 was used for all experiments. This master slag contained 86 ppmw boron while the ferrosilicon alloys contained less than 1 ppmw boron. SiO_2-rich binary slags have previously been shown to have an equilibrium time of approximately 6 hours. The same holding time was considered to be sufficient for the experiments with ferrosilicon since the slag was less viscous and hence should have an equilibrium time of less than 6 hours. The alloy compositions are shown together with the results in table 5.12 and it is seen that the slag compositions are the same after all experiments.

Table 5.12: Concentration of boron and calcium in silicon and boron in slag after experiments. Iron concentration in silicon is given on the left hand side and slag compositions after the experiments are given on the right hand side of the table.

ID.	Fe (wt%)	B in slag (ppmw)	B in Si (ppmw)	Ca in Si (ppmw)	CaO (wt%)	SiO_2 (wt%)
FS1	50	63.1 ± 2.3	23.2 ± 4.3	67 ± 36	51.6	47.9
FS2	35	70.4 ± 4.9	22.7 ± 2.4	279 ± 95	51.2	48.3
FS3	25	63.5 ± 4.6	24.3 ± 4.7	838 ± 80	51.2	48.2
FS4	15	66.3 ± 1.6	25.1 ± 2.6	1787 ± 183	51.6	47.9
FS5	0	66.0 ± 3.0	25.7 ± 2.9	3172 ± 274	51.3	48.2

Uncertainty is given as 95% confidence intervals based on the analysis of three replicate splits.

Figure 5.29 shows the distribution coefficient as a function of silicon content in ferrosilicon and it is seen that metal composition does not have any significant influence on the distribution coefficient of boron. The distribution coefficient is between 2.6 and 3.1 for all metal compositions. In figure 5.30 is it seen that the calcium concentration is strongly dependent of metal composition. The calcium concentration decreases drastically with increasing iron content. This is as expected since iron and calcium is immiscible while calcium and silicon forms intermediate silicides.

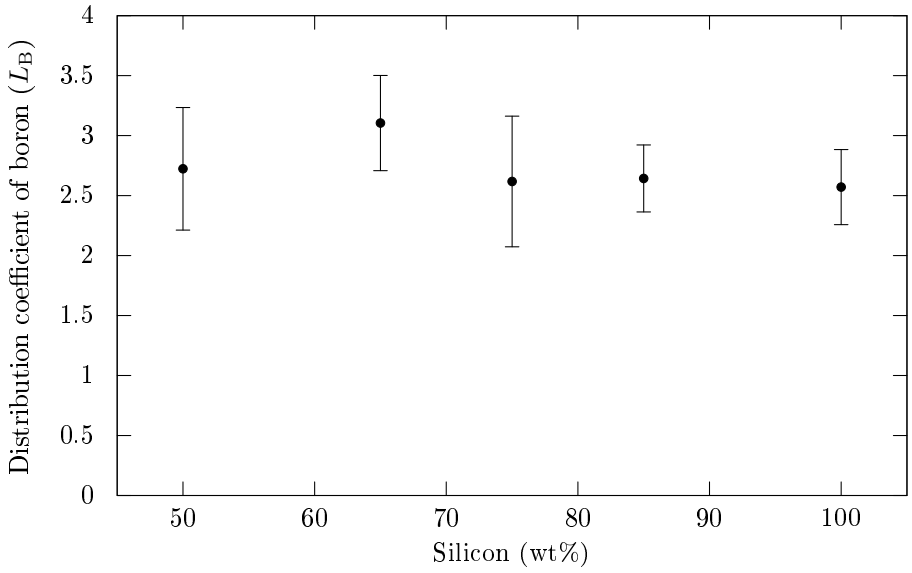

Figure 5.29: Distribution coefficient of boron as a function of silicon concentration in ferrosilicon.

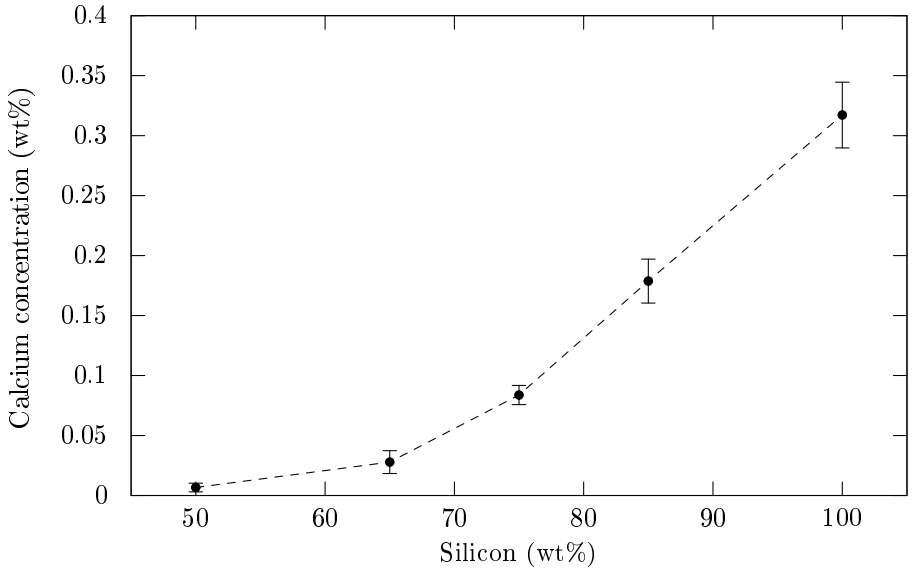

Figure 5.30: Calcium concentration in ferrosilicon as a function of silicon concentration in ferrosilicon.

5.6 Mass loss and slag composition

The mass loss from the system is most likely to be caused by reaction between SiO_2 in the slag and the graphite crucible. Also the reaction between SiO_2 in the slag and the silicon melt may be contributing to the mass loss. Other mass losses may also occur as will be shown below.

The binary CaO-SiO_2 system

The reaction

$$SiO_2(l) + C(s) = SiO(g) + CO(g) \tag{5.2}$$

is assumed to the dominating mechanism for mass loss in the binary CaO-SiO_2 system. This can be calculated using thermochemical data and mass loss together with the geometry of the system. It must also be assumed that some of the calcium oxide is also lost for the mass balance to add up, as will be shown below. CaO can be lost through evaporation of calcium from silicon and by the reaction $CaO(l) + C(s) = Ca(g) + CO(g)$. No attempt has been done here to determine the dominating mechanism for loss of calcium and it is assumed that all CaO is lost through evaporation of calcium from silicon in the following calculations. The 9 hour experiment is chosen for the calculations where the mass loss was measured to be 3.34 g. Some CaO is reduced and absorbed into silicon, but the concentration of calcium in silicon is so low that the influence on final slag composition can be neglected in the following calculations. Some SiO_2 will as mentioned also be lost through the reaction

$$SiO_2(l) + Si(l) = 2SiO(g) \tag{5.3}$$

For reaction (5.2) we have from the NIST-JANAF Tables (1998) that $\Delta G_1 = 49.146$ kJ/mol at 1600 °C, and for reaction (5.3) we have $\Delta G_2 = 73.653$ kJ/mol at 1600 °C. The equilibrium constants are hence $K_1 = 4.3 \cdot 10^{-2}$ and $K_1 = 8.8 \cdot 10^{-3}$ respectively. From figure 5.1 we can estimate the reaction interface between slag and silicon to be approximately half the size of the reaction interface between slag and graphite. Hence the relative magnitude of the reaction (5.2) to reaction (5.3) can be estimated to be $K_1/K_2 \cdot 2 \approx 10$.

First we can estimate the mass of carbon that has reacted with SiO_2 to form SiO and CO gas after 9 hours

$$\begin{aligned} \Delta m_C &= \frac{0.9 \cdot \Delta m}{M_{SiO_2} + M_C} \cdot M_C \\ &= \frac{0.9 \cdot 3.34g}{60.1 + 12.0} \cdot 12.0 = 0.50g \end{aligned} \tag{5.4}$$

Secondly we can estimate the mass of silicon that has reacted with SiO_2 to

form SiO gas

$$\begin{aligned}\Delta m_{\mathrm{Si}} &= \frac{0.1 \cdot \Delta m}{\mathrm{M}_{\mathrm{SiO_2}} + \mathrm{M}_{\mathrm{Si}}} \cdot \mathrm{M}_{\mathrm{Si}} \\ &= \frac{0.1 \cdot 3.34\mathrm{g}}{60.1 + 28.1} \cdot 28.1 = 0.11\mathrm{g} \end{aligned} \tag{5.5}$$

Using these mass losses together with the initial and final concentration of CaO we can estimate the mass loss of CaO from the slag

$$\begin{aligned}\Delta m_{\mathrm{CaO}} &= m_{\mathrm{CaO,in}} - m_{\mathrm{CaO,9h}} \\ &= m_{\mathrm{slag,in}} \cdot w_{\mathrm{CaO,in}} - m_{\mathrm{slag,9h}} \cdot w_{\mathrm{CaO,9h}} \\ &= 15.03\mathrm{g} \cdot 0.362 - (15.03 - (3.34 - 0.50 - 0.11))\mathrm{g} \cdot 0.421 \\ &= 0.26\mathrm{g} \end{aligned} \tag{5.6}$$

where w is the mass fraction. Hence we lose $3.34 - 0.26 = 3.08$g from the reaction between carbon and SiO_2 and the reaction between silicon and SiO_2. We can now recalculate the mass of carbon from equation (5.4) to be 0.46 g and the mass of silicon from equation (5.5) to be 0.10 g. Using these values in equation (5.6) gives a loss of CaO of 0.28 g. Inserting this value back into equations (5.4) and (5.5) gives the same losses as previously calculated and further iterations are therefore not necessary. The rest of the mass loss has to be from SiO_2 where $\Delta m_{\mathrm{SiO_2}} = 3.34 - 0.28 - 0.46 - 0.10 = 2.50$g. Using this mass loss we can estimate the concentration of SiO_2 in the slag after 9 hours.

$$\begin{aligned} w_{\mathrm{SiO_2,9h}} &= \frac{m_{\mathrm{SiO_2,in}} - \Delta m_{\mathrm{SiO_2}}}{m_{\mathrm{slag,9h}}} \\ &= \frac{15.03\mathrm{g} \cdot 0.637 - 2.50\mathrm{g}}{15.03\mathrm{g} - (3.34 - 0.46 - 0.10)\mathrm{g}} = 0.578 \end{aligned} \tag{5.7}$$

which is almost the same as the measured concentration of 57.7 wt% confirming that the calculations are self-consistent. We can therefore conclude that the dominating reaction for mass loss is $SiO_2 + C = SiO + CO$, as proposed.

The binary MgO-SiO_2 system

It can be calculated if the reaction between SiO_2 and carbon to form SiO and CO gas is the correct mechanism for mass loss in the same way as in the binary CaO-SiO_2 system. MgO and Mg are volatile and may also be lost from the system and we can estimate the loss of MgO from the slag using the mass loss together with the measured MgO concentration in the slag. The reaction $\mathrm{MgO}(l) + \mathrm{C}(s) = \mathrm{Mg}(g) + \mathrm{CO}(g)$ is assumed to be negligible. The 9 hours experiment is chosen for the following mass balance calculation. A

small amount of MgO is reduced and absorbed into the silicon phase, but the concentration of magnesium in silicon after 9 hours is so small that change of slag composition due to this reaction is neglected. The same procedure as in the binary CaO-SiO_2 system can therefore be used.

First we can estimate the mass of carbon that has reacted to CO gas after 9 hours using equation (5.4)

$$\Delta m_{\mathrm{C}} = \frac{0.9 \cdot 1.28\mathrm{g}}{60.1 + 12.0} \cdot 12.0 = 0.19\mathrm{g} \tag{5.8}$$

Then we can estimate the mass of silicon that has reacted with SiO_2

$$\Delta m_{\mathrm{Si}} = \frac{0.1 \cdot 1.28\mathrm{g}}{60.1 + 28.1} \cdot 28.1 = 0.04\mathrm{g} \tag{5.9}$$

Using these mass losses together with the initial and final concentration of MgO we can use equation (5.6) to estimate the mass loss of MgO from the slag

$$\Delta m_{\mathrm{MgO}} = 4.99\mathrm{g} \cdot 0.339 - (4.99 - (1.28 - 0.19 - 0.4))\mathrm{g} \cdot 0.406 = 0.09\mathrm{g} \tag{5.10}$$

Hence we lose $1.28 - 0.09 = 1.19$g mass from the reaction between carbon and SiO_2. We can now recalculate the mass of carbon reacted from equation (5.4) to be 0.18 g and the mass of silicon reacted from equation (5.5) to be 0.04 g. Using this value in equation (5.6) gives a mass loss of MgO of 0.10 g. Inserting this value into equations (5.4) and (5.5) gives the same values as calculated before and further iterations are therefore not necessary. The rest of the mass loss has to be from SiO_2 where $\Delta m_{\mathrm{SiO_2}} = 1.28 - 0.10 - 0.18 - 0.04 = 0.96$g. Using this mass loss in equation 5.7 we can estimate the concentration of SiO_2 in the slag after 9 hours.

$$w_{\mathrm{SiO_2,9h}} = \frac{4.99\mathrm{g} \cdot 0.655 - 0.96\mathrm{g}}{4.99\mathrm{g} - (1.28 - 0.18 - 0.04)\mathrm{g}} = 0.587 \tag{5.11}$$

where w is the mass fraction. This is almost the same as the measured concentration of 58.6 wt% confirming that the calculations are self-consistent. We can therefore conclude that the dominating reaction for mass loss is $SiO_2 + C = SiO + CO$, as proposed, with a small additional loss of MgO.

The ternary CaO-MgO-SiO_2 system

At low SiO_2 concentration in the ternary CaO-MgO-SiO_2 system the SiO_2 concentration is seen to be almost unchanged after 6 hours holding time implying that mass loss of SiO_2 is not dominating in this part of the slag system. Experiment CMS13 in table 5.5 had a mass loss of 2.55 g and was chosen to

estimate the mass losses in this part of the slag system. At first we can calculate the change of slag mass due to reduction of CaO and MgO. The mass of silicon oxidized to SiO_2 can be calculated form calcium and magnesium concentration in silicon

$$\Delta \mathrm{m_{Si}} = 0.5 \cdot m_{\mathrm{Me,in}}(\frac{w_{\mathrm{Ca}}}{\mathrm{M_{Ca}}} + \frac{w_{\mathrm{Mg}}}{\mathrm{M_{Mg}}}) \cdot \mathrm{M_{Si}} = 0.08\mathrm{g} \tag{5.12}$$

where w is the mass fraction of the respective element in silicon $m_{\mathrm{Me,in}} = 15.04$ is the mass of the silicon phase. The total mass of the silicon phase after reduction of CaO and MgO is hence

$$m_{\mathrm{Me,red}} = m_{\mathrm{Me,in}} + w_{\mathrm{Ca}} \cdot m_{\mathrm{Me}} + w_{\mathrm{Mg}} \cdot m_{\mathrm{Me}} - \Delta \mathrm{m_{Si}} = 15.13\mathrm{g} \tag{5.13}$$

and the mass of the slag phase have to be reduced equally from 15.03 to 14.94 g. A hypothetical initial slag composition after reduction of CaO and MgO before any mass loss can then be calculated. The initial concentration of CaO in the slag phase after the reduction of CaO and MgO is

$$w_{\mathrm{CaO,red}} = (w_{\mathrm{CaO,in}} \cdot m_{\mathrm{slag,in}} - \frac{w_{\mathrm{Ca}} \cdot m_{\mathrm{Me,in}}}{\mathrm{M_{Ca}}} \cdot \mathrm{M_{CaO}})/m_{\mathrm{slag,red}} = 0.302 \tag{5.14}$$

and the initial concentration of MgO after reduction can similarly be found to be 22.9 wt% while the concentration of SiO_2 is 46.7 wt%. A similar calculation as with the mass loss of the binary slag systems can be done using these concentrations, but the mass losses of CaO and MgO are calculated first in this case. The mass loss of CaO is

$$\Delta \mathrm{m_{CaO}} = w_{\mathrm{CaO,red}} \cdot m_{\mathrm{slag,red}} - w_{\mathrm{CaO,end}} \cdot m_{\mathrm{slag,end}} = 0.25\mathrm{g} \tag{5.15}$$

and the mass loss of MgO can be calculated in the same way to be 1.08 g. The remaining mass loss of 1.21 g can be used equations (5.4) and (5.5) to estimate the mass loss of carbon and silicon to be 0.18 and 0.04 g respectively. Subtracting these losses from the total mass loss gives us a new estimate for the mass loss from the slag and the mass loss of CaO and MgO can be recalculated to be 0.18 and 1.03 g respectively. The mass loss of carbon and silicon can then be recalculated to be 0.17 and 0.04 g respectively and the mass loss of CaO and MgO can then be recalculated to be 0.18 and 1.04 g respectively. Further iterations give the same values and the remaining mass loss of 1.13 g has to be SiO_2. The final concentration of SiO_2 in the slag can be estimated

$$w_{\mathrm{SiO_2},end} = \frac{m_{\mathrm{SiO_2,red}} - \Delta m_{\mathrm{SiO_2}}}{m_{\mathrm{slag,end}}} = 0.464 \tag{5.16}$$

which is close to the measured concentration of 46.5 wt% confirming that the calculations are self-consistent. It is seen that the mass loss of MgO is on the same level as the mass loss of SiO_2 in this part of the ternary CaO-MgO-SiO_2 slag system.

The ternary CaO-Al_2O_3-SiO_2 system

A significant reduction of CaO and Al_2O_3 is seen in this system at high Al_2O_3 concentrations. The change of slag composition due to this is clearly visible in figure 5.31. The mass balance calculation given below reveals that the initial change of slag composition is in line with the change after longer holding times. A hypothetical initial slag composition after reduction of calcium and aluminium to the measured concentration in silicon after 3 hours should follow the same linear trend as the other measurements. At first we can calculate the mass of silicon oxidized when calcium and aluminium is reduced.

$$\Delta m_{Si} = m_{Me,in}(0.5 \cdot \frac{w_{Ca}}{M_{Ca}} + 0.75 \cdot \frac{w_{Al}}{M_{Al}}) \cdot M_{Si} = 0.40g \qquad (5.17)$$

and using (5.13) with magnesium replaced with aluminium we can calculate the mass of the silicon phase after reduction to be 15.00 g + 0.12 g = 15.12 g. The mass of the slag phase will be equally reduced from 15.00 g to 14.88 g. Using equation (5.14) we can calculate the initial concentration of CaO in the slag after reduction to be 34.8 wt%. The concentration of Al_2O_3 and SiO_2 is in the same way found to be 37.8 and 27.2 wt% respectively. The calculated hypothetical initial composition is seen in figure 5.31 to be completely in line with the data for longer holding times.

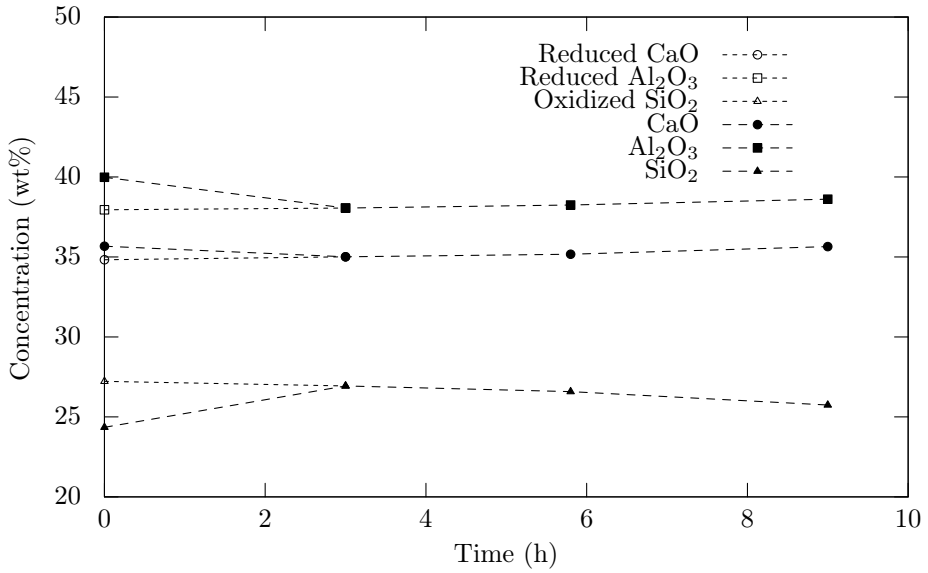

Figure 5.31: CaO, SiO_2 and Al_2O_3 concentration in slag as a function of time with a hypothetical initial slag composition after reduction of CaO and Al_2O_3.

We can estimate the mass losses after 9 hours by first calculating the composition after reduction in the same way as above. After that we can use

equation (5.14) to estimate the loss of CaO and Al_2O_3 from the slag to be 0.08 and 0.24 g respectively. Then we can estimate the loss of carbon and silicon in reaction with SiO_2 using equations (5.4) and (5.5) to be 0.06 and 0.01 g. After subtracting these from the mass loss we can recalculate the loss of CaO and Al_2O_3 and iterate to convergence at 0.05 and 0.20 g mass loss of CaO and Al_2O_3 respectively. The calculated carbon and silicon losses converge to 0.07 and 0.02 g. The remaining mass loss of 0.40 g has to be SiO_2 and using equation (5.16) we can estimate the final concentration of SiO_2 to be 25.7 wt% which is the same as the measured concentration. The reaction between SiO_2 and carbon is hence the dominating reaction, but a significant amount of Al_2O_3 is also lost.

Summary of mass loss calculations

The calculated losses for different slag systems are given in table 5.13. The losses reflect to some extent the thermodynamic activities of the slag components. In these calculations the losses of carbon from the crucible and silicon from the silicon melt scales with the loss of SiO_2, but are approximately 5 and 25 times lower respectively. The loss of CaO is around 10 to 15 % of the loss of SiO_2. In the MgO-SiO_2 system (MS5) the loss of MgO is about 10 % of the SiO_2 loss. For a CaO-MgO-SiO_2 slag with a relatively low SiO_2 content and high MgO content (CMS13) the mass losses of these two oxides are seen to be similar. With the CaO-Al_2O_3-SiO_2 slag (CAS3) the loss of Al_2O_3 is seen to be half of the SiO_2 loss. Hence, loss of SiO_2 dominates for silica rich slags while losses of MgO and Al_2O_3 also are at a similar level for slags with a lower SiO_2 content where these oxides are a major component of the slag.

Table 5.13: Calculated loss of carbon, silicon and oxides from the crucible, silicon melt and slag respectively. Losses are given in grams.

ID.	C	Si	SiO_2	CaO	MgO	Al_2O_3	Total loss
CS4	0.46	0.10	2.50	0.28	0	0	3.34
MS5	0.18	0.04	0.96	0	0.10	0	1.28
CMS13	0.17	0.04	1.13	0.18	1.04	0	2.55
CAS3	0.07	0.02	0.40	0.05	0	0.20	0.74

Chapter 6

Discussion

The results found in this work are compared with data from literature in the first part of this chapter. Activity data for slag forming oxides and $BO_{1.5}$ in the CaO-SiO_2, MgO-SiO_2 and CaO-MgO-SiO_2 systems are then calculated using the experimental data and their trends. Activities of calcium, magnesium and aluminium at infinite dilution in silicon are also determined. The activities of boron and calcium at infinite dilution in ferrosilicon are found before mass transfer is considered. The accuracy and reproducibility of data found in the present work is discussed and industrial consequences are discussed in the end of this chapter.

6.1 The distribution coefficient of boron

The distribution coefficient of boron in the binary CaO-SiO_2 system found in the present study is shown in figure 6.1 together with results from previous works and it is seen that the results from the present work is mostly in the middle between the results from previous works. The linear fit to the data found in the present work gives

$$L_B = 0.449 \cdot V + 1.89 \tag{6.1}$$

where V is the CaO/SiO_2 mass ratio.

The distribution coefficient is found to be higher than in the work by Suzuki et al. (1990). The values found by Suzuki et al. may however not be equilibrium values due to a holding time of just 2 hours as compared to the 6 hours found to be required in the present work for a SiO_2-rich slag. A closer agreement is found with the values from Weiss and Schwerdtfeger (1994). This indicates that boron behaves as a Henrian solute up to 1.25 wt% B_2O_3 in slag and 0.23 wt% boron in silicon which is even higher than the range investigated by Teixeira et al. (2009). A linear trend is found for the distribution coefficient of boron in the present work as opposed to the u-shaped trend found by Teixeira et al. The present work agree well with the work by Teixeira et al. in

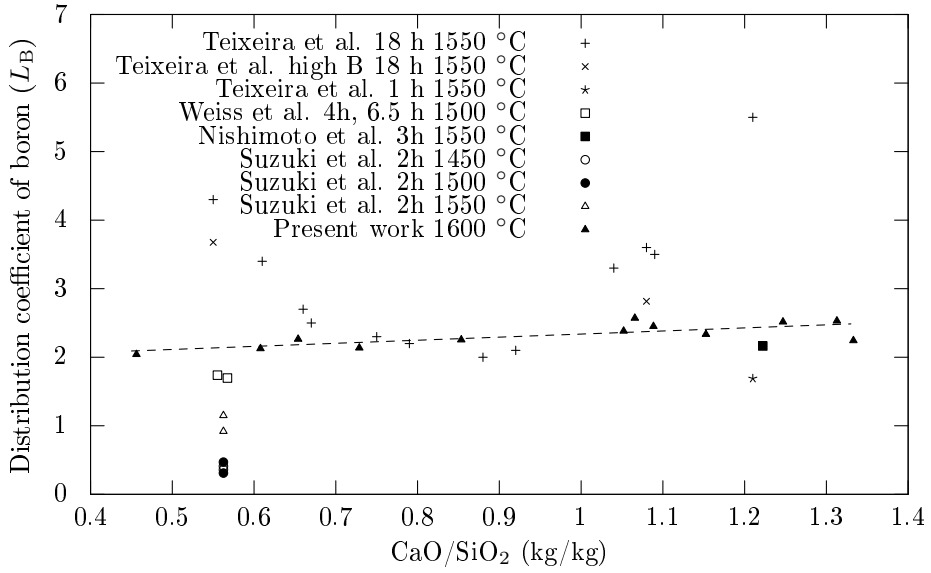

Figure 6.1: Distribution coefficient of boron in the binary CaO-SiO_2 system.

the mid-range of the CaO-SiO_2 system while Teixeira et al. found higher values in both the SiO_2-rich end and the CaO-rich end of the system. No obvious reason for this difference has been found since both systems are considered to be at equilibrium. A closer agreement is found with the value they found for one hour holding time but their value is somewhat lower. A holding time of one hour may however not be sufficient to reach equilibrium considering that Nishimoto et al. (2012) found the equilibrium time to be two hours close to that slag composition. The value of the distribution coefficient found by Nishimoto et al. is in good agreement with the present work. Other works that includes the binary system are for different reasons discussed earlier not considered here.

The equilibrium values for the distribution coefficient of boron in the binary MgO-SiO_2 system are shown in figure 6.2. The experiment with 15 g slag and 15 g boron doped silicon was seen in figure 5.12 to have a somewhat lower recovery of boron than the other experiments, but the deviation was not considered to be large enough for this experiment to be discarded. There are no results from previous work with respect to the distribution coefficient of boron in this system.

Two works have previously been conducted in the ternary CaO-MgO-SiO_2 system and they are compared with the present work in figure 6.3. It is seen that the present work is more in agreement with the work by White et al. (2012) than the work by Suzuki et al. (1990). Also the results from the binary systems in the present work are included because replacing CaO with MgO was found to have no significant influence on the distribution coefficient. The

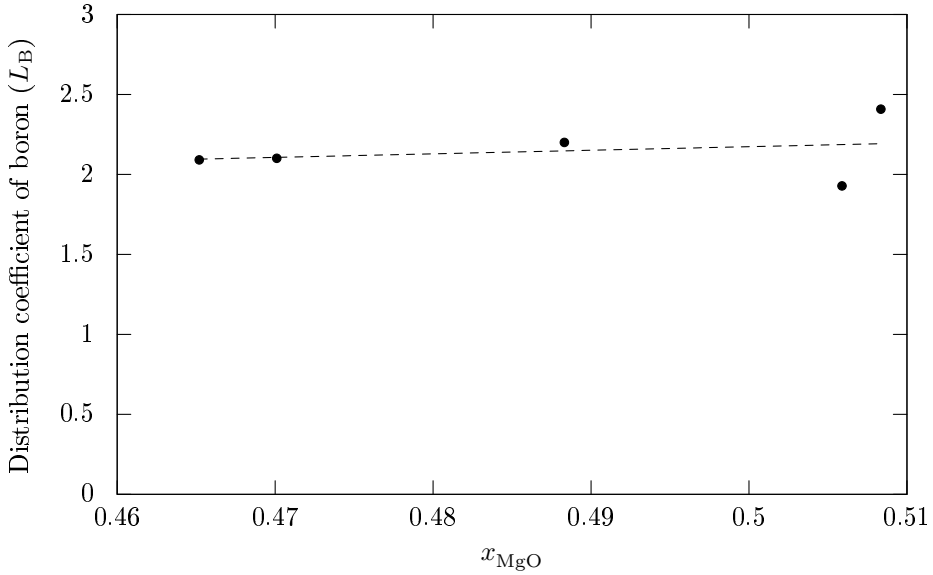

Figure 6.2: Distribution coefficient of boron in the binary MgO-SiO_2 system as found in the present work.

work by Suzuki et al. was performed at 1450 °C with a holding time of two hours. Two hours have been shown by Nishimoto et al. (2012) et al. to be the equilibrium time at 1550 °C for a CaO-rich binary calcium silicate slag. The equilibrium time at 1450 °C is expected to be longer and the work by Suzuki et al. may therefore not have reached equilibrium. The slag compositions in the present work and the work by White et al. and Suzuki et al. are shown in figure 6.4. Only the initial slag composition was given in the work by Suzuki et al. and it may have changed somewhat in reaction with carbon and elemental silicon in the same way as shown for the present work.

The distribution coefficient of boron found in the present work in the CaO-Al_2O_3-SiO_2 system is compared with the work by Johnston and Barati (2010) in figure 6.5 and it is seen that the results from the present work agree very well with their work. The concentration of CaO in the present work was $x_{CaO} = 0.437 \pm 0.004$ (SD) for the 'Low CaO' series and $x_{CaO} = 0.527 \pm 0.014$ (SD) for the 'High CaO' series. The distribution coefficient of boron has already been found to be almost unaffected by CaO content in the slag and the similarity of the results with different CaO content here is in accordance with that finding. The agreement between the present work and the work by Johnston and Barati also supports this finding since the values agree so well when plotted as a function of $x_{Al_2O_3}/(x_{SiO_2} + x_{Al_2O_3})$ ratio even if the slag composition is significantly different with respect to CaO. Five of the slags in the work by Johnston et al. contained significantly less CaO than the other

slags, and the distribution coefficient for four of these slags are seen to be on the low side of the trend in figure 6.5. This is in agreement with the small decreasing trend of the distribution coefficient with decreasing CaO content in the slag found in the present work for the binary CaO-SiO_2 system. The trend seen in figure 3.4 is therefore mainly caused by changing Al_2O_3/SiO_2 ratio and not changing CaO/SiO_2 mass ratio.

The work by Fujiwara et al. (2002) is also shown in figure 6.5 and is seen to follow the same trend as the present work and the work by Johnston and Barati. The Al_2O_3 content in the work by Fujiwara et al. has been estimated on the assumption that the slag composition is fixed at the liquidus line by the Al_2O_3 saturation. The final slag composition in the present work, the work by Fujiwara et al. and the work by Johnston and Barati are shown in figure 6.6. The slag in the work by Johnston and Barati also contained 2 - 4 wt% MgO and this is seen to have changed the composition at Al_2O_3 saturation at 1500 °C to be similar to the liquidus line at 1600 °C.

Johnston and Barati (2010) also investigated a quaternary CaO-MgO-Al_2O_3-SiO_2 slag at MgO-saturation where the sum $x_{CaO} + x_{MgO}$ was constant at 0.648 ± 0.12 (SD). The mole fraction of MgO varied from 0.309 to 0.429 with a corresponding variation of the mole fraction of CaO from 0.340 to 0.230. The MgO and CaO content have been shown in the present work to have no influence on the distribution coefficient of boron in the ternary CaO-MgO-SiO_2 system. The results they obtained in the quaternary system is therefore also included in figure 6.5 and is seen to agree well with the trend found for the ternary CaO-Al_2O_3-SiO_2 system.

All data in the ternary CaO-Al_2O_3-SiO_2 and the quaternary CaO-MgO-Al_2O_3-SiO_2 system is seen to follow a linear decreasing trend with increasing $x_{Al_2O_3}/(x_{SiO_2}+x_{Al_2O_3})$. A linear fit of the data is also shown in figure 6.5 and extrapolation to $x_{SiO_2} = 0$ gives a distribution coefficient of boron close to zero. The oxygen partial pressure will no longer be controlled by the equilibrium between silicon and SiO_2 since we have a binary CaO-Al_2O_3 or ternary CaO-MgO-Al_2O_3 slag system in equilibrium with an alloy without silicon. Without any SiO_2 (and hence also elemental silicon) in the system the partial pressure of oxygen will be too low to oxidize boron. The distribution coefficient of boron should therefore be zero when $x_{SiO_2} = 0$.

From the ternary CaO-Al_2O_3-SiO_2 and quaternary CaO-MgO-Al_2O_3-SiO_2 system we therefore have that boron decreases linearly as a function of $x_{Al_2O_3}/(x_{SiO_2} + x_{Al_2O_3})$. An equation for the distribution coefficient of boron in the quaternary CaO-MgO-Al_2O_3-SiO_2 system can be made by requiring that L_B should be zero for $x_{SiO_2} = 0$.

$$L_B = L_B^0 \cdot \frac{x_{SiO_2}}{x_{SiO_2} + x_{Al_2O_3}} \tag{6.2}$$

where L_B^0 is the distribution coefficient of boron for $x_{Al_2O_3} = 0$.

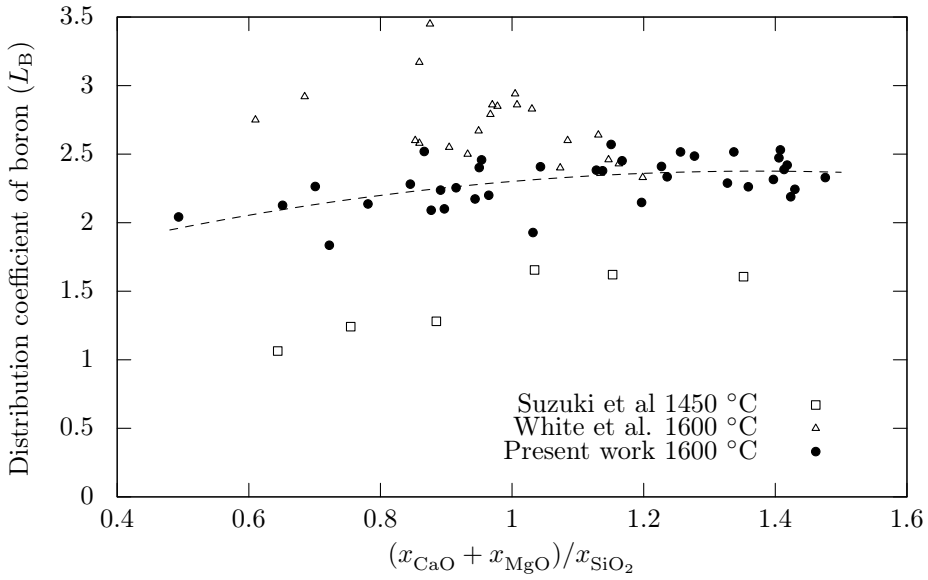

Figure 6.3: The distribution coefficient of boron as found in present and previous works in the ternary CaO-MgO-SiO_2 system.

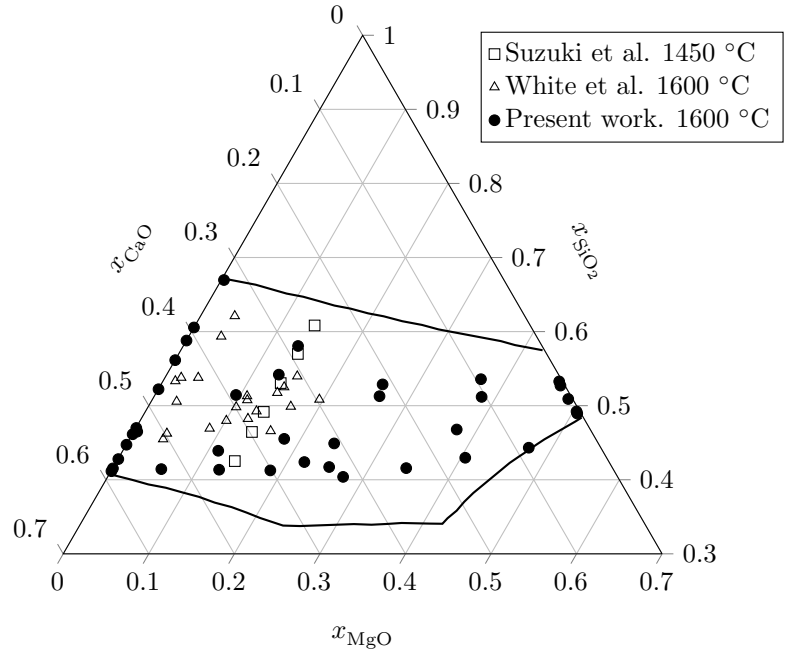

Figure 6.4: Final slag compositions in the ternary CaO-MgO-SiO_2 system in the present study and the study by White et al. Only initial slag compositions were given in the study by Suzuki et al.

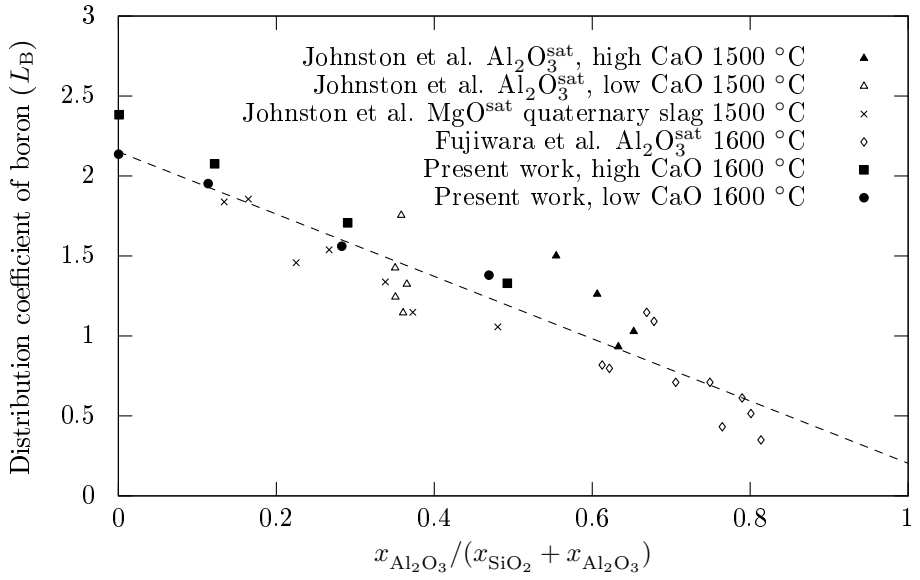

Figure 6.5: The distribution coefficient of boron as a function of Al_2O_3 content as found in present and previous works.

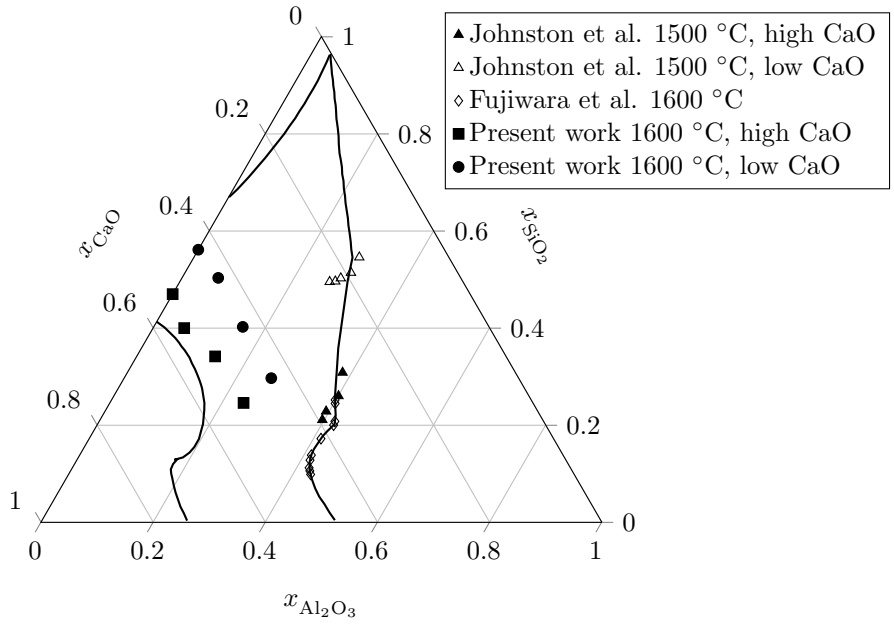

Figure 6.6: Final slag composition in the present work and the work by Johnston et al. shown together estimated final slag composition in the work by Fujiwara et al. The slag in the work by Johnston et al. also contained 2 - 4 wt% MgO.

6.2 Concentration of slag forming elements in silicon in equilibrium with slags.

The calcium concentration in silicon in equilibrium with binary CaO-SiO_2 slags as found in present and previous works are shown in figure 6.7. The concentrations found in the present work agree well with previous works in the SiO_2-rich part of the system while the concentrations are somewhat lower in the CaO-rich end of the system. A closer view of the SiO_2-rich part of the system is shown in figure 6.8 and it is seen that the results are in good agreement with previous works in this part of the system. The trend found in the present work is also indicated in the figure. The values obtained in the present work are slightly higher than the results by Morita et al. at 1600 °C while the values from Weiss et al. at SiO_2 saturation at 1600 °C are about half of the value obtained in the present work. The liquidus line at 1600 °C was found from Jung et al. (2005) to be at $x_{SiO_2} = 0.4138$ and $x_{SiO_2} = 0.6707$.

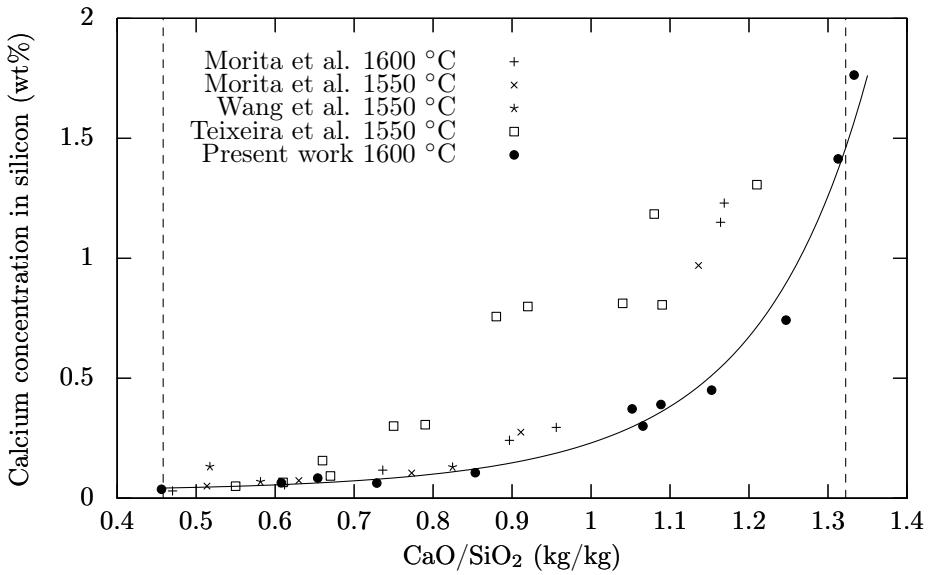

Figure 6.7: Calcium concentration in silicon in equilibrium with binary CaO-SiO_2 slags. Only works that extends across a large region of the slag system is shown. The liquidus lines at 1600°C after Jung et al. (2005) is also indicated as dashed lines in the figure.

Morita et al. (2000) have previously determined two values of the magnesium concentration in silicon in equilibrium with binary MgO-SiO_2 slags and these values are shown together with the values from the present work in figure 6.9. The liquidus line at 1600 °C was found from Wu et al. (1993) to be at $x_{SiO_2} = 0.4879$ and $x_{SiO_2} = 0.5575$.

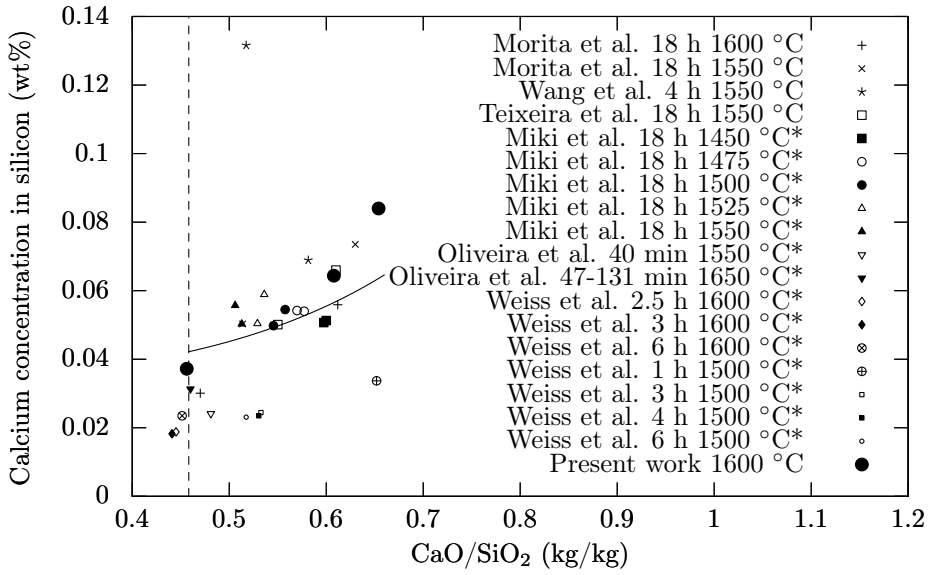

Figure 6.8: Calcium concentration in silicon in equilibrium with binary CaO-SiO_2 slags in the SiO_2-rich part of the system. The liquidus line at 1600°C after Jung et al. (2005) and the non-linear fit is also indicated in the figure.

The calcium and magnesium concentration in silicon in equilibrium with CaO-MgO-SiO_2 slags are shown in figures 6.10 and 6.12. These results can be compared with the previous work by Morita et al. (2000) in figures 6.11 and 6.13. A relatively good agreement is seen between the work by Morita et al. and the present work for both calcium and magnesium. It can however be seen, as have already been seen in the binary CaO-SiO_2 system, that Morita et al. obtained somewhat higher calcium concentrations in the CaO-rich part of the system.

There are no other works at 1600 °C in the same part of the CaO-Al_2O_3-SiO_2 system as the present work. Morita et al. (2000) and Wang et al. (2001) investigated the whole liquid region of the CaO-Al_2O_3-SiO_2 system at 1550 °C. The values obtained in the work by Wang et al. are somewhat scattered as have already been shown for the binary CaO-SiO_2 system. Wang et al. and Schei et al. (1998) have estimated isoconcentration curves in this slag system at 1550 °C. The calcium concentrations in silicon found in the present work are compared with the work by Wang et al. and Schei et al. in figure 6.14. It is seen that the calcium concentration for the most SiO_2-rich slag in the present work fits well with the previous works while the calcium concentration in silicon in equilibrium with a 37.9%CaO-37.2%SiO_2-24.9%Al_2O_3 slag is seen to be in best agreement with Schei et al. The other slags in the present work are seen to be outside the region of the isoconcentration curves from the works by Wang et al. and Schei et al.

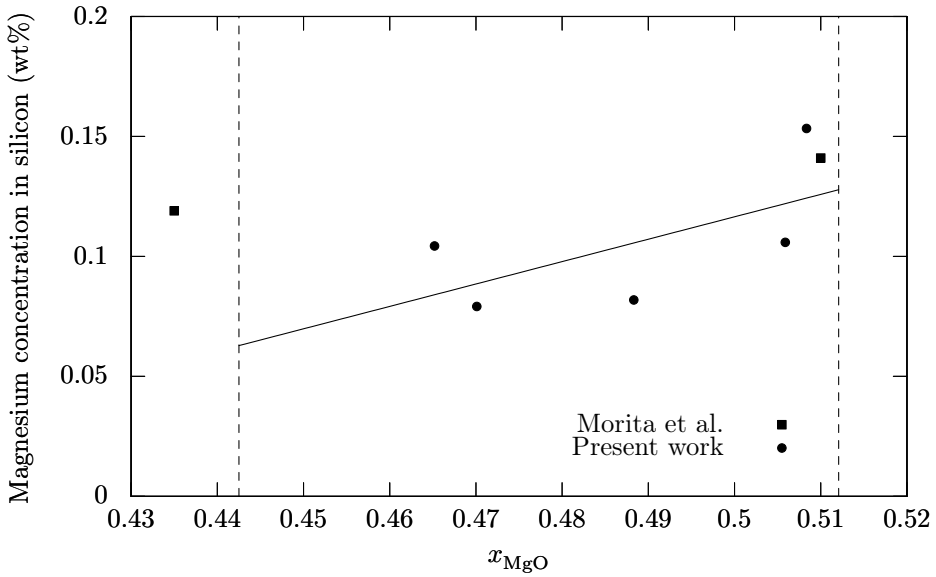

Figure 6.9: Magnesium concentration in silicon in equilibrium with binary MgO-SiO_2 slags at 1600 °C as found in present work and the work by Morita et al. The liquidus lines at 1600 °C from the phase diagram by Wu et al. (1993) are indicated as dashed lines. (* Silica saturated systems)

The aluminium concentrations in silicon found in the present work is compared with Wang et al. (2001) and Schei et al. (1998) in figure 6.15. The aluminium concentration in silicon in equilibrium with the most SiO_2-rich slag in the present work is in best agreement with the work by Schei et al. while the aluminium concentration in equilibrium with the other slags are higher than found in the works by Wang et al. and Schei et al.

The present work is also in relatively good agreement with the concentrations measured by Morita et al. (2000) for the three experiments with lowest CaO concentration. The concentrations in experiment CAS4 and CAS5 are somewhat higher than the concentrations found by Morita et al. at 1550 °C while experiment CAS6 is outside the liquidus region at 1550 °C.

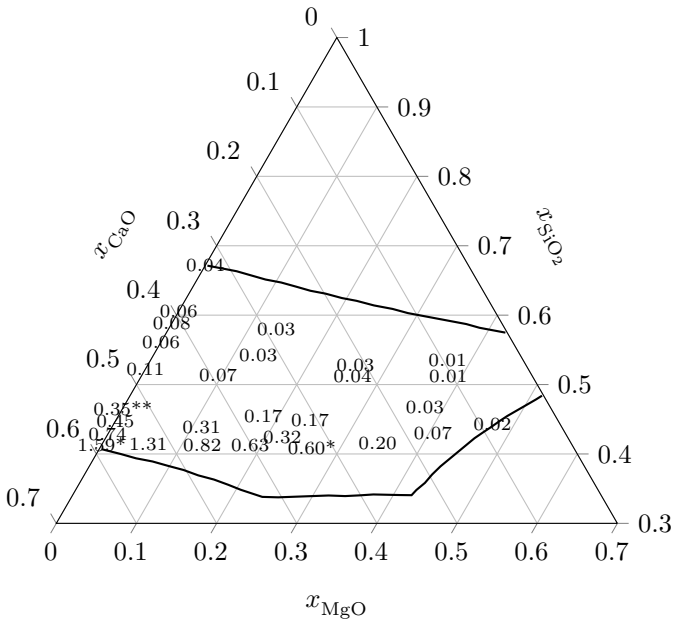

Figure 6.10: Concentration of calcium in silicon in equilibrium with ternary CaO-MgO-SiO_2 slags as found in the present study. (* Mean value of two experiments. ** Mean value of three experiments.)

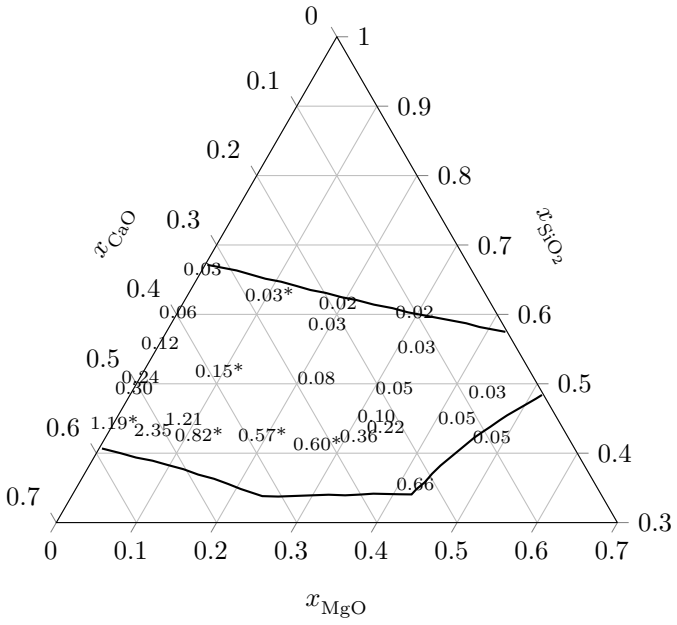

Figure 6.11: Concentration of calcium in silicon in equilibrium with ternary CaO-MgO-SiO_2 slags as found by Morita et al. (2000). (* Mean value of two experiments.)

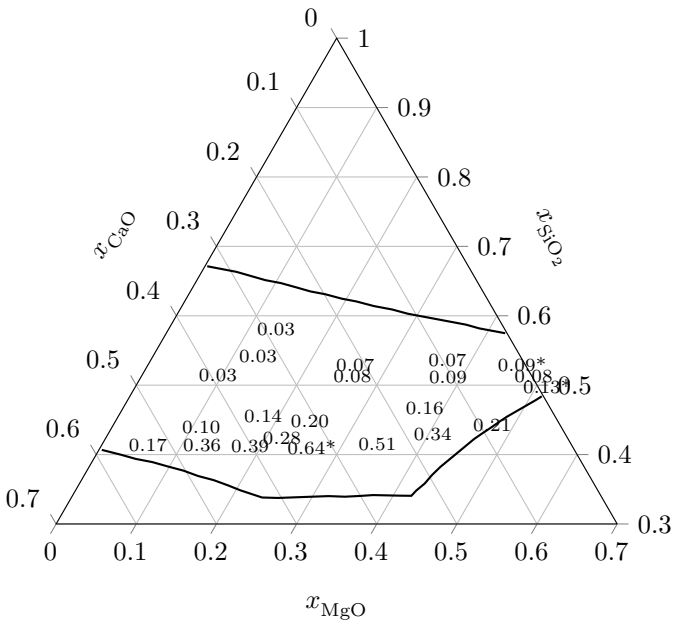

Figure 6.12: Concentration of magnesium in silicon in equilibrium with ternary CaO-MgO-SiO_2 slags as found in the present study. (* Mean value of two experiments.)

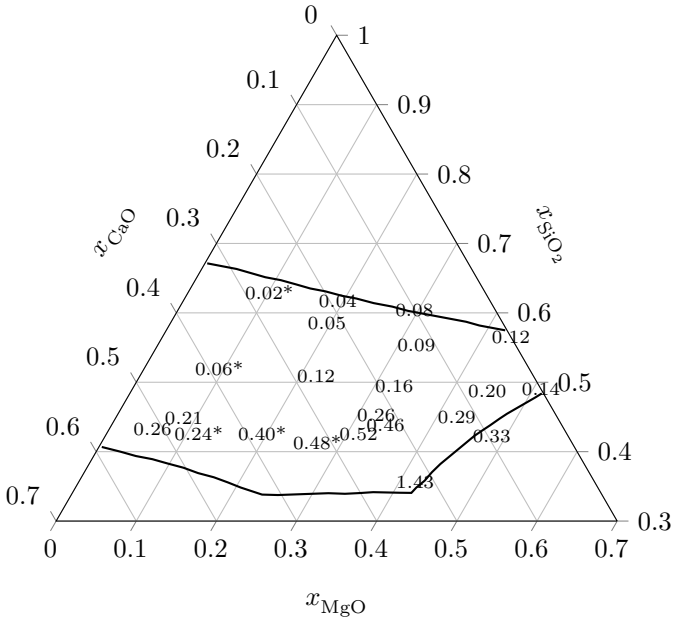

Figure 6.13: Concentration of magnesium in silicon in equilibrium with ternary CaO-MgO-SiO_2 slags as found by Morita et al. (2000). (* Mean value of two experiments.)

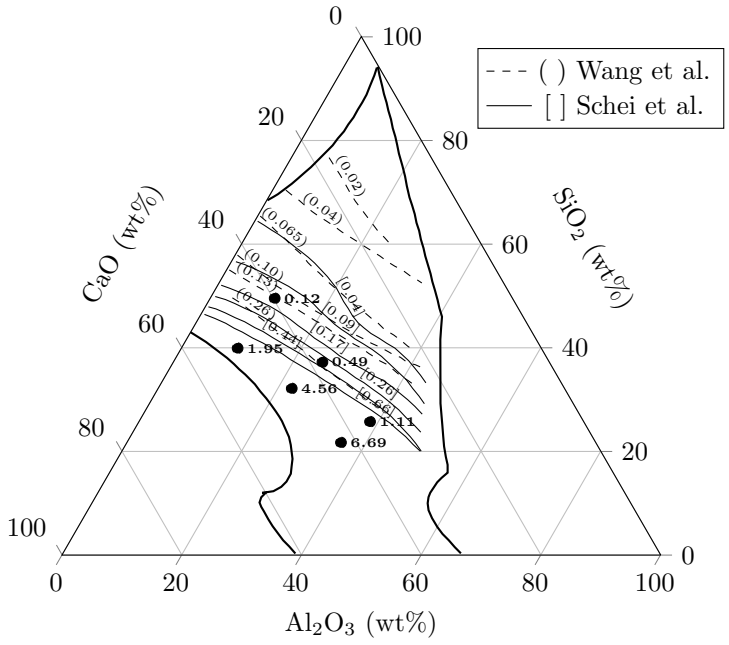

Figure 6.14: Isoconcentration curves for calcium at 1550 °C found in previous works compared with the present work at 1600 °C.

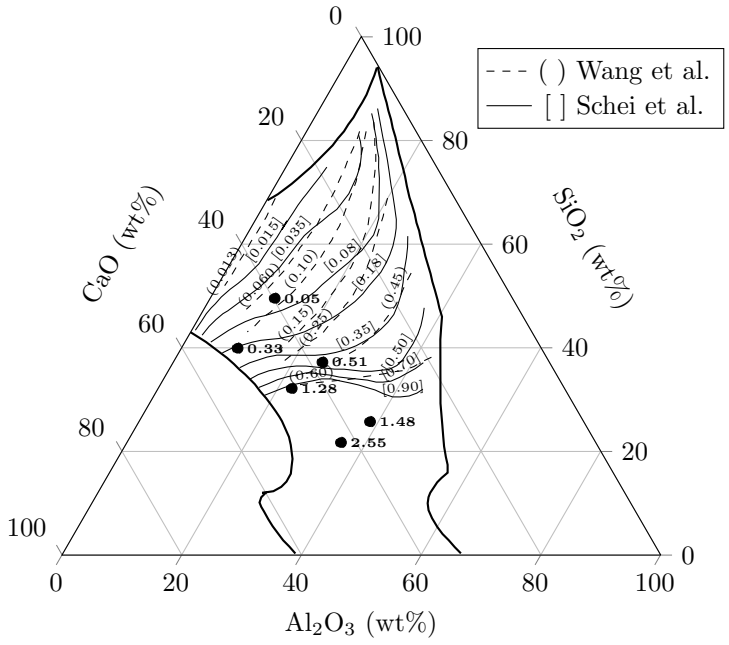

Figure 6.15: Isoconcentration curves for aluminium at 1550 °C found in previous works compared with the present work at 1600 °C.

6.3 Activities in the binary CaO-SiO_2 system

The best fit to the calcium concentration in silicon as a function of CaO/SiO_2 mass ratio is shown in 6.7. This fit is expressed by

$$[\%\mathrm{Ca}] = \exp(3.002 \cdot V^2 - 1.2481 \cdot V - 3.2241) \tag{6.3}$$

where $V = \mathrm{CaO/SiO_2}$ (kg/kg). The concentration of calcium can be used to determine the activity of CaO and SiO_2 by Gibbs Duhem integration as shown by Morita et al. (2000) and Morita et al. (2002). For the determination of the activity of SiO_2 a slightly modified version of the derivation by Morita et al. is given below.

The Gibbs-Duhem equation gives

$$x_{\mathrm{SiO_2}} \mathrm{d}\ln\gamma_{\mathrm{SiO_2}} + x_{\mathrm{CaO}} \mathrm{d}\ln\gamma_{\mathrm{CaO}} = 0 \tag{6.4}$$

and by introducing $B = \gamma^2_{\mathrm{CaO}}/\gamma_{\mathrm{SiO_2}}$ we get

$$\begin{aligned}
& x_{\mathrm{SiO_2}} \mathrm{d}\ln\gamma_{\mathrm{SiO_2}} + x_{\mathrm{CaO}} \mathrm{d}\ln(B\gamma_{\mathrm{SiO_2}})^{1/2} = 0 \\
\Longrightarrow \quad & x_{\mathrm{SiO_2}} \mathrm{d}\ln\gamma_{\mathrm{SiO_2}} + 1/2 x_{\mathrm{CaO}} \mathrm{d}\ln B + 1/2 x_{\mathrm{CaO}} \mathrm{d}\ln\gamma_{\mathrm{SiO_2}} = 0 \\
\Longrightarrow \quad & (x_{\mathrm{SiO_2}} + 1/2 x_{\mathrm{CaO}}) \mathrm{d}\ln\gamma_{\mathrm{SiO_2}} = -1/2 x_{\mathrm{CaO}} \mathrm{d}\ln B \\
\Longrightarrow \quad & \mathrm{d}\ln\gamma_{\mathrm{SiO_2}} = \frac{-x_{\mathrm{CaO}}}{1+x_{\mathrm{SiO_2}}} \mathrm{d}\ln B
\end{aligned} \tag{6.5}$$

Integration gives

$$\ln\gamma_{\mathrm{SiO_2}} = \int_{x^0_{\mathrm{CaO}}}^{x_{\mathrm{CaO}}} \frac{-x_{\mathrm{CaO}}}{1+x_{\mathrm{SiO_2}}} \mathrm{d}\ln B + \ln\gamma^0_{\mathrm{SiO_2}} \tag{6.6}$$

We have the equilibrium

$$\mathrm{SiO_2}(s) + 2\mathrm{Ca}(l) = \mathrm{Si}(l) + 2\mathrm{CaO}(s) \tag{6.7}$$

with

$$\begin{aligned}
K &= \frac{a^2_{\mathrm{CaO}} \cdot a_{\mathrm{Si}}}{a_{\mathrm{SiO_2}} \cdot a^2_{\mathrm{Ca}}} \\
&= \frac{x^2_{\mathrm{CaO}} \gamma^2_{\mathrm{CaO}} \cdot x_{\mathrm{Si}}}{x_{\mathrm{SiO_2}} \gamma_{\mathrm{SiO_2}} \cdot x^2_{\mathrm{Ca}} \gamma^2_{\mathrm{Ca}}}
\end{aligned} \tag{6.8}$$

where silicon is assumed to follow Raoult's law. Morita et al. (2000) has shown that Raoult's law is obeyed when x_{Si} is above 0.98. By rearranging equation (6.8) we get

$$B = \gamma^2_{\mathrm{CaO}}/\gamma_{\mathrm{SiO_2}} = \frac{K \cdot x_{\mathrm{SiO_2}} \cdot x^2_{\mathrm{Ca}} (\gamma^0_{\mathrm{Ca}} \exp(\epsilon^{\mathrm{Ca}}_{\mathrm{Ca}} x_{\mathrm{Ca}}))^2}{x^2_{\mathrm{CaO}} \cdot x_{\mathrm{Si}}} \tag{6.9}$$

and since γ^0_{Ca} and K is constant we get

$$\mathrm{d}\ln B = \mathrm{d}\ln\left(\frac{x_{\mathrm{SiO_2}}\cdot x^2_{\mathrm{Ca}}\exp(2\epsilon^{\mathrm{Ca}}_{\mathrm{Ca}}x_{\mathrm{Ca}})}{x^2_{\mathrm{CaO}}\cdot x_{\mathrm{Si}}}\right) \tag{6.10}$$

From Miki et al. (1999) we have that $\epsilon^{\mathrm{Ca}}_{\mathrm{Ca}} = 7.58$ at 1600 °C. The integral (6.6) can now be numerically evaluated and the activity of SiO_2 as obtained in the present work is compared with previous works in figure 6.16. It is seen that the activity found in the present work is somewhat higher than found in most of the other works. A good agreement with Rein and Chipman (1965) is seen for the SiO_2-rich side while the activity of SiO_2 is found to be somewhat higher for lower SiO_2 content in the slag. The activity of SiO_2 found in the present work close to Ca_2SiO_4 saturation is however found to be in good agreement with other works. The activity of SiO_2 found in the present work can be expressed by the formula

$$\begin{aligned} a_{\mathrm{SiO_2}} &= x_{\mathrm{SiO_2}}\exp(2154.432x^5_{\mathrm{SiO_2}} - 6458.771x^4_{\mathrm{SiO_2}} + 7818.517x^3_{\mathrm{SiO_2}} \\ &\quad -4796.372x^2_{\mathrm{SiO_2}} + 1497.522x_{\mathrm{SiO_2}} - 190.7277) \end{aligned} \tag{6.11}$$

We have saturation with Ca_2SiO_4 at the liquidus line on the CaO-rich side of the liquid region in the binary CaO-SiO_2 system. The activity of CaO at Ca_2SiO_4 saturation can be calculated using the activity of SiO_2 and thermochemical data. From the NIST-JANAF Tables (1998) we have that the Gibbs energy of formation of SiO_2 (solid cristobalite) is -575.914 kJ/mol at 1600 °C and that the Gibbs energy of formation of CaO(s) is -426.199 kJ/mol. From Barin (1995) we have that the Gibbs energy of formation of Ca_2SiO_4 is -1573.218 kJ/mol at 1600 °C. The activity of CaO can thus be calculated from the activity of SiO_2 at Ca_2SiO_4 saturation from the equilibrium

$$\mathrm{Ca_2SiO_4} = 2\mathrm{CaO} + \mathrm{SiO_2} \tag{6.12}$$

where $K = 9.10\cdot 10^{-5}$. Using this equilibrium we get

$$a_{\mathrm{CaO}} = \sqrt{\frac{9.10\cdot 10^{-5}}{0.0842}} = 3.29\cdot 10^{-4} \tag{6.13}$$

The activity of CaO can now be determined by Gibbs-Duhem integration of the activity of SiO_2 and it is compared with other works in figure 6.17. The activity found in the present work is somewhat higher than found in other works, but it is in good agreement with Rein and Chipman in the SiO_2-rich end of the system. The activity found in the present work is somewhat lower than found by Rein and Chipman for higher CaO content in the slag and at Ca_2SiO_4 saturation the activity of CaO is found to be somewhat higher than found by Rein and Chipman. The formula

$$\begin{aligned} a_{\mathrm{CaO}} &= x_{\mathrm{CaO}}\exp(882.284x^5_{\mathrm{CaO}} - 1765.11x^4_{\mathrm{CaO}} + 1453.86x^3_{\mathrm{CaO}} \\ &\quad -590.304x^2_{\mathrm{CaO}} + 115.678x_{\mathrm{CaO}} - 13.3528) \end{aligned} \tag{6.14}$$

reproduces the activity of CaO found in the present work.

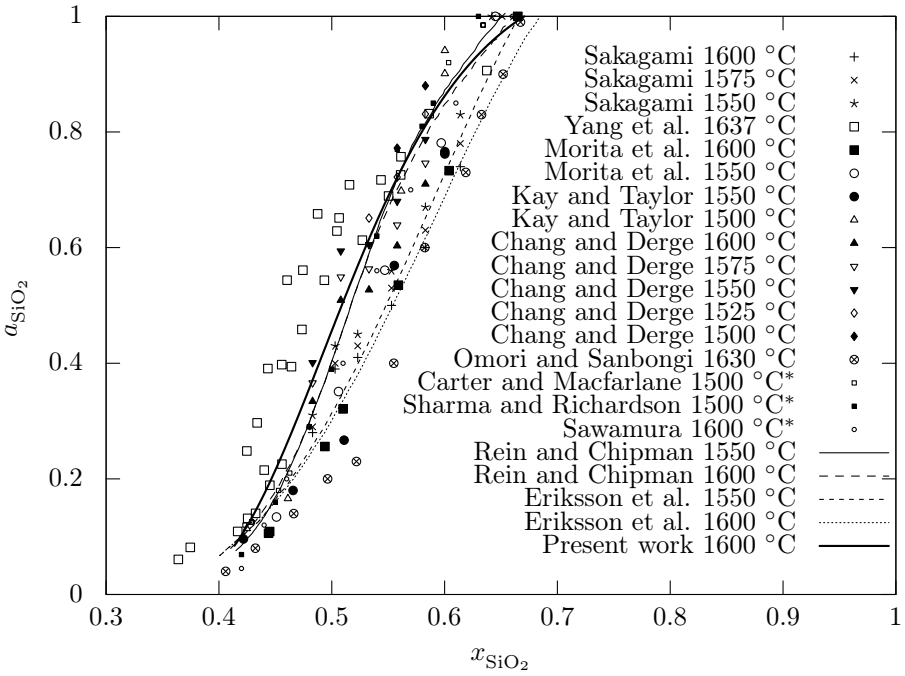

Figure 6.16: Activity of SiO_2 in the binary CaO-SiO_2 slag system as found in the present work compared with previous works. (* Determined by Gibbs-Duhem integration of the activty of CaO)

The activities of CaO and SiO_2 can be used to calculate the activity coefficient of calcium at infinite dilution in silicon. For the reaction

$$2\mathrm{Ca}(l) + \mathrm{O}_2(g) = 2\mathrm{CaO}(s) \tag{6.15}$$

the Gibbs energy change from the NIST-JANAF Tables is -869.028 kJ/mol. Hence the equilibrium constant for reaction (6.7) is $6.70 \cdot 10^{-9}$ and the activity coefficient of calcium is

$$\ln \gamma^0_{\mathrm{Ca}} = \ln \left(\frac{K \cdot a^2_{\mathrm{CaO}} \cdot x_{\mathrm{Si}}}{a_{\mathrm{SiO}_2} \cdot x^2_{\mathrm{Ca}} \exp(2\epsilon^{\mathrm{Ca}}_{\mathrm{Ca}} x_{\mathrm{Ca}})} \right) = -7.09 \tag{6.16}$$

It should be noted that this activity coefficient is calculated to be the same from any point across the entire liquid region using the present data, which confirms the self-consistency of the calculations. The activity coefficient is compared with other works in figure 6.18 and it is seen to be in best agreement with Pinto and Takano (2000). The activity coefficient found by Miki et al. (1999) was as discussed earlier found using a different value for the Gibbs energy of formation of CaO than found in the NIST-JANAF Tables.

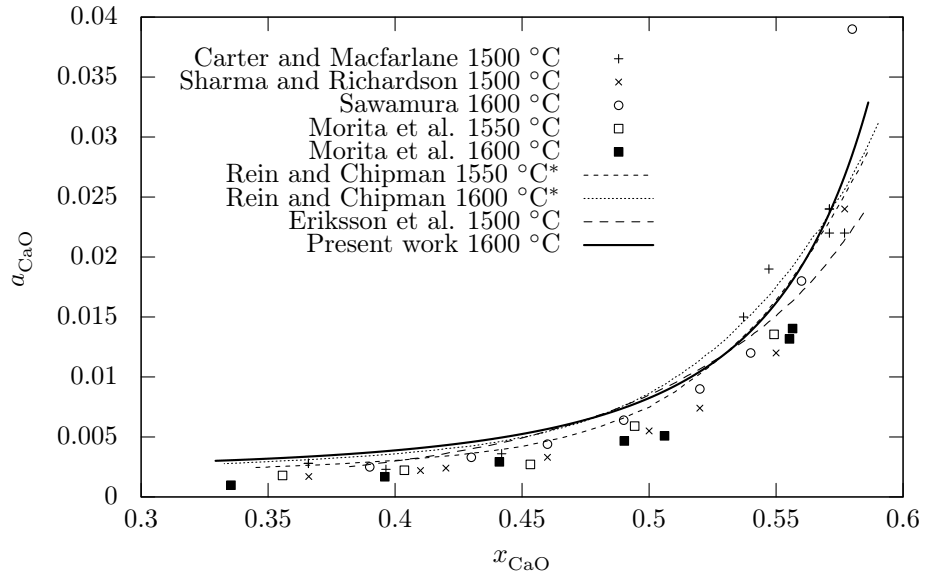

Figure 6.17: Activity of CaO in the binary CaO-SiO_2 slag system as found in the present work compared with previous works. (* Determined by Gibbs-Duhem integration of the activty of SiO_2)

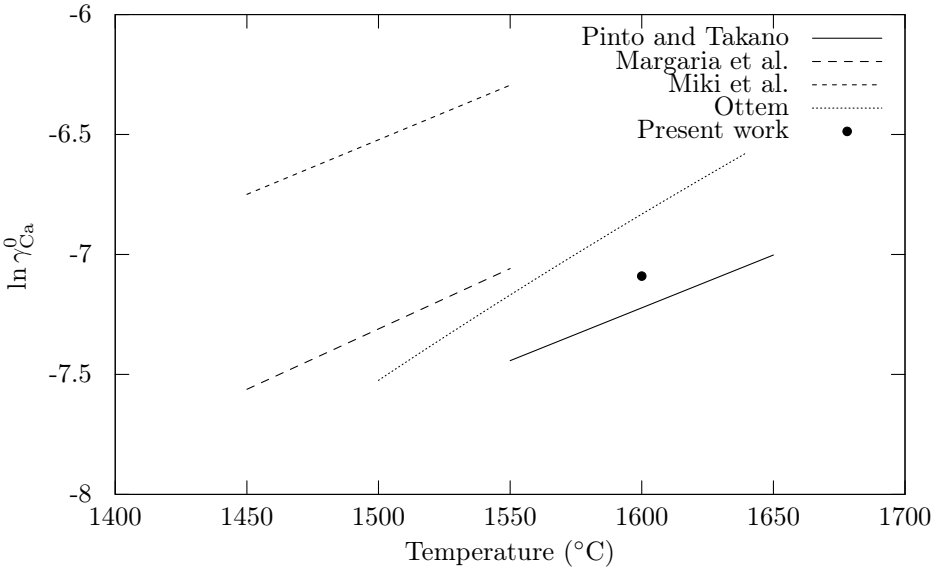

Figure 6.18: Activity coefficient of Ca at infinite dilution in silicon as found in the present work compared with previous works.

6.4 Activities in the binary MgO-SiO_2 system

In the MgO-SiO_2 system we have the equilibrium

$$SiO_2(s) + 2Mg(l) = Si(l) + 2MgO(s) \tag{6.17}$$

between slag and silicon. This equilibrium is equivalent with the equilibrium between a CaO-SiO_2 slag and silicon. The integral for the activity coefficient of SiO_2 is hence given by

$$\ln \gamma_{SiO_2} = \int_{x^0_{MgO}}^{x_{MgO}} \frac{-x_{MgO}}{1 + x_{SiO_2}} \mathrm{d} \ln B + \ln \gamma^0_{SiO_2} \tag{6.18}$$

where

$$\mathrm{d} \ln B = \mathrm{d} \ln \left(\frac{x_{SiO_2} \cdot x^2_{Mg}}{x^2_{MgO} \cdot x_{Si}} \right) \tag{6.19}$$

The self-interaction coefficient of magnesium has been neglected because it is not known at 1600 °C and because the concentration range of Mg in silicon is relatively small. A linear fit is shown in figure 6.9 and it is expressed by

$$x_{Mg} = 0.01079 x_{MgO} - 0.00405 \tag{6.20}$$

This linear fit is used for equation (6.18) to find the activity of SiO_2. The activity of SiO_2 found in the present work is given by the polynomial

$$a_{SiO_2} = 273.63 x^3_{SiO_2} - 395.13 x^2_{SiO_2} + 193.58 x_{SiO_2} - 31.526 \tag{6.21}$$

and it is compared with previous works in figure 6.19. It is seen that the activity of SiO_2 is found to be somewhat lower than in previous works. The magnesium concentrations measured in silicon are somewhat scattered and the slope in the linear fit used for the integration is therefore somewhat uncertain. Less slope would have given an activity of SiO_2 more in agreement with other works.

At the liquidus line in the MgO-rich end of the liquid region we have saturation with Mg_2SiO_4 that has a Gibbs energy of formation of -1326.229 kJ/mol according to Barin (1995). The Gibbs energy of formation of MgO is -345.887 kJ/mol according to the NIST-JANAF Tables. Using these data the activity of MgO can be calculated from the activity of SiO_2 at Mg_2SiO_4 saturation from the equilibrium

$$Mg_2SiO_4 = 2MgO + SiO_2 \tag{6.22}$$

where $K = 0.0233$. The activity of MgO at Mg_2SiO_4 saturation is hence

$$a_{MgO} = \sqrt{\frac{0.0233}{0.644}} = 0.190 \tag{6.23}$$

This value was used to find the activity of MgO across the liquid region by Gibbs-Duhem integration of the activity of SiO_2 and the activity is given by

$$a_{MgO} = -2.3075x_{MgO}^2 + 3.2589x_{MgO} - 0.8735 \tag{6.24}$$

The activity of MgO can also be found by direct integration in the same way as for the activity of SiO_2. It is compared with previous works in figure 6.19. The activity is seen to be in best agreement with Kambayashi and Kato (1983) in the MgO-rich end of the system while it is in best agreement with Rein and Chipman (1965) in the SiO_2-rich end of the system. Kambayashi and Kato found the liquid region to go to much higher MgO content in the slag than in the presently known phase diagram. The uncertainty of the activity curve for MgO found in the present work is the same as for SiO_2.

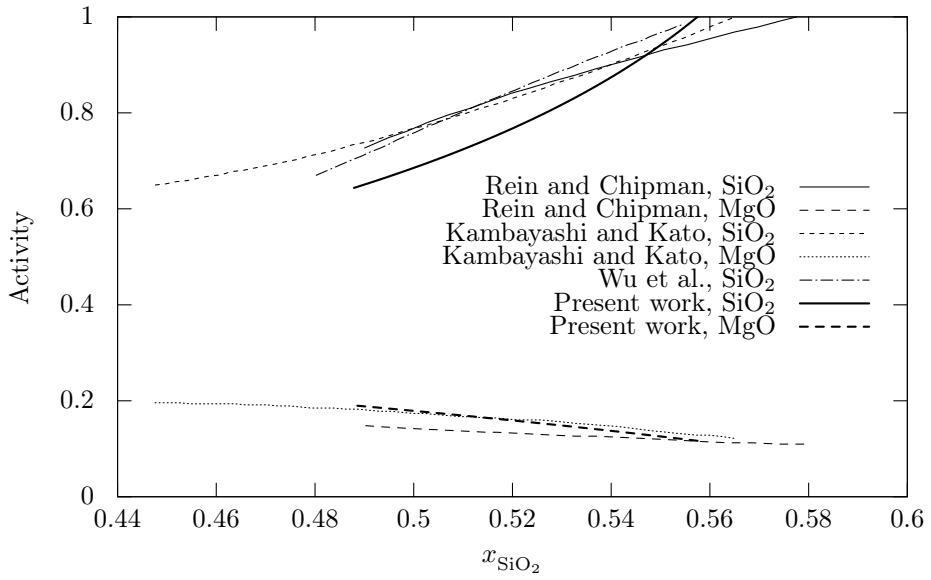

Figure 6.19: Activity of MgO and SiO_2 at 1600 °C in a binary CaO-SiO_2 slag as found in the present work compared with previous works.

The activity coefficient of magnesium at infinite dilution in silicon can be calculated in the same way as the activity coefficient of calcium was calculated in the binary CaO-SiO_2 system. The reaction

$$2Mg(l) + O_2(g) = 2MgO(s) \tag{6.25}$$

have a Gibbs energy change of -738.086 kJ/mol at 1600 °C according to the NIST-JANAF Tables. Hence the equilibrium constant for reaction (6.17) is $3.00 \cdot 10^{-5}$. The activity coefficient of magnesium at infinite dilution in silicon

can then be calculated from the present data to be

$$\gamma^0_{\mathrm{Mg}} = \sqrt{\frac{K \cdot a^2_{\mathrm{MgO}} \cdot x_{\mathrm{Si}}}{a_{\mathrm{SiO_2}} \cdot x^2_{\mathrm{Mg}}}} = 0.88 \tag{6.26}$$

An extrapolation of the activity coefficient found by Miki et al. (1998) to 1600 °C gives $\gamma^0_{\mathrm{Mg}} = 0.22$. The activity coefficient found in the present work therefore indicates less deviation from ideal behaviour than found by Miki et al.

6.5 Activities in the ternary CaO-MgO-SiO_2 system

Determination of activities in the ternary CaO-MgO-SiO_2 system has not been attempted by Gibbs-Duhem integration because the integral must be started from saturation with either MgO or SiO_2. Extrapolation even further than shown in the binary MgO-SiO_2 system would be necessary and the uncertainties are therefore considered to be too large for a good estimate of activities. A calculation of the activity of CaO and MgO is however possible using the determined activity coefficients γ^0_{Ca} and γ^0_{Mg} together with the determined activity of SiO_2 in the binary CaO-SiO_2 system and the iso-activity lines for SiO_2 in figure 3.14.

A decent linear estimate of the iso-activity lines for SiO_2 can be made by observing that the lines are parallel to the liquidus line close to SiO_2 saturation in figure 3.14. The iso-line for $a_{\mathrm{SiO_2}} = 0.1$ by Jung et al. (2005) is chosen as representative for the region with low SiO_2 content. Based on these two observations an expression for the iso-lines was found:

$$C = \frac{x_{\mathrm{CaO}} + x_{\mathrm{MgO}}(0.97 - 0.63 x_{\mathrm{SiO_2}})}{x_{\mathrm{SiO_2}}} \tag{6.27}$$

where the $C = x_{\mathrm{CaO}}/x_{\mathrm{SiO_2}}$ at the starting point for each iso-line in the binary CaO-SiO_2 system.

The calculated activities of CaO is compared with the work by Rein and Chipman (1965) and the work by Morita et al. (2002) in figure 6.20. The activities in the binary CaO-SiO_2 system have already been shown to be in good agreement with the work by Rein and Chipman. The present work is in the middle between the work by Morita et al. and the work by Rein and Chipman in the SiO_2-rich part of the ternary system while it is in best agreement with the work by Rein and Chipman in the CaO-rich part of the ternary system.

The calculated activities of MgO are compared with the work by Rein and Chipman and the work by Morita et al. in figure 6.21. The present work is seen to follow the iso-activity curves of Morita et al. better than the curves found by Rein and Chipman. The activities of MgO found in the present work

is however approximately 25% lower than the iso-activity curve for $a_{\mathrm{MgO}} = 0.3$ and approximately 35% lower than the curve for $a_{\mathrm{MgO}} = 0.2$.

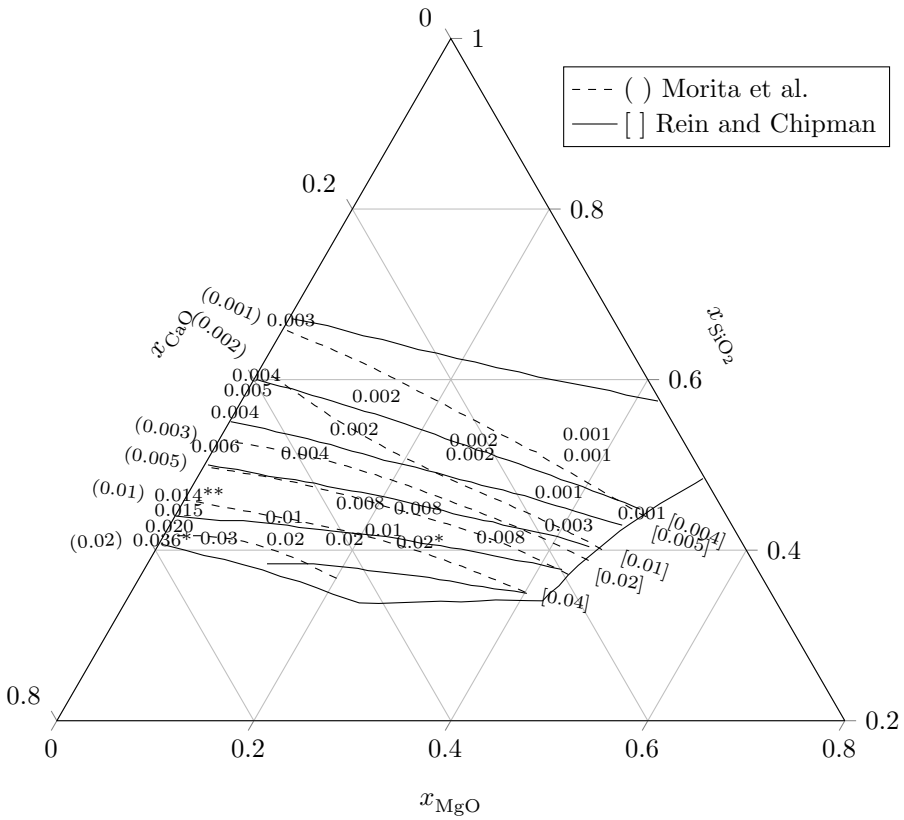

Figure 6.20: Calculated activities of CaO, shown as numbers without parentheses, in the ternary CaO-MgO-SiO_2 system compared with previous works. (* Mean value of two experiments. ** Mean value of three experiments.)

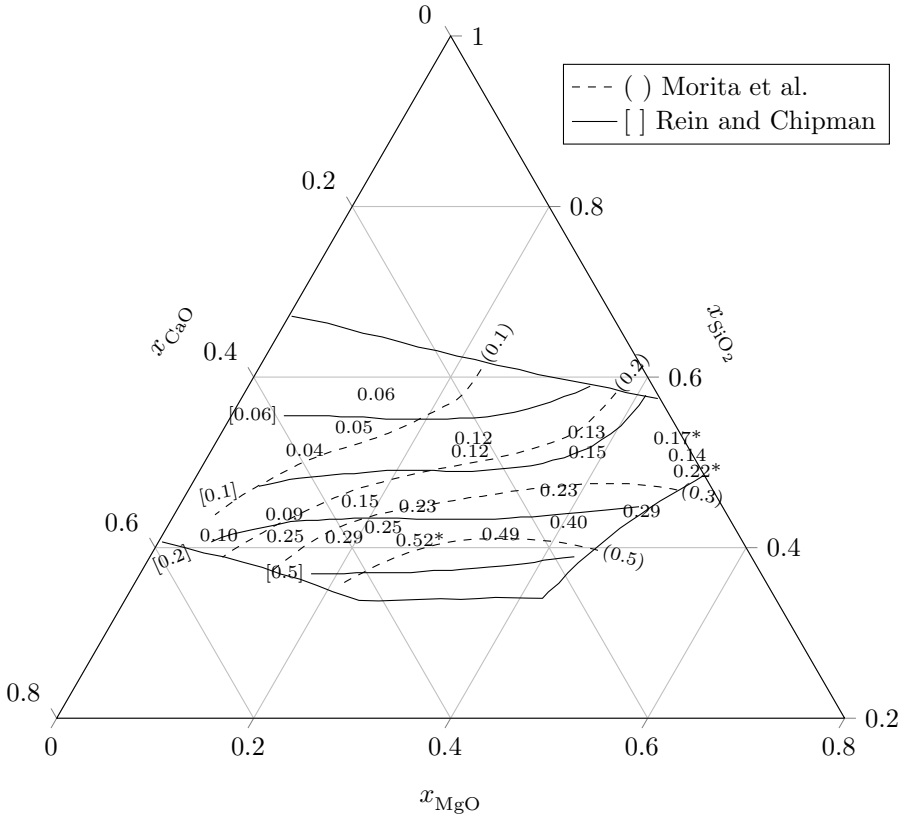

Figure 6.21: Calculated activities of MgO, shown as numbers without parentheses, in the ternary CaO-MgO-SiO_2 system compared with previous works. (* Mean value of two experiments.)

6.6 Activities in the ternary CaO-Al_2O_3-SiO_2 system

The calcium concentration in silicon in equilibrium with ternary CaO-Al_2O_3-SiO_2 slags can be estimated using activity data together with the activity coefficient of calcium determined in the present work. The self-interaction coefficient of calcium in silicon found by extrapolation of the data by Miki et al. (1999) was also used in the calculation while interaction between calcium and aluminium has been neglected. Activities of CaO and SiO_2 were taken from the work by Rein and Chipman (1965) and calculated using FactSage. These values are shown in table 6.1 where the values from Rein and Chipman has been estimated from the iso-activity lines in their work. Rein and Chipman did not determine any iso-activity lines for low Al_2O_3 concentrations and the activities for Al_2O_3 in this region may therefore be inaccurate. The estimated calcium concentration using these data is compared with the concentrations found in the present work in table 6.2.

The concentrations calculated using activity data for CaO and SiO_2 from FactSage is seen to be in better agreement with the present work than the calculated values using activity data from Rein and Chipman (1965). The experiments CAS6 and CAS7 have a relatively high concentration of calcium in silicon and the calculations are most accurate close to infinite dilution. Deviations between calculated values and measured values may therefore be expected for these experiments. The most notable deviation between measured value and calculated value using FactSage is therefore in experiment CAS7. The activty of SiO_2 may therefore be higher or the activity of CaO may be lower than the values from FactSage. More measurements would however be necessary confirm this deviation.

Table 6.1: Activities of slags in the ternary CaO-Al_2O_3-SiO_2 system.

	FactSage			Rein and Chipman		
ID.	a_{CaO}	a_{SiO_2}	$a_{Al_2O_3}$	a_{CaO}	a_{SiO_2}	$a_{Al_2O_3}$
CAS4	0.032	0.037	0.032	0.03	0.085	0.002
CAS5	0.033	0.024	0.151	0.038	0.030	0.070
CAS6	0.043	0.012	0.223	0.065	0.009	0.203
CAS7	0.006	0.235	0.026	0.006	0.330	0.003
CAS8	0.010	0.084	0.277	0.013	0.160	0.099
CAS3	0.015	0.040	0.437	0.03	0.030	0.336

The activities from FactSage were selected for estimation of the activity coefficient of aluminium at infinite dilution in silicon based on the calculations for calcium in the ternary CaO-Al_2O_3-SiO_2 system. The self-interaction coefficient of aluminium found by Miki et al. (1999) was also used in the calculation. The calculated activity coefficient of aluminium is shown in table 6.2 for experiments CAS3 to CAS8. These estimates are somewhat scattered

Table 6.2: Calcium concentration in wt% in silicon found in the present work compared with calculated concentrations using activity data from literature. Estimated activity coefficient of aluminium at infinite dilution in silicon estimated using activity data from FactSage is shown on the right hand side of the table.

ID.	Calcium in silicon (wt%) Measured	FactSage	Rein and Chipman	Al in Si (wt%)	γ^0_{Al}
CAS4	1.95	2.06	1.33	0.33	0.66
CAS5	4.56	2.58	2.62	1.28	0.43
CAS6	6.69	4.26	6.42	2.55	0.36
CAS7	0.12	0.17	0.15	0.05	0.97
CAS8	0.49	0.49	0.44	0.51	0.67
CAS3	1.11	1.00	2.13	1.48	0.43

but some of the experiments can be considered more reliable for estimation of the activity coefficient. An estimate of the activity coefficient of aluminium at infinite dilution in silicon can be made if we exclude the experiments where the aluminium concentration was above 1 wt% and experiment CAS7 since it was deviating for calcium. The two experiments we are left with are CAS4 and CAS8 which are almost identical with respect to the activity coefficient of aluminium even if the concentration of calcium in silicon is 2% for experiment CAS4. An average of these two experiments gives $\gamma^0_{Al} = 0.66$. This is somewhat higher than the value of 0.23 found by extrapolation of the data found by Miki et al. to 1600 °C. The activity coefficient found in the present work is also somewhat higher than the activity coefficient found by Margaria et al. (1996) where $\gamma^0_{Al} = 0.45 \pm 0.09$ and the activity coefficient of 0.53 which they calculated from the work by Weiss and Schwerdtfeger (1994). The experiments CAS3 and CAS5 are seen to be in best agreement with the work by Margaria et al. but the aluminium and calcium concentrations in silicon are not as close to infinite dilution as in experiments CAS4 and CAS8 which for this reason are considered to be more reliable for the estimation of γ^0_{Al}.

6.7 The activity of $BO_{1.5}$ at infinite dilution in slags

In this section the activity coefficient of $BO_{1.5}$ is always at infinite dilution even if it is just referred to as the activity coefficient of $BO_{1.5}$. It can be calculated from the data obtained in the present work using thermochemical data. The best estimate of the activity coefficient of boron at infinite dilution in silicon is given by Yoshikawa and Morita (2005) as discussed in chapter 2.2. Using their equation (2.4) the activity coefficient is found to be $\gamma_B^0 = 3.84$ at 1600 °C. An estimate of the activity coefficient of boron oxide at infinite dilution in slag can now be made using the reaction

$$B(l) + 3/4SiO_2(s) = BO_{1.5}(l) + 3/4Si(l) \tag{6.28}$$

where

$$B(l) + 3/4O_2(g) = BO_{1.5}(l) \tag{6.29}$$

have a Gibbs energy change of -427.490 kJ/mol according to the NIST-JANAF Tables. The equilibrium constant for reaction (6.28) is thus $K = 0.75$. By rearranging equation (2.22) and approximating that boron is infinitely diluted in silicon and slag we get

$$\gamma^0_{BO_{1.5}} = \frac{K \cdot \gamma^0_B \cdot a^{3/4}_{SiO_2}}{k_{x\to\%} \cdot L_B \cdot x^{3/4}_{Si}} \tag{6.30}$$

where silicon has been assumed to follow Raoult's law and

$$k_{x\to\%} = \frac{\frac{[\%Si]}{M_{Si}} + \frac{[\%Ca]}{M_{Ca}}}{\frac{(\%SiO_2)}{M_{SiO_2}} + \frac{(\%CaO)}{M_{CaO}}} \tag{6.31}$$

in the binary CaO-SiO_2 system. The activity coefficient of $BO_{1.5}$ can be calculated using the linear fit for the distribution coefficient of boron shown as a dashed line in figure 6.1 together with the activity of SiO_2 found in the present work. The activity coefficient of $BO_{1.5}$ is compared with the activity coefficient of SiO_2 in figure 6.22 and it is seen that the activity coefficient of $BO_{1.5}$ is somewhat lower but follows approximately the same trend. In figure 6.23 is the activity coefficient of $BO_{1.5}$ plotted against the activity coefficient of SiO_2 and they are seen to be relatively well correlated. The linear fit shown in the figure gives $\gamma^0_{BO_{1.5}} = 0.41\gamma_{SiO_2}$.

The same procedure can be used to find the activity coefficient of boron in the binary MgO-SiO_2 system using the linear fit for the distribution coefficient of boron shown in figure 6.2 and the activity of SiO_2 found by Gibbs-Duhem integration. Also in this system the activity coefficient of boron is somewhat lower and following the same trend as the activity coefficient of SiO_2 as can be seen in figure 6.24. In this system we have $\gamma^0_{BO_{1.5}} = 0.42\gamma_{SiO_2}$

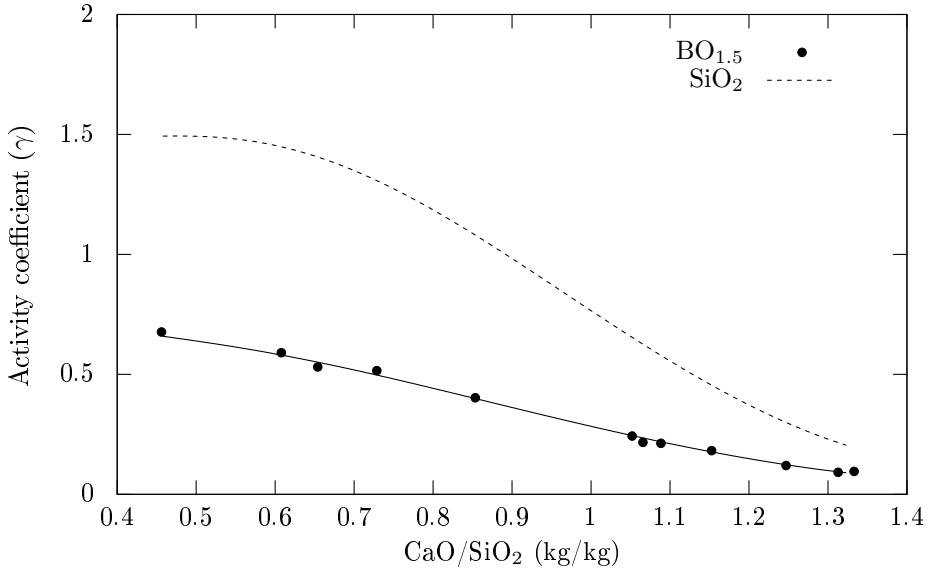

Figure 6.22: Activity coefficient of $BO_{1.5}$ at infinite dilution in slag and activity coefficient of SiO_2 in the binary CaO-SiO_2 system as found in the present work.

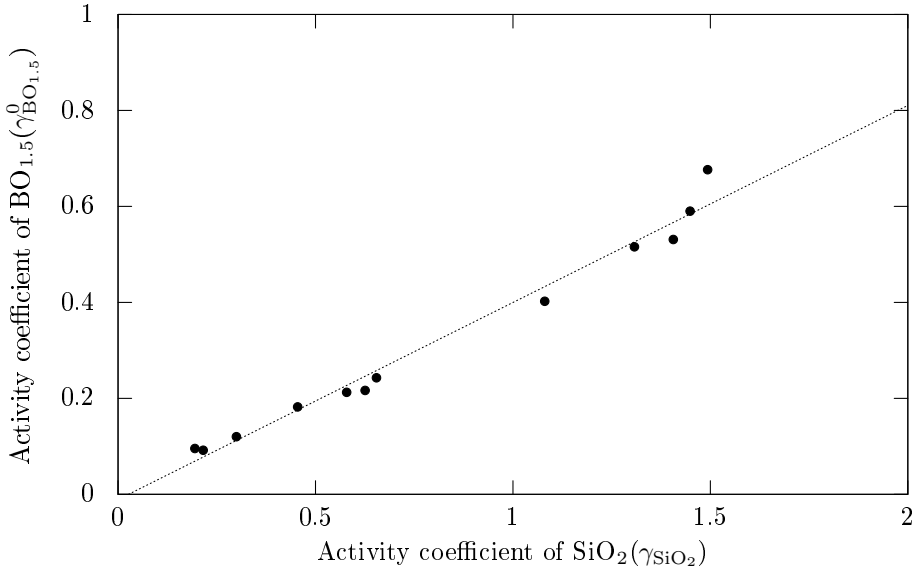

Figure 6.23: Correlation between the activity coefficient of $BO_{1.5}$ at infinite dilution in slag and activity coefficient of SiO_2 in the binary CaO-SiO_2 system as found in the present work.

Using equation 6.27 to calculate the activity of SiO_2 we can compare the activity coefficient of SiO_2 and $BO_{1.5}$ across the entire ternary CaO-MgO-

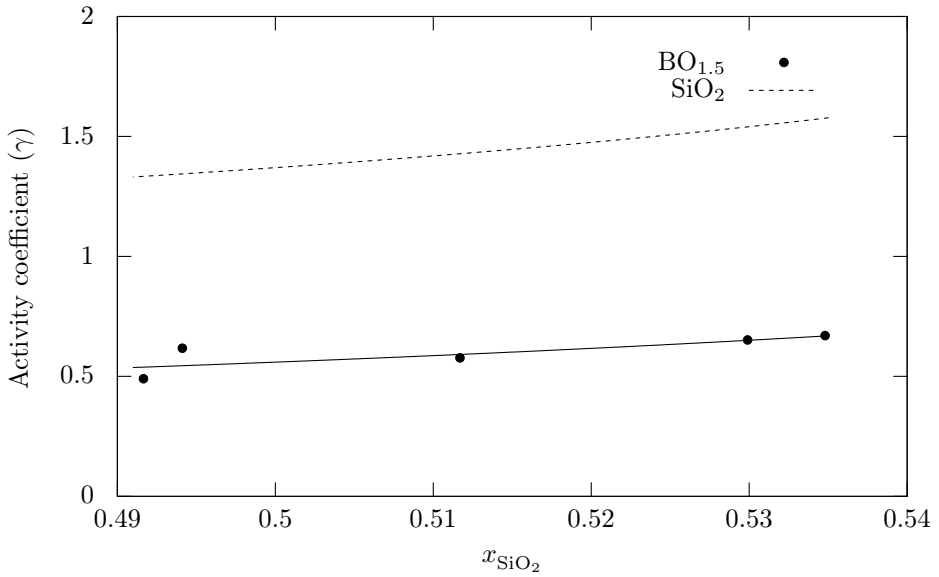

Figure 6.24: Activity coefficient of $BO_{1.5}$ at infinite dilution in slag and activity coefficient of SiO_2 in the binary MgO-SiO_2 system as found in the present work.

SiO_2 system. The activity coefficient of $BO_{1.5}$ in the ternary system can be calculated in the same way as for the binary systems where the activity of SiO_2 from the binary system is extended into the ternary system by replacing x_{SiO_2} in equation (6.11) with $1/(1+C)$. The calculated activity coefficient of $BO_{1.5}$ is compared with the activity coefficient of SiO_2 in figure 6.25 and the coefficients are seen to be correlated across the entire system. The activity coefficient of SiO_2 is larger for higher SiO_2 content in the slag and the same is also true for $BO_{1.5}$. In this system the linear correlation is given by $\gamma^0_{BO_{1.5}} = 0.38\gamma_{SiO_2}$. The activity coefficient of $BO_{1.5}$ is seen to be somewhat more scattered in the SiO_2-rich part of the system.

Activity coefficients in the ternary CaO-Al_2O_3-SiO_2 system can be estimated in the same way as in the previously discussed systems using the activity data from FactSage shown in table 6.1. Possible interactions between boron and calcium and between boron and aluminium have been neglected even if the concentration of both calcium and aluminium is relatively high. The ratio between the activity coefficient of $BO_{1.5}$ and SiO_2 are shown as a function of $x_{Al_2O_3}$ in figure 6.26 and it is seen that the activity coefficient of $BO_{1.5}$ becomes larger than the activity coefficient of SiO_2 when Al_2O_3 is added to the system. The ratio of activity coefficients for experiment CS4 and CS7 in the binary CaO-SiO_2 system and a linear fit forced through $\gamma^0_{BO_{1.5}}/\gamma_{SiO_2} = 0.38$ at $x_{Al_2O_3} = 0$ are also shown in the figure.

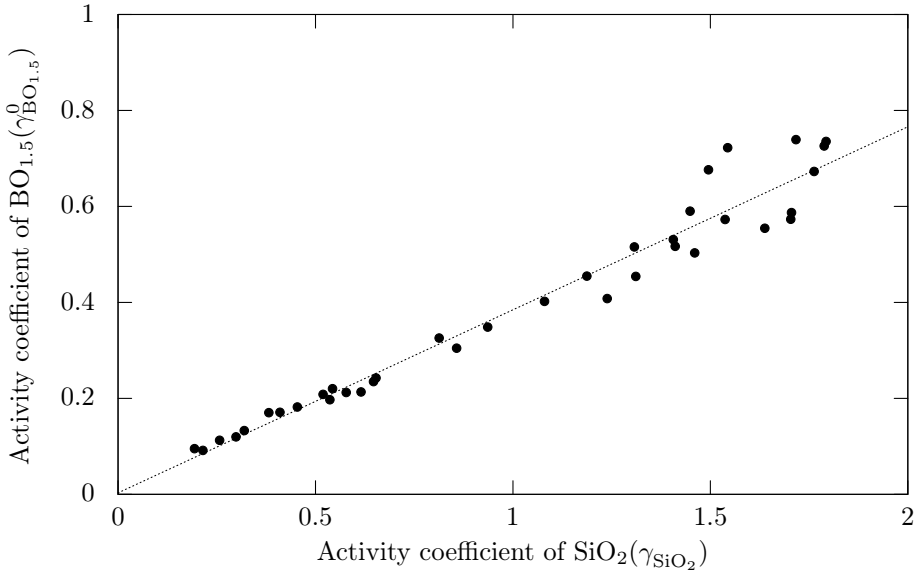

Figure 6.25: Activity coefficient of $BO_{1.5}$ at infinite dilution in slag compared with the activity coefficient of SiO_2 in the ternary CaO-MgO-SiO_2 system. The activity coefficients increase with increasing SiO_2 content in the slag.

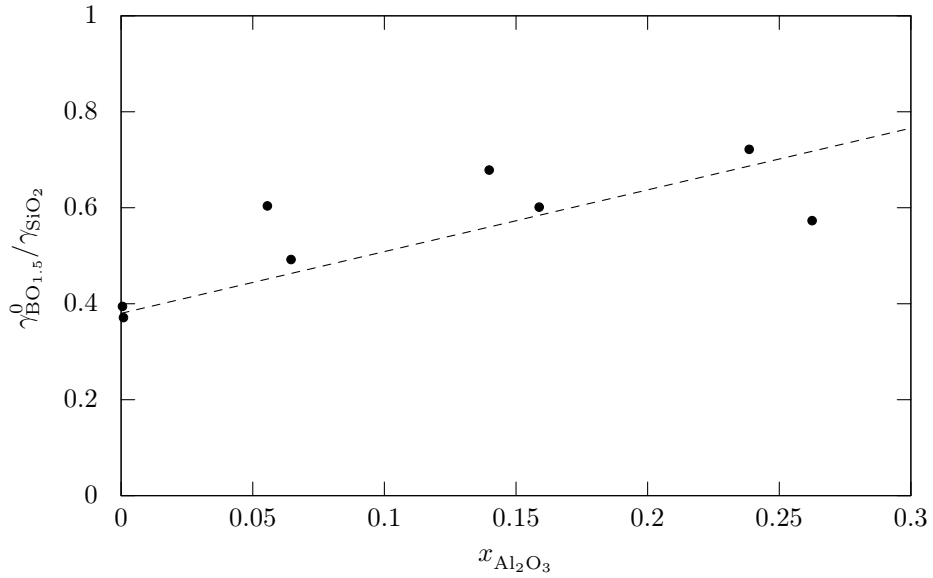

Figure 6.26: Ratio of the activity coefficient of $BO_{1.5}$ at infinite dilution in slag and activity coefficient of SiO_2 as a function of $x_{Al_2O_3}$ in the ternary CaO-Al_2O_3-SiO_2 system.

6.8 Activities of calcium and boron in ferrosilicon

The distribution of calcium and boron between a binary 51.7%CaO-48.3%SiO_2 slag and ferrosilicon has been investigated in the present work, and both calcium and boron is present as a dilute species in silicon for all experiments in this system. The equation

$$[\%Ca] = \exp(-8.8393 \cdot 10^{-4} \cdot [\%Si]^2 + 0.2120[\%Si] - 13.4594) \qquad (6.32)$$

gives a good fit to the experimental data as shown in figure 6.27. This equation can be merged with equation (6.3) to get one unified equation for the calcium concentration in ferrosilicon in equilibrium with CaO-SiO_2 slags. The calcium concentration with 100% silicon is chosen to be according to equation (6.3) and hence we get the unified equation to be

$$[\%Ca] = \exp(3.002 \cdot V^2 - 1.2481 \cdot V - 8.839 \cdot 10^{-4} \cdot [\%Si]^2 + 0.212[\%Si] - 15.5848) \qquad (6.33)$$

where V is the CaO/SiO_2 mass ratio and [%Si] is the concentration of silicon in ferrosilicon. This equation can be used to calculate the concentration of calcium in ferrosilicon in equilibrium with a binary CaO-SiO_2 slag for ferrosilicon containing up to 50 wt% iron.

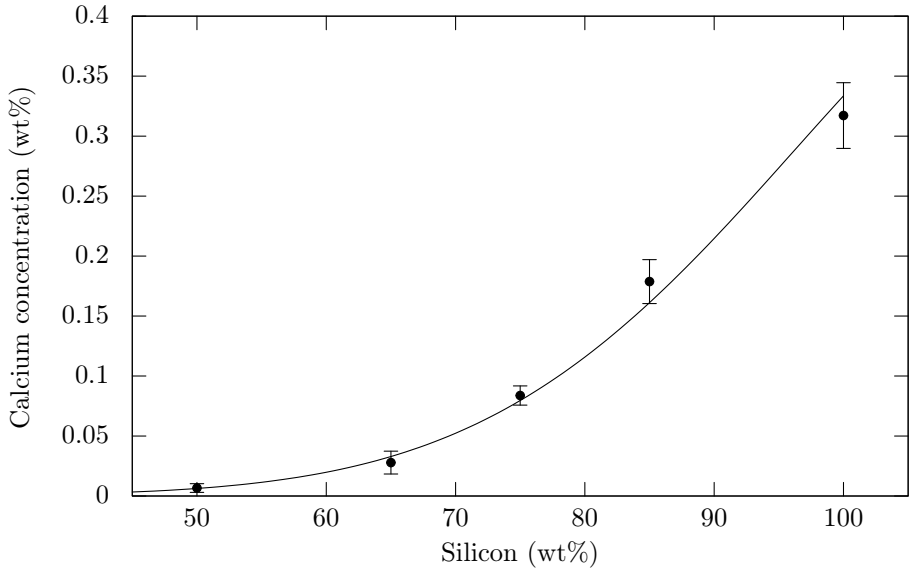

Figure 6.27: Calcium concentration in ferrosilicon as a function of silicon concentration in ferrosilicon with a non-linear fit.

The carbon solubility in ferrosilicon is low in the range investigated in this work as can be seen in figure 6.28. Interaction between carbon and other impurity elements in the alloy was therefore assumed to be negligible.

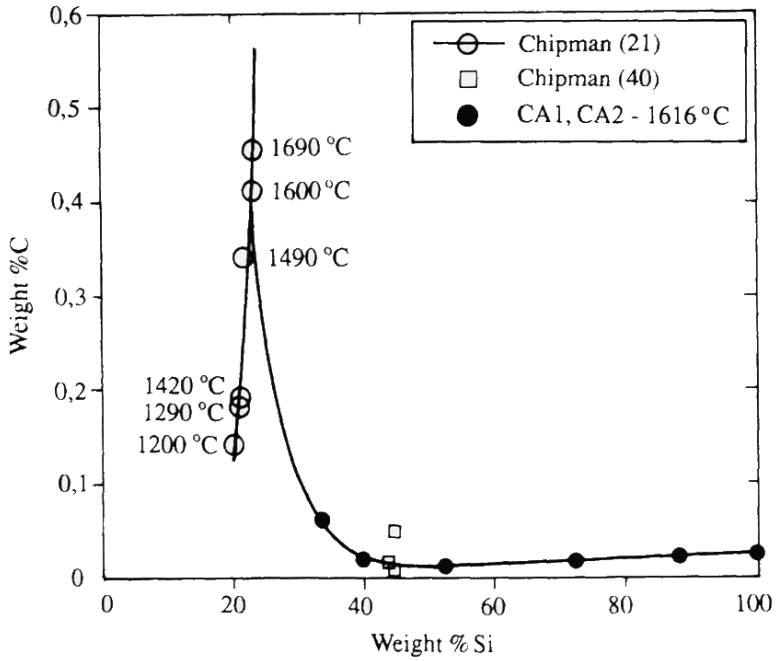

Figure 6.28: Carbon solubility in ferrosilicon (Schei et al., 1998).

The activity coefficient of calcium at infinite dilution in ferrosilicon can be calculated using the activity coefficient at infinite dilution in silicon as a starting point. The concentration of calcium in ferrosilicon in silicon is controlled by equilibrium (6.7). The activity of CaO and SiO_2 is constant since the slag composition is constant and we get the following expression for the activity coefficient of calcium in ferrosilicon

$$\ln \gamma^0_{\text{Ca in FeSi}} = \ln \gamma^0_{\text{Ca}} + \ln \left(\frac{a_{\text{Si}} x^2_{\text{Ca},0}}{a_{\text{Si},0} x^2_{\text{Ca}}} \right) \tag{6.34}$$

where $a_{\text{Si},0} = 1$ and $x_{\text{Ca},0}$ is given by equation (6.32) at 100% Si. Figure 6.29 shows the activity coefficient as a function of $x_{\text{Fe}}/x_{\text{Si}}$ and the negative interaction of calcium with silicon is seen to be cancelled of the positive interaction with iron at $x_{\text{Fe}}/x_{\text{Si}} = 0.52$. The activity coefficient can be expressed by the linear fit shown in the figure which is given by

$$\ln \gamma^0_{\text{Ca in FeSi}} = -7.09 + 13.8 \frac{x_{\text{Fe}}}{x_{\text{Si}}} \tag{6.35}$$

The activity coefficient of boron in ferrosilicon can also be calculated. Having a constant activity of SiO_2 and constant $\gamma^0_{\text{BO}_{1.5}}$ we get

$$\ln \gamma^0_{\text{B in FeSi}} = \ln \gamma^0_{\text{B}} + \ln \left(\frac{L_{\text{B}} k_{x\to\%} a^{3/4}_{\text{Si}}}{L^0_{\text{B}} k^0_{x\to\%} a_{\text{Si},0}} \right) \tag{6.36}$$

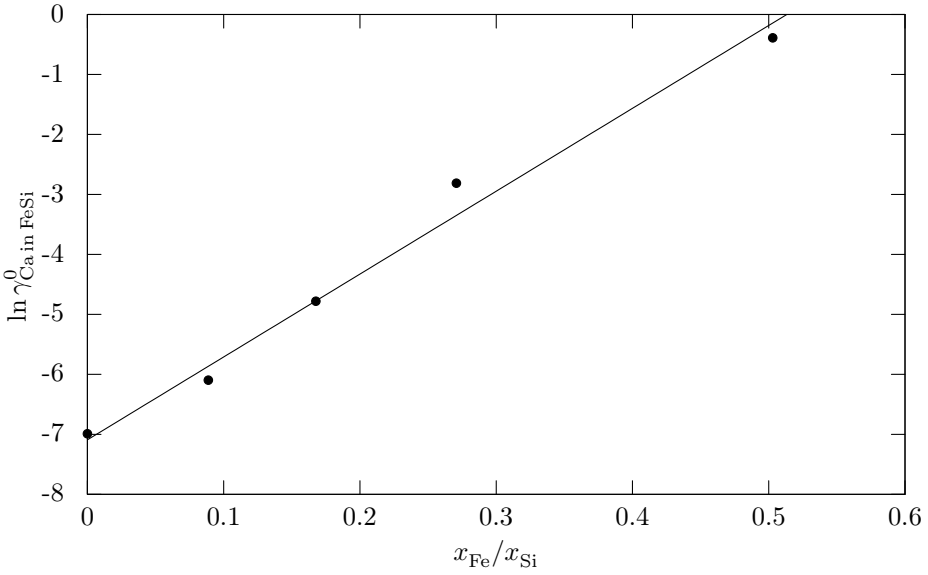

Figure 6.29: Activity coefficient of calcium at infinite dilution in ferrosilicon as a function of alloy composition.

where L^0_{B} is taken from the experiment with 100% silicon, $k^0_{x\to\%}$ is calculated using the average slag composition after the five experiments and $a_{\text{Si},0} = 1$. The activity of silicon in ferrosilicon is taken from Elliott et al. (1963). The calculated activity coefficient of boron in ferrosilicon is shown in figure 6.30 and it is seen that the activity coefficient of boron decreases with increasing iron content in the alloy. The activity coefficient can be expressed by the linear fit

$$\ln \gamma^0_{\text{B in FeSi}} = 1.34 - 1.21 \frac{x_{\text{Fe}}}{x_{\text{Si}}} \tag{6.37}$$

which is also shown in the figure.

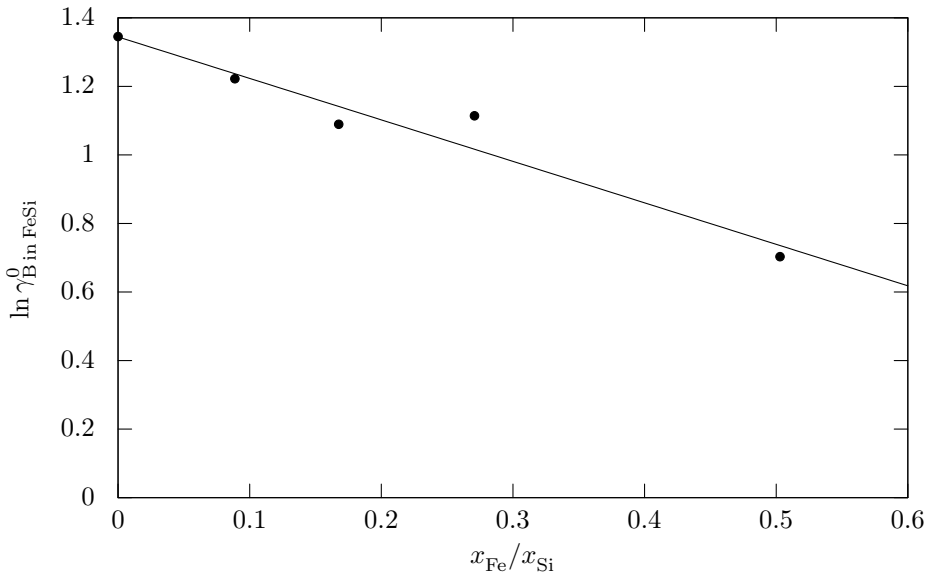

Figure 6.30: Activity coefficient of boron at infinite dilution in ferrosilicon.

6.9 Transfer of boron between slag and silicon

An estimate of the mass transfer coefficient can be made for the binary CaO-SiO_2 system based on the results in the present work. Equation (2.26) is given below and it is seen that this equation is in terms of the boron concentration in silicon.

$$\frac{[\overline{\%B}] - [\%B]_{eq}}{[\%B]_{in} - [\%B]_{eq}} = \exp\left(-\frac{k_t \rho A_s t}{M}\left(1 + \frac{M}{M_s L_B}\right)\right) \tag{6.38}$$

where $[\overline{\%B}]$ is the average concentration of boron in silicon at the time t. The rest of the transport equation is unchanged where $[\%B]_{in}$ is the initial boron concentration in silicon, $[\%B]_{eq}$ is the boron concentration in silicon at chemical equilibrium, k_t is the total mass transfer coefficient, ρ is the density of silicon, A_s is the slag/silicon interface area, M is the total mass of silicon, M_s is the total mass of slag, and L_B is the distribution coefficient of boron.

A mass transfer equation in terms of the ratio between the boron concentration in slag and in silicon would be more appropriate for an evaluation of the results in the present work. Such an equation can be derived in a similar way as equation (2.26), as will be shown below.

Figure 2.4 shows the concentration profile when boron is transferred to slag. Boron will not be homogeneously distributed in the bulk phases since convection is limited in the system. Mean concentration in slag ($\overline{\%B}$) and silicon $[\overline{\%B}]$ is therefore used here. The work by Krystad et al. (2012) and Nishimoto et al. (2012) indicates, as discussed in chapter 2.3.2, that the mass transfer equation holds as a good approximation for the behaviour of the system even if the bulk phases may not be completely mixed. The initial boron concentration in slag is approximately zero and the molar flux of boron, $\dot{n}$, is hence from silicon to slag.

$$\dot{n} = \frac{k_s \rho_s}{100 M_B}\left((\%B)_i - (\overline{\%B})\right) \tag{6.39}$$

and the molar flux in silicon is

$$\dot{n} = \frac{k\rho}{100 M_B}\left([\overline{\%B}] - [\%B]_i\right) \tag{6.40}$$

The reaction at the interface is assumed to be at equilibrium. Hence the concentration ratio at the interface is equal to the distribution coefficient of boron

$$L_B = \frac{(\%B)_i}{[\%B]_i} \tag{6.41}$$

Equation (6.40) can therefore be rearranged and multiplied with the distribution coefficient to get

$$(\%B)_i = [\overline{\%B}] \cdot L_B - \frac{\dot{n} 100 M_B}{k\rho} \cdot L_B \tag{6.42}$$

which can be inserted into (6.39) to get

$$\dot{n} = \frac{k_\mathrm{s}\rho_\mathrm{s}}{100\mathrm{M_B}} \left([\overline{\%\mathrm{B}}] \cdot L_\mathrm{B} - \frac{\dot{n}100\mathrm{M_B}}{k\rho} \cdot L_\mathrm{B} - (\overline{\%\mathrm{B}}) \right) \tag{6.43}$$

and rearrangement gives

$$\dot{n}100\mathrm{M_B} \left(\frac{1}{k_\mathrm{s}\rho_\mathrm{s}} + \frac{1}{k\rho} \cdot L_\mathrm{B} \right) = [\overline{\%\mathrm{B}}] \cdot L_\mathrm{B} - (\overline{\%\mathrm{B}}) \tag{6.44}$$

Nishimoto et al. (2012) have as discussed earlier shown that transfer of boron is controlled by the slag phase and the mass transfer coefficient in silicon can therefore be neglected. The slag investigated in the present study in the binary CaO-SiO_2 system is more viscous than the slag in the study by Nishimoto et al. causing the transfer of boron even more likely to be controlled by the slag phase. Hence it is assumed that the total mass transfer coefficient is equal to the mass transfer coefficient in the slag phase, and we get

$$\dot{n} = \frac{k_\mathrm{s}\rho_\mathrm{s}}{100\mathrm{M_B}} \left([\overline{\%\mathrm{B}}] \cdot L_\mathrm{B} - (\overline{\%\mathrm{B}}) \right) \tag{6.45}$$

The molar flux can also be expressed by the differential change of boron content in slag

$$\dot{n} = \frac{\mathrm{d}}{\mathrm{d}t} \left(\frac{M_\mathrm{s}(\overline{\%\mathrm{B}})}{100\mathrm{M_B}A_\mathrm{i}} \right) \tag{6.46}$$

where A_i is the area of the interface and M_s is the mass of the slag. This equation can be combined with equation (6.45) to give

$$\frac{\mathrm{d}(\overline{\%\mathrm{B}})}{\mathrm{d}t} = \frac{k_\mathrm{s}\rho_\mathrm{s}A_\mathrm{i}}{M_\mathrm{s}} \left([\overline{\%\mathrm{B}}] \cdot L_\mathrm{B} - (\overline{\%\mathrm{B}}) \right) \tag{6.47}$$

we can divide this equation by [%B] and define a non-equilibrium distribution coefficient $C_\mathrm{B} = (\overline{\%\mathrm{B}})/[\overline{\%\mathrm{B}}]$ to get

$$\frac{1}{[\overline{\%\mathrm{B}}]} \frac{\mathrm{d}(\overline{\%\mathrm{B}})}{\mathrm{d}t} = \frac{k_\mathrm{s}\rho_\mathrm{s}A_\mathrm{i}}{M_\mathrm{s}} (L_\mathrm{B} - C_\mathrm{B}) \tag{6.48}$$

Also the left side of the equation must be in terms of C_B if the integral is to be evaluated. We can achieve this by observing that the mass of boron must remain constant in the system

$$\frac{\mathrm{d}}{\mathrm{d}t} \left(M_\mathrm{s}(\overline{\%\mathrm{B}}) + M[\overline{\%\mathrm{B}}] \right) = 0 \tag{6.49}$$

which gives

$$\frac{\mathrm{d}}{\mathrm{d}t}[\overline{\%\mathrm{B}}] = -\frac{\mathrm{d}}{\mathrm{d}t} \left(\frac{M_\mathrm{s}}{M}(\overline{\%\mathrm{B}}) \right) \tag{6.50}$$

where M is the mass of silicon. Hence we get

$$\frac{1}{[\overline{\%\mathrm{B}}]}\frac{\mathrm{d}(\overline{\%\mathrm{B}})}{\mathrm{d}t} = \frac{1}{1+\frac{M_\mathrm{s}}{M}C_\mathrm{B}}\frac{\mathrm{d}C_\mathrm{B}}{\mathrm{d}t} = \frac{k_\mathrm{s}\rho_\mathrm{s}A_\mathrm{i}}{M_\mathrm{s}}\left(L_\mathrm{B}-C_\mathrm{B}\right) \tag{6.51}$$

and the equation can be rearranged and integrated

$$\int_{C_\mathrm{B}^0}^{C_\mathrm{B}} \frac{\mathrm{d}C_\mathrm{B}}{\left(1+\frac{M_\mathrm{s}}{M}C_\mathrm{B}\right)\left(L_\mathrm{B}-C_\mathrm{B}\right)} = \int_0^t \frac{k_\mathrm{s}\rho_\mathrm{s}A_\mathrm{i}}{M_\mathrm{s}}\mathrm{d}t \tag{6.52}$$

which gives

$$\frac{1}{1+\frac{M_\mathrm{s}}{M}L_\mathrm{B}}\ln\left(\frac{(1+\frac{M_\mathrm{s}}{M}C_\mathrm{B})(L_\mathrm{B}-C_\mathrm{B}^0)}{(L_\mathrm{B}-C_\mathrm{B})(1+\frac{M_\mathrm{s}}{M}C_\mathrm{B}^0)}\right) = \frac{k_\mathrm{s}\rho_\mathrm{s}A_\mathrm{i}}{M_\mathrm{s}}\cdot t \tag{6.53}$$

In the binary CaO-SiO_2 system we start with approximately 100 times more boron in silicon than slag, and provided that L_B and $\frac{M}{M_\mathrm{s}}$ is close to or larger than unity we can assume C_B^0 to be zero. The equation becomes independent of the initial concentration of boron in silicon as long as these assumptions are valid.

$$\frac{M_\mathrm{s}}{\rho_\mathrm{s}A_\mathrm{i}(1+\frac{M_\mathrm{s}}{M}L_\mathrm{B})}\ln\left(\frac{1-\frac{1}{L_\mathrm{B}}C_\mathrm{B}}{1+\frac{M_\mathrm{s}}{M}C_\mathrm{B}}\right) = -k_\mathrm{s}t \tag{6.54}$$

The boron content in silicon also has to be so low that boron is a dilute species in the system for the above equation to be valid. We can estimate the interfacial area between slag and silicon from figure 5.4 to be 8.0 cm^2. The equilibrium time has been found to be 6 hours, but the slag composition changes with holding time and the mean of initial slag composition and the composition after 6 hours is therefore chosen to be the representative composition. From the Slag Atlas (1995) we have a density of 2.54 $\mathrm{g/cm}^3$ of this slag composition. The mass of the slag after 9 hours have been estimated in chapter 5.6 to be 12.25 g. We can assume the mass to change linearly with time and get the mass of the slag to be 13.2 g after half the equilibrium time. The mass of silicon after half the equilibrium time can in the same way be estimated to be $15.04\mathrm{g} - 0.10\mathrm{g}/3 \approx 15.0$ g. The distribution coefficient of boron is estimated by the mean value of experiment CS3-CS5 in table 5.1 to be 2.18. These experiments are not included in the regression since exponential regression is very sensitive to measurement errors in experiments close to equilibrium. The left hand side of equation (6.54) can now be plotted as a function of time and the mass transfer coefficient of boron is given by the slope of the linear fit in figure 6.31. Hence the mass transfer coefficient is found to be $k_\mathrm{s} = 5.2\cdot 10^{-7}$ m/s for the binary 37.9%CaO-62.1%SiO_2 system. The mass transfer coefficient in the slag will, as mentioned above, be equal to the total mass transfer coefficient since mass transfer is controlled by the slag phase. The linear fit is seen not to intersect with the x-axis when time is

zero. The most probable explanation for this delayed onset of mass transfer is that the slag and silicon may not have been completely melted when the system reached 1600 °C. The mass transfer coefficient should only be used as an informative value since it is based on just two experiments with a shorter holding time than the equilibrium time.

The mass transfer coefficient found by Krystad et al. (2012) at 1650 °C with a similar slag composition is 3.3-3.5 times higher than the mass transfer coefficient found in the present work, and the mass transfer coefficient Krystad et al. found at 1600 °C with a 50%CaO-50%SiO_2 slag is 6.7 times higher than the mass transfer coefficient found in the present work. The viscosity becomes lower with increasing temperature and decreasing SiO_2 content in the slag as can be seen in figure 2.7. The mass transfer coefficient in the present work should therefore be lower than at 1650 °C for the same slag composition and lower than with a 50%CaO-50%SiO_2 slag at 1600 °C. The present work does in other words agree well with the results found by Krystad et al.

The experiments in the binary MgO-SiO_2 system showed a very delayed onset of mass transfer. In figure 5.11 the mass transfer is seen to have started after three hours and to be at equilibrium after six hours. The reason for this delayed onset of mass transfer may have been that some of the holding time was required to melt the slag and silicon in the same way as in the binary CaO-SiO_2 system. Another reason may have been that the slag composition initially was outside the liquid region as discussed earlier. There are no experiments with holding times between 3 and 6 hours when the mass transfer took place, and therefore no data for a mass transfer calculation. The time from onset of mass transfer to equilibrium is reached is maximum three hours, which is twice as fast as in the binary system. The mass of the experiments in this system is one third of the mass in the binary CaO-SiO_2 system and this downscaling from the binary system should make the mass transfer approximately 30 % faster. The mass transfer is however at least 50 % faster indicating that the mass transfer coefficient is somewhat higher than in the binary CaO-SiO_2 system which agree with the findings of Krystad et al.

All the equilibrium time experiments in the 35.0%CaO-38.1%Al_2O_3-26.9% SiO_2 (composition after 3 hours holding time) system are seen to be equilibrium values and a mass transfer calculation is therefore not possible for this system either. The mass transfer coefficient must however be significantly higher than for the binary 37.9%CaO-62.1%SiO_2 system since equilibrium is reached at least twice as fast.

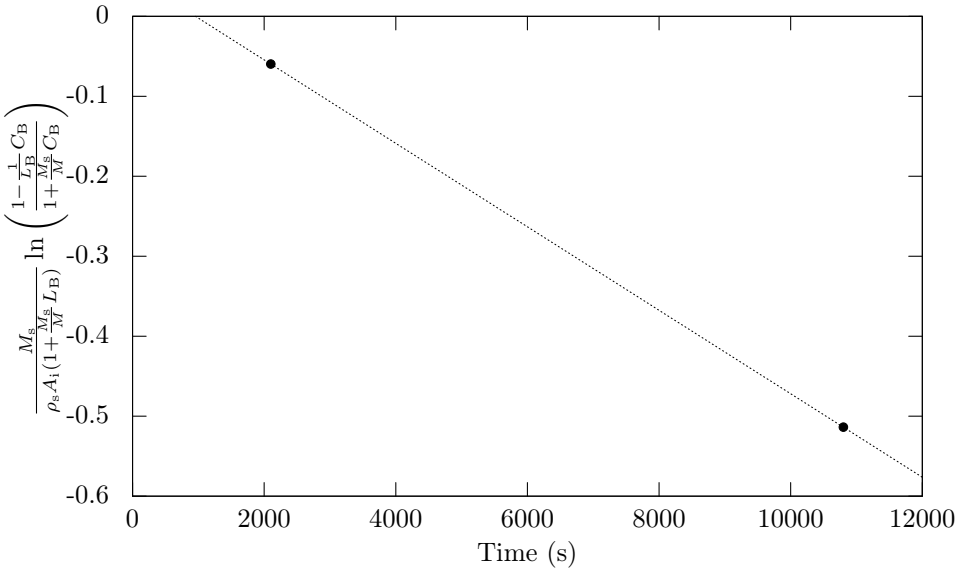

Figure 6.31: Plot where the mass transfer coefficient of boron is given by the slope.

6.10 Accuracy and reproducibility experimental data

The experiments in the present work have been shown to be at equilibrium both by determination of the equilibrium time and by equilibration by transfer of boron from slag to silicon and from silicon to slag. A holding time of six hours have been shown to be necessary to reach equilibrium for the most viscous slags in the present work while equilibrium is reached faster for less viscous slags. Transfer of calcium, magnesium and aluminium from slag to silicon has also been shown to reach equilibrium at least as fast as the transfer of boron.

The analysis of boron concentration is seen to be under good statistical control since similar experiments gives approximately the same distribution coefficient of boron. A recovery of boron close to 100% for most experiments shows that the total boron content in the system remains constant. No boron is lost or introduced to the system from before the experiments are started to the final analysis of slag and silicon. The distribution coefficient is measured to be the same at an external laboratory as when performing the analyses using in house equipment. The same agreement between in house equipment and an external was found with respect to calcium in silicon. The concentration of boron in both slag and silicon was measured to be lower at the external laboratory. Such a bias does however not influence the measured distribution coefficient of boron since it is the same for both slag and silicon. Boron in slag and silicon from the same experiments was measured during the same analytical run to minimize measurement error caused by instrument bias. Using this approach makes the determined distribution coefficient independent of instrument calibration and potential long term drift of the instrument.

Some of the slag is lost during the experiments due to reaction with the graphite crucible. Some calcium, magnesium and aluminium are also lost when the activities of the respective oxides are at their highest in the different slag systems. The change of slag composition is in any case relatively small and slag and silicon will therefore reach equilibrium and remain in equilibrium even if the slag composition changes.

The initial change of slag composition in the Al_2O_3-rich region of the CaO-Al_2O_3-SiO_2 system is shown to be caused by reduction of CaO and Al_2O_3 where the measured concentration of calcium and aluminium in silicon has been shown in figure 5.31 to be very well correlated with the change of slag composition. This serves as a confirmation of accurate measurement of calcium and aluminium in silicon.

Most of the experiments in the MgO-SiO_2 system were performed at an external laboratory and these experiments agree well with respect to boron when compared with experiments using the in-house equipment. Also the measured magnesium concentration was found to be in reasonable agreement but the magnesium concentration from the experiments at the external labo-

ratory are somewhat higher than with in-house equipment for holding times of 6 and 9 hours.

Silicon was premelted in a graphite crucible where also the crucible wall above silicon was wetted with silicon in one of the experiments. This served as a barrier for reaction between slag and graphite and caused mass loss to be relatively low for this experiment. This demonstrates that the type of graphite used for experiments can influence change of slag composition during experiments.

The in-house XRF instrument used for analysis of slag composition was calibrated against standard reference materials for all the major oxides used in the present work. The good agreement between analysed slag composition and the known liquidus line at SiO_2 saturation in the binary CaO-SiO_2 system is a reassurance of the accuracy of these analyses. Also the good agreement between targeted and measured composition of the master slags serves as a quality assurance of the measurements of slag composition.

6.11 Industrial consequences

Industrial slags for boron removal can from a thermodynamic point of view have any composition in the ternary CaO-MgO-SiO_2 system. The efficiency of the slag for boron removal will be approximately the same independently of slag composition in this system. Al_2O_3 should be avoided since the distribution coefficient decreases with increasing amount of this oxide. The distribution coefficient of boron between silicon and slags can also be used to a good approximation for refining of ferrosilicon.

A distribution coefficient of boron equal to two can reduce the boron content in silicon by 67% if the same amount of slag as silicon is used for refining provided that the slag does not contain any boron initially. Using several ladles where slag is reused in a counter-current flow process can improve the efficiency. If three ladles are used in this way we get a 93.3% reduction of the boron content in silicon. Using more ladles or a continuous counter-current flow system would have a even higher efficiency. With $L_B = 2$ we would in any case have a physical limit of purification of 50% of the initial boron content in the slag. It would for example be impossible to get below 0.5 ppmw boron in silicon if the slag contains 1 ppmw boron initially with $L_B = 2$.

Calcium and magnesium will be present in silicon after slag refining with a CaO-MgO-SiO_2 slag and will have to be removed after the slag refining. This can for example be done by vacuum refining, leaching or directional solidification or alternatively by a combination of these processes. Impurities in the slag with less stable oxides than SiO_2 should be kept at a minimum since they will be reduced into the silicon melt.

Chapter 7

Conclusion

The present work has been conducted with the aim of finding more accurate data for the distribution of boron between silicon and CaO-SiO_2, MgO-SiO_2, CaO-MgO-SiO_2 and CaO-Al_2O_3-SiO_2 slags.

A critical review of all published values of the distribution coefficient has been conducted. Non-equilibrium systems was identified and eliminated so that the distribution coefficient could be more accurately determined from literature data. Large differences between different works could still be observed in most slag systems but the highest equilibrium values were observed in the binary CaO-SiO_2 and ternary CaO-MgO-SiO_2 systems.

A complete review of the distribution of other components than boron in the system has also been conducted. Other relevant thermodynamic properties were also reviewed to give a good base for comparison with the present work. The following equilibrium distributions have been determined:

- The distribution of boron and calcium between silicon and binary CaO-SiO_2 slags.
- The distribution of boron and magnesium between silicon and binary MgO-SiO_2 slags.
- The distribution of boron, calcium, and magnesium between silicon and ternary CaO-MgO-SiO_2 slags.
- The distribution of boron, calcium, and aluminium between silicon and ternary CaO-Al_2O_3-SiO_2 slags.
- The distribution of boron and calcium between binary CaO-SiO_2 slags and ferrosilicon.

The following thermodynamic activity data have been determined:

- Activities of CaO, SiO_2 and $BO_{1.5}$ in binary CaO-SiO_2 slags.
- Activities of CaO, MgO, SiO_2 and $BO_{1.5}$ in ternary CaO-MgO-SiO_2 slags.
- Activity coefficients of calcium, magnesium and aluminium at infinite dilution in silicon
- The activity coefficient of boron and calcium at infinite dilution in ferrosilicon

7.1 Determined thermodynamic data

The distribution coefficient of boron was found to be between 2 and 2.5 in the binary CaO-SiO_2, MgO-SiO_2 and ternary CaO-MgO-SiO_2 systems at 1600 °C.

The distribution coefficient of boron in the binary CaO-SiO_2 system was found to follow a linear trend where the distribution coefficient increased from 2 at SiO_2 saturation to 2.5 at Ca_2SiO_4 saturation. A linear fit to the present work in the binary CaO-SiO_2 system is given by

$$L_B = 0.449 \cdot V + 1.89 \tag{7.1}$$

where V is the CaO/SiO_2 mass ratio. The distribution coefficient of boron has been found to be in between the values found in previous works. Most of the previous works has been conducted at a lower temperature than the present work but all of them except the work by Suzuki et al. (1990) is in reasonable agreement with the present work at certain slag compositions. The work by Suzuki et al. in this binary system has been shown to have a too short holding time to reach equilibrium. A similar slag composition in the present work had an equilibrium time of six hours at 1600 °C while Suzuki et al. used a holding time of 2 hours.

The distribution coefficient of boron in the ternary CaO-MgO-SiO_2 system was found to be independent of slag composition with L_B between 2 and 2.5 across the entire liquid region at 1600 °C. The present work has a distribution coefficient of boron that is slightly lower than the only work by White et al. (2012). The distribution coefficient is approximately 1.5 times higher than in a previous work at 1450 °C.

The distribution coefficient of boron was found to decrease linearly with $x_{SiO_2}/(x_{SiO_2} + x_{Al_2O_3})$ in the ternary CaO-Al_2O_3-SiO_2 system at 1600 °C. This decrease was found to be in good agreement with previous works in the same system even if one of the previous works were conducted at a lower temperature. Previous works in the quaternary CaO-MgO-Al_2O_3-SiO_2 system was also found to fit well with the results in the ternary CaO-Al_2O_3-SiO_2

system. This supports the finding in the present work in the ternary CaO-MgO-SiO_2 system that replacing CaO with MgO has no influence on the distribution coefficient of boron. Based on this the equation

$$L_B = L_B^0 \cdot \frac{x_{SiO_2}}{x_{SiO_2} + x_{Al_2O_3}} \tag{7.2}$$

was proposed for slags containing Al_2O_3 where L_B^0 is the distribution coefficient of boron for $x_{Al_2O_3} = 0$.

The concentration of calcium in silicon in equilibrium with binary CaO-SiO_2 slags was measured and found to follow the relation

$$[\%Ca] = \exp(3.002 \cdot V^2 - 1.2481 \cdot V - 3.2241) \tag{7.3}$$

where V is the CaO/SiO_2 mass ratio. This expression was used to determine the activity of CaO and SiO_2 in the slag by Gibb-Duhem integration. The integral was shown to only be dependent on slag composition, the concentration of calcium in silicon and the self-interaction coefficient of calcium. The activity of SiO_2 is given by the polynomial fit

$$\begin{aligned} a_{SiO_2} &= x_{SiO_2} \exp(2154.432x_{SiO_2}^5 - 6458.771x_{SiO_2}^4 + 7818.517x_{SiO_2}^3 \\ &\quad -4796.372x_{SiO_2}^2 + 1497.522x_{SiO_2} - 190.7277) \end{aligned} \tag{7.4}$$

while the activity of CaO is given by

$$\begin{aligned} a_{CaO} &= x_{CaO} \exp(882.284x_{CaO}^5 - 1765.11x_{CaO}^4 + 1453.86x_{CaO}^3 \\ &\quad -590.304x_{CaO}^2 + 115.678x_{CaO} - 13.3528) \end{aligned} \tag{7.5}$$

The activities was used together with the concentration of calcium in silicon to determine the activity coefficient of calcium at infinite dilution in silicon to be

$$\ln \gamma_{Ca}^0 = -7.09 \tag{7.6}$$

at 1600 °C. This value is in good agreement with most previous experimental works.

The same procedure as for the binary CaO-SiO_2 system was used to determine the activity of MgO and SiO_2 in the binary MgO-SiO_2 system. The concentration of magnesium in silicon was approximated by the linear fit

$$x_{Mg} = 0.01079x_{MgO} - 0.00405 \tag{7.7}$$

The activity of SiO_2 found using this function for magnesium in silicon is given by

$$a_{SiO_2} = 273.63x_{SiO_2}^3 - 395.13x_{SiO_2}^2 + 193.58x_{SiO_2} - 31.526 \tag{7.8}$$

and the activity of MgO is given by

$$a_{MgO} = -2.3075x_{MgO}^2 + 3.2589x_{MgO} - 0.8735 \tag{7.9}$$

The activities was used to calculate the activity coefficient of magnesium at infinite dilution in silicon to be

$$\gamma^0_{\mathrm{Mg}} = 0.88 \tag{7.10}$$

at 1600 °C which is somewhat higher than found by an extrapolation of the work by Miki et al. (1999).

The activity coefficients of calcium and magnesium were used together with the measured concentrations of calcium and magnesium to determine activities of CaO and MgO in the ternary CaO-MgO-SiO_2 system. These activities were found to be in good agreement with values from previous works. An extrapolation of the activity SiO_2 found in the binary CaO-SiO_2 system into the ternary CaO-MgO-SiO_2 system was used for this calculation.

The activity coefficient of aluminium at infinite dilution in silicon was estimated using activity data for Al_2O_3 and SiO_2 from FactSage together with the aluminium concentration in silicon in equilibrium with ternary CaO-Al_2O_3-SiO_2 slags to be

$$\gamma^0_{\mathrm{Al}} = 0.66 \tag{7.11}$$

at 1600 °C. This value is somewhat higher than found in previous experimental works.

The activity coefficient of $BO_{1.5}$ at infinite dilution in slag was found to found to follow the same trend as the activity coefficient of SiO_2 in the binary CaO-SiO_2, CaO-MgO and ternary CaO-MgO-SiO_2 systems at 1600 °C. This correlation is also the main cause why the distribution coefficient of boron is more or less independent of slag composition in this system. The activity coefficient was found to be given by

$$\gamma^0_{\mathrm{BO}_{1.5}} = 0.38\gamma_{\mathrm{SiO}_2} \tag{7.12}$$

across the entire CaO-MgO-SiO_2 system. This relation was found to be almost the same in both the the binary CaO-SiO_2 system and the binary MgO-SiO_2 system.

The activity coefficient of $BO_{1.5}$ at infinite dilution in the ternary CaO-Al_2-SiO_2 system was found to increase relatively to the activity coefficient of SiO_2 with increasing Al_2O_3 content in the slag. This increase explains the decrease of the distribution coefficient with increasing Al_2O_3 content in the slag.

The distribution coefficient between a binary 51.7%CaO-48.3%SiO_2 slag and ferrosilicon containing up to 50% iron was found to be unchanged with alloy composition. This means that the distribution coefficient found between pure silicon and slags can be used as a good estimate of the distribution coefficient of boron between ferrosilicon and slags.

The concentration of calcium was found to decrease with increasing iron content in the alloy. This is as expected since silicon forms silicides with

calcium while iron and calcium is immiscible. An equation for calcium concentration in ferrosilicon in equilibrium with binary CaO-SiO_2 slags was found to be

$$[\%\mathrm{Ca}] = \exp(3.002 \cdot V^2 - 1.2481 \cdot V - 8.839 \cdot 10^{-4} \cdot [\%\mathrm{Si}]^2 + 0.212[\%\mathrm{Si}] - 15.5848) \tag{7.13}$$

where V is the CaO/SiO_2 mass ratio and [%Si] is the concentration of silicon in ferrosilicon.

The activity coefficient of calcium at infinite dilution in ferrosilicon was found to follow the relation

$$\ln \gamma^0_{\mathrm{Ca\,in\,FeSi}} = -7.09 + 13.8 \frac{x_{\mathrm{Fe}}}{x_{\mathrm{Si}}} \tag{7.14}$$

while the activity coefficient of boron was found to follow the relation

$$\ln \gamma^0_{\mathrm{B\,in\,FeSi}} = 1.34 - 1.21 \frac{x_{\mathrm{Fe}}}{x_{\mathrm{Si}}} \tag{7.15}$$

7.2 Kinetic data

Kinetic data for boron removal was also studied and an alternative equation for determination of the mass transfer coefficient of boron has been derived:

$$\frac{1}{1 + \frac{M_\mathrm{s}}{M} L_\mathrm{B}} \ln \left(\frac{(1 + \frac{M_\mathrm{s}}{M} C_\mathrm{B})(L_\mathrm{B} - C^0_\mathrm{B})}{(L_\mathrm{B} - C_\mathrm{B})(1 + \frac{M_\mathrm{s}}{M} C^0_\mathrm{B})} \right) = \frac{k_\mathrm{s} \rho_\mathrm{s} A_\mathrm{i}}{M_\mathrm{s}} \cdot t \tag{7.16}$$

where

$$C_\mathrm{B} = (\overline{\%\mathrm{B}})/[\overline{\%\mathrm{B}}] \tag{7.17}$$

$(\overline{\%\mathrm{B}})$ and $[\overline{\%\mathrm{B}}]$ is the concentration of boron in slag and silicon respectively. This equation can be used to determine the mass transfer coefficient of boron by simultaneous measurement of the boron concentration in slag and silicon. This can give a more reliable estimate of the mass transfer coefficient if the boron concentration in slag and silicon from the same experiments are measured during the same analytical run because instrument bias will be eliminated.

The mass transfer coefficient was estimated to be

$$k_\mathrm{s} = 5.2 \cdot 10^{-7} \mathrm{m/s} \tag{7.18}$$

for a binary 37.9%CaO - 62.1%SiO_2 slag using this equation. The total mass transfer coefficient is equal to the mass transfer coefficient in the slag because the mass transfer is controlled by the slag phase. The mass transfer coefficient found in the present work is in good agreement with previous works.

7.3 Industrial consequences and future work

A ternary CaO-MgO-SiO_2 slag can be used to remove boron from silicon provided that the initial boron content in slag is less than twice as large as the target level of boron in silicon. Thermodynamically the slag can have any composition in this system and maintain approximately the same refining efficiency. Al_2O_3 should be avoided as a slag component if the aim is to reduce the boron content in silicon. Calcium and magnesium will be present in silicon after slag refining with a CaO-MgO-SiO_2 slag and additional refining steps are needed to bring the content these to solar grade silicon levels. The distribution coefficient of boron between silicon and slags can also be used to a good approximation for refining of ferrosilicon.

An investigation of the temperature dependence of the distribution coefficient of boron would be an interesting extension of the present work. Determination of the distribution coefficient of phosphorous would also be very useful since phosphorous also is a challenging element to remove from silicon. An investigation of the distribution coefficient of boron where other elements have been added to silicon would also be interesting. Ma et al. (2013) have done one such study very recently where tin was added to the system and the distribution coefficient of boron was found to increase significantly.

Bibliography

J. D. Baird and J. Taylor. Reaction between silica and carbon and the activity of silica in slag solution. *Transactions of the Faraday Society*, 54:526–539, 1958.

I. Barin. *Thermochemical Data of Pure Substances*, volume 2. Wiley-VCH Verlag GmbH, third edition, 1995.

J. Cai, J. Li, W. Chen, C. Chen, and X. Luo. Boron removal from metallurgical silicon using CaO-SiO_2-CaF_2 slags. *Transactions of Nonferrous Metals Society of China*, 21(6):1402 – 1406, 2011.

P. T. Carter and T. G. Macfarlane. Thermodynamics of Slag Systems Part II - The thermodynamic properties of CaO-SiO_2 slags. *The Journal of the Iron and Steel Institute*, 185:62–66, 1957.

L. C. Chang and G. Derge. An Elecrochemical Study of the Properties of Molten Slags og the Systems CaO-SiO_2 and CaO-Al_2O_3-SiO_2. *Metals technology*, 13, 1946.

M. W. Chase. NIST-JANAF Thermochemical Tables. *Journal of Physical and Chemical Reference Data*, Monograph 9, 1998.

J. Chipman. The Free Energy of Silica. *Journal of the American Chemical Society*, 83(7):1762–1763, 1961.

Y. Delannoy. Purification of silicon for photovoltaic applications. *Journal of Crystal Growth*, 360:61 – 67, 2012.

J. Dietl and M. Wohlschläger. Process for purifying metallurgical-grade silicon. Patent. US 4304763, 1981.

Z. Ding, W. Ma, K. Wei, J. Wu, Y. Zhou, and K. Xie. Boron removal from metallurgical-grade silicon using lithium containing slag. *Journal of Non Crystalline Solids*, 358:2708–2712, 2012.

V. D. Eisenhuttenleute, editor. *Slag Atlas*. Verlag Stahleisen GmbH, 2nd edition, 1995.

J. Elliott, M. Gleiser, and V. Ramakrishna. *Thermochemistry for steelmaking, Volume II.* Addison-Wesley Pub. Co., 1963.

E. Enebakk, A. K. Søiland, J. T. Håkedal, and R. Tronstad. Dopant specification of compensated silicon for solar cells of equal efficiency and yield as standard solar cells. In *3rd Int. Workshop on Crystalline Silicon Solar Cells, Trondheim (Norway)*, 2009.

T. Engh, C. Simensen, and O. Wijk. *Principles of metal refining.* Oxford science publications. Oxford University Press, Incorporated, 1992.

EPIA and Greenpeace. Solar Generation 6, 2011.

G. Eriksson, P. Wu, M. Blander, and A. D. Pelton. Critical evaluation and optimization of the thermodynamic properties and phase diagrams of the MnO-SiO_2 and CaO-SiO_2 systems. *Canadian Metallurgical Quarterly*, 33 (1):12–21, 1994.

H. Fujiwara, L. J. Yuan, K. Miyata, E. Ichise, and R. Otsuka. Distribution Equilibria of the Metallic Elements and Boron between Si Based Liquid Alloys and CaO-Al_2O_3-SiO_2. *Journal of the Japan Institute of Metals*, 60 (1):65–71, 2002.

J. C. Fulton and J. Chipman. Slag-metal-graphite reactions and the activity of silica in lime-alumina-silica slags. *Journal of Metals*, 200:1136–1146, 1954.

D. Gaskell. *Introduction to the Thermodynamics of Materials.* Taylor & Francis, 2008.

W. M. Haynes, editor. *Handbook of Chemistry and Physics.* CRC Press, Boca Raton, Florida, 93rd edition, 2012. URL `http://www.hbcpnetbase.com`. [Online; accessed 02.04.2013].

W. A. Hermann. Quantifying global exergy resources. *Energy*, 31(12):1685–1702, 2006.

V. Hoffmann, K. Petter, J. Djordjevic-Reiss, E. Enebakk, J. T. Håkedal, R. Tronstad, T. Vlasenko, I. Buchovskaja, S. Beringov, and M. Bauer. First results on idustrialization of elkem solar at Pillar JSC and Q-Cells. In *Proc. 23rd European Photovoltaic Solar Energy Conference*, 2008.

R. Hopkins and A. Rohatgi. Impurity effects in silicon for high efficiency solar cells. *Journal of Crystal Growth*, 75(1):67–79, 1986.

IPCC. Climate Change 2007: Synthesis Report. Contribution of Working Groups I, II and III to the Fourth Assessment Report of the Intergovernmental Panel on Climate Change, 2007. [Core Writing Team, Pachauri, R.K and Reisinger, A. (eds.)]. IPCC, Geneva, Switzerland, 104 pp.

K. Jacob and V. Varghese. Controversy on the free energy of formation of CaO - additional evidence in support of thermochemical data. *Metallurgical and Materials Transactions B*, 27(4):647–651, 1996.

M. Johnston and M. Barati. Distribution of impurity elements in slag-silicon equilibria for oxidative refining of metallurgical silicon for solar cell applications. *Solar Energy Materials and Solar Cells*, 94(12):2085 – 2090, 2010.

M. D. Johnston, L. T. Khajavi, M. Li, S. Sokhanvaran, and M. Barati. High-temperature refining of metallurgical-grade silicon: A review. *JOM*, 64(8): 935–945, 2012. ISSN 1047-4838.

I.-H. Jung, S. A. Decterov, and A. D. Pelton. Critical thermodynamic evaluation and optimization of the CaO-MgO-SiO_2 system. *Journal of the European Ceramic Society*, 25(4):313–333, 2005.

M. R. Kalyanram, T. G. Macfarlane, and H. B. Bell. The activity of calcium oxide in slags in the systems CaO-MgO-SiO_2, CaO-Al_2O_3-SiO_2, and CaO-MgO-Al_2O_3-SiO_2 at 1500 °C. *Journal of The Iron and Steel Institute*, 195: 58–64, 1960.

S. Kambayashi and E. Kato. A thermodynamic study of (magnesium oxide + silicon dioxide) by mass spectrometry. *The Journal of Chemical Thermodynamics*, 15(8):701 – 707, 1983.

D. A. R. Kay and J. Taylor. Activities of silica in the lime + alumina + silica system. *Transactions of the Faraday Society*, 56:1372–1386, 1960.

E. Krystad, K. Tang, and G. Tranell. The Kinetics of Boron Transfer in Slag Refining of Silicon. *The Journal of The Minerals, Metals and Materials Society*, 64(8):968–972, 2012.

D. Luo, N. Liu, Y. ping Lu, G. liang Zhang, and T. ju Li. Removal of boron from metallurgical grade silicon by electromagnetic induction slag melting. *Transactions of Nonferrous Metals Society of China*, 21(5):1178 – 1184, 2011. ISSN 1003-6326.

D. Lynch. Winning the global race for solar silicon. *JOM*, 61(11):41–48, 2009. ISSN 1047-4838.

X. Ma, T. Yoshikawa, and K. Morita. Removal of boron from silicon-tin solvent by slag treatment. *Metallurgical and Materials Transactions B*, 44 (3):528–533, 2013.

H. Mao, M. Hillert, M. Selleby, and B. Sundman. Thermodynamic Assessment of the CaO-Al_2O_3-SiO_2 System. *Journal of the American Ceramic Society*, 89(1):298–308, 2006.

T. Margaria, M. Rebiere, F. Traversaz, and C. Dumay. Silicon refining: Experimental studies and industrial means to control silicon quality. In *Proc. Silicon for the Chemical Industry III*, pages 21–31, 1996.

T. Miki, K. Morita, and N. Sano. Thermodynamic properties of aluminum, magnesium, and calcium in molten silicon. *Metallurgical and Materials Transactions B*, 29(5):1043–1049, 1998.

T. Miki, K. Morita, and N. Sano. Thermodynamic Properties of Si-Al, -Ca, -Mg Binary and Si-Ca-Al, -Ti, -Fe Ternary alloys. *Materials Transactions, JIM*, 40(10):1108–1116, 1999.

K. Morita, K. Kume, and N. Sano. A Newly Developed Method for Determining SiO_2 Activity of the Silicate Slags Equilibrated with Molten Silicon Alloys. *ISIJ International*, 40(6):554–560, 2000.

K. Morita, K. Kume, and N. Sano. Activity measurement of silicate slags equilibrated with molten silicon alloys. *Scandinavian Journal of Metallurgy*, 31(3):178–183, 2002.

O. Morton. Solar energy: A new day dawning?: Silicon Valley sunrise. *Nature*, 443:19–22, 2006.

E. Myrhaug and H. Tveit. Material Balances of Trace Elements in the Ferrosilicon and Silicon Processes. In *Electric Furnace Conference Proceedings*, pages 591–604, 2000.

H. Nishimoto, Y. Kang, T. Yoshikawa, and K. Morita. The Rate of Boron Removal from Molten Silicon by CaO-SiO_2 Slag and Cl_2 Treatment. *High Temperature Materials and Processes*, 31(4-5):471–477, 2012.

E. F. Nordstrand and M. Tangstad. Removal of Boron from Silicon by Moist Hydrogen Gas. *Metallurgical and Materials Transactions B*, 43(4):814–822, 2012. ISSN 1073-5615.

H. Ohta and H. Suito. Activities in CaO-SiO_2-Al_2O_3 slags and deoxidation equilibria of Si and Al. *Metallurgical and Materials Transactions B*, 27(6): 943–953, 1996.

Y. Omori and K. Sanbongi. Activity of CaO in the Slag of CaO-SiO_2-Al_2O_3 System. *Journal of the Japan Institute of Metals*, 25(2):1873–1878, 1961.

L. Ottem. Equilibria between molten silicon and SiO_2-CaO-Al_2O_3 slags at 1550 °C. Report STF34 F93112, SINTEF, 1993. Cited from Schei et al. (1998).

E. O. Pinto and C. Takano. Activity of calcium in dilute liquid Si-Ca alloy. *Metallurgical and Materials Transactions B*, 31(6):1267–1272, 2000.

R. H. Rein and J. Chipman. Activities in the Liquid Solution SiO_2-CaO-MgO-Al_2O_3 at 1600 °C. *Transactions of the Metallurgical Society of AIME*, 233: 415–425, 1965.

REN21. Renewables 2013 Global Status Report, 2013. URL `http://www.ren21.net/REN21Activities/GlobalStatusReport.aspx`. (Paris: REN21 Secretariat).

M. Rey. The thermodynamic activity of silica and of oxides in silicate melts. *Discussions of the Faraday Society*, 4:257–265, 1948.

F. D. Richardson. Thermodynamic aspects of molten slags. In *Proc. The Physical Chemistry of Melts*, pages 75–95, 1953.

J. Safarian, G. Tranell, and M. Tangstad. Thermodynamic and Kinetic Behavior of B and Na Through the Contact of B-Doped Silicon with Na_2O-SiO_2 Slags. *Metallurgical and Materials Transactions B*, pages 1–13, 2013. ISSN 1073-5615.

R. Sakagami. Electrochemical study on molten slags (II). *Tetsu-to-Hagane*, 39(7), 1953a.

R. Sakagami. Electrochemical study on molten slags (III). *Tetsu-to-Hagane*, 39(11), 1953b.

K. Sawamura. Activity of CaO in the Binary System CaO-SiO_2. *Tetsu-to-Hagane*, 47(14):1873–1878, 1961.

A. Schei, J. Tuset, and H. Tveit. *Production of High Silicon Alloys*. Tapir Forlag, 1998.

C. E. Schürmann, P. Fünders, and D. H. Litterscheidt. Vapor pressure of calcium above calcium-silicon- and calcium-aluminum melts and also above calcium-aluminum-silicon alloys. *Archiv für das Eisenhüttenwesen*, 46(8): 473–476, 1975.

SEMI. PV17-1012, Specification for Virgin Silicon Feedstock Materials for Photovoltaic Applications, 2012.

R. A. Sharma and F. D. Richardson. The solubility of calcium sulphide and activities in lime-silica melts. *The Journal of the Iron and Steel Institute*, 200:373–379, 1962.

A.-K. Søiland, J.-O. Odden, B. Sandberg, K. Friestad, J. Håkedal, E. Enebakk, and S. Braathen. Solar Silicon from a metallurgical route by Elkem Solar - a viable alternative to virgin polysilicon. In *Proc. 6th International workshop on Crystalline Silicon for Solar Cells*, 2012.

K. Suzuki, T. Sugiyama, K. Takano, and N. Sano. Thermodynamics for Removal of Boron from Metallurgical Silicon by Flux Treatment. *Journal of the Japan Institute of Metals*, 54(2):168–172, 1990.

M. Tanahashi, T. Fujisawa, and C. Yamauchi. Activity of Boron in Molten Silicon. *Shigen-to-Sozai*, 114(11):807–812, 1998.

M. Tanahashi, Y. Shinpo, T. Fujisawa, and C. Yamauchiy. Distribution Behavior of Boron between SiO_2-saturated $NaO_{0.5}$-CaO-SiO_2 Flux and Molten Silicon. *Shigen-to-Sozai*, 118(7):497–505, 2002.

L. A. V. Teixeira and K. Morita. Removal of Boron from Molten Silicon Using CaO-SiO_2 Based Slags. *ISIJ International*, 49(6):783–787, 2009.

L. A. V. Teixeira, Y. Tokuda, T. Yoko, and K. Morita. Behavior and State of Boron in CaO-SiO_2 Slags during Refining of Solar Grade Silicon. *ISIJ International*, 49(6):777–782, 2009.

H. C. Theuerer. Removal of Boron from Silicon by Hydrogen Water Vapor Treatment. *Journal of Metals*, 75(8):1316–1319, 1956.

R. Thomas. *Practical Guide to ICP-MS*. Marcel Dekker, New York, New York, 2004.

F. A. Trumbore. Solid solubilities of impurity elements in germanium and silicon. *Bell System Technical Journal*, 39(1):205–233, 1960.

J. K. Tuset. Principles of silicon refining. In *Proc. International Seminar on Refining and Alloying of Liquid Aluminium and Ferro-Alloys*, pages 50–69, 1985.

T. Wakasugi and N. Sano. Re-evaluation of standard free energy of formation of CaO. *Metallurgical Transactions B*, 20(3):431–433, 1989.

X. Wang, W. zhong Ding, K. Tang, G. chang Jiang, and K. di Xu. Experimental thermodynamic research on equilibrium between silicon alloy and SiO_2-CaO-Al_2O_3 melt. *Transactions of Nonferrous Metals Society of China*, 11(4):535–539, 2001.

T. Weiss and K. Schwerdtfeger. Chemical Equilibria between Silicon and Slag Melts. *Metallurgical and Materials Transactions B*, 25(4):497–504, 1994.

J. White, C. Allertz, K. Forwald, and D. Sichen. The Distribution of Boron between SiO_2-CaO-MgO Slags and Liquid Silicon at Controlled Oxygen and Nitrogen Potentials. In *Proc. Ninth International Conference on Molten Slags, Fluxes and Salts*, 2012.

P. Wu, G. Eriksson, A. D. Pelton, and M. Blander. Prediction of the Thermodynamic Properties and Phase Diagrams of Silicate Systems: Evaluation of the FeO-MgO-SiO_2 System. *ISIJ International*, 33(1):26–35, 1993.

L. Yang, C. L. McCabe, and R. Miller. A Summary of Some Experimental Work on the Activity of Silica in Liquid Silicate Systems. In *Proc. The Physical Chemistry of Steelmaking*, pages 63–64, 1958.

T. Yoshikawa and K. Morita. Thermodynamic Property of B in Molten Si and Phase Relations in the Si-Al-B System. *Materials Transactions*, 46: 1335–1340, 2005.

L. Zhang, Y. Tan, F. M. Xu, J. Y. Li, H. Y. Wang, and Z. Gu. Removal of Boron from Molten Silicon using Na_2O-CaO-SiO_2 Slags. *Separation Science and Technology*, 48(7):1140–1144, 2013.

Z. Zhang, J. Zhou, Y. Zuo, and Y. Tian. Activity of CaO in liquid CaO-Al_2O_3-SiO_2 system. *Acta Metallurgica Sinica - Chinese Edition*, 22(3):256–264, 1986.